Volume 67A
Number 2
Mar.–Apr. 1963

Physics and Chemistry

6

U.S. DEPARTMENT OF COMMERCE

SECTION A

JOURNAL OF RESEARCH

NATIONAL BUREAU OF STANDARDS

Journal of Research

of the

National Bureau of Standards

A. Physics and Chemistry

MAR.–APR. • 1963

VOLUME • 67A

NUMBER • 2

Editor: C. W. Beckett

Associate Editors: D. D. Wagman
I. M. Richardson

Publication dates:
Feb. 1, Apr. 1, June 1, Aug. 1, Oct. 1, Dec. 1, 1963.

JOURNAL OF RESEARCH

The National Bureau of Standards Journal of Research reports research and development in the fields of activity shown at right. Also included from time to time are survey articles on topics closely related to the Bureau's scientific and technical program.

The Journal is published in four separate sections as follows:

A. Physics and Chemistry

Contains papers of interest primarily to scientists working in these fields. Issued six times a year. Annual subscription: domestic, $4.00; foreign, $4.75.

B. Mathematics and Mathematical Physics

Presents studies and compilations designed mainly for the mathematician and the theoretical physicist. Issued quarterly. Annual subscription: domestic, $2.25; foreign, $2.75.

C. Engineering and Instrumentation

Reports research and development results of interest chiefly to the engineer and the applied scientist. Issued quarterly. Annual subscription: domestic, $2.25; foreign, $2.75.

D. Radio Propagation

Reports work in radio propagation, upper atmospheric physics, and communications. Issued six times a year. Annual subscription: domestic, $4.00; foreign, $4.75.

U.S. DEPARTMENT OF COMMERCE
Luther H. Hodges, Secretary

NATIONAL BUREAU OF STANDARDS
A. V. Astin, Director

Functions and Activities

The functions of the National Bureau of Standards are set forth in the Act of Congress, March 3, 1901, as amended. These include the development and maintenance of the national standards of measurement and the provision of means and methods for making measurements consistent with these standards; the determination of physical constants and properties of materials; the development of methods and instruments for testing materials, devices, and structures; advisory services to government agencies on scientific and technical problems; invention and development of devices to serve special needs of the Government; and the development of standard practices, codes, and specifications. The work includes basic and applied research, development, engineering, instrumentation, testing, evaluation, calibration services, and various consultation and information services. The Bureau also serves as the Federal technical research center in a number of specialized fields. The scope of activities of the National Bureau of Standards is suggested in the following listing of the divisions and sections engaged in technical work.

Washington, D.C.

Electricity. Resistance and Reactance. Electrochemistry. Electrical Instruments. Magnetic Measurements. Dielectrics. High Voltage.

Metrology. Photometry and Colorimetry. Refractometry. Photographic Research. Length. Engineering Metrology. Mass and Scale. Volumetry and Densimetry.

Heat. Temperature Physics. Heat Measurements. Cryogenic Physics. Equation of State. Statistical Physics.

Radiation Physics. X-ray. Radioactivity. Radiation Theory. High Energy Radiation. Radiological Equipment. Nucleonic Instrumentation. Neutron Physics.

Analytical and Inorganic Chemistry. Pure Substances. Spectrochemistry. Solution Chemistry. Standard Reference Materials. Applied Analytical Research. Crystal Chemistry.

Mechanics. Sound. Pressure and Vacuum. Fluid Mechanics. Engineering Mechanics. Rheology. Combustion Controls.

Polymers. Macromolecules: Synthesis and Structure. Polymer Chemistry. Polymer Physics. Polymer Characterization. Polymer Evaluation and Testing. Applied Polymer Standards and Research. Dental Research.

Metallurgy. Engineering Metallurgy. Microscopy and Diffraction. Metal Reactions. Metal Physics. Electrolysis and Metal Deposition.

Inorganic Solids. Engineering Ceramics. Glass. Solid State Chemistry. Crystal Growth. Physical Properties. Crystallography.

Building Research. Structural Engineering. Fire Research. Mechanical Systems. Organic Building Materials. Heat Transfer. Inorganic Building Materials. Metallic Building Materials.

Applied Mathematics. Numerical Analysis. Computation. Statistical Engineering. Mathematical Physics. Operations Research.

Data Processing Systems. Components and Techniques. Computer Technology. Measurements Automation. Engineering Applications. Systems Analysis.

Atomic Physics. Spectroscopy. Infrared Spectroscopy. Solid State Physics. Electron Physics. Atomic Physics.

Instrumentation. Engineering Electronics. Electron Devices. Electronic Instrumentation. Mechanical Instruments. Basic Instrumentation.

Physical Chemistry. Thermochemistry. Surface Chemistry. Organic Chemistry. Molecular Spectroscopy. Molecular Kinetics. Mass Spectrometry.

Office of Weights and Measures

Boulder, Colo.

Cryogenic Engineering. Cryogenic Equipment. Cryogenic Processes. Properties of Materials. Cryogenic Technical Services.

Central Radio Propagation Laboratory

Ionosphere Research and Propagation. Low Frequency and Very Low Frequency Research. Ionosphere Research. Prediction Services. Sun-Earth Relationships. Field Engineering. Radio Warning Services. Vertical Soundings Research.

Radio Propagation Engineering. Data Reduction Instrumentation. Radio Noise. Tropospheric Measurements. Tropospheric Analysis. Propagation-Terrain Effects. Radio-Meteorology. Lower Atmosphere Physics.

Radio Systems. Applied Electromagnetic Theory. High Frequency and Very High Frequency Research. Modulation Research. Antenna Research. Navigation Systems.

Upper Atmosphere and Space Physics. Upper Atmosphere and Plasma Physics. Ionosphere and Exosphere Scatter. Airglow and Aurora. Ionospheric Radio Astronomy.

Radio Standards Laboratory

Radio Physics. Radio Broadcast Service. Radio and Microwave Materials. Atomic Frequency and Time-Interval Standards. Millimeter-Wave Research.

Circuit Standards. High Frequency Electrical Standards. Microwave Circuit Standards. Electronic Calibration Center.

Order all publications from the Superintendent of Documents
U.S. Government Printing Office, Washington 25, D.C.

Use of funds for printing this publication approved by the Director of the Bureau of the Budget (June 19, 1961).

JOURNAL OF RESEARCH of the National Bureau of Standards—A. Physics and Chemistry
Vol. 67A, No. 2, March–April 1963

Third Spectrum of Palladium (Pd III)

A. G. Shenstone*

(November 2, 1962)

The Pd III spectrum has been observed from 688 to 2991 A, and the earlier analysis has been revised and extended. The number of Pd III lines here reported is 1,110, of which 917 are classified as combinations of 57 even energy levels with 111 of odd parity. The interpretation has been aided by theoretical predictions of the approximate positions of expected energy levels. Spectral terms from the $4d^8$, $4d^7\,ns^1$, and $4d^6\,5s^1\,5p^1$ configurations are designated. Eight limit terms are in the $4d^7\,ns^1$ configurations. The earlier ionization potential, 33.0 electron volts derived from the $(ns^1)\,^{3,5}\mathrm{F}$ series (n=5,6) by means of a Ritz formula, remains unchanged.

1. Introduction

Although a table of energy levels of the third spectrum of palladium was published in Atomic Energy Levels Vol. III[1] [1] in 1958, no description of the spectrum itself has appeared in print. Since the original analysis was done, I have made new measurements of the spectrum lines and have corrected and added to the analysis. While I was engaged in that work, the thesis of Dr. Yehudi Shadmi appeared in June 1961, with the title "A Systematic Treatment of the Low Configurations in the Spectra of the Transition Elements." His research extended the theoretical work started by Professor Racah [2] so that he was able to make a calculation of the even levels of the third spectra of the iron period and the first, second, and third spectra of the second long period. Palladium III was an important spectrum in that last group, being the last spectrum in the period of any considerable complication. Shadmi, who was in Princeton at the Institute for Advanced Study in 1961–62, also was good enough to ask one of his colleagues, Zvi Shimoni, in Jerusalem to calculate for me the positions of the odd levels of Pd III. As a result I have been able to correct the analysis in a number of points. They are discussed below.

2. Observations

The method of excitation of the spectrum was the same as that used for Ni III [3] with a number of refinements. The spark was operated in helium by using a transformer-condenser circuit with an auxiliary spark gap. The gap was a mercury gap, formerly part of an old induction furnace, and its present use gave considerably sharper spectra than the air gap used in recent years. Figure 1 shows the design of this useful and quiet gap. The accuracy of the level scheme was considerably improved by new measurements of all the longer wavelength lines by means of our 21 ft 30,000 line per inch grating in a Paschen mounting. The lines of the third spectrum were first spotted by observing their polarity in spectra taken with a stigmatic mounting at smaller dispersion. This was necessary, of course, because of the great astigmatism of the Paschen instrument. The accurate measures were extended to the λ 1944 line of Cu II and were based on the copper lines as standards [4]. This wavelength range overlaps the strong oxygen absorption bands with the consequence that some strong Pd III lines are missing on the high dispersion photographs, and others are much weakened. This probably means that all the measurements below about 2000 A may be inaccurate due to absorption on one side or the other of the lines. In the part of the spectrum measured with the vacuum instrument only, the accuracy is somewhat better than in previous papers from this laboratory because of recent improvements in standards [5]. In table 1 from 1946 to 2197 A two sets of intensity estimates are listed: LG denotes the large grating and VG denotes the vacuum grating.

3. Analysis

The electronic structures which are responsible for Pd III are analogous, of course, to those of Ni III, but the change in the n's of the electrons produces very large differences in the level structure. The total spreads of energy in $4d^8$ and $4d^7\,5s$ are only about 0.78 of those in $3d^8$ and $3d^7\,4s$ but the spread of most of the individual terms is larger by a factor of over two. In consequence, there is a much greater mixing of terms and a great decrease in the individuality of the levels so that it becomes chiefly a matter of taste or convenience to use Russell-Saunders notation for many of the even levels and for a majority of the odd levels. The names chosen are mainly based on relative intensities of combinations, but some are based on analogy with other spectra. This leads to a considerable number of differences between my choice and those of

*Present address: Princeton University.
[1] Figures in brackets indicate the literature references at the end of this paper.

670682—63——1

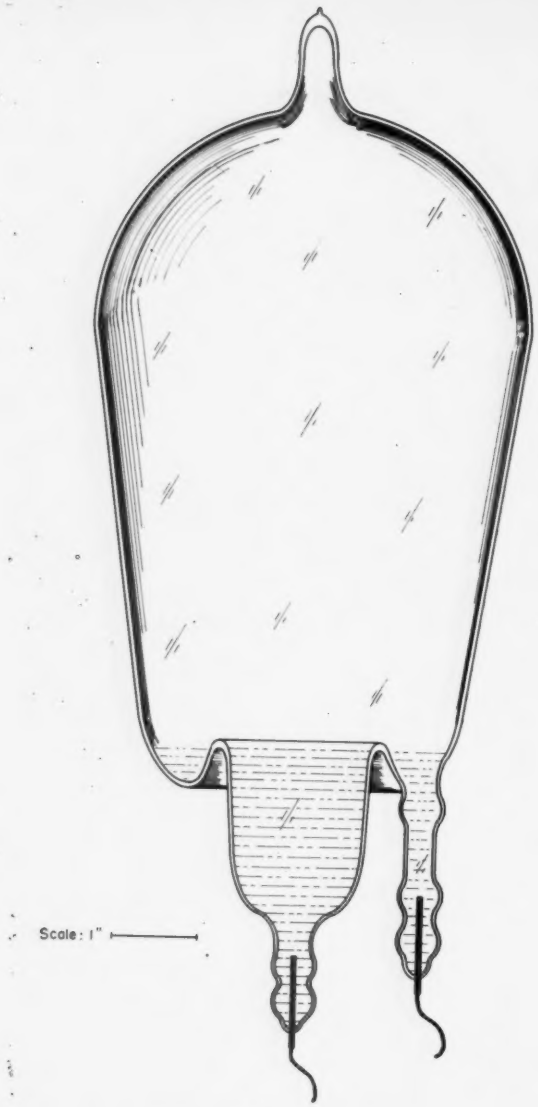

FIGURE 1. *Mercury spark gap.*

Shadmi and Shimoni although the numerical agreements between theory and observation are extraordinarily good.

4. Configurations $4d^8$ and $4d^7\,5s$

Shadmi's allocations differ from mine in one case only, the interchange of $a\,^1D_2$ and $a\,^3P_2$. The evidence for this change from intensities is ambiguous and I have preferred to retain my original choice.

There are, however, cases in which the theory does not predict significant mixing of identities, but where the experimental evidence does. The most important example is the mixing of $b\,^3F_3$ and $a\,^5P_3$ which are only 453 cm^{-1} apart. That they share their combining properties to a very considerable extent is shown by the following selected pairs of intensities. With $z\,^5S^\circ_2$ the intensities are 200 and 300; with $z\,^3F^\circ_2$ 200 and 200; with $z\,^3G^\circ_4$ 500 and 250; with $z\,^3D^\circ_3$ 200 and 200; with $z\,^5P^\circ_3$ 150 and 200.

Two corrections amongst the even levels should be noted. $c\,^3P_0$ was incorrectly copied in my original manuscript and is now corrected. I have found, also, a new level $b\,^3D_1$ which fits both theory and observation better than the one which was previously reported and is now deleted. The only missing level of $4d^7\,5s$ is $(b\,^2D)^1D_2$. A thorough search has been made for it with no result in spite of the guidance of Shadmi's prediction.

As usual, the $^1S_0$ of the d^8 structure is missing. Its predicted position is so high that most of its combinations would lie in regions of the spectrum where very few lines have been observed. However, the theoretically predicted positions of $a\,^1S_0$ and $(b\,^2D)^1P^\circ_1$ differ by 118140 and there is a strong isolated and unidentified line at 117804 cm^{-1}. Since the sole parent of $d^8\,^1S_0$ in d^7 is $b\,^2D$ this combination should be the strongest of all those possible. The only other lines which fall near predicted positions are the questionable ones at 82861 and 82800 cm^{-1}. If one of these is taken as $c\,^3P_1 - (b\,^2D)^1P^\circ_1$ then $a\,^1S_0$ falls at 41112 or 41051 both of which are close to the predicted position 41196.

5. Configuration $4d^7\,5p$

Although Shimoni's calculated odd levels agree numerically very well indeed with the empirical levels, there are many differences of interpretation. He gave in his communication to me the percentage composition of all the levels; and if one were to name each level to agree with its major component, there would be at least 15 more differences in interpretation than the 14 chosen by Shimoni.

Oddly enough, in the case of the important quintets built on the ^4F of Pd IV Shimoni has chosen identifications which agree with mine, even though the percentage composition could in some levels lead to changes, and even though, also, this is the only set of levels for which I have used names based on an analogy in disagreement with the evidence of the intensities. In the isoelectronic sequences which begin with Fe I and Ru I, the identification of these levels in the arc spectra is the same whether based on intensities or g-values. It is quite otherwise in Co II [6] where the pattern of levels differs markedly from Fe I and where the evidence of the g-values is in considerable disagreement with the intensities. Since in Ni III, Rh II [1] and Pd III the pattern is more like Co II than Fe I, I have chosen the levels of Pd III by analogy with Co II and therefore in disagreement with the intensities. Figure 2 shows the two choices. In the triplet triad built on ^4F of Pd IV, Shimoni has again chosen in agreement with me al-

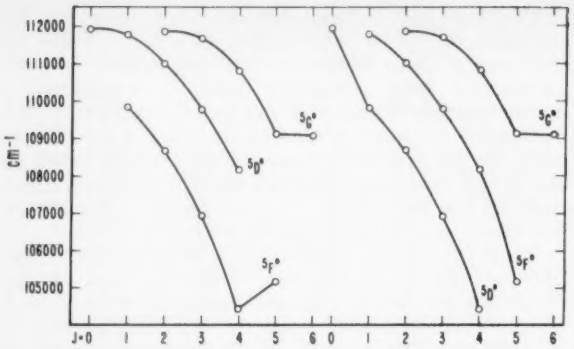

FIGURE 2. $4d^7\,5p\,{}^5D°$, F°, G°, *as identified by analogy with* Co II *(on left) and by intensities (on right).*

though the percentage composition of $z\,{}^3F_3^\circ$ and $z\,{}^3D_3^\circ$ is slightly in favor of an interchange. The intensities are somewhat ambiguous.

In the region of energies from 119000 to 129000 there are 45 odd levels, of which ten are named differently by Shimoni and myself. Figure 3 is a plot to show the two arrangements. The intensities are in favor of my identifications but there are certainly fundamental questions to be answered. For instance, the composition given for my $z\,{}^5P_3^\circ$ is 49 percent $({}^4P){}^5D°$, 17 percent $({}^4P){}^3D°$, 14 percent $({}^4F){}^5D°$, so that ${}^5P°$ should be a very minor constituent in disagreement with the intensity observations. My $z\,{}^5P_2^\circ$ also has no major ${}^5P°$ character in its makeup. These few examples indicate a very wide divergence in this respect between experiment and theory and a detailed examination would appear to be of importance. The levels at 119187 and 125477 which Shimoni calls respectively $({}^2P){}^3P_1^\circ$ and $({}^4P){}^3S_1^\circ$ could be interchanged and the lower one labeled $({}^2P){}^3S_1^\circ$ from intensities. The choice I made for 119187 $({}^2P){}^3P_1^\circ$ however fits the intensities best.

In this part of the analysis, Shimoni's predictions of the positions of $({}^2P){}^3P_0^\circ$ and $({}^4P){}^3P_0^\circ$ made it possible for me to find these two levels, which are always elusive because of the paucity of combinations of levels of $J=0$. Amongst the higher terms there are a few more differences of naming, but more important is the fact that Shimoni's predictions led me to discover that my $w\,{}^3F_2^\circ$ is in reality $w\,{}^3G_3^\circ$; that my $x\,{}^1F_3^\circ$ is $w\,{}^3F_2^\circ$ and that my old $w\,{}^3G_3^\circ$ is spurious. This cleared up the difficulty, that I had one too many levels with $J=3$. The only odd set of terms that is incomplete is the one based on the higher of the ${}^2D$ terms of $4d^7$. $w\,{}^3P°$ seems excellent but the fragments of ${}^3F°$ and ${}^3D°$ are all quite uncertain. They were chosen to fit the Shimoni analysis but the fact that levels such as $^3F_4^\circ$, which should give stronger lines, are missing makes them all doubtful. The level given in A. E. L. as $w\,{}^3D_3^\circ$ is certainly spurious.

It is of considerable importance to find an accurate ionization potential by means of series and I, therefore, made a great effort to identify the levels of $4d^7({}^4F)6s$ and $4d^7({}^4F)5d$ which should lie at about 170,000 to 175,000, making combinations with the $5p$ levels in the range 1450 to 1700 A. Long exposures were made in this region and every possible

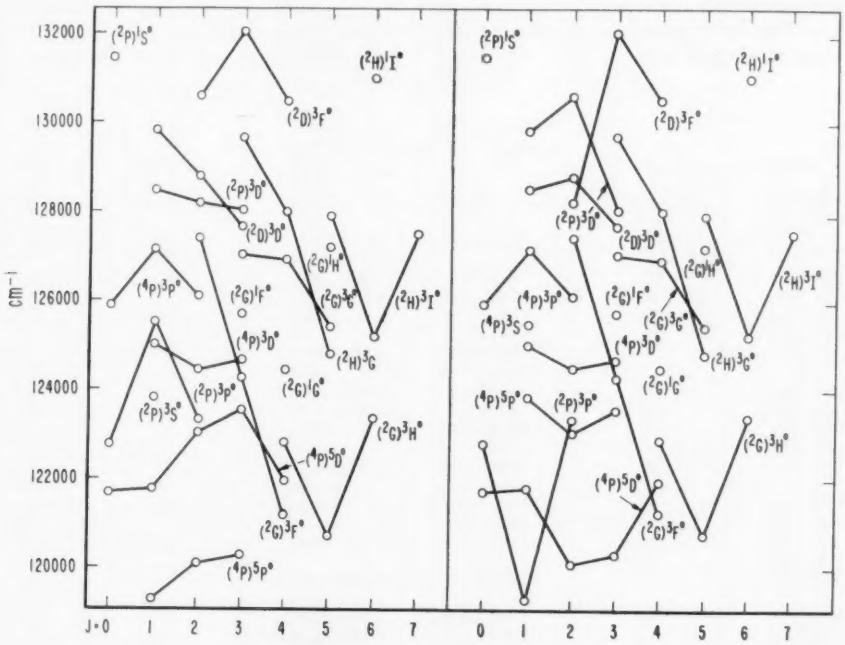

FIGURE 3. *Some levels of $4d^7\,5p$ as identified in this paper (on left) and as identified by Shimoni (on right).*

line measured. The results were very disappointing, only 12 levels being retained as probably real. This is all the more surprising in that many complete terms were found in the corresponding structures of Co III. Of the levels here listed 1_5 is probably $6s\ ^5F_5$ as given in A. E. L.; 2_4 is perhaps $6s\ ^5F_4$ and 11_4 is about correct for $6s\ ^3F_4$. The remainder cannot be identified except that it is certain that all but 11 and 12 are quintets. I cannot, therefore, give any evidence that will improve our knowledge of the ionization potential.

6. Configurations $4d^6\,5s^2$ and $4d^6\,5s\,5p$

There remains the problem of the terms $4d^6\,5s^2\ ^5D$ and the various odd triads from $4d^6(^5D)5s\ 5p$. The position of the even ^5D can be estimated from a consideration of various other spectra [7] as being between 128000 and 133000. Recently Shadmi has calculated the position for me as $131{,}500 \pm 1{,}000$ cm^{-1}. The structure $4d^6\,5s\,5p$ yields two sets of quintets based respectively on ^6D and ^4D of $4d^6\,5s$. By analogy with Ru I, where both sets are identified, one can estimate that they should be separated by about 10,000 cm^{-1}. Also the lower triad gives lines in combination with the even ^5D of nearly the same wave number as $4d^7\,5s$–$4d^7\,5p$ which lie at about 54,000 cm^{-1}. This would place the lower $4d^6\,5s\,5p$ quintet triad around 185,500 $\pm 1{,}000$ and no levels at all have been found in that region. The higher quintets should lie about 10,000 higher and they may be represented by the levels 1 to 7°. This is an unsatisfactory conclusion because in both Fe I and Ru I the lower triad gives considerably stronger lines than the upper one.

The line list includes all the lines that can be assigned to Pd III with some certainty. Only in the region from 1500 to 1650 A where I took excessively long exposures have I eliminated a a considerable number of the measured lines which appear to be more probably due to Pd IV. Especially in this region some new source which develops the Pd III spectrum more completely and eliminates most of the lines of Pd IV is necessary if the higher structures are to be identified with any certainty.

There are a few unidentified lines in the region 680 to 800 A which are probably due to the structure $4d^6\ 5s\ 5p$. In the region 1450 to 1700 A the many unidentified lines are undoubtedly due to structures $4d^7\ 6s$ and $4d^7\ 5d$ as discussed above or to Pd IV. In the part longer than 1950 A there are five unidentified lines of considerable strength. The only structures to which they can be attributed are $4d^7(b\ ^2D)5s$ and $5p$, but no logical way of fitting them into the term scheme has been found.

The accuracy with which Shadmi's and Shimoni's predictions fit the numerical data makes it obvious that when a theoretical analysis of that kind is available, the experimentalist would be unwise to ignore it. Very definite empirical evidence would be necessary to justify any large difference between theory and experiment.

This research has been in part supported by the Higgins Fund of Princeton University. Mrs. Charlotte Moore Sitterly and the National Bureau of Standards have assisted in the preparation of the manuscript. I am much indebted to Mr. Zvi Shimoni for his kind permission to use his unpublished results in any way I wished.

TABLE 1. *List of lines of* Pd III

Wavelength λ (Vac)	Intensity	Wave number	Identification
688. 743	10	145192. 0	$a\ ^5F_5$—7^0_4
689. 456	20	145041. 9	$a\ ^5F_5$—6^0_4
689. 542	50	145023. 8	$a\ ^5F_5$—$5^0_{5,4}$
691. 575	10	144597. 5	
692. 626	5	144378. 1	$a\ ^5F_5$—4^0_4
692. 830	20	144335. 6	$a\ ^1D_2$—$w\ ^3P^0_1$
693. 426	2	144211. 5	$a\ ^1D_2$—$v\ ^3F^0_2$
694. 961	10	143893. 0	
695. 319	15	143818. 9	
695. 907	50	143697. 4	$a\ ^1D_2$—$w\ ^3P^0_2$
696. 937	2	143484. 6	
697. 054	2	143460. 9	
700. 043	20	142848. 4	$a\ ^5F_4$—$5^0_{5,4}$
700. 122	15	142832. 5	
704. 335	5	141977. 9	$a\ ^3F_4$—$w\ ^3F^0_4$
704. 626	50	141919. 2	$a\ ^3P_1$—$w\ ^3P^0_0$
704. 850	3	141874. 2	$a\ ^3F_4$—$w\ ^3G^0_5$
705. 490	200	141745. 5	Pd IV?
707. 797	150	141283. 4	$a\ ^3F_4$—$v\ ^3D^0_3$
708. 125	15	141218. 0	$a\ ^5F_3$—6^0_4

TABLE 1. *List of lines of* Pd III—Continued

Wavelength λ (Vac)	Intensity	Wave number	Identification
708. 731	10	141097. 2	$a\ ^3P_1—w\ ^3P^\circ_1$
709. 885	100	140867. 8	$a\ ^3P_1—w\ ^3P^\circ_1$
711. 954	100	140458. 5	$a\ ^3P_1—w\ ^3P^\circ_2$
712. 730	10	140305. 6	$a\ ^5F_5—1^\circ_4$
712. 958	50	140260. 9	
713. 928	15	140072. 1	$a\ ^5F_4—2^\circ_{3,4}$
714. 625	30	139933. 5	$a\ ^3P_2—w\ ^3P^\circ_1$
715. 041	1	139852. 1	
715. 237	1	139813. 1	
715. 997	0	139665. 3	
716. 121	0	139641. 2	
717. 904	100	139294. 3	$a\ ^3P_2—w\ ^3P^\circ_2$
718. 124	10	139251. 7	
719. 474	100	138990. 4	$a\ ^3F_5—v\ ^3D^\circ_3$
720. 213	5	138847. 8	
720. 964	10	138703. 2	$a\ ^5F_3—3^\circ_2$
720. 997	20	138696. 8	
721. 568	3	138587. 0	
722. 447	15	138419. 2	$a\ ^5F_3—2^\circ_{3,4}$
723. 935	50	138132. 4	$a\ ^5F_4—1^\circ_4$ and $a\ ^1G_4—v\ ^3F^\circ_3$
724. 348	15	138053. 8	$a\ ^3F_3—v\ ^3D^\circ_3$
725. 646	15	137808. 2	
725. 732	10	137791. 9	$a\ ^3F_3—x\ ^1G^\circ_4$
725. 934	1	137753. 5	
726. 766	5	137595. 8	$a\ ^5F_2—3^\circ_2$
727. 100	50	137532. 6	$a\ ^3F_2—v\ ^3D^\circ_2$
727. 720	200	137415. 4	$a\ ^3F_2—v\ ^3D^\circ_1$
728. 149	20	137334. 5	$a\ ^3F_3—x\ ^1D^\circ_2$
728. 616	3	137246. 5	$a\ ^3F_3—w\ ^3F^\circ_3$
730. 371	5	136916. 7	$a\ ^5F_1—3^\circ_2$
730. 733	3	136848. 9	$a\ ^3F_4—y\ ^1H^\circ_5$
731. 830	5	136643. 8	
732. 073	3	136598. 3	$a\ ^3F_2—v\ ^3D^\circ_3$
732. 704	3	136480. 8	$a\ ^5F_3—1^\circ_4$
734. 961	15	136061. 6	
736. 260	30	135821. 6	$a\ ^3F_3—w\ ^3G^\circ_4$
736. 452	10	135786. 2	$a\ ^3F_2—w\ ^3F^\circ_3$
736. 696	10	135741. 2	
737. 359	5	135619. 1	
737. 822	3	135534. 0	
738. 793	150	135355. 9	$a\ ^3F_4—y\ ^1F^\circ_3$
743. 776	15	134449. 0	
747. 693	20	133744. 7	
747. 779	50	133729. 3	$a\ ^3F_2—w\ ^3G^\circ_3$
748. 577	10	133586. 8	
753. 002	3	132801. 7	$a\ ^3F_2—x\ ^3P^\circ_1$
754. 862	15	132474. 5	$a\ ^3F_2—w\ ^3F^\circ_2$
755. 300	2	132397. 7	$a\ ^5P_3—7^\circ_4$
755. 426	3	132375. 6	
755. 859	15	132299. 8	$a\ ^3F_4—y\ ^3H^\circ_5$
756. 137	50	132251. 1	$a\ ^5P_3—6^\circ_4$
756. 853	100	132126. 0	$a\ ^3F_3—y\ ^1F^\circ_3$
757. 412	100	132028. 5	$a\ ^3P_2—x\ ^1F^\circ_3$
757. 631	5	131990. 3	$a\ ^3F_3—x\ ^3P^\circ_2$ and $a\ ^1D_2—v\ ^3D^\circ_2$
758. 308	50	131872. 6	$a\ ^1D_2—v\ ^3D^\circ_1$
758. 839	10	131780. 2	
759. 629	2	131643. 2	
759. 945	5	131588. 5	$a\ ^5P_3—4^\circ_4$
763. 058	500	131051. 6	$a\ ^1D_2—v\ ^3D^\circ_3$
764. 192	3	130857. 2	

TABLE 1. *List of lines of* Pd III—Continued

Wavelength λ (Vac)	Intensity	Wave number	Identification
764.447	5	130813.5	
766.102	5?	130530.9	$a\ ^3F_2—x\ ^3P_2$
766.424	500	130476.0	$a\ ^3F_4—x\ ^3F_4^\circ$
767.265	50	130333.0	$a\ ^1D_2—x\ ^1D_2^\circ$
767.773	2	130246.8	$a\ ^1D_2—w\ ^3F_3^\circ$
767.930	3	130220.2	$a\ ^3F_3—y\ ^3H_4^\circ$
768.762	5	130079.3	
770.873	10	129723.0	$a\ ^3F_3—y\ ^1D_2^\circ$
771.105	10	129684.0	$a\ ^3F_4—y\ ^3G_3^\circ$
771.497	10	129618.1	
772.110	200	129515.2	$a\ ^3F_3—z\ ^1D_2^\circ$
774.416	3	129129.5	
776.315	100	128813.6	$a\ ^3F_3—x\ ^3F_3^\circ$
776.507	200	128781.8	$a\ ^1G_4—x\ ^1F_3^\circ$
776.681	150	128753.0	$a\ ^3P_1—v\ ^3D_2^\circ$
778.783	50	128405.5	$a\ ^3P_0—v\ ^3D_1^\circ$
779.483	15	128290.2	$a\ ^3P_1—3_2^\circ$?
779.636	50	128265.0	$a\ ^3F_2—y\ ^1D_2^\circ$
780.115	100	128186.2	$a\ ^1D_2—w\ ^3G_3^\circ$
781.019	2000	128037.8	$a\ ^3F_4—w\ ^3D_3^\circ$
783.344	100	127657.8	$a\ ^3F_4—x\ ^3D_3^\circ$
783.783	150	127586.7	$a\ ^3P_2—v\ ^3D_2^\circ$
784.361	20	127492.3	$a\ ^3F_2—y\ ^3S_1^\circ$
784.985	200	127391.0	$a\ ^3F_3—x\ ^3F_3^\circ$
785.184	20	127358.7	$a\ ^3F_2—x\ ^3F_3^\circ$
785.883	150	127245.4	$a\ ^3F_3—x\ ^3F_4^\circ$
786.244	3	127187.0	$a\ ^3F_4—z\ ^1H_5^\circ$
786.828	50	127092.6	$a\ ^3P_1—x\ ^1D_2^\circ$
787.314	200	127014.1	$a\ ^3F_4—x\ ^3G_3^\circ$
787.837	100	126929.8	$a\ ^1D_2—w\ ^3F_2^\circ$
787.950	200	126911.6	$a\ ^3F_4—x\ ^3G_4^\circ$
789.356	15	126685.5	
789.583	200	126649.1	$a\ ^3P_2—v\ ^3D_3^\circ$
790.192	150	126551.5	$a\ ^1D_2—y\ ^1P_1^\circ$
790.800	10	126454.2	$a\ ^3F_3—y\ ^3G_3^\circ$
794.078	500	125932.2	$a\ ^3F_2—x\ ^3F_2^\circ$
795.585	50	125693.7	$a\ ^3F_4—z\ ^1F_3^\circ$
796.384	150	125567.6	$a\ ^3F_3—x\ ^3D_2^\circ$
797.517	500	125389.2	$a\ ^3F_4—x\ ^3G_5$
799.013	200	125154.4	$a\ ^3F_2—x\ ^3D_1^\circ$
799.202	200	125124.8	$a\ ^1D_2—y\ ^1F_3^\circ$
800.025	500	124996.1	$a\ ^3F_2—y\ ^3G_3^\circ$
800.103	500	124983.9	$a\ ^3F_3—w\ ^3D_2^\circ$
801.223	50	124809.2	$a\ ^3F_3—w\ ^3D_3^\circ$
801.570	200*d*	124755.2	$a\ ^3F_4—y\ ^3G_3^\circ$ and $a\ ^3F_3—y\ ^3G_4^\circ$
802.286	150	124643.8	$a\ ^3F_4—y\ ^3D_3^\circ$
803.665	500	124429.9	$a\ ^3F_4—z\ ^1G_4^\circ$ and $a\ ^3F_3—x\ ^3D_3^\circ$
804.688	30	124271.8	$a\ ^3P_1—x\ ^3P_0^\circ$
804.900	5	124239.0	$a\ ^3F_4—y\ ^3F_3^\circ$
805.725	40	124111.8	$a\ ^3F_2—x\ ^3D_2^\circ$
806.317	50	124020.7	$a\ ^3P_1—x\ ^3P_1^\circ$
807.672	50	123812.6	$a\ ^3F_2—w\ ^3D_1^\circ$
807.827	150	123788.9	$a\ ^3F_3—x\ ^3G_3^\circ$ and $a\ ^3P_0—x\ ^3P_1^\circ$
808.497	30	123686.3	$a\ ^3F_3—x\ ^3G_4^\circ$
809.536	100	123527.5	$a\ ^3F_2—w\ ^3D_2^\circ$
809.695	150	123503.3	$a\ ^3F_4—y\ ^5D_3^\circ$
810.336	75	123405.6	$a\ ^1G_4—v\ ^3D_3^\circ$
810.928	10	123315.5	$a\ ^3P_1—y\ ^1P_1^\circ$
812.086	50	123139.7	$a\ ^1G_4—x\ ^1G_4^\circ$
812.443	30	123085.6	$a\ ^3P_0—y\ ^1P_1^\circ$

TABLE 1. *List of lines of* Pd III—Continued

Wavelength λ (Vac)	Intensity	Wave number	Identification
813. 192	100	122972. 2	$a\ ^3F_2$—$x\ ^3D_3^0$
813. 989	150*d*	122851. 8	$a\ ^3F_3$—$y\ ^3P_2^0$ and $a\ ^3P_2$—$x\ ^3P_1^0$?
814. 524	100	122771. 1	$a\ ^3F_4$—$z\ ^3H_4^0$
815. 053	200	122691. 4	$a\ ^3F_2$—$y\ ^3F_3^0$
816. 221	200	122515. 8	$a\ ^1D_2$—$z\ ^1D_2^0$
816. 400	15	122489. 0	$a\ ^1D_2$—$z\ ^1P_1^0$
816. 563	200	122464. 5	$a\ ^3F_3$—$z\ ^1F_3^0$
818. 679	200	122148. 0	$a\ ^3P_2$—$y\ ^1P_1^0$
820. 012	100	121949. 4	$a\ ^1D_2$—$y\ ^3S_1^0$
820. 342	75	121900. 4	$a\ ^3F_4$—$y\ ^5D_4^0$
820. 917	20	121815. 0	$a\ ^1D_2$—$x\ ^3F_3^0$
821. 162	5	121778. 7	
821. 353	50	121750. 3	$a\ ^3P_1$—$x\ ^3P_2^0$
823. 643	300	121411. 8	$a\ ^3F_3$—$y\ ^3D_3^0$?
825. 076	150	121200. 9	$a\ ^3F_3$—$z\ ^1G_4^0$
825. 345	500	121161. 5	$a\ ^3F_4$—$y\ ^3F_4^0$
826. 411	400	121005. 2	$a\ ^3F_3$—$y\ ^3F_3^0$ and $a\ ^3F_2$—$z\ ^1F_3^0$
828. 359	30	120720. 6	$a\ ^3P_2$—$y\ ^1F_3^0$
828. 595	15	120686. 2	$a\ ^3F_4$—$z\ ^3H_5^0$
829. 316	300	120581. 3	$a\ ^3P_2$—$x\ ^3P_2^0$?
830. 639	30	120389. 2	$a\ ^1D_2$—$x\ ^3F_2^0$
831. 334	15	120288. 6	$a\ ^3F_2$—$y\ ^3D_1^0$
833. 627	15	119957. 7	$a\ ^3F_2$—$y\ ^3D_2^0$
834. 978	50	119763. 6	$a\ ^3F_3$—$y\ ^3D_2^0$
836. 041	30	119611. 3	$a\ ^1D_2$—$x\ ^3D_1^0$
836. 476	100	119549. 2	$a\ ^3F_2$—$y\ ^3F_3^0$
836. 948	100	119481. 7	$a\ ^3P_1$—$y\ ^1D_2^0$
837. 146	200	119453. 5	$a\ ^1D_2$—$y\ ^3G_3^0$
838. 414	30	119272. 8	$a\ ^3P_1$—$z\ ^1D_2^0$
839. 693	20	119091. 1	$a\ ^3F_2$—$z\ ^3S_1^0$
840. 214	100	119017. 3	$a\ ^3P_0$—$z\ ^1P_1^0$
840. 579	500	118965. 6	$a\ ^1G_4$—$y\ ^1H_5^0$
842. 376	50?	118711. 8	$a\ ^3P_1$—$y\ ^3S_1^0$
842. 675	2	118669. 7	$a\ ^3F_3$—$y\ ^5D_4^0$
843. 392	5	118568. 8	$a\ ^1D_2$—$x\ ^3D_2^0$
845. 268	50	118305. 7	$a\ ^3F_2$—$y\ ^5D_3^0$
845. 525	100	118269. 7	$a\ ^1D_2$—$w\ ^3D_1^0$
846. 687	30	118107. 4	$a\ ^3P_2$—$z\ ^1D_2^0$
847. 342	100	118016. 1	$a\ ^3P_1$—$z\ ^1S_0^0$
847. 582	30	117982. 7	$a\ ^1D_2$—$w\ ^3D_2^0$
847. 943	50	117932. 4	$a\ ^3F_3$—$y\ ^3F_4^0$
848. 868	100	117803. 9	
850. 733	20	117545. 7	$a\ ^3P_2$—$y\ ^3S_1^0$
851. 240	200	117475. 7	$a\ ^1G_4$—$y\ ^1F_3^0$
851. 589	100	117427. 5	$a\ ^1D_2$—$x\ ^3D_3^0$
851. 717	300	117409. 9	$a\ ^3P_2$—$x\ ^3F_3^0$
853. 610	50	117149. 5	$a\ ^1D_2$—$y\ ^3F_2^0$
854. 354	100	117047. 5	$a\ ^3F_2$—$y\ ^5D_1^0$
854. 766	30	116991. 0	$a\ ^3F_3$—$z\ ^5P_3^0$
855. 294	150	116918. 8	$a\ ^1D_2$—$y\ ^3P_1^0$
856. 071	50	116812. 7	$a\ ^3F_3$—$z\ ^5P_2^0$
856. 249	10	116788. 5	$a\ ^1D_2$—$x\ ^3G_3^0$
856. 470	500	116758. 3	$a\ ^1G_4$—$y\ ^1G_4^0$
858. 238	100	116517. 7	$a\ ^3F_4$—$z\ ^3G_3^0$
859. 309	10	116372. 5	$a\ ^3P_1$—$x\ ^3D_1^0$
862. 165	2	115987. 1	$a\ ^3P_2$—$x\ ^3F_2^0$
863. 200	200	115848. 0	$a\ ^1D_2$—$y\ ^3P_2^0$
864. 044	500	115734. 8	$a\ ^3F_4$—$z\ ^3D_3^0$
865. 285	200	115568. 8	$a\ ^1G_4$—$y\ ^3H_4^0$
866. 075	150	115463. 4	$a\ ^1D_2$—$z\ ^1F_3^0$

TABLE 1. *List of lines of* Pd III—Continued

Wavelength λ (Vac)	Intensity	Wave number	Identification
866.896	20	115354.0	$a\ ^3F_2 - z\ ^5P_2^\circ$
867.087	100	115328.6	$a\ ^3P_1 - x\ ^3D_2^\circ$
867.699	100	115247.3	$a\ ^1D_2 - z\ ^3P_1^\circ$
867.992	75	115208.4	$a\ ^3P_2 - x\ ^3D_1^\circ$
869.203	2	115047.9	$a\ ^3P_2 - y\ ^3G_3^\circ$
869.330	10	115031.1	$a\ ^3P_1 - w\ ^3D_1^\circ$
870.437	150	114884.8	$a\ ^3F_4 - z\ ^3G_4^\circ$
871.061	100	114802.5	$a\ ^3P_0 - w\ ^3D_1^\circ$
871.491	75	114745.8	$a\ ^1D_2 - y\ ^3D_1^\circ$ and $a\ ^3P_1 - w\ ^3D_2^\circ$
873.057	200	114540.0	$a\ ^5F_2 - z\ ^5P_1^\circ$
873.977	200	114419.4	$a\ ^1G_4 - y\ ^3H_5^\circ$
875.587	15	114209.0	$a\ ^1D_2 - y\ ^3D_2^\circ$
875.931	100	114164.2	$a\ ^3P_2 - x\ ^3D_3^\circ$ and $a\ ^1G_4 - x\ ^3F_2^\circ$
877.897	10	113910.9	$a\ ^3P_1 - y\ ^3F_2^\circ$
878.732	400	113800.3	$a\ ^3F_4 - z\ ^3F_3^\circ$
880.590	500	113560.2	$a\ ^3F_3 - z\ ^3D_2^\circ$
881.442	30	113450.4	$a\ ^3P_0 - y\ ^3P_1^\circ$
882.690	50	113290.0	$a\ ^3F_3 - z\ ^3G_3^\circ$
882.814	20	113274.1	$a\ ^1D_2 - y\ ^5D_3^\circ$
884.304	50	113083.2	$a\ ^1D_2 - z\ ^3P_2^\circ$
884.766	5	113024.2	$a\ ^3P_2 - x\ ^3D_3^\circ$
885.913	300	112877.9	$a\ ^3F_2 - z\ ^3D_1^\circ$
886.820	100	112762.4	$a\ ^1D_2 - y\ ^5D_2^\circ$
888.842	500	112505.9	$a\ ^3F_4 - z\ ^3G_5^\circ$ and $a\ ^3F_3 - z\ ^3D_3^\circ$ and $a\ ^3F_4 - z\ ^3F_2^\circ$
889.294	1000	112448.7	$a\ ^3F_4 - z\ ^3F_4^\circ$
889.476	10	112425.7	$a\ ^3P_1 - y\ ^3P_0^\circ$
889.801	5	112384.6	$a\ ^3P_2 - x\ ^3G_3^\circ$
892.029	100	112103.9	$a\ ^3F_2 - z\ ^3D_2^\circ$
892.793	150	112008.0	$a\ ^3P_1 - z\ ^3P_1^\circ$
894.197	30	111832.1	$a\ ^3F_2 - z\ ^3G_3^\circ$
894.428	1	111803.2	$a\ ^1G_4 - y\ ^3G_3^\circ$
894.614	50	111780.0	$a\ ^3P_0 - z\ ^3P_1^\circ$
895.599	100	111657.1	$a\ ^3F_3 - z\ ^3G_4^\circ$
895.804	30	111631.5	$a\ ^3F_4 - z\ ^5G_3^\circ$
896.813	200	111505.9	$a\ ^1D_2 - y\ ^5D_1^\circ$ and $a\ ^3P_1 - y\ ^3D_1^\circ$
897.300	3	111445.4	$a\ ^3P_2 - y\ ^3P_2^\circ$
900.423	150	111058.9	$a\ ^3P_2 - z\ ^1F_3^\circ$
900.490	300	111050.6	$a\ ^3F_2 - z\ ^3F_3^\circ$ and $a\ ^3F_2 - z\ ^3D_3^\circ$
901.130	50	110970.9	$a\ ^3P_1 - y\ ^3D_2^\circ$
902.178	20	110842.8	$a\ ^3P_2 - z\ ^3P_1^\circ$
902.904	400	110749.3	$a\ ^3F_4 - z\ ^5G_4^\circ$
904.390	400	110571.8	$a\ ^3F_3 - z\ ^3F_3^\circ$
906.531	30	110310.6	$a\ ^3P_1 - z\ ^3S_1^\circ$
908.876	100	110026.0	$a\ ^1G_4 - z\ ^3I_5^\circ$
909.003	50	110010.6	$a\ ^3P_2 - y\ ^3D_3^\circ$
909.152	30	109992.6	$a\ ^1D_2 - z\ ^5P_3^\circ$
910.373	50	109845.0	$a\ ^3P_1 - z\ ^3P_2^\circ$
910.921	10	109779.0	$a\ ^1G_4 - x\ ^3D_3^\circ$
911.367	15	109725.3	$a\ ^3F_4 - z\ ^5D_3^\circ$
912.376	10	109603.9	$a\ ^3P_2 - y\ ^3F_3^\circ$
914.858	100	109306.5	$a\ ^1G_4 - z\ ^1H_5^\circ$
915.134	20	109273.6	$a\ ^3P_1 - z\ ^3P_0^\circ$
915.582	200	109220.1	$a\ ^3F_3 - z\ ^3F_4^\circ$
916.467	100	109114.6	$a\ ^3F_2 - z\ ^3F_3^\circ$
916.783	200	109077.1	$a\ ^3F_4 - z\ ^5G_5^\circ$
917.136	10	109035.0	$a\ ^1G_3 - x\ ^3G_4^\circ$
917.450	100	108997.8	$a\ ^1D_2 - z\ ^5P_1^\circ$
918.524	5	108870.3	$a\ ^3P_2 - y\ ^5D_3^\circ$
920.136	3	108679.5	$a\ ^3P_2 - z\ ^3P_2^\circ$
921.026	30	108574.5	$a\ ^3F_3 - z\ ^5G_2^\circ$

TABLE 1. *List of lines of* Pd III—Continued

Wavelength λ (Vac)	Intensity	Wave number	Identification
922. 498	200	108401. 3	$a\ ^3F_3—z\ ^5G^0_3$
922. 855	5	108359. 4	$a\ ^3P_2—y\ ^5D^0_2$
925. 617	10	108036. 0	$a\ ^3P_0—y\ ^5D^0_1$
927. 526	100	107813. 7	$a\ ^1G_3—z\ ^1F^0_3$
930. 151	100	107509. 4	$a\ ^1G_4—x\ ^3G^0_5$
931. 641	20	107337. 4	$a\ ^1D_2—z\ ^3D^0_1$
933. 573	5	107115. 3	$a\ ^3F_2—z\ ^5G^0_2$
933. 700	10	107100. 8	$a\ ^3P_2—y\ ^5D^0_1$
935. 623	10	106880. 6	$a\ ^1G_4—y\ ^3G^0_5$
938. 311	50	106574. 5	$a\ ^3P_1—z\ ^5P^0_2$
938. 435	50	106560. 4	$a\ ^1D_2—z\ ^3D^0_2$
939. 014	5	106494. 7	$a\ ^3F_3—z\ ^5D^0_3$
940. 825	5	106289. 7	$a\ ^1D_2—z\ ^3G^0_3$
941. 145	1	106253. 6	$a\ ^3F_2—z\ ^5D^0_2$
947. 606	30	105529. 0	$a\ ^3P_0—z\ ^5P^0_1$
947. 780	300	105507. 0	$a\ ^1D_2—z\ ^3D^0_3$ and $a\ ^1D_2—z\ ^3F^0_2$
948. 652	5	105412. 7	$a\ ^3F_3—z\ ^5F^0_2$
956. 077	50	104594. 0	$a\ ^3P_2—z\ ^5P^0_1$
957. 681	75	104418. 9	$a\ ^3F_4—z\ ^5F^0_4$
960. 643	100	104096. 9	$a\ ^3P_1—z\ ^3D^0_1$
962. 753	100	103868. 8	$a\ ^3P_0—z\ ^3D^0_1$
965. 516	300	103571. 6	$a\ ^1D_2—z\ ^3F^0_3$
967. 865	200	103320. 2	$a\ ^3P_1—z\ ^3D^0_2$
968. 223	3	103281. 9	$a\ ^1G_4—y\ ^3F^0_4$
972. 689	100	102807. 8	$a\ ^1G_4—z\ ^3H^0_5$
977. 805	100	102269. 9	$a\ ^3P_1—z\ ^3F^0_2$
981. 503	10	101884. 6	$a\ ^3P_2—z\ ^3G^0_3$
989. 103	20	101101. 7	$a\ ^3P_2—z\ ^3F^0_2$ and $a\ ^3P_2—z\ ^3D^0_3$
996. 768	10	100324. 2	
1005. 080	5	99494. 6	$a\ ^1D_2—z\ ^3D^0_2$
1008. 385	30	99168. 5	$a\ ^3P_2—z\ ^3F_3$
1016. 947	3	98333. 5	$a\ ^3P_1—z\ ^3G^0_2$
1057. 415	5	94570. 2	$a\ ^1G_4—z\ ^3F^0_4$
1078. 978	5	92680. 3	
1088. 450	0	91873. 8	
1094. 603	2	91357. 3	
1096. 531	3	91196. 7	$a\ ^1G_4—z\ ^3G^0_3$
1097. 779	3	91093. 0	
1144. 970	5	87338. 5?	
1145. 316	10	87312. 1?	
1206. 840	15	82861. 0?	
1207. 729	5	82800. 0?	
1400. 767	3	71389. 5	
1406. 351	2	71106. 0	
1407. 798	1	71033. 1	$a\ ^3G_5—x\ ^1G^0_4$
1424. 896	3	70180. 6	$c\ ^3F_3—v\ ^3F^0_3$
1433. 903	15	69739. 8	$b\ ^3F_4—y\ ^3H^0_5$
1437. 464	20	69567. 0	$a\ ^5P_2—y\ ^1F^0_3$
1440. 393	2	69425. 5	$a\ ^3G_4—w\ ^3F^0_3$
1443. 488	2	69276. 6	$b\ ^3F_3—y\ ^1F^0_3$
1447. 175	2	69100. 1	$b\ ^3P_1—v\ ^3D^0_1$
1448. 898	3	69018. 0	$c\ ^3F_2—v\ ^3F^0_2$
1449. 615	50	68983. 8	$a\ ^5F_5—y\ ^5D^0_4$
1461. 673	5	68414. 8	$a\ ^5F_4—y\ ^5D^0_3$
1465. 296	10	68245. 6	$a\ ^5F_5—y\ ^3F^0_4$
1468. 830	0	68081. 4	$a\ ^3H_4—x\ ^1F^0_3$
1477. 144	10*h*	67698. 2	$a\ ^5F_3—y\ ^3D^0_2$
1481. 768	2	67486. 9	$b\ ^3F_3—z\ ^1D^0_2$
1483. 042	2*h*	67429. 0	
1484. 379	15	67368. 2	$a\ ^3G_4—w\ ^3G^0_3$ and $z\ ^5F^0_5—9_5$

TABLE 1. *List of lines of* Pd III—Continued

Wavelength λ (Vac)	Intensity	Wave number	Identification
1488.092	50	67200.1	$a\ ^3H_6 - w\ ^3G^0_5$
1488.662	1	67174.4	
1494.462	10	66913.7	$z\ ^5F^0_4 - 5_{5,4}$
1496.704	10	66813.5	
1496.764	30	66810.8	$a\ ^5F_4 - y\ ^5D^0_4$
1497.868	10	66761.6	$a\ ^5F_3 - y\ ^5D^0_3$
1499.314	20	66697.2	
1501.606	1	66595.4	$a\ ^5F_2 - y\ ^3D^0_2$
1502.036	3	66576.3	$b\ ^1G_4 - w\ ^3F^0_4$
1502.154	10	66571.1	$a\ ^5F_3 - z\ ^3P^0_2$
1502.378	2	66561.1	
1502.577	10	66552.3	
1502.842	10	66540.6	
1504.402	1	66471.6	$b\ ^1G_4 - w\ ^3G^0_5$
1505.400	100	66427.5	
1505.658	3	66416.1	
1505.854	5	66407.5	$z\ ^5F^0_5 - 6_4$
1505.987	3	66401.6	
1509.399	3	66251.5	$a\ ^5F_3 - y\ ^5D^0_2$
1510.323	10	66211.0	
1510.872	5	66186.9	$z\ ^5F^0_5 - 5_{5,4}$
1512.401	15	66120.0	
1513.475	5	66073.1	$a\ ^5F_4 - y\ ^3F^0_4$
1514.137	15*h*	66044.2	
1515.934	40	65965.9	$z\ ^5F^0_4 - 3_5$
1517.183	200	65911.6	$z\ ^5F^0_4 - 2_4$
1517.614	15	65892.9	
1518.097	1	65871.9	$b\ ^3F_2 - y\ ^1D^0_2$
1518.732	20	65844.4	
1518.924	20	65836.1	
1519.104	10	65828.3	$c\ ^3P_2 - v\ ^3D^0_3$
1519.320	5	65818.9	
1519.635	3	65805.3	
1520.946	5	65748.6	$a\ ^3D_3 - w\ ^3F^0_4$
1522.134	10	65697.2	
1522.641	5	65675.4	
1522.841	50*h*	65666.7	
1523.558	2	65635.8	$b\ ^3F_2 - z\ ^1P^0_1$?
1523.688	3	65630.2	$a\ ^3G_3 - w\ ^3G^0_3$
1524.038	10	65615.2	$b\ ^1G_4 - x\ ^1G^0_4$
1524.634	30	65589.5	
1524.842	10	65580.6	
1525.183	5	65565.9	$a\ ^5P_1 - z\ ^1P^0_1$
1526.249	50*h*	65520.1	$z\ ^5D^0_4 - 11_4$
1526.397	5	65513.8	
1526.515	10	65508.7	
1526.876	200*h*	65493.2	$z\ ^5F^0_5 - 4_6$
1527.247	20	65477.3	$b\ ^3F_4 - w\ ^3D^0_3$
1527.462	5	65468.1	$a\ ^5F_2 - z\ ^3P^0_2$
1528.756	20*h*	65412.7	$z\ ^5F^0_4 - 1_5$
1529.862	30	65365.4	$b\ ^3F_3 - x\ ^3F^0_2$
1530.960	10	65318.5	
1531.757	5	65284.5	
1532.516	0	65252.2	$a\ ^5F_1 - z\ ^3S^0_1$
1532.813	20*h*	65239.5	$z\ ^5F^0_5 - 3_5$
1534.092	40*h*	65185.1	$z\ ^5F^0_5 - 2_4$
1534.718	2	65158.6	$a\ ^5F_3 - y\ ^5D^0_4$
1534.941	2	65149.1	$a\ ^5F_2 - y\ ^5D^0_2$
1535.304	50	65133.7	$a\ ^5F_4 - z\ ^5P^0_3$
1536.172	5H?	65096.9	$b\ ^3F_4 - x\ ^3D^0_3$

TABLE 1. *List of lines of* Pd III—Continued

Wavelength λ (Vac)	Intensity	Wave number	Identification
1537. 234	15	65051. 9	$a\ ^3D_3 - v\ ^3D_3^\circ$
1538. 140	10*h*	65013. 6	
1538. 319	3	65006. 0	
1538. 538	50*h*	64996. 8	
1539. 371	15*h*	64916. 6	
1540. 072	50	64932. 0	
1540. 496	5*h*	64914. 2	
1541. 031	15*h*	64891. 6	$z\ ^5F_3^\circ - 8_3$
1542. 630	100	64824. 4	
1542. 859	20*h*	64814. 7	
1543. 034	15	64807. 4	
1543. 609	20*h*	64783. 2	$z\ ^5F_3^\circ - 7_{4,3}$
1543. 955	2	64768. 7	$a\ ^3P_2 - x\ ^3F_3^\circ$
1544. 121	2	64761. 8	
1545. 127	30*h*	64719. 6	
1545. 605	3*h*	64699. 6	
1545. 953	200*h*	64685. 0	$z\ ^5F_5^\circ - 1_5$
1546. 601	3*h*	64657. 9	$z\ ^5F_3^\circ - 6_4$
1547. 656	20	64613. 8	
1547. 896	15*h*	64603. 8	
1549. 864	5	64521. 8	
1550. 048	5	64514. 1	
1550. 284	1	64504. 3	
1550. 743	5	64485. 2	$b\ ^3P_1 - x\ ^3P_1^\circ$?
1550. 860	5	64480. 4	
1551. 221	5*h*	64465. 3	$a\ ^5F_1 - y\ ^5D_2^\circ$
1552. 832	10*h*	64398. 5	$z\ ^5D_4^\circ - 9_5$
1553. 917	15	64353. 5	$b\ ^3F_4 - x\ ^3G_4^\circ$
1554. 058	15	64347. 7	
1555. 002	15*h*	64308. 6	$a\ ^3G_4 - y\ ^1F_3^\circ$
1557. 013	10*h*	64225. 5	
1557. 570	2	64202. 6	
1557. 935	10	64187. 5	
1559. 067	10*h*	64140. 9	
1560. 091	10	64098. 8	$a\ ^3D_1 - v\ ^3D_2^\circ$
1561. 669	50*h*	64034. 1	
1563. 131	1	63974. 2	$a\ ^5P_3 - y\ ^3G_3^\circ$
1564. 622	20	63913. 2	
1564. 782	20	63906. 7	
1565. 210	20	63889. 2	$a\ ^5F_2 - y\ ^5D_1^\circ$
1567. 835	3	63782. 2	
1571. 016	5	63653. 1	
1571. 197	3*h*	63645. 7	$b\ ^1G_4 - w\ ^3G_4^\circ$
1572. 101	5	63609. 1	
1573. 295	20*h*	63560. 9	$z\ ^5D_4^\circ - 7_{4,3}$
1573. 744	3	63542. 7	$b\ ^3F_2 - x\ ^3D_2^\circ$
1574. 844	5	63498. 4	$z\ ^5G_6^\circ - 9_5$
1575. 128	50	63486. 9	
1575. 279	15	63480. 8	$a\ ^5F_3 - z\ ^5P_3^\circ$
1575. 492	1*h*	63472. 2	
1575. 806	5*h*	63459. 6	$z\ ^5G_4^\circ - 10_4$
1576. 371	0	63436. 8	$z\ ^5F_3^\circ - 2_4$
1579. 746	50	63301. 3	$a\ ^5F_3 - z\ ^5P_2^\circ$
1580. 275	5	63280. 1	
1581. 212	1*h*	63242. 6	$a\ ^1F_3 - w\ ^3P_2^\circ$
1581. 855	10	63216. 9	$z\ ^5D_4^\circ - 5_{5,4}$
1582. 055	50	63208. 9	$b\ ^3P_0 - x\ ^3P_1^\circ$
1582. 110	50	63206. 7	$a\ ^5F_1 - y\ ^5D_1^\circ$
1582. 861	15	63176. 7	
1583. 047	10	63169. 3	

TABLE 1. *List of lines of* Pd III—Continued

Wavelength λ (Vac)	Intensity	Wave number	Identification
1584. 167	10	63124. 7	$a\ ^5F_1 - y\ ^5D^o_0$
1584. 445	1	63113. 6	$a\ ^3D_2 - v\ ^3D^o_1$
1584. 637	3	63105. 9	
1585. 046	15*h*	63089. 7	$a\ ^5P_3 - x\ ^3D^o_2$
1585. 258	15	63081. 2	$a\ ^3H_5 - w\ ^3G^o_4$
1586. 982	3	63012. 7	$b\ ^1G_4 - w\ ^3G^o_3$
1591. 033	3	62852. 2	
1591. 603	3	62829. 7	$b\ ^3F_4 - x\ ^3G^o_5$
1591. 924	3	62817. 1	$a\ ^3D_3 - w\ ^3G^o_4$
1594. 158	2	62729. 0	$b\ ^3F_3 - y\ ^3G^o_4$
1594. 836	3*h*	62702. 4	$a\ ^3H_4 - v\ ^3D^o_3$
1596. 892	300	62621. 6	
1598. 242	2	62568. 7	
1600. 637	1*h*	62475. 1	$z\ ^3G^o_5 - 6_4$
1601. 901	30	62425. 8	$a\ ^5P_2 - w\ ^3D^o_2$
1602. 314	20	62409. 7	
1602. 489	20	62402. 9	$b\ ^3F_3 - x\ ^3D^o_3$ and $a\ ^3G_4 - y\ ^3H^o_4$
1604. 755	3	62314. 8	$a\ ^3G_5 - y\ ^3H^o_5$
1605. 053	5	62303. 2	$a\ ^3D_2 - w\ ^3F^o_3$
1605. 710	2*h*	62277. 7	
1606. 096	200*h*	62262. 8	
1606. 269	15	62256. 1	$z\ ^5G^o_5 - 5_{5,4}$
1606. 417	5	62250. 3	$a\ ^5P_2 - w\ ^3D^o_3$
1607. 613	2*h*	62204. 0	
1607. 760	20	62198. 3	$a\ ^5F_2 - z\ ^5P^o_2$
1607. 921	10	62192. 1	
1608. 127	0*h*	62184. 2	$a\ ^3D_3 - w\ ^3G^o_3$
1608. 404	3	62173. 4	$a\ ^3H_6 - y\ ^1H^o_5$
1610. 754	10*h*	62082. 7	$b\ ^3F_4 - y\ ^3D^o_3$
1610. 972	1	62074. 3	
1611. 156	3*h*	62067. 2	
1611. 422	3	62057. 0	
1612. 025	3*h*	62033. 8	$c\ ^3P_2 - x\ ^3P^o_1$
1613. 236	2*h*	61987. 2	
1613. 800	5	61965. 5	
1613. 983	5	61958. 5	
1615. 575	3*h*	61897. 5	
1615. 987	5*h*	61881. 7	
1616. 295	100	61869. 9	$a\ ^5P_2 - x\ ^3D^o_3$ and $b\ ^3F_4 - z\ ^1G^o_4$
1616. 746	1	61852. 6	$a\ ^3G_3 - y\ ^1G^o_4$
1616. 941	1	61845. 2	
1617. 700	1*h*	61816. 2	
1618. 472	10*h*	61786. 7	$z\ ^5G^o_4 - 10_4$
1618. 700	2*h*	61778. 0	
1619. 088	20	61763. 2	$b\ ^3F_3 - x\ ^3G^o_3$
1619. 244	100	61757. 2	
1619. 464	5	61748. 8	
1619. 598	5	61743. 7	
1620. 346	5	61715. 2	$z\ ^5D^o_4 - 1_5$
1620. 628	50	61704. 5	
1620. 905	50	61693. 9	
1621. 124	0	61685. 6	$c\ ^3P_1 - x\ ^3P^o_0$
1621. 324	1*h*	61678. 0	
1621. 663	1	61665. 1	
1621. 831	2	61658. 7	$b\ ^3F_3 - x\ ^3G^o_4$
1622. 106	5	61648. 3	
1622. 777	100	61622. 8	$z\ ^5G^o_6 - 4_6$
1623. 623	1	61590. 7	$a\ ^5P_2 - y\ ^3F^o_2$
1623. 836	0	61582. 6	
1624. 295	10	61565. 2	$a\ ^3G_5 - y\ ^3H^o_5$

TABLE 1. *List of lines of* Pd III—Continued

Wavelength λ (Vac)	Intensity	Wave number	Identification
1625.073	2	61535.7	
1626.098	10*h*	61496.9	
1626.609	2*h*	61477.6	
1627.006	3	61462.6	
1628.091	5	61421.6	$b\ ^3F_2 - w\ ^3D_1^\circ$
1629.118	5	61382.9	$a\ ^5F_2 - z\ ^5P_1^\circ$
1629.327	3*h*	61375.0	
1629.484	20*h*	61369.1	$z\ ^5G_6^\circ - 3_5$
1629.681	1	61361.7	$a\ ^5P_2 - y\ ^3P_1^\circ$
1630.246	3	61340.4	
1630.355	20*h*	61336.3	
1630.836	150	61318.2	
1631.091	3*h*	61308.7	$z\ ^5G_5^\circ - 3_5$
1631.836	5*h*	61280.7	$z\ ^3F_4^\circ - 12_4$
1632.389	2	61259.9	
1632.558	3	61253.6	$a\ ^3G_4 - y\ ^3H_5^\circ$
1632.669	5*h*	61249.4	
1633.365	15*h*	61223.3	$z\ ^5G_3^\circ - 12_4$
1634.355	15	61186.2	$z\ ^3F_4^\circ - 11_4$
1634.987	1	61162.6	
1635.518	3	61142.7	
1635.678	10	61136.7	
1635.758	10	61133.7	$b\ ^3F_3 - w\ ^3D_2^\circ$
1635.984	30	61128.7	$z\ ^3G_5^\circ - 11_4$
1636.838	1	61093.4	
1638.343	10	61037.3	$z\ ^5G_4^\circ - 8_3$
1638.716	10	61023.4	
1639.271	1	61002.7	
1639.428	2	60996.9	$a\ ^3G_4 - x\ ^3F_3^\circ$
1639.750	2	60984.9	
1640.049	0	60973.8	$a\ ^3G_5 - z\ ^1I_6^\circ$
1640.928	1	60941.1	
1641.294	1	60927.5	$z\ ^5G_4^\circ - 7_{4,3}$
1641.913	3	60904.6	$z\ ^5G_3^\circ - 10_4$
1643.532	10*h*	60844.6	$z\ ^5D_2^\circ - 8_3$
1643.758	15*h*	60836.2	
1644.092	2	60823.8	$b\ ^3F_3 - y\ ^3P_2^\circ$
1644.311	5*h*	60815.7	$z\ ^5G_6^\circ - 1_5$
1644.679	15*h*	60802.1	$z\ ^5G_4^\circ - 6_4$
1645.689	5*h*	60764.8	
1645.977	5*h*	60754.2	$z\ ^5G_5^\circ - 1_5$
1646.158	1	60747.5	
1647.440	10	60700.2	$a\ ^5F_1 - z\ ^5P_1^\circ$
1648.443	3	60663.3	$a\ ^3G_3 - y\ ^3H_4^\circ$
1648.859	10	60648.0	$a\ ^5F_4 - z\ ^3D_3^\circ$
1649.257	1	60633.4	
1650.608	5	60583.7	$z\ ^5G_4^\circ - 5_{5,4}$
1651.365	1	60556.0	
1651.529	30	60550.0	
1653.774	3	60467.8	$a\ ^3H_4 - w\ ^3G_4^\circ$
1656.423	10	60371.1	$a\ ^5P_3 - y\ ^3P_2^\circ$
1657.185	20	60343.4	
1658.392	10	60299.4	$b\ ^3F_2 - y\ ^3F_2^\circ$
1658.788	2*h*	60285.0	
1658.925	5	60280.0	
1660.297	10	60230.2	
1660.363	10	60227.8	$a\ ^5P_1 - y\ ^3F_2^\circ$
1660.754	2	60213.6	$a\ ^1H_5 - x\ ^1G_4^\circ$
1660.809	2	60211.6	$b\ ^3F_4 - z\ ^3H_4^\circ$
1663.199	1	60125.1	

TABLE 1. *List of lines of* Pd III—Continued

Wavelength λ (Vac)	Intensity	Wave number	Identification
1663.620	3	60109.9	
1666.723	10	59998.0	$a\ ^5P_1-y\ ^3P_1^\circ$ and $b\ ^3P_2-z\ ^1D_2^\circ$
1667.045	10*h*	59986.4	$a\ ^5P_3-z\ ^1F_3^\circ$
1667.639	5	59965.0	
1667.804	5	59959.1	
1667.968	15	59953.2	$b\ ^1G_4-y\ ^1F_3^\circ$
1668.664	5*h*	59928.2	$z\ ^3F_3^\circ-12_4$
1668.873	1	59920.7	$z\ ^5G_3^\circ-6_4$
1669.068	1	59913.7	
1669.284	10*h*	59905.9	$a\ ^5P_2-z\ ^1F_3^\circ$
1670.361	1	59867.3	$c\ ^3F_4-x\ ^1F_3^\circ$
1670.795	0	59851.7	
1670.986	0	59844.9	
1671.090	1	59841.2	
1671.282	20	59834.3	$a\ ^3H_4-w\ ^3G_3^\circ$ and $z\ ^3F_3^\circ-11_4$
1672.313	15III?	59797.4	$a\ ^5F_4-z\ ^3G_4^\circ$
1672.878	5*h*	59777.2	$a\ ^5F_3-z\ ^3G_3^\circ$
1673.246	5	59764.1	$c\ ^3P_2-x\ ^3P_2^\circ$
1673.924	10	59739.9	$b\ ^3P_1-z\ ^1D_2^\circ$
1674.428	5*h*	59721.8	$a\ ^5F_2-z\ ^3D_1^\circ$
1674.669	5	59713.3	$b\ ^3P_1-z\ ^1P_1^\circ$
1675.331	20	59689.7	$a\ ^5P_2-z\ ^3P_1^\circ$
1676.580	3	59645.2	
1677.275	10*h*	59620.5	$a\ ^3D_1-x\ ^3P_0^\circ$
1678.112	30	59590.8	$a\ ^5F_5-z\ ^3G_5^\circ$
1679.731	50	59533.3	$a\ ^5F_5-z\ ^3F_4^\circ$
1681.162	3	59482.7	$a\ ^1P_1-v\ ^3D_1^\circ$
1682.478	5*h*	59436.1	$b\ ^3P_2-y\ ^3S_1^\circ$
1682.676	1	59429.1	$a\ ^3G_4-x\ ^3F_4^\circ$
1683.408	0	59403.3	
1684.379	0	59369.1	$a\ ^3D_1-x\ ^3P_1^\circ$
1685.790	50*h*	59319.4	$a\ ^3D_2-x\ ^3P_1^\circ$
1686.348	2	59299.7	$b\ ^3P_2-x\ ^3F_3^\circ$
1687.530	5	59258.2	$a\ ^3G_3-x\ ^3F_3^\circ$
1688.167	15*h*	59235.8	$b\ ^1G_4-y\ ^1G_4^\circ$
1688.438	5	59226.3	
1689.447	1	59191.0	
1689.547	1	59187.5	$a\ ^5P_2-y\ ^3D_1^\circ$
1689.809	30*h*	59178.3	$b\ ^3P_1-y\ ^3S_1^\circ$
1689.851	10	59176.8	$b\ ^3F_3-z\ ^1G_4^\circ$
1690.223	0	59163.8	$c\ ^3P_1-x\ ^3P_2^\circ$
1690.359	2	59159.0	
1691.343	5	59124.6	$a\ ^3D_3-y\ ^1F_3^\circ$
1693.736	15*h*	59041.1	$a\ ^3D_1-w\ ^3F_2^\circ$
1693.797	10	59039.0	$a\ ^5F_1-z\ ^3D_1^\circ$
1695.053	5	58995.2	$a\ ^5F_3-z\ ^3D_3^\circ$ and $a\ ^5F_3-z\ ^3F_2^\circ$
1695.282	30	58987.2	$a\ ^3D_3-x\ ^3P_2^\circ$
1695.480	5	58980.5	$b\ ^3F_3-y\ ^3F_3^\circ$
1696.487	5	58945.3	$a\ ^5F_2-z\ ^3D_2^\circ$
1696.760	50*h*	58935.9	$a\ ^5P_3-y\ ^3D_3^\circ$
1696.994	50	58927.7	$a\ ^5P_1-y\ ^3P_2^\circ$ and $a\ ^3D_3-w\ ^3G_3^\circ$
1698.283	5	58883.0	
1701.897	10	58758.0	
1702.667	10	58731.4	$a\ ^5P_3-y\ ^3D_2^\circ$
1704.330	100	58674.1	$a\ ^5F_2-z\ ^3G_3^\circ$
1704.436	20	58670.4	$a\ ^3H_4-y\ ^1G_4^\circ$
1704.670	1	58662.4	$a\ ^3D_1-y\ ^1P_1^\circ$
1705.435	3	58636.1	$a\ ^3G_4-y\ ^3G_3^\circ$
1706.061	2	58614.6	$b\ ^3F_2-z\ ^1F_3^\circ$
1706.400	50	58600.8	$b\ ^3F_4-y\ ^3F_4^\circ$

TABLE 1. *List of lines of* Pd III—Continued

Wavelength λ (Vac)	Intensity	Wave number	Identification
1708. 251	5	58539. 4	
1708. 568	100	58528. 5	$a\ ^5P_3-y\ ^3F_3^\circ$
1714. 506	10	58325. 8	$a\ ^5P_1-z\ ^3P_1^\circ$
1715. 140	3	58304. 3	$b\ ^3D_1-u\ ^3D_1^\circ$
1716. 286	2	58265. 3	$a\ ^3H_4-y\ ^1H_5^\circ$
1716. 367	50	58262. 6	$a\ ^5F_1-z\ ^3D_2^\circ$
1716. 804	10	58247. 8	$b\ ^3F_3-y\ ^5D_3^\circ$ and $c\ ^3P_0-y\ ^1P_1^\circ$
1719. 856	200	58144. 4	$a\ ^5F_3-z\ ^5G_4^\circ$
1720. 015	3	58139. 0	
1721. 798	10	58078. 8	$b\ ^1D_2-v\ ^3D_3^\circ$
1722. 735	150	58047. 2	$b\ ^1G_4-y\ ^3H_4^\circ$
1724. 179	1	57998. 6	$a\ ^3G_5-y\ ^3G_4^\circ$
1724. 407	50	57991. 0	$a\ ^5P_2-z\ ^3S_1^\circ$
1727. 124	5	57899. 7	$b\ ^3P_0-y\ ^3S_1^\circ$ and $z\ ^3D_3^\circ-11_4$
1727. 209	2	57896. 9	$b\ ^3F_2-y\ ^3D_1^\circ$
1727. 375	100	57891. 3	$a\ ^5F_2-z\ ^3D_3^\circ$ and $a\ ^5F_2-z\ ^3F_3^\circ$
1727. 875	5	57874. 6	$b\ ^3P_2-x\ ^3F_2^\circ$?
1728. 162	10	57864. 9	$b\ ^3D_2-u\ ^3D_1^\circ$
1729. 125	40	57832. 7	$a\ ^5F_5-z\ ^5G_4^\circ$
1730. 245	40	57795. 3	$a\ ^5P_3-y\ ^5D_3^\circ$
1731. 974	50	57737. 6	$b\ ^3F_3-y\ ^5D_2^\circ$
1732. 634	250	57715. 6	$a\ ^5P_2-y\ ^5D_3^\circ$
1734. 273	3	57661. 0	$b\ ^3F_4-z\ ^5P_3^\circ$
1738. 140	1	57532. 8	
1738. 363	5	57525. 4	$a\ ^5P_2-z\ ^3P_2^\circ$
1739. 657	10	57482. 6	$a\ ^3H_5-y\ ^3H_4^\circ$
1741. 619	500	57417. 8	$a\ ^5F_4-z\ ^3G_5^\circ$
1743. 342	2	57361. 1	$a\ ^5F_4-z\ ^3F_4^\circ$
1745. 562	150	57288. 1	$c\ ^3P_2-z\ ^1D_2^\circ$
1745. 657	5	57285. 0	$a\ ^5P_3-y\ ^5D_2^\circ$
1748. 097	50	57205. 06	$a\ ^5P_2-y\ ^5D_2^\circ$
1748. 204	5	57201. 56	$a\ ^3G_5-z\ ^1H_5^\circ$
1752. 543	10	57059. 94	$a\ ^5F_5-z\ ^3F_5^\circ$
1752. 881	5	57048. 94	$a\ ^3D_3-x\ ^3P_2^\circ$
1754. 668	2	56990. 84	$a\ ^3G_4-w\ ^3D_3^\circ$
1756. 322	40	56937. 17	$a\ ^3G_4-y\ ^3G_4^\circ$
1757. 561	20	56897. 03	$a\ ^3G_3-y\ ^3G_3^\circ$ and $b\ ^1G_4-y\ ^3H_3^\circ$
1758. 187	400	56876. 77	$a\ ^3H_6-y\ ^3H_5^\circ$
1759. 356	3	56838. 98	$b\ ^3P_1-x\ ^3D_1^\circ$
1761. 339	3	56774. 99	$a\ ^3H_4-y\ ^1F_3^\circ$
1762. 852	5	56726. 26	$c\ ^3P_2-y\ ^3S_1^\circ$
1764. 219	50	56682. 31	$c\ ^3F_2-v\ ^3D_1^\circ$
1764. 883	0	56660. 98	$c\ ^3P_1-z\ ^1P_1^\circ$
1765. 403	200	56644. 29	$b\ ^3F_3-y\ ^5D_4^\circ$
1765. 908	2	56628. 09	$a\ ^5P_1-z\ ^3S_1^\circ$
1766. 458	5	56610. 46	$a\ ^3G_4-x\ ^3D_3^\circ$
1766. 652	5	56604. 24	
1768. 588	5	56542. 3	$a\ ^5F_4-z\ ^5G_3^\circ$
1772. 285	0	56424. 33	$b\ ^5F_2-y\ ^5D_3^\circ$
1775. 162	300	56332. 89	$a\ ^3H_5-y\ ^3H_5^\circ$
1778. 256	1	56234. 87	$b\ ^3F_2-z\ ^3P_2^\circ$
1779. 629	300	56191. 49	$a\ ^5P_3-y\ ^5D_4^\circ$
1780. 617	200	56160. 31	$a\ ^5F_5-z\ ^5G_5^\circ$
1780. 952	30	56149. 74	$c\ ^3F_3-w\ ^3F_4^\circ$
1781. 262	150	56139. 97	$a\ ^3G_4-z\ ^1H_5^\circ$
1782. 548	4000	56099. 47	$a\ ^5F_5-z\ ^5G_6^\circ$
1784. 367	300	56042. 28	$a\ ^1H_5-y\ ^1H_5^\circ$
1786. 419	150	55977. 91	$a\ ^1F_3-x\ ^1F_3^\circ$
1786. 666	5	55970. 17	$a\ ^3G_4-x\ ^3G_3^\circ$
1787. 091	10	55956. 86	$a\ ^5F_2-z\ ^3F_3^\circ$

TABLE 1. *List of lines of* Pd III—Continued

Wavelength λ (Vac)	Intensity	Wave number	Identification
1789. 987	200	55866. 33	$a\ ^3G_4 - x\ ^3G_4^\circ$
1790. 106	2	55862. 61	$c\ ^3F_2 - v\ ^3D_3^\circ$
1790. 772	100	55841. 84	$a\ ^5P_1 - y\ ^5D_2^\circ$
1792. 274	5	55795. 04	$b\ ^3P_1 - x\ ^3D_2^\circ$
1793. 533	2?	55755. 87	$b\ ^3P_2 - w\ ^3D_1^\circ$
1795. 083	150	55707. 73	$a\ ^5F_3 - z\ ^3F_4^\circ$
1796. 616	100	55660. 20	$a\ ^5F_4 - z\ ^5G_4^\circ$
1799. 107	100	55583. 13	$a\ ^3H_5 - y\ ^3H_6^\circ$
1801. 877	5	55497. 68	$b\ ^3P_1 - w\ ^3D_1^\circ$
1803. 315	150	55453. 43	$a\ ^5P_3 - y\ ^3F_4^\circ$ and $c\ ^3F_3 - v\ ^3D_3^\circ$
1804. 176	75	55426. 96	$c\ ^3P_1 - z\ ^1S_0^\circ$
1804. 908	400	55404. 48	$a\ ^3G_5 - x\ ^3G_5^\circ$
1808. 544	250	55293. 10	$b\ ^3P_2 - w\ ^3D_3^\circ$
1809. 873	3	55252. 50	$a\ ^3G_3 - w\ ^3D_3^\circ$
1811. 605	150	55199. 67	$a\ ^5F_5 - z\ ^5D_4^\circ$ and $a\ ^3G_3 - y\ ^3G_4^\circ$
1811. 975	200	55188. 40	$c\ ^3F_3 - x\ ^1G_4^\circ$
1812. 094	150	55184. 77	$c\ ^3F_4 - w\ ^3F_4^\circ$
1812. 322	3	55177. 83	$a\ ^3G_5 - z\ ^3I_6^\circ$
1812. 713	3	55165. 93	$c\ ^3P_2 - x\ ^3F_2^\circ$
1813. 523	150	55141. 29	$c\ ^3F_2 - x\ ^1D_2^\circ$
1814. 217	3	55120. 20	$a\ ^1P_1 - x\ ^3P_0^\circ$
1815. 574	250	55079. 00	$c\ ^3F_4 - w\ ^3G_5^\circ$
1816. 147	2	55061. 62	$a\ ^5F_3 - z\ ^5G_2^\circ$
1816. 447	50	55052. 53	$c\ ^3F_2 - w\ ^3F_3^\circ$
1818. 464	200	54991. 46	$a\ ^3H_5 - z\ ^1I_6^\circ$
1819. 274	150	54966. 98	$b\ ^3F_3 - z\ ^5P_3^\circ$
1821. 066	3	54912. 9	$b\ ^3P_2 - x\ ^3D_2^\circ$
1821. 839	50	54889. 59	$a\ ^5F_3 - z\ ^5G_3^\circ$
1822. 409	50	54872. 42	$a\ ^3G_3 - x\ ^3D_3^\circ$
1822. 515	200	54869. 23	$a\ ^3H_4 - y\ ^3H_4^\circ$ and $a\ ^1P_1 - x\ ^3P_1^\circ$
1823. 774	1	53831. 36	$a\ ^3D_1 - y\ ^1D_2^\circ$
1825. 654	50	54774. 89	$a\ ^3G_5 - y\ ^3G_5^\circ$
1829. 670	3*h*	54654. 66	$b\ ^3F_2 - y\ ^5D_1^\circ$
1829. 918	50	54647. 26	$a\ ^3G_4 - z\ ^1F_3^\circ$
1830. 063	150	54642. 93	$c\ ^3F_3 - w\ ^3F_3^\circ$
1830. 311	100	54635. 52	$a\ ^5F_4 - z\ ^5D_3^\circ$
1831. 753	200	54592. 51	$a\ ^3G_3 - y\ ^3F_2^\circ$
1832. 067	150	54583. 16	$a\ ^5P_1 - y\ ^5D_1^\circ$
1832. 404	5	54573. 12	$a\ ^3D_2 - z\ ^1D_2^\circ$
1832. 666	50	54565. 32	$c\ ^3P_1 - x\ ^3F_2^\circ$
1833. 300	100	54546. 45	$a\ ^3D_2 - z\ ^1P_1^\circ$
1834. 386	250	54514. 15	$a\ ^5P_3 - z\ ^5P_3^\circ$
1834. 832	100	54500. 90	$a\ ^5P_1 - y\ ^5D_0^\circ$
1835. 265	150	54488. 04	$c\ ^3F_4 - v\ ^3D_3^\circ$
1836. 672	250	54446. 30	$a\ ^3G_5 - z\ ^1G_4^\circ$
1837. 073	200	54434. 42	$a\ ^5P_2 - z\ ^5P_3^\circ$
1838. 101	3*h*	54403. 97	$b\ ^3P_2 - y\ ^3P_1^\circ$
1838. 594	10	54389. 39	$a\ ^3D_3 - x\ ^3F_2^\circ$
1840. 166	50	54342. 92	$a\ ^3G_4 - x\ ^3G_5^\circ$
1840. 438	30	54334. 89	$a\ ^5P_3 - z\ ^5P_2^\circ$
1842. 305	10	54279. 83	$b\ ^1G_4 - y\ ^3G_4^\circ$
1842. 546	1	54272. 73	$b\ ^3P_2 - x\ ^3G_3^\circ$
1843. 148	150	54255. 00	$a\ ^5P_2 - z\ ^5P_2^\circ$
1843. 490	400	54244. 94	$a\ ^3D_3 - x\ ^3F_4^\circ$
1843. 940	250	54231. 70	$a\ ^3G_2 - x\ ^3G_3^\circ$
1845. 020	50	54199. 95	$a\ ^5F_3 - z\ ^5D_2^\circ$
1845. 945	10	54172. 79	
1846. 306	3	54162. 20	$a\ ^1P_1 - y\ ^1P_1^\circ$
1846. 842	2	54146. 5	$b\ ^3P_1 - y\ ^3P_1^\circ$
1847. 473	250	54127. 99	$a\ ^3G_3 - x\ ^3G_4^\circ$

TABLE 1. *List of lines of* Pd III—Continued

Wavelength λ (Vac)	Intensity	Wave number	Identification
1849. 755	5	54061. 2	$a\ ^3D_1 - y\ ^3S_1^\circ$
1851. 592	1500	54007. 58	$a\ ^5F_3 - z\ ^5G_4^\circ$
1852. 274	2000	53987. 69	$a\ ^5F_4 - z\ ^5G_5^\circ$
1853. 283	15	53958. 30	$a\ ^5F_2 - z\ ^5G_3^\circ$
1856. 161	200	53874. 64	$a\ ^3D_2 - x\ ^3F_3^\circ$
1856. 504	50	53864. 68	$a\ ^5F_2 - z\ ^5D_1^\circ$
1857. 558	200	53834. 12	$a\ ^1H_5 - y\ ^1G_4^\circ$
1859. 206	1000	53786. 40	$a\ ^5F_2 - z\ ^5G_2^\circ$
1861. 514	30	53719. 71	$a\ ^3H_4 - y\ ^3H_5^\circ$
1861. 740	40	53713. 19	$a\ ^3G_4 - y\ ^3G_5^\circ$
1862. 947	10	53678. 39	$c\ ^3F_4 - w\ ^3F_3^\circ$
1864. 040	5	53646. 9	$c\ ^3P_0 - y\ ^3S_1^\circ$
1865. 782	150	53596. 83	$a\ ^3G_4 - y\ ^3D_3^\circ$
1866. 421	50	53578. 48	$b\ ^1D_2 - y\ ^1P_1^\circ$
1870. 487	150	53463. 44	$a\ ^3H_4 - x\ ^3F_3^\circ$
1871. 263	100	53439. 84	$a\ ^5P_2 - z\ ^5P_1^\circ$
1873. 197	200	53384. 67	$a\ ^3G_4 - z\ ^1G_4^\circ$
1874. 629	1500	53343. 89	$a\ ^3G_5 - z\ ^3H_5^\circ$
1874. 969	15	53334. 21	$b\ ^3P_2 - y\ ^3P_2^\circ$
1875. 469	100	53320. 00	$a\ ^5F_1 - z\ ^5D_0^\circ$
1877. 027	400	53275. 74	$a\ ^5F_1 - z\ ^5G_2^\circ$
1879. 041	15	53218. 64	$c\ ^3F_3 - w\ ^3G_4^\circ$
1880. 064	250	53189. 68	$a\ ^3G_4 - y\ ^3F_3^\circ$
1880. 326	300	53182. 27	$a\ ^5F_1 - z\ ^5D_1^\circ$
1880. 547	50	53176. 02	$b\ ^3F_4 - z\ ^3D_3^\circ$
1881. 382	3	53152. 4	
1882. 072	2	53132. 9	
1883. 352	500	53096. 82	$a\ ^5F_2 - z\ ^5D_2^\circ$
1884. 080	5	53076. 30	$b\ ^3P_1 - y\ ^3P_2^\circ$
1885. 834	2000	53026. 94	$a\ ^5F_4 - z\ ^5D_4^\circ$
1886. 978	50	52994. 79	$c\ ^3F_2 - w\ ^3G_3^\circ$
1887. 398	1000	52982. 99	$a\ ^5F_3 - z\ ^5D_3^\circ$
1888. 070	15	52964. 14	$b\ ^3F_2 - z\ ^5P_2^\circ$
1888. 575	1*h*	52949. 98	$b\ ^3P_2 - z\ ^1F_3^\circ$
1890. 047	15	52908. 74	$a\ ^3G_3 - z\ ^1F_3^\circ$
1890. 645	15	52892. 00	$a\ ^5P_1 - z\ ^5P_2^\circ$ and $b\ ^3P_1 - y\ ^3P_0^\circ$
1891. 341	1500	52872. 54	$a\ ^3H_6 - z\ ^3I_7^\circ$
1891. 475	10?	52868. 79	$b\ ^3P_0 - y\ ^3P_1^\circ$
1896. 003	2	52742. 5	$c\ ^3P_1 - x\ ^3D_2^\circ$
1896. 352	5	52732. 82	$b\ ^3P_2 - z\ ^3P_1^\circ$
1899. 486	50	52645. 82	$a\ ^1H_5 - y\ ^3H_4^\circ$
1901. 177	5	52598. 99	$a\ ^1P_1 - x\ ^3P_2^\circ$
1901. 679	50	52585. 11	$c\ ^3F_3 - w\ ^3G_3^\circ$
1901. 767	50	52582. 68	$b\ ^1G_4 - y\ ^3G_4^\circ$ and $c\ ^3P_2 - w\ ^3D_3^\circ$
1904. 255	2	52513. 98	$a\ ^3H_6 - z\ ^1H_5^\circ$
1904. 721	75	52501. 13	$a\ ^3D_1 - x\ ^3F_2^\circ$
1905. 673	2	52474. 90	$b\ ^3P_1 - z\ ^3P_1^\circ$
1906. 122	50	52462. 54	$b\ ^3D_2 - v\ ^3F_3^\circ$
1906. 529	20	52451. 34	$a\ ^3D_2 - x\ ^3F_2^\circ$
1906. 768	5	52444. 8	$c\ ^3P_1 - w\ ^3D_1^\circ$
1907. 874	20	52414. 36	$a\ ^5F_1 - z\ ^5D_2^\circ$
1913. 729	150	52254. 00	$c\ ^3F_4 - w\ ^3G_4^\circ$
1914. 616	4000	52229. 79	$a\ ^5F_5 - z\ ^5F_5^\circ$
1915. 592	5	52203. 18	$c\ ^3P_2 - x\ ^3D_3^\circ$
1917. 281	150	52157. 20	$c\ ^3P_1 - w\ ^3D_2^\circ$
1917. 472	200	52152. 00	$b\ ^1D_2 - y\ ^1F_3^\circ$
1917. 580	5	52149. 06	$b\ ^3F_2 - z\ ^5P_1^\circ$
1920. 250	6	52076. 55	$a\ ^5P_1 - z\ ^5P_1^\circ$
1922. 443	250	52017. 15	$a\ ^3H_5 - y\ ^3G_4^\circ$
1922. 522	100	52015. 01	$b\ ^1D_2 - x\ ^3P_2^\circ$

TABLE 1. *List of lines of* Pd III—Continued

Wavelength λ (Vac)	Intensity		Wave number	Identification
1924. 061	10		51973. 40	$b\ ^3P_1 - y\ ^3D_1^\circ$
1925. 324	30		51939. 31	$a\ ^3H_5 - z\ ^3I_5^\circ$
1925. 472	300		51935. 32	$a\ ^5F_2 - z\ ^5F_1^\circ$
1926. 254	5		51914. 23	$a\ ^3G_5 - y\ ^5D_4^\circ$
1926. 770	500		51900. 33	$a\ ^5F_3 - z\ ^5F_2^\circ$ and $b\ ^3P_2 - y\ ^3D_3^\circ$
1927. 545	10		51879. 46	$a\ ^5F_2 - z\ ^5D_3^\circ$
1930. 330	1000		51804. 61	$a\ ^5F_4 - z\ ^5F_5^\circ$
1931. 090	400		51784. 22	$b\ ^1G_4 - z\ ^1H_5^\circ$
1931. 293	5		51778. 78	$a\ ^5P_2 - z\ ^3D_1^\circ$
1932. 729	5		51740. 31	$c\ ^3F_2 - w\ ^3F_2^\circ$
1933. 324	40		51724. 39	$a\ ^3G_4 - z\ ^3H_4^\circ$
1933. 442	30		51721. 23	$a\ ^3D_1 - x\ ^3D_1^\circ$
1934. 439	15		51694. 57	$b\ ^3P_2 - y\ ^3D_2^\circ$ and $c\ ^3P_2 - y\ ^3P_1^\circ$
1937. 430	15		51614. 77	$b\ ^1G_4 - x\ ^3G_3^\circ$
1938. 273	3*h*		51592. 32	$b\ ^3D_3 - v\ ^3F_3^\circ$
1939. 404	1*h*		51562. 23	$c\ ^3P_2 - x\ ^3G_3^\circ$
1940. 447	50		51534. 52	$b\ ^3F_3 - z\ ^3D_2^\circ$ and $b\ ^1F_3 - v\ ^3D_2^\circ$
1941. 262	20		51512. 88	$a\ ^3D_2 - y\ ^3G_3^\circ$
1941. 332	100		51511. 02	$b\ ^1G_4 - x\ ^3G_4^\circ$
1941. 639	2000		51502. 88	$a\ ^5F_5 - z\ ^5F_4^\circ$
1943. 600	50		51450. 9	$a\ ^3G_4 - y\ ^3F_3^\circ$
1944. 123	50		51437. 07	$b\ ^3P_1 - y\ ^3D_2^\circ$
1944. 537	200		51426. 12	$a\ ^3D_3 - x\ ^3D_3^\circ$
	(LG)	(VG)		
1946. 509	5	50	51374. 02	$a\ ^5F_3 - z\ ^5D_4^\circ$
1948. 160	0	50	51330. 49	$c\ ^3F_3 - w\ ^3F_2^\circ$ and $b\ ^3D_1 - v\ ^3F_2^\circ$
1948. 460(v)	-------	20	51322. 58	$c\ ^3P_1 - y\ ^3F_2^\circ$
1949. 048(v)	-------	100	51307. 10	$c\ ^3P_0 - x\ ^3D_1^\circ$
1949. 483	5	50	51295. 65	$a\ ^1F_3 - w\ ^3F_4^\circ$
1950. 459	5	50	51269. 98	
1951. 117(v)	-------	200	51252. 69	$a\ ^5F_1 - z\ ^5F_1^\circ$
1951. 562	50	400	51241. 01	$b\ ^3F_4 - z\ ^3F_3^\circ$
1954. 027	3	300	51176. 37	$a\ ^3G_5 - y\ ^3F_4^\circ$
1956. 886	10	150	51101. 60	$a\ ^3H_4 - y\ ^3G_3^\circ$
1957. 192	5	50	51093. 61	$c\ ^3P_1 - y\ ^3P_1^\circ$
1957. 632	1	3	51082. 12	$a\ ^5P_3 - z\ ^3D_2^\circ$
1959. 477	5	30	51034. 03	$b\ ^3P_2 - z\ ^3S_1^\circ$
1960. 139	2	20	51016. 79	$b\ ^3D_2 - w\ ^3P_1^\circ$
1960. 688	1	5	51002. 51	$a\ ^5P_2 - z\ ^3D_2^\circ$
1962. 858	15	150	50946. 12	$a\ ^3H_5 - x\ ^3G_4^\circ$
1965. 025	1	3	50889. 94	$b\ ^3D_2 - v\ ^3F_2^\circ$
1966. 479	3	10	50852. 31	$a\ ^3G_4 - y\ ^5D_4^\circ$
1968. 632	10	150	50796. 70	$a\ ^5F_2 - z\ ^5F_2^\circ$
1969. 051	10	100	50785. 89	$a\ ^3D_3 - x\ ^3G_3^\circ$
1969. 423	2	10	50776. 29	$b\ ^3P_1 - z\ ^3S_1^\circ$
1970. 108	10	50	50758. 64	$b\ ^3P_2 - y\ ^5D_3^\circ$
1970. 607	0	3	50745. 79	$a\ ^1H_5 - y\ ^3H_6^\circ$
1971. 175	0	2	50731. 16	$a\ ^5P_2 - z\ ^3G_3^\circ$
1971. 747	20	200	50716. 45	$a\ ^3H_6 - x\ ^3G_5^\circ$
1972. 294	25	300	50702. 38	$a\ ^3G_5 - z\ ^3H_5^\circ$
1972. 575	3	100	50695. 21	$b\ ^3P_0 - y\ ^3D_1^\circ$
1973. 241	3	30	50678. 05	$a\ ^3D_1 - x\ ^3D_2^\circ$
1975. 185	20	200	50628. 17	$a\ ^3D_2 - x\ ^3D_2^\circ$
1975. 350	20	150	50623. 94	$c\ ^3P_2 - y\ ^3P_2^\circ$
1977. 528	50	300	50568. 18	$b\ ^3P_2 - z\ ^3P_2^\circ$
1979. 130	0	1	50527. 25	$a\ ^3G_3 - z\ ^3P_2^\circ$

TABLE 1. *List of lines of* Pd III—Continued

Wavelength λ (Vac)	Intensity		Wave number	Identification
1980. 609	5	50	50489. 52	$a\ ^3H_6 - z\ ^3I^\circ_6$
1980. 695	5	200	50487. 33	$b\ ^3F_2 - z\ ^3D^\circ_1$
1980. 860	5	200	50483. 12	$b\ ^3F_3 - z\ ^3F^\circ_2$
1980. 940	10	300	50481. 08	$b\ ^3F_3 - z\ ^3D^\circ_3$
1984. 886	5	50	50380. 73	$a\ ^3D_1 - w^3D^\circ_1$ and $b\ ^3D_2 - w\ ^3P^\circ_2$
1986. 705	15	100	50334. 60	$a\ ^1F_3 - x\ ^1G^\circ_4$
1986. 856	15	150	50330. 77	$a\ ^3D_2 - w^3D^\circ_1$ and $a\ ^1P_1 - y\ ^1D^\circ_2$
1988. 412	30	200	50291. 39	$b\ ^1G_4 - z\ ^1F^\circ_3$
1990. 470	3	10	50239. 39	$c\ ^3P_2 - z\ ^1F^\circ_3$
1993. 841	20*h*	200	50154. 45	$a\ ^1H_5 - z\ ^1I^\circ_6$
1993. 951	10	150	50151. 68	$a\ ^5F_3 - z\ ^5F^\circ_3$
1995. 105	1	2	50122. 68	$a\ ^1P_1 - z\ ^1D^\circ_2$
1995. 429	15	100	50114. 54	$a\ ^5F_1 - z\ ^5F^\circ_2$ and $a\ ^3G_4 - y\ ^3F^\circ_4$
1996. 168	2	20	50095. 98	$a\ ^1P_1 - z\ ^1P^\circ_1$
1996. 294	3	20	50092. 82	$a\ ^3D_1 - w^3D^\circ_2$
1996. 545	30	300	50086. 52	$a\ ^3H_6 - y\ ^3G^\circ_5$
1997. 735	10	50	50056. 69	$a\ ^5F_4 - z\ ^5F^\circ_5$
1998. 802	10	200	50029. 97	$a\ ^5P_3 - z\ ^3F^\circ_2$
1998. 879	10	200	50028. 04	$a\ ^5P_3 - z\ ^3D^\circ_3$
1999. 099	5	100	50022. 54	$c\ ^3P_2 - z\ ^3P^\circ_1$
2000. 390	20	200	49990. 25	$b\ ^3P_1 - y\ ^5D^\circ_2$
2000. 554	40	300	49986. 15	$a\ ^3G_3 - z\ ^3H^\circ_4$
2001. 345	3	30	49966. 40	$c\ ^3P_0 - w\ ^3D^\circ_1$
2002. 159	50	800	49946. 08	$b\ ^3F_4 - z\ ^3G^\circ_5$
2004. 473	50	1000	49888. 42	$b\ ^3F_4 - z\ ^3F^\circ_4$
2004. 898	3	20	49877. 85	$a\ ^1F_3 - v\ ^3D^\circ_2$
2005. 295	0	2	49867. 97	$a\ ^3D_2 - w\ ^3D^\circ_3$?
2006. 119	10	50	49847. 49	$a\ ^3D_3 - y\ ^3P^\circ_2$
2006. 485	1	3	49838. 40	$c\ ^3P_1 - y\ ^3P^\circ_0$
2010. 174	3	10	49746. 94	$b\ ^1D_2 - y\ ^1D^\circ_2$
2010. 504	5	75	49738. 77	$b\ ^3P_1 - z\ ^3P^\circ_0$
2011. 613	50	250	49711. 35	$b\ ^3F_2 - z\ ^3D^\circ_2$
2014. 478	50	500	49640. 65	$a\ ^3G_4 - z\ ^3H^\circ_5$
2014. 868	50	500	49631. 04	$b\ ^3F_3 - z\ ^3G^\circ_4$
2018. 623	15	75	49538. 72	$b\ ^1D_2 - z\ ^1D^\circ_2$
2019. 151	2	15	49525. 77	$c\ ^3F_3 - y\ ^1F^\circ_3$
2019. 332	2	15	49521. 33	$c\ ^3P_2 - y\ ^3D^\circ_1$
2019. 820	10	75	49509. 36	$b\ ^3D_3 - w\ ^3P^\circ_2$
2020. 690	1	5	49488. 05	$a\ ^3D_2 - x\ ^3D^\circ_3$
2022. 653	100	500	49440. 02	$b\ ^3F_2 - z\ ^3G^\circ_3$
2023. 375	2*h*	25	49422. 38	$a\ ^3H_3 - x\ ^3G^\circ_5$ and $c\ ^3P_1 - z\ ^3P^\circ_1$
2025. 582	5	35	49368. 53	
2026. 043	5	150	49357. 29	$b\ ^1G_4 - y\ ^3G^\circ_5$
2027. 158	20	300	49330. 15	$a\ ^5F_4 - z\ ^5F^\circ_4$
2027. 353	30	500	49325. 40	$a\ ^3H_4 - z\ ^3I^\circ_5$
2030. 110	3	10	49258. 41	$a\ ^3D_1 - y\ ^3F^\circ_2$
2030. 828	3	5	49241. 00	$b\ ^1G_4 - y\ ^3D^\circ_3$
2032. 699	50	500	49195. 68	$a\ ^3H_5 - z\ ^3I^\circ_6$
2032. 975	20	200	49189. 00	$c\ ^3P_2 - y\ ^3D^\circ_3$
2033. 419	30	400	49178. 26	$a\ ^5P_3 - z\ ^3G^\circ_4$
2036. 077	1	2	49114. 06	$a\ ^3G_3 - y\ ^5D^\circ_4$
2038. 804	1	2	49048. 36	$a\ ^5F_2 - z\ ^5F^\circ_3$
2039. 610	10	200	49028. 98	$b\ ^1G_4 - z\ ^1G^\circ_4$
2041. 268	2	20	48989. 16	$b\ ^3P_2 - y\ ^5D^\circ_1$
2041. 441	5	200	48985. 01	$c\ ^3P_2 - y\ ^3D^\circ_2$
2041. 787	0	2	48976. 71	$b\ ^1D_2 - y\ ^3S^\circ_1$
2044. 125	3	50	48920. 69	$c\ ^3P_1 - y\ ^3D^\circ_1$
2047. 177	2	10	48847. 75	$a\ ^3D_2 - x\ ^3G^\circ_3$
2047. 500	2	10	48840. 05	$b\ ^1D_2 - x\ ^3F^\circ_3$
2047. 758	3	25	48833. 90	$b\ ^1G_4 - y\ ^3F^\circ_3$

TABLE 1. *List of lines of* Pd III—Continued

Wavelength λ (Vac)	Intensity		Wave number	Identification
2049. 945	3	25	48781. 80	$c\ ^3P_2 - y\ ^3F^\circ_3$
2055. 110	30	500	48659. 20	$b\ ^3F_2 - z\ ^3F^\circ_2$
2055. 271	3	5	48655. 38	$a\ ^3H_6 - z\ ^3H^\circ_6$
2055. 415	3	20	48651. 98	
2957. 352	1	10	48606. 17	$a\ ^3H_4 - z\ ^1H^\circ_5$
2059. 277	3	50	48560. 73	$c\ ^3F_4 - y\ ^1F^\circ_3$
2059. 881	10	150	48546. 49	$b\ ^3F_3 - z\ ^3F^\circ_3$
2063. 381	2	25	48464. 15	$a\ ^3H_5 - z\ ^1G^\circ_4$
2064. 565	1	10	48436. 35	$a\ ^3H_4 - x\ ^3G^\circ_3$
2065. 587	0?	0	48412. 39	$a\ ^3D_3 - y\ ^3D^\circ_3$
2066. 802	0?	1	48383. 93	$c\ ^3P_1 - y\ ^3D^\circ_2$
2067. 148	1	15	48375. 83	$a\ ^3G_3 - y\ ^3F^\circ_4$
2067. 639	10	150	48364. 34	$a\ ^1F_3 - w\ ^3G^\circ_4$
2069. 356	5	20	48324. 21	$c\ ^3P_2 - z\ ^3S^\circ_1$
2074. 349	1	2	48207. 90	$a\ ^3D_3 - y\ ^3D^\circ_2$
2075. 205	100	200	48188. 01	$b\ ^3F_3 - z\ ^5G^\circ_4$
2079. 268	10	75	48093. 85	$a\ ^5P_3 - z\ ^3F^\circ_3$
2081. 225	5	15	48048. 63	$c\ ^3P_2 - y\ ^5D^\circ_3$
2083. 106	2	5	48005. 24	$a\ ^3D_3 - y\ ^3F^\circ_3$
2089. 500	3	10	47858. 34	$c\ ^3P_2 - z\ ^3P^\circ_2$
2095. 073	0	1	47731. 03	$a\ ^1F_3 - w\ ^3G^\circ_3$
2095. 400	2	10	47723. 58	$c\ ^3P_1 - z\ ^3S^\circ_1$
2097. 436	1	5	47677. 26	$a\ ^5F_3 - z\ ^5F^\circ_4$
2098. 436	2	10	47654. 54	
2099. 959	2	10	47619. 98	$c\ ^3F_3 - y\ ^3H^\circ_4$
2103. 919	2	10	47530. 35	$c\ ^3F_2 - y\ ^1D^\circ_2$
2104. 175	10	50	47524. 56	$a\ ^3D_2 - z\ ^1F^\circ_3$
2106. 269	5	25	47477. 32	$b\ ^3P_2 - z\ ^5P^\circ_3$
2107. 358	5	20	47452. 78	$b\ ^3P_0 - y\ ^5D^\circ_1$
2111. 082	30	200	47369. 07	$b\ ^1G_4 - z\ ^3H^\circ_4$
2111. 406	2	5	47361. 81	$a\ ^3H_5 - z\ ^3H^\circ_6$
2111. 600	1	2	47357. 45	$a\ ^3D_1 - z\ ^3P^\circ_1$
2113. 820	2	5	47307. 72	$a\ ^3D_2 - z\ ^3P^\circ_1$
2113. 980	2	10	47304. 14	
2114. 253	3	20	47295. 79	$c\ ^3F_2 - z\ ^1P^\circ_1$
2115. 413	5	25	47272. 09	$a\ ^3D_3 - y\ ^5D^\circ_3$
2116. 077	0?	0	47257. 26	$a\ ^3G_3 - z\ ^5P^\circ_2$ and $c\ ^3P_1 - z\ ^3P^\circ_2$
2118. 912	0	1	47194. 03	$b\ ^3F_3 - z\ ^3F^\circ_4$
2119. 551	50	150	47179. 80	$a\ ^1H_5 - y\ ^3G^\circ_4$
2120. 277	5	20	47163. 65	$b\ ^3F_4 - z\ ^5D^\circ_3$
2122. 204	3	10	47120. 82	$c\ ^3F_3 - y\ ^1D^\circ_2$
2122. 544	3	10	47113. 28	$a\ ^3H_4 - z\ ^1F^\circ_3$
2123. 070	5	20	47101. 60	$a\ ^1H_5 - z\ ^3I^\circ_5$
2123. 967	5	50	47081. 71	$a\ ^3D_3 - z\ ^3P^\circ_2$
2124. 351	30	200	47073. 20	$b\ ^3F_3 - z\ ^5S^\circ_2$
2125. 851	3	20	47039. 99	$b\ ^3P_1 - z\ ^5P^\circ_2$
2130. 495	1	1	46937. 45	$c\ ^3P_1 - y\ ^5D^\circ_2$
2131. 632	0	0	46912. 41	$c\ ^3F_3 - z\ ^1D^\circ_2$
2136. 530	2	15	46804. 87	$a\ ^3H_5 - z\ ^3H^\circ_4$
2138. 506	1	5	46761. 62	$a\ ^3D_3 - y\ ^5D^\circ_2$
2139. 438	1	3	46741. 25	$a\ ^5P_2 - z\ ^3F^\circ_4$
2140. 286	1	3	46722. 73	$b\ ^3F_2 - z\ ^3F^\circ_3$
2144. 988	50	400	46620. 31	$a\ ^5P_3 - z\ ^5S^\circ_2$
2148. 663	50	300	46540. 57	$a\ ^5P_2 - z\ ^5S^\circ_2$
2149. 815	50	500	46515. 63	$b\ ^3F_4 - z\ ^5G^\circ_3$
2150. 681	0	0	46496. 90	$b\ ^1G_4 - y\ ^5D^\circ_4$
2151. 339	30	75	46482. 68	$b\ ^3P_2 - z\ ^5P^\circ_1$
2151. 604	15	75	46476. 95	$a\ ^1F_3 - w\ ^3F^\circ_2$
2156. 290	2	5	46375. 95	$b\ ^3F_3 - z\ ^5G^\circ_3$
2158. 899	2	3	46319. 91	$a\ ^3D_1 - y\ ^3D^\circ_2$

TABLE 1. *List of lines of* Pd III—Continued

Wavelength λ (Vac)	Intensity		Wave number	Identification
2161. 226	2	5	46270. 03	$a\ ^3D_2 - y\ ^3D^\circ_2$
2163. 367	5	20	46224. 24	$b\ ^3P_1 - z\ ^5P^\circ_1$?
2165. 551	1	5	46177. 62	$a\ ^1P_1 - x\ ^3D^\circ_2$
2168. 785	1	2	46109. 34	$a\ ^1H_5 - x\ ^3G^\circ_4$
2170. 757	3	5	46066. 88	$a\ ^3D_2 - y\ ^3F^\circ_3$
2173. 219	50	100	46014. 69	$a\ ^3H_6 - z\ ^3H^\circ_5$
2177. 550	20	500	45923. 17	$a\ ^3P_2 - z\ ^5G^\circ_3$
2177. 625	30		45921. 59	$a\ ^3P_2 - z\ ^5D^\circ_1$
2180. 990	3	15	45850. 74	$a\ ^3H_4 - z\ ^1G^\circ_4$
2185. 368	5	15	45758. 88	$b\ ^1G_4 - y\ ^3F^\circ_4$
2188. 840	5	15	45686. 30	$b\ ^3F_3 - z\ ^5D^\circ_2$
2189. 220	2	5	45678. 37	$c\ ^3P_1 - y\ ^5D^\circ_1$
2190. 311	15	20	45655. 62	$a\ ^3H_4 - y\ ^3F^\circ_3$
2193. 162	1	3	45596. 27	$c\ ^3P_1 - y\ ^5D^\circ_0$
2195. 157	3	10	45554. 83	$b\ ^3F_4 - z\ ^5D^\circ_4$
2197. 537	2	2	45505. 49	$c\ ^3F_4 - y\ ^3H^\circ_5$
λ (Air)				
2197. 414	50		45493. 83	$b\ ^3F_4 - z\ ^5G^\circ_4$
2209. 297	2		45249. 16	$c\ ^3F_4 - x\ ^3F^\circ_3$
2212. 815	15		45177. 23	$a\ ^3P_1 - z\ ^5S^\circ_2$
2219. 512	1		45040. 93	$a\ ^5P_3 - z\ ^5G^\circ_4$
2221. 113	1?		45008. 47	$b\ ^1D_2 - w\ ^3D^\circ_2$
2226. 444	1		44900. 71	$a\ ^3G_3 - z\ ^3G^\circ_4$
2230. 382	1		44821. 44	$b\ ^3P_2 - z\ ^3D^\circ_1$
2233. 079	15		44767. 29	$c\ ^3P_2 - z\ ^5P^\circ_3$
2236. 636	5		44696. 12	$a\ ^5P_1 - z\ ^5D^\circ_0$
2236. 971	3		44689. 43	$a\ ^3G_4 - z\ ^3D^\circ_3$
2239. 923	3		44630. 56	$b\ ^3F_2 - z\ ^5D^\circ_1$
2243. 548	15		44558. 44	$a\ ^5P_1 - z\ ^5D^\circ_1$
2243. 865	15		44552. 14	$b\ ^3F_2 - z\ ^5G^\circ_3$
2248. 054	5		44469. 13	$b\ ^3F_3 - z\ ^5D^\circ_3$
2253. 671	50		44358. 31	$a\ ^1H_5 - z\ ^3I^\circ_6$
2271. 183	3		44016. 31	$a\ ^5P_3 - z\ ^5F^\circ_3$
2271. 786	5		44004. 63	$a\ ^3G_3 - z\ ^3D^\circ_2$
2272. 429	3		43992. 18	$a\ ^5P_2 - z\ ^5F^\circ_1$
2272. 683	3		43987. 27	$c\ ^3P_1 - z\ ^5P^\circ_2$
2275. 310	20		43936. 48	$a\ ^5P_2 - z\ ^5D^\circ_3$
2279. 155	5		43862. 37	$b\ ^3F_2 - z\ ^5D^\circ_2$
2279. 674	2		43852. 38	$c\ ^3F_3 - y\ ^3G^\circ_3$
2282. 893	15		43790. 55	$a\ ^5P_1 - z\ ^5D^\circ_2$
2283. 059	15		43787. 37	$b\ ^3P_1 - z\ ^3D^\circ_2$
2288. 604	10		43681. 29	$c\ ^3F_4 - x\ ^3F^\circ_4$
2291. 446	100		43627. 12	$a\ ^1H_5 - z\ ^1G^\circ_4$
2304. 155	3		43386. 51	$b\ ^3F_3 - z\ ^5F^\circ_2$
2309. 531	30		43285. 52	$b\ ^3P_0 - z\ ^3D^\circ_1$
2326. 609	5		42967. 82	$c\ ^3F_3 - x\ ^3D^\circ_2$
2328. 456	3		42933. 74	$a\ ^5P_3 - z\ ^5F^\circ_2$
2332. 796	20		42853. 87	$a\ ^5P_2 - z\ ^5F^\circ_2$
2339. 280	10		42735. 10	$b\ ^3P_1 - z\ ^3F^\circ_2$
2341. 146	5		42701. 05	$b\ ^3F_2 - z\ ^5F^\circ_1$
2344. 206	3		42645. 31	$b\ ^3F_2 - z\ ^5D^\circ_3$
2345. 108	2		42628. 90	$a\ ^5P_1 - z\ ^5F^\circ_1$
2352. 769	10		42490. 11	$b\ ^1D_2 - z\ ^1F^\circ_3$
2354. 230	40		42463. 74	$a\ ^3G_5 - z\ ^3F^\circ_4$
2357. 346	30		42407. 62	$a\ ^5P_3 - z\ ^5D^\circ_4$
2358. 748	1		42382. 41	$c\ ^3F_3 - w\ ^3D^\circ_2$

TABLE 1. *List of lines of* Pd III—Continued

Wavelength λ (Air)	Intensity	Wave number	Identification
2371. 514	10	42154. 29	$c\ ^3F_3 - y\ ^3G^0_4$
2374. 180	5	42106. 95	$a\ ^3H_4 - z\ ^3H^0_5$
2382. 102	1	41966. 93	$a\ ^1H_5 - z\ ^3H^0_4$
2390. 045	3	41827. 47	$c\ ^3F_3 - x\ ^3D^0_3$
2400. 907	5	41638. 25	$b\ ^3F_3 - z\ ^5F^0_3$
2403. 297	5	41596. 85	$c\ ^3F_2 - x\ ^3G^0_3$
2405. 273	10	41562. 68	$b\ ^3F_2 - z\ ^5F^0_2$
2409. 452	3	41490. 60	$a\ ^5P_1 - z\ ^5F^0_2$
2411. 244	1	41459. 76	$a\ ^3G_4 - z\ ^3G^0_5$
2432. 034	30	41105. 38	$a\ ^5P_2 - z\ ^5F^0_3$
2434. 468	2	41064. 28	$c\ ^3P_2 - z\ ^3G^0_3$
2452. 415	100	40763. 79	$a\ ^3G_5 - z\ ^5G^0_4$
2463. 281	10	40583. 99	$a\ ^3G_4 - z\ ^5G^0_3$
2464. 800	1	40558. 98	$a\ ^3D_3 - z\ ^3D^0_2$
2474. 980	3	40392. 16	$c\ ^3F_4 - z\ ^1H^0_5$
2477. 138	20	40356. 98	$a\ ^1H_5 - y\ ^3F^0_4$
2481. 424	3	40287. 28	$a\ ^3D_3 - z\ ^3G^0_3$
2482. 262	0	40273. 68	$c\ ^3F_2 - z\ ^1F^0_3$
2485. 440	15	40222. 19	$c\ ^3F_4 - x\ ^3G^0_3$
2491. 862	10	40118. 53	$c\ ^3F_4 - x\ ^3G^0_4$
2512. 510	3	39788. 86	$b\ ^1D_2 - y\ ^5D^0_2$
2527. 320	10	39555. 71	$c\ ^3F_2 - y\ ^3D^0_1$
2530. 563	30	39505. 02	$a\ ^3D_3 - z\ ^3D^0_3$
2537. 507	5	39396. 92	$a\ ^3D_3 - z\ ^3D^0_2$
2548. 741	20	39223. 29	$c\ ^3F_2 - y\ ^3D^0_3$
2552. 613	40	39163. 79	$b\ ^3F_3 - z\ ^5F^0_4$
2562. 201	3	39017. 25	$a\ ^3G_3 - z\ ^5G^0_2$
2568. 684	10	38918. 78	$a\ ^3H_5 - z\ ^3G^0_4$
2582. 478	50	38710. 91	$a\ ^5P_3 - z\ ^5F^0_4$
2585. 251	2	38669. 39	$b\ ^3D_2 - v\ ^3D^0_2$
2586. 231	2	38654. 74	$a\ ^3D_3 - z\ ^3G^0_4$
2588. 506	10	38620. 77	$a\ ^3D_2 - z\ ^3D^0_2$
2589. 796	5	38601. 53	$c\ ^3F_3 - z\ ^1G^0_4$
2590. 233	5	38595. 02	$c\ ^3F_4 - x\ ^3G^0_5$
2603. 449	5	38399. 10	$b\ ^1G_4 - z\ ^3F^0_3$
2606. 982	30	38347. 08	$c\ ^3P_2 - z\ ^3F^0_3$
2633. 216	100	37965. 06	$c\ ^3F_4 - y\ ^3G^0_5$
2634. 993?	0	37939. 46	$b\ ^3P_1 - z\ ^5D^0_2$
2635. 019?	0	37939. 08	$a\ ^3H_4 - z\ ^3G^0_3$
2641. 307	15	37848. 77	$c\ ^3F_4 - y\ ^3D^0_3$
2642. 389	30	37833. 27	$a\ ^3H_6 - z\ ^3G^0_5$
2656. 200	2	37636. 57	$c\ ^3F_4 - z\ ^1G^0_4$
2660. 878	30	37570. 40	$a\ ^3D_3 - z\ ^3F^0_3$
2661. 512	10	37561. 26	$b\ ^3D_3 - w\ ^3F^0_4$
2667. 088	3	37482. 93	$c\ ^3F_3 - z\ ^3P^0_2$
2669. 224	3	37452. 94	$b\ ^3D^0_1 - x\ ^1D^0_2$
2690. 055	3	37162. 93	$c\ ^3F_3 - y\ ^5D^0_2$
2690. 583	2	37155. 64	$a\ ^3H_4 - z\ ^3D^0_3$
2699. 478	2	37033. 21	
2700. 920	5	37013. 44	$b\ ^3D_2 - x\ ^1D^0_2$
2706. 182	2	36941. 48	$c\ ^3F_2 - z\ ^3H^0_4$
2707. 428	15	36924. 48	$b\ ^3D_2 - w\ ^3F^0_3$
2711. 170	20	36873. 52	$c\ ^3P_2 - z\ ^5S^0_2$
2711. 830	10	36864. 54	$b\ ^3D_3 - v\ ^3D^0_3$
2723. 362	3	36709. 80	$c\ ^3F_4 - y\ ^5D^0_3$?
2740. 287	40	36481. 74	$a\ ^3H_5 - z\ ^3F^0_4$
2752. 981	10	36313. 53	$c\ ^3F_2 - y\ ^5D^0_1$
2759. 369	15	36229. 46	$a\ ^1F_3 - x\ ^3G^0_4$
2765. 868	15	36144. 34	$b\ ^3D_3 - x\ ^1D_2$?
2771. 623	3	36069. 29	$c\ ^3F_3 - y\ ^5D^0_4$

TABLE 1. *List of lines of* Pd III—Continued

Wavelength λ (Air)	Intensity	Wave number	Identification
2788. 880	2	35846. 12	$a\ ^3G_4 - z\ ^5F_3^\circ$
2803. 903	0	35654. 07	$c\ ^3P_1 - z\ ^5D_1^\circ$
2805. 109	0	35638. 74	$b\ ^3P_1 - z\ ^5F_2^\circ$
2805. 622	0	35632. 22	$a\ ^3D_2 - z\ ^3F_3^\circ$
2816. 152	1	35499. 00	$b\ ^3P_0 - z\ ^5F_1^\circ$
2829. 496	30	35331. 59	$c\ ^3F_3 - y\ ^3F_4^\circ$
2855. 481	10	35010. 08	$a\ ^1F_3 - z\ ^1F_3^\circ$
2865. 653	15*d*?	34885. 82	$c\ ^3P_1 - z\ ^5D_2^\circ$
2867. 235	5	34866. 57	$b\ ^3D_2 - w\ ^3G_3^\circ$
2884. 642	2	34656. 18	
2886. 811	20	34630. 15	$b\ ^3D_3 - w\ ^3G_4^\circ$
2896. 227	15	34517. 56	$a\ ^3D_3 - z\ ^5G_4^\circ$
2903. 308	20	34433. 38	$a\ ^3G_5 - z\ ^5F_4^\circ$
2905. 890	30	34402. 79	$a\ ^3H_6 - z\ ^5G_5^\circ$
2909. 303	1	34362. 43	$b\ ^1D_2 - z\ ^3D_1^\circ$
2917. 191	5	34269. 52	$c\ ^3P_2 - z\ ^5D_3^\circ$
2922. 030	20	34212. 77	$c\ ^3F_3 - z\ ^5P_2^\circ$
2927. 543	5	34148. 35	$b\ ^3P_2 - z\ ^5F_3^\circ$
2935. 841	5	34051. 83	$b\ ^3D_1 - w\ ^3F_2^\circ$
2949. 616	15	33892. 81	$c\ ^3F_4 - z\ ^3H_5^\circ$
2987. 648	3	33461. 38	$a\ ^3D_2 - z\ ^5G_3^\circ$
2990. 708	5	33427. 15	$c\ ^3F_4 - z\ ^5P_3^\circ$

TABLE 2. Pd III *even levels*

Configuration	Name	Observed	Calculated	Obs-Calc	Name (Shadmi)
$4d^8$	$a\ ^3F_4$	0. 00	2	−2	
$4d^8$	$a\ ^3F_3$	3229. 3	3227	2	
$4d^8$	$a\ ^3F_2$	4687. 5	4728	−40	
$4d^8$	$a\ ^1D_2$	10229. 3	10330	−101	$^3P_2$
$4d^8$	$a\ ^3P_1$	13468. 9	13394	75	
$4d^8$	$a\ ^3P_0$	13697. 5	13636	62	
$4d^8$	$a\ ^3P_2$	14634. 4	14768	−134	$^1D_2$
$4d^8$	$a\ ^1G_4$	17879. 3	17824	55	
$4d^8$	$a\ ^1S_0$		41196		
$4d^7(^4F)5s$	$a\ ^5F_5$	52916. 0	52885	31	
$4d^7(^4F)5s$	$a\ ^5F_4$	55088. 6	55040	49	
$4d^7(^4F)5s$	$a\ ^5F_3$	56741. 64	56697	45	
$4d^7(^4F)5s$	$a\ ^5F_2$	57844. 93	57806	39	
$4d^7(^4F)5s$	$a\ ^5F_1$	58527. 3	58492	35	
$4d^7(^4F)5s$	$b\ ^3F_4$	62560. 75	62397	164	
$4d^7(^4F)5s$	$b\ ^3F_3$	65255. 08	65181	74	
(^4P)	$a\ ^5P_3$	65707. 92	65689	19	
(^4P)	$a\ ^5P_2$	65787. 75	65817	−29	
(^4F)	$b\ ^5F_2$	67078. 93	66986	93	
(^4P)	$a\ ^5P_1$	67151. 03	67195	−44	
(^2G)	$a\ ^3G_3$	69985. 44	70034	−49	
(^2G)	$a\ ^3G_4$	71047. 05	71027	20	
(^2P)	$b\ ^3P_2$	72744. 82	72859	−114	
(^2G)	$a\ ^3G_3$	72785. 64	72791	−5	
(^2P)	$b\ ^3P_1$	73002. 81	73096	−93	
(^2P)	$b\ ^3P_0$	74280. 92	74320	−39	
(^2H)	$a\ ^3H_6$	74673. 57	74741	−67	
(^2G)	$b\ ^1G_4$	75402. 52	75336	67	
(^4P)	$c\ ^3P_2$	75454. 65	75447	8	
(^2H)	$a\ ^3H_5$	75967. 39	75971	−4	
(^4P)	$c\ ^3P_1$	76055. 46	76193	−138	
($a\ ^2D$)	$a\ ^3D_3$	76231. 26	76235	−4	
($a\ ^2D$)	$a\ ^3D_1$	78119. 50	78210	−90	
($a\ ^2D$)	$a\ ^3D_2$	78169. 48	78125	44	
(^4P)	$c\ ^3P_0$	78533. 8	78682	−148	
(^2H)	$a\ ^3H_4$	78580. 62	78525	56	
(^2H)	$a\ ^1H_5$	80804. 43	80802	2	
(^2P)	$a\ ^1P_1$	82619. 94	82809	−189	

TABLE 2. Pd III *even levels*—Continued

Configuration	Name	Observed	Calculated	Obs-Calc	Name (Shadmi)
(a ^{2}D)	b ^{1}D$_2$	83203. 94	83113	91	
(^{2}F)	c ^{3}F$_2$	85420. 33	85494	−74	
(^{2}F)	c ^{3}F$_3$	85829. 98	85940	−110	
(^{2}F)	c ^{3}F$_4$	86794. 85	86937	−142	
(^{2}F)	a ^{1}F$_3$	90684. 00	90857	−173	
(b ^{2}D)	b ^{3}D$_1$	103109. 0	102858	251	
(b ^{2}D)	b ^{3}D$_2$	103548. 42	103296	252	
(b ^{2}D)	b ^{3}D$_3$	104418. 18	104124	294	
(b ^{2}D)	^{1}D$_2$		108183		
$4d^7(^4\mathrm{F})6s$ or $4d^7(^4\mathrm{F})5d$	1_5	169831. 0			
	2_4	170330. 2?			
	3_5	170384. 7			
	4_6	170638. 4?			
	$5_{5,4}$	171332. 5			
	6_4	171551. 5			
	$7_{4,3}$	171676. 6			
	8_3	171785. 7?			
	9_5	172573. 9			
	10_4	172535. 8			
	11_4	173635. 8			
	12_4	173730. 0			

TABLE 3. Pd III *odd levels*

Configuration	Name	Observed	Calculated	Obs-Calc	Name (Shimoni)
$4d^7(^4\mathrm{F})5p$	z ^{5}F$_4^\circ$	104418. 86	104535	−116	
$4d^7(^4\mathrm{F})5p$	z ^{5}F$_5^\circ$	105145. 6	105030	116	
$4d^7(^4\mathrm{F})5p$	z ^{5}F$_3^\circ$	106893. 27	106934	−41	
$4d^7(^4\mathrm{F})5p$	z ^{5}D$_4^\circ$	108115. 59	107968	148	
$4d^7(^4\mathrm{F})5p$	z ^{5}F$_2^\circ$	108641. 62	108637	5	
$4d^7(^4\mathrm{F})5p$	z ^{5}G$_6^\circ$	109015. 5	108675	340	
$4d^7(^4\mathrm{F})5p$	z ^{5}G$_5^\circ$	109076. 37	108884	192	
$4d^7(^4\mathrm{F})5p$	z ^{5}D$_3^\circ$	109724. 26	109622	102	
$4d^7(^4\mathrm{F})5p$	z ^{5}F$_1^\circ$	109779. 95	109760	20	
$4d^7(^4\mathrm{F})5p$	z ^{5}G$_4^\circ$	110748. 86	110496	253	
$4d^7(^4\mathrm{F})5p$	z ^{5}D$_2^\circ$	110941. 34	110870	71	
$4d^7(^4\mathrm{F})5p$	z ^{5}G$_3^\circ$	111631. 06	111370	261	
$4d^7(^4\mathrm{F})5p$	z ^{5}D$_1^\circ$	111709. 50	111759	−49	
$4d^7(^4\mathrm{F})5p$	z ^{5}G$_2^\circ$	111802. 44	111606	196	
$4d^7(^4\mathrm{F})5p$	z ^{5}D$_0^\circ$	111847. 15	111962	−115	
(^{4}P)	z ^{5}S$_2^\circ$	112328. 25	112717	−389	
(^{4}F)	z ^{3}F$_4^\circ$	112449. 15	112383	66	
(^{4}F)	z ^{3}G$_5^\circ$	112506. 83	112281	226	
(^{4}F)	z ^{3}F$_3^\circ$	113801. 73	113852	−50	
(^{4}F)	z ^{3}G$_4^\circ$	114886. 14	114765	121	
(^{4}F)	z ^{3}D$_3^\circ$	115736. 24	115572	164	
(^{4}F)	z ^{3}F$_2^\circ$	115738. 07	115758	−20	
(^{4}F)	z ^{3}G$_3^\circ$	116518. 9	116436	83	
(^{4}F)	z ^{3}D$_2^\circ$	116790. 27	116681	109	
(^{4}F)	z ^{3}D$_1^\circ$	117566. 34	117640	−74	
(^{4}P)	z ^{5}P$_1^\circ$	119227. 56	119187	41	(^{2}P)^{3}P$_1^\circ$
(^{4}P)	z ^{5}P$_2^\circ$	120042. 76	120188	−145	(^{4}P)^{5}D$_2^\circ$
(^{4}P)	z ^{5}P$_3^\circ$	120222. 00	120183	39	(^{4}P)^{5}D$_3^\circ$
(^{2}G)	z ^{3}H$_5^\circ$	120687. 62	120776	−88	
(^{2}G)	y ^{3}F$_4^\circ$	121161. 42	121228	−67	
(^{4}P)	y ^{5}D$_0^\circ$	121651. 73	121662	−10	
(^{4}P)	y ^{5}D$_1^\circ$	121733. 85	121635	99	
(^{4}P)	y ^{5}D$_4^\circ$	121899. 35	121729	170	
(^{2}P)	z ^{3}P$_0^\circ$	122741. 65	123212	−470	
(^{2}G)	z ^{3}H$_4^\circ$	122771. 61	122931	−159	
(^{4}P)	y ^{5}D$_2^\circ$	122992. 91	123099	−106	(^{4}P)^{5}P$_2^\circ$
(^{2}P)	z ^{3}P$_2^\circ$	123312. 96	123673	−360	
(^{2}G)	z ^{3}H$_3^\circ$	123329. 95	123309	21	
(^{4}P)	y ^{5}D$_3^\circ$	123503. 32	123382	121	(^{4}P)^{5}P$_3^\circ$
(^{3}P)	z ^{5}S$_1^\circ$	123778. 95	123905	−126	(^{4}P)^{5}P$_1^\circ$

TABLE 3. Pd III *odd levels*—Continued

Configuration	Name	Observed	Calculated	Obs-Calc	Name (Shadmi)
(^{2}G)	$y\ ^3F^o_3$	124236. 40	124133	103	
(^{2}G)	$z\ ^1G^o_4$	124431. 47	124691	−260	
(^{4}P)	$y\ ^3D^o_2$	124439. 49	124436	3	
(^{4}P)	$y\ ^3D^o_3$	124643. 61	124628	16	
(^{2}H)	$y\ ^3G^o_5$	124759. 94	124910	−150	
(^{4}P)	$y\ ^3D^o_1$	124976. 06	125099	−123	
(^{2}H)	$z\ ^3I^o_6$	125163. 08	125181	−18	
(^{2}G)	$x\ ^3G^o_5$	125389. 89	125279	111	
(^{2}P)	$z\ ^3P^o_1$	125477. 21	125396	81	(^{4}P)^{3}S$_1$
(^{2}G)	$z\ ^1F^o_3$	125694. 00	125576	118	
(^{4}P)	$y\ ^3P^o_0$	125893. 86	126028	−134	
(^{4}P)	$y\ ^3P^o_2$	126078. 67	126261	−182	
(^{2}G)	$x\ ^3G^o_4$	126913. 52	127037	−123	
(^{2}G)	$x\ ^3G^o_3$	127017. 16	127145	−128	
(^{4}P)	$y\ ^3P^o_1$	127149. 07	127224	−75	
(^{2}G)	$z\ ^1H^o_5$	127187. 01	127179	8	
(^{2}G)	$y\ ^3F^o_2$	127377. 9	127451	−73	
(^{2}H)	$z\ ^3I^o_7$	127546. 1	127374	172	
($a\ ^2$D)	$x\ ^3D^o_3$	127657. 51	127728	−70	
(^{2}H)	$z\ ^3I^o_8$	127906. 01	127830	76	
(^{2}H)	$y\ ^3G^o_4$	127984. 23	127948	36	
(^{2}P)	$w\ ^3D^o_3$	128037. 98	128127	−89	
(^{2}P)	$w\ ^3D^o_2$	128212. 4	128047	165	(^{2}D)^{3}F$_2$
(^{2}P)	$w\ ^3D^o_1$	128500. 19	128723	−223	(^{2}D)^{3}D$_1$
($a\ ^2$D)	$x\ ^3D^o_2$	128797. 57	128868	−70	
(^{2}H)	$y\ ^3G^o_3$	129682. 29	129681	1	
($a\ ^2$D)	$x\ ^3D^o_1$	129841. 2	129840	1	(^{2}P)^{3}D$_1$
($a\ ^2$D)	$x\ ^3F^o_4$	130476. 14	130542	−66	
($a\ ^2$D)	$x\ ^3F^o_2$	130620. 71	130674	−53	(^{2}P)^{3}D$_2$
(^{2}H)	$z\ ^1I^o_6$	130958. 84	130864	95	
(^{2}P)	$z\ ^1S^o_0$	131482. 4	131512	−30	
(^{2}H)	$y\ ^3H^o_6$	131550. 18	131693	−143	
($a\ ^2$D)	$x\ ^3F^o_3$	132043. 98	132031	+13	
(^{4}P)	$y\ ^3S^o_1$	132180. 62	132653	−472	(^{2}P)^{3}S$_1$
(^{2}H)	$y\ ^3H^o_5$	132300. 34	132373	−73	
(^{2}P)	$z\ ^1P^o_1$	132715. 87	132975	−259	
($a\ ^2$D)	$z\ ^1D^o_2$	132742. 60	132576	167	($a_^2$D)^{3}P$_2$
(^{2}P)	$y\ ^1D^o_2$	132950. 75	133114	−163	
(^{2}H)	$y\ ^3H^o_4$	133449. 96	133584	−134	
(^{2}H)	$y\ ^1G^o_4$	134638. 1	134783	−145	
($a\ ^2$D)	$x\ ^3P^o_2$	135218. 90	134832	387	(^{2}D)^{1}D$_2$
($a\ ^2$D)	$y\ ^1F^o_3$	135355. 67	135412	−56	
($a\ ^2$D)	$y\ ^1P^o_1$	136782. 2	136949	−167	
(^{2}H)	$y\ ^1H^o_5$	136846. 5	136908	−61	
(^{2}F)	$w\ ^3F^o_2$	137160. 95	137515	−354	
($a\ ^2$D)	$x\ ^3P^o_1$	137489. 2	137415	74	
($a\ ^2$D)	$x\ ^3P^o_0$	137741. 1	137659	82	
(^{2}F)	$w\ ^3G^o_3$	138414. 99	138499	−84	
(^{2}F)	$w\ ^3G^o_4$	139048. 34	139188	−140	
(^{2}F)	$w\ ^3F^o_3$	140472. 90	140631	−158	
(^{2}F)	$x\ ^1D^o_2$	140561. 87	140820	−258	
(^{2}F)	$x\ ^1G^o_4$	141018. 60	141168	−149	
(^{2}F)	$v\ ^3D^o_3$	141282. 72	141116	167	
(^{2}F)	$w\ ^3G^o_5$	141873. 9	141897	−23	
(^{2}F)	$w\ ^3F^o_4$	141979. 44	142139	−160	
(^{2}F)	$v\ ^3D^o_1$	142102. 6	141902	201	
(^{2}F)	$v\ ^3D^o_2$	142218. 4?	142091	127	
(^{2}F)	$x\ ^1F^o_3$	146662. 4	146266	396	
($b\ ^2$D)	$w\ ^3P^o_2$	153928. 1	153766	162	
($b\ ^2$D)	$v\ ^3F^o_2$	154438. 4?	154464	−26	
($b\ ^2$D)	$w\ ^3P^o_1$	154566. 9	154422	145	
($b\ ^2$D)	$w\ ^3P^o_0$	155388. 1	155229	159	
($b\ ^2$D)	$v\ ^3F^o_3$	156010. 7?	155840	171	
($b\ ^2$D)	$^3F^o_4$		157947		
($b\ ^2$D)	$^1F^o_3$		159169		
($b\ ^2$D)	$^1P^o_1$		159336		
($b\ ^2$D)	$w\ ^3D^o_1$	161413. 3	161411	2	
($b\ ^2$D)	$^3D^o_2$		161489		
($b\ ^2$D)	$^1D^o_2$		162638		
($b\ ^2$D)	$^3D^o_3$		163362		

TABLE 3. Pd III *odd levels*—Continued

Configuration	Name	Observed	Calculated	Obs-Calc	Name (Shadmi)
$4d^8(^3D)5s\ 5p$	1°_4	193222?			
$4d^8(^3D)5s\ 5p$	$2^\circ_{3,4}$	195161?			
$4d^8(^3D)5s\ 5p$	3°_2	195444?			
$4d^8(^3D)5s\ 5p$	4°_4	197296?			
$4d^8(^3D)5s\ 5p$	$5^\circ_{3,4}$	197939			
$4d^8(^3D)5s\ 5p$	6°_4	197959			
$4d^8(^3D)5s\ 5p$	7°_4	198107			

TABLE 4. *Observed terms of* Pd III

Configuration	Terms		
$4d^8$	$a\ ^3P\ a\ ^1D\ a\ ^3F\ a\ ^1G$		
	$nx=5s$	$nx=5p$	$nx=6s$ or $5d$
$4d^7(^4F)nx$	$a\ ^5F$ $b\ ^3F$	$z\ ^5D^\circ z\ ^5F^\circ z\ ^5G^\circ$ $z\ ^3D^\circ z\ ^3F^\circ z\ ^3G^\circ$	1 to 12 Inclusive.
(^4P)	$a\ ^5P$ $c\ ^3P$	$z\ ^5S^\circ z\ ^5P^\circ y\ ^5D^\circ$ $y\ ^3S^\circ y\ ^3P^\circ y\ ^3D^\circ$	
(^2G)	$a\ ^3G$ $b\ ^1G$	$y\ ^3F^\circ x\ ^3G^\circ z\ ^3H^\circ$ $z\ ^1F^\circ z\ ^1G^\circ z\ ^1H^\circ$	
(^2P)	$b\ ^3P$ $a\ ^1P$	$z\ ^3S^\circ z\ ^3P^\circ w\ ^3D^\circ$ $z\ ^1S^\circ z\ ^1P^\circ y\ ^1D^\circ$	
(^2H)	$a\ ^3H$ $a\ ^1H$	$y\ ^3G^\circ y\ ^3H^\circ z\ ^3I^\circ$ $y\ ^1G^\circ y\ ^1H^\circ z\ ^1I^\circ$	
$(a\ ^2D)$	$a\ ^3D$ $b\ ^1D$	$x\ ^3P^\circ x\ ^3D^\circ x\ ^3F^\circ$ $y\ ^1P^\circ z\ ^1D^\circ y\ ^1F^\circ$	
(^2F)	$c\ ^3F$ $a\ ^1F$	$v\ ^3D^\circ w\ ^3F^\circ w\ ^3G^\circ$ $x\ ^1D^\circ x\ ^1F^\circ x\ ^1G^\circ$	
$(b\ ^2D)$	$b\ ^3D$	$w\ ^3P^\circ u\ ^3D^\circ v\ ^3F^\circ$	
$4d^8\ 5s\ 5p$		1 to 7° Inclusive	

7. References

[1] C. E. Moore, Atomic Energy Levels, NBS Circ. 467, III 1958.
[2] G. Racah, Bull. Res. Council of Israel Sect. F **1,** 1 (1959); G. Racah and Y. Shadmi, Bull. Res. Council of Israel Sect. F **1,** 15 (1959).
[3] A. G. Shenstone, J. Opt. Soc. Am. **44,** 749 (1954).
[4] J. Reader, K. W. Meissner, and K. L. Andrew, J. Opt. Soc. Am. **50,** 221 (1960).
[5] P. G. Wilkinson, J. Opt. Soc. Am. **45,** 862 (1955).
[6] J. H. Findlay, Phys. Rev. **36,** 5 (1930).
[7] M. A. Catalán, F. Rohrlich, and A. G. Shenstone, Proc. Roy. Soc. **221,** 421 (1954).

(Paper 67A2–197)

JOURNAL OF RESEARCH of the National Bureau of Standards—A. Physics and Chemistry
Vol. 67A, No. 2, March–April 1963

Broadening of the Rotational Lines of Carbon Monoxide by HCl and by Argon[1]

R. J. Thibault, J. H. Jaffe,[2] and Earle K. Plyler

(November 2, 1962)

The present work deals with the broadening of rotational lines of the carbon monoxide 2–0 band by both argon and hydrogen chloride. A high resolution grating spectrometer with a spectral slit width of 0.07 cm^{-1} was used, necessitating only a small correction in observed half-width values. Sufficiently small contributions of CO self-broadening were obtained by using long pathlength cells of 12 meters for CO-argon mixture and 1 meter for CO-HCl mixture. Half-width results, which are considered accurate to within ±5 percent, are presented in the form of a table and by a graph.

It is to be hoped that the study of widths, shapes, and shifts of lines in molecular absorption spectra will eventually lead to a wealth of information about intermolecular forces. While the results obtained thus far have not been incorporated into a more complete kinetic theory, a considerable amount of information regarding molecular interactions has been obtained at high pressures by Vodar [1].[3] He has shown that diatomic molecules at pressures greater than 40 atm lose their individual rotational lines and develop a Q branch. At lower pressures the rotational lines are broadened by an increase in pressure.

Several interesting phenomena have been observed. Most interesting is the J-dependence of line width and shift. That is to say, in a given absorption band, each individual line is broadened and shifted differently. The majority of the published work has been on HCl gas pressurized by itself and by a variety of foreign gases. HCl was an obvious first choice because it has a simple spectrum with well reported and fairly wide lines. But in order to extend the range of observations it is now desirable to make measurements on other molecules.

Self-broadening of carbon monoxide lines has been measured [2, 3, 4] and foreign gas broadening of CO due to CO_2 has been also reported [5]. In this study the broadening of lines in the 2–0 band of CO due to argon and HCl was determined. These lines are narrow and a spectrometer of very high resolving power is required. Line width is proportional to the pressure of the broadening gas and better accuracy is obtained by using high pressures. In practice a compromise must be drawn between the advantages of broad lines and the difficulties of making reliable corrections for the overlapping of adjacent lines.

The spectrometer used was the grating instrument described by Plyler and Blaine [6], used double passed. In the region of the band under study the spectral slit width was 0.07 cm^{-1}.

The half width γ of a line is defined as half its width at half its maximum height on the plot of extinction coefficient (in cm^{-1}) versus frequency (in cm^{-1}). The half width of a line in the spectrum of a mixture of gases may be expressed as the sum of contributions from each component of the mixture

$$\gamma=\gamma_A^0 P_A+\Sigma\gamma_i^0 P_i$$

where γ_A^0 is the broadening constant (in cm^{-1} atm^{-1}) of the absorbing gas and γ_i^0 the broadening constant of the ith foreign gas. The half widths of the lines actually observed were between 0.1 and 0.2 cm^{-1}. The ratio of slit width to line width was between 0.3 and 0.1, and accordingly small enough to make possible the accurate application of direct-instrumental corrections after the manner of Kostkowski and Bass [7]. The correction tables of Izatt [8] were used for the purpose, since these embrace a larger range of values than those presented by Kostkowski and Bass. The instrumental correction to the line half width amounted in most cases to between 1 and 5 percent and the largest correction was 8 percent.

It was decided not to depend upon the published values for the self-broadening constant of CO and for this reason long absorbing paths were used so that the quantity of CO was negligible by comparison with the quantity of foreign gas broadener.

The broadening constants listed in the table were calculated from the spectra of samples under the following conditions:

3 mm CO+4 atm argon; pathlength 12 M
20 mm CO+3 atm argon; pathlength 12 M
50 mm CO+2.22 atm HCl; pathlength 1 M

[1] This work was supported in part by the Cambridge Air Force Research Center.
[2] Guestworker from the Weizmann Institute of Science, Rehovoth, Israel.
[3] Figures in brackets indicate the literature references at the end of this paper.

The unsmoothed results are shown in table 1. Each point in figure 1 represents the mean of the values for corresponding lines in the P and R branches.

Babrov, Ameer, and Benesch [9] have reported the widths of HCl lines broadened by CO. This is the first available set of data on line widths with complementary pairs of gases. It is hoped that by using the combined data and by making plausible assumptions about the relationship between the partial collision diameters in the two cases, direct information about interaction energies will be forthcoming. Calculations along these lines are in progress.

TABLE I. γ° (cm^{-1} atm^{-1}) *of* CO *lines due to broadening by* HCl *and by* Ar

|m|	γ°_{HCl}		γ°_{Ar}	
	P-branch	*R* branch	*P*-branch	*R*-branch
1	0.096	0.095	0.069	0.070
2	.081	.090	.064	.063
3	.082	.081	.058	.057
4	.079	.078	.056	.051
5	073	073	.052	.048
6	.075	.078	.049	.048
7	.072	.075	.045	.046
8	.077	.073	.042	.043
9	.075	.070	.042	.043
10	.079	.076	.044	.041
11	.076	.075	.043	.042
12		.075	.042	.041
13		.071		.041
14	.074	.073	.042	.042
15		.073		.038
16		.072		.042
17	.073	.072		.042
18		.072		.042
19		.072	.040	.035
20			.039	.038
21			.037	.036
22				.033
23				.036

NOTE: While the present work was in process of publication, values for the half-width parameters of CO broadened by argon were reported by Rank and co-workers. See D. H. Rank, D. P. Eastman, B. S. Rao, and T. A. Wiggins, J. Mol. Spec. **10,** 34 (1963).

(Paper 67A2–198)

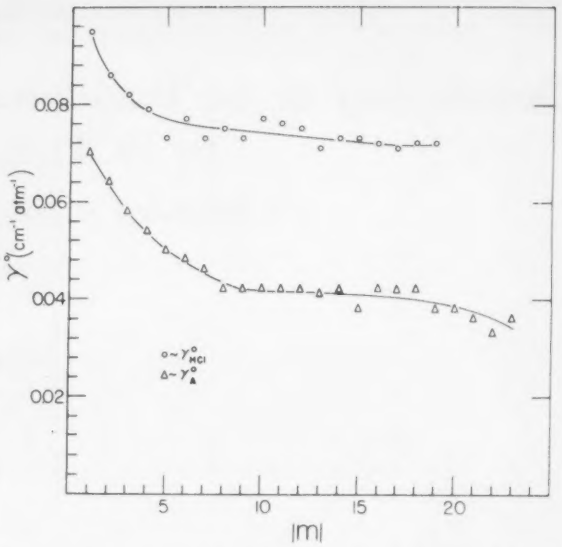

FIGURE 1.—*A plot showing the broadening constants,* γ° (cm^{-1} atm^{-1}), *for* CO *lines of the 2–0 band as a function of* |m|.

The circles represent the broadening produced by HCl and the triangles represent the broadening produced by argon.

References

[1] G. C. Turrell, H. Vu, and B. Vodar, J. Chem. Phys. **33,** 315 (1960).

[2] D. R. Eaton and H. W. Thompson, Proc. Roy. Soc. London, **A251,** 475 (1959).

[3] H. J. Kostkowski and A. M. Bass, J. Quant. Spectroy. Radiative Transfer **1,** 177 (1961).

[4] W. S. Benedict, R. Herman, G. Moore, and S. Silverman, Astrophys. J. **135,** 277 (1962).

[5] Earle K. Plyler and R. J. Thibault, J. Research NBS **66A,** 435 (1962).

[6] E. K. Plyler and L. R. Blaine, J. Research NBS **62,** 7 (1959).

[7] H. J. Kostkowski and A. M. Bass, J. Opt. Soc. Am. **46,** 1960 (1956).

[8] J. R. Izatt, Progress Report, J. Hopkins Univ., Lab. of Astrophys. and Phys. Meteorology (1960).

[9] H. Babrov, G. Ameer, and W. Benesch, J. Chem. Phys. **33,** 145 (1960).

JOURNAL OF RESEARCH of the National Bureau of Standards—A. Physics and Chemistry
Vol. 67A, No. 2, March–April 1963

Theory of Frustrated Total Reflection Involving Metallic Surfaces

T. R. Young and B. D. Rothrock

(November 30, 1962)

The theory for frustrated total reflection has been developed for the case where the third medium is metallic of complex index. Using parallel polarized light a unique minimum in reflectance occurs at a definite film thickness. Experimental verification of the theory is made and indicates the theory applicable to the precise measurement of thin contact films existing between metallic and dielectric surfaces.

1. Introduction

In the field of precise length measurement there exists the need to measure precisely the proximity of two surfaces. One or both surfaces may be plane. Frequently at least one of the surfaces is transparent to visible light. For instance, in the interferometric determinations of the lengths of metallic end standards called gage blocks, a transparent plate may be contacted to one of the end surfaces and the optical length between the surface of this plate and the noncontacted surface of the gage block is determined. The practical length, or calibrated length, of the gage block is obtained from the optical length by correcting for the phase change difference occurring at reflection from the two dissimilar surfaces. Thus the practical length of the gage block is dependent upon the thickness of the film existing between the contacted surfaces. A transparent contacting plate, usually of quartz, is often used rather than a plate of material similar to the metallic gage block to facilitate visual examination of the contacted surfaces. A satisfactory contacting is considered to be one that provides a uniform grayness over the contacted area.

The literature indicates some inconsistency in the measured values of wringing film thickness. These measurements range from -2.4 to $+2.8$ μin. for lapped metallic surfaces. For optically polished glass surfaces, the recent measurements by Bruce and Thornton [1] [1] indicate a variation in thickness for different surfaces of ± 0.4 μin. Negative values are explained by the investigators as being caused by an intermeshing of the high points of the surfaces. Although some of this inconsistency in results may be due to systematic error or the use of questionable assumptions, there is a distinct possibility that wringing film thickness is dependent upon the material forming the surface, the planeness of the surfaces involved and the surface finish. However, there is evidence that the film thickness is not critically dependent upon the type of oil used as a wringing agent where this is employed to purposely contaminate lapped surfaces to facilitate contacting [2, 3]. Furthermore, whereas different values of wringing film thickness have been reported, many investigators agree that the thickness of a wringing film between two given surfaces is repeatable to a fraction of a microinch [1, 2, 3].

For the measurement of the practical length of gage blocks to an accuracy of 0.1 μin., it is obvious that stringent control and measurement of wringing film thickness are required. Practically speaking, it is useless to devise methods of length measurement of gage blocks that eliminate wringing films when the blocks measured will eventually be used in wring combinations with other blocks to achieve specifically desired lengths. What seems to be required is a measurement facility that will directly determine the wringing film thickness between two surfaces to an accuracy better than 0.01 interference fringe (0.1 μin.).

Another common occurrence that arises in length measurements is the need to measure the proximity of a plane surface and a spherical surface. This proximity may be either posi-

[1] Figures in brackets indicate the literature references at the end of this paper.

tive or negative, negative in the sense that a contacting of a spherical and plane surface will result in deformation if a contact pressure is present. Although this deformation may be determined theoretically, it is questionable in all cases, particularly in the case of small contact pressure, that the theoretical assumptions are valid. In the case of positive proximity, an interference pattern of Newton's Rings is frequently used to determine the distance between a plane and the vertex of a spherical surface. Figure 1A shows such a pattern formed between a glass surface and a steel ball. The diameter of at least one ring is obtained for each of several wavelengths of light. Knowing the approximate diameter, the distance between the plane and the ball can be determined by extrapolating the fractional order patterns to the vertex and applying the method of coincidences. As in all interference length measurements, correction for phase change at reflection must be made, but in this case correction for dispersion of phase change is also required. Furthermore, the distance between ball and plane must be held constant during the time required to obtain interference patterns for each wavelength.

This paper indicates the results of an investigation into the possibility of employing frustrated total reflection to the problems described above.

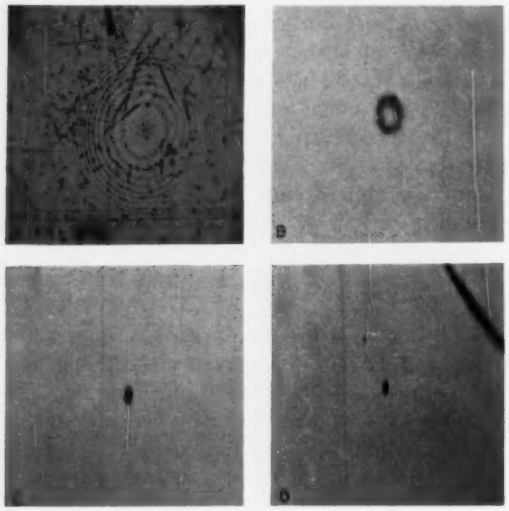

FIGURE 1A. *Newton's Rings obtained by interference between glass boundary surface and steel ball of figure 9.*

Angle of incidence is less than the critical angle. B,C,D. Reflectance patterns obtained by frustrated total reflection at angles 45, 65, and 75°.

2. Theory

Total internal reflection occurs when light is incident at an angle θ upon an interface between two media having indices of refraction μ_1 and μ_2 such that $\frac{\mu_1}{\mu_2} \sin \theta > 1$ where $\mu_1 > \mu_2$. Here μ_1 and μ_2 refer to the refractive indices of the incident and refractive media respectively. However, the energy associated with the incident light is transmitted into the refractive medium a short distance before it returns into the incident medium [4].

If a third material is positioned in the region of this energy transmission, this material will transmit or absorb part of the energy and prevent its return to the incident medium. This effect is referred to as frustrated total reflection.

It has been shown that for an all-dielectric system, the relative amount of energy intercepted depends upon the polarization of the incident light, the thickness of the refractive film, the optical constants of the three media involved, the wavelength of the incident light and the angle of incidence [5].

In this development of the theory of frustrated total reflection involving metallic frustrating media, it is assumed that a right-hand coordinate system, as shown in figure 2, is used.

Light from the positive Z space having a refractive index μ_1 is incident at an angle θ_1 upon an interface represented by the xy plane at $Z=0$. A dielectric film of refractive index μ_2 exists between planes $Z=0$ and $Z=-d$. Let θ_2 represent the angle of refraction in this medium. A boundary surface exists at $Z=-d$, forming an interface between the dielectric film and a medium having refractive index μ_3, where μ_3 may be complex. Let θ_3 represent the angle of refraction in this medium.

The electric vectors represented in figure 2 are the resultant of all incident, transmitted, and reflected waves. For instance, E'_{1p} is the resultant of parallel polarizations of all components that are contributed by multireflections from surfaces at $Z=0$ and $Z=-d$.

The components of the electric vectors polarized in the plane of incidence are indicated by $E_{\nu p}$ where ν is an integer indicating the medium. Prime quantities refer to components associated with reflected waves. Positive components are indicated by the arrows in figure 2. Components of the electric vectors polarized perpendicularly to the plane of incidence are indicated by $E_{\nu s}$. Positive components of $E_{\nu s}$ have a direction parallel to the positive y axis.

In general, the parallel and the perpendicular components of the electric vectors may be expressed by

$$
\begin{aligned}
E_{\nu s} &= A_{\nu s} e^{i\left[\omega t - \frac{2\pi}{\lambda_\nu}(x \sin\theta_\nu - Z_\nu \cos\theta_\nu)\right]} && \nu = 1, 2, 3 \\
E_{\nu p} &= A_{\nu p} e^{i\left[\omega t - \frac{2\pi}{\lambda_\nu}(x \sin\theta_\nu - Z_\nu \cos\theta_\nu)\right]} && Z_1 = Z,\ \infty \geq Z \geq 0 \\
E'_{\nu s} &= A'_{\nu s} e^{i\left[\omega t - \frac{2\pi}{\lambda_\nu}(x \sin\theta_\nu + Z_\nu \cos\theta_\nu)\right]} && Z_2 = Z,\ 0 \geq Z \geq -d \\
E'_{\nu p} &= A'_{\nu p} e^{i\left[\omega t - \frac{2\pi}{\lambda_\nu}(x \sin\theta_\nu + Z_\nu \cos\theta_\nu)\right]} && Z_3 = Z,\ -d \geq Z \geq -\infty
\end{aligned}
\qquad (1)
$$

where

A is the amplitude of the electric vector
ω is the angular velocity
t is the time

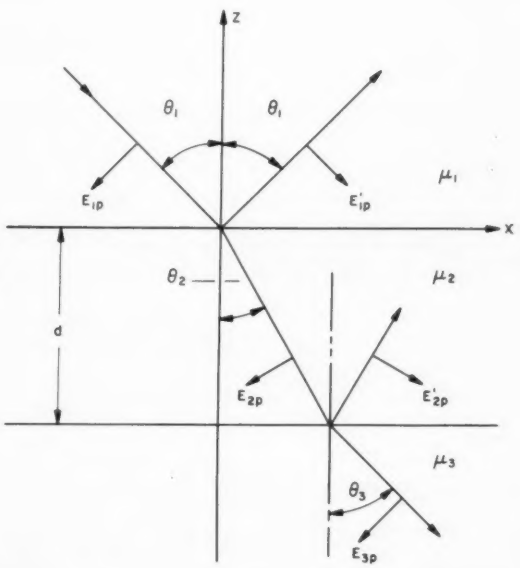

FIGURE 2. *Representation of the resultant electric vectors of light polarized parallel to the plane of incidence for all incident, reflected, and transmitted waves.*

Plane of incidence is in the plane of the paper.

and λ_ν is the wavelength in medium ν.

From Snell's Law

$$\sin\theta_1 = n_{12}\sin\theta_2$$
$$\sin\theta_2 = n_{23}\sin\theta_3 \tag{2}$$

where

$$n_{12} = \frac{\mu_2}{\mu_1}$$

and

$$n_{23} = \frac{\mu_3}{\mu_2}.$$

Applying the conditions of continuity for electromagnetic waves at the boundaries $Z=0$ and $Z=-d$, the relationships between amplitudes are obtained.

For the polarization perpendicular to the plane of incidence

$$A_{1s} + A'_{1s} = A_{2s} + A'_{2s}$$
$$A_{1s} - A'_{1s} = (A_{2s} - A'_{2s}) n_{12} \frac{\cos\theta_2}{\cos\theta_1}$$
$$A_{2s}e^{u} + A'_{2s}e^{-u} = A_{3s}e^{q}$$
$$A_{2s}e^{u} - A'_{2s}e^{-u} = A_{3s}e^{q} n_{23} \frac{\cos\theta_3}{\cos\theta_2} \tag{3}$$

and for the polarization parallel to the plane of incidence

$$A'_{1p} - A_{1p} = (A'_{2p} - A_{2p}) \frac{\cos\theta_2}{\cos\theta_1}$$
$$A'_{1p} + A_{1p} = n_{12}(A_{2p} + A'_{2p})$$
$$A'_{2p}e^{-u} - A_{2p}e^{u} = -A_{3p}e^{q} \frac{\cos\theta_3}{\cos\theta_2}$$
$$A'_{2p}e^{-u} + A_{2p}e^{u} = n_{23}A_{3p}e^{q} \tag{4}$$

where

$$u = \frac{-i2\pi\mu_2 d\cos\theta_2}{\lambda_0}$$

and

$$q = \frac{-i2\pi\mu_3 d\cos\theta_3}{\lambda_0}$$

where

λ_0 = vacuum wavelength.

The ratios of the reflected to the incident amplitudes are obtained for the perpendicular and for the parallel polarizations by the use of eqs (3) and (4), respectively.

$$\frac{-A'_{1s}}{A_{1s}} = \frac{\cosh u\left(1 - \dfrac{\cos\theta_1}{n_{12}n_{23}\cos\theta_3}\right) + \sinh u\left(\dfrac{\cos\theta_1}{n_{12}\cos\theta_2} - \dfrac{\cos\theta_2}{n_{23}\cos\theta_3}\right)}{\cosh u\left(1 + \dfrac{\cos\theta_1}{n_{12}n_{23}\cos\theta_3}\right) - \sinh u\left(\dfrac{\cos\theta_1}{n_{12}\cos\theta_2} + \dfrac{\cos\theta_2}{n_{23}\cos\theta_3}\right)} \tag{5}$$

and

$$\frac{A'_{1p}}{A_{1p}} = \frac{\cosh u\left(\dfrac{\cos\theta_3}{n_{12}n_{23}\cos\theta_2} - \dfrac{\cos\theta_1}{\cos\theta_2}\right) + \sinh u\left(\dfrac{\cos\theta_1\cos\theta_3}{n_{23}\cos^2\theta_2} - \dfrac{1}{n_{12}}\right)}{\sinh u\left(\dfrac{\cos\theta_1\cos\theta_3}{n_{23}\cos^2\theta_2} + \dfrac{1}{n_{12}}\right) - \cosh u\left(\dfrac{\cos\theta_3}{n_{12}n_{23}\cos\theta_2} + \dfrac{\cos\theta_1}{\cos\theta_2}\right)}. \tag{6}$$

For the condition of total internal reflection

$$\frac{\sin^2\theta_1}{n_{12}^2}>1$$

and from eq (2)

$$\cos\theta_2=\frac{-i}{n_{12}}\sqrt{\sin^2\theta_1-n_{12}^2}\ ^{2}. \tag{7}$$

Using this value of $\cos\theta_2$ in eqs (5) and (6), the ratio of reflected to incident amplitudes are

$$\frac{-A'_{1s}}{A_{1s}}=\frac{\sinh u[\sin^2\theta_1-n_{12}^2+n_{12}n_{23}\cos\theta_1\cos\theta_3]+i\sqrt{\sin^2\theta_1-n_{12}^2}[\cos\theta_1-n_{12}n_{23}\cos\theta_3]\cosh u}{\sinh u[\sin^2\theta_1-n_{12}^2-n_{12}n_{23}\cos\theta_1\cos\theta_3]-i\sqrt{\sin^2\theta_1-n_{12}^2}[\cos\theta_1+n_{12}n_{23}\cos\theta_3]\cosh u} \tag{8}$$

for the perpendicular polarization, and

$$\frac{A'_{1p}}{A_{1p}}=\frac{\sinh u[n_{12}^3\cos\theta_1\cos\theta_3+n_{23}(\sin^2\theta_1-n_{12}^2)]-i\sqrt{\sin^2\theta_1-n_{12}^2}[n_{12}\cos\theta_3-n_{12}^2n_{23}\cos\theta_1]\cosh u}{\sinh u[n_{12}^3\cos\theta_1\cos\theta_3-n_{23}(\sin^2\theta_1-n_{12}^2)]+i\sqrt{\sin^2\theta_1-n_{12}^2}[n_{12}\cos\theta_3+n_{12}^2n_{23}\cos\theta_1]\cosh u} \tag{9}$$

for the parallel polarization.

Equations (8) and (9) may be used to determine the magnitude and phase of the reflected electric vector when an all-dielectric system is being considered. For such a system the reflectance for the perpendicular component is given by

$$R_s=\frac{A'_{1s}A'^{*}_{1s}}{A_{1s}^2}=\frac{B-C}{B+C} \tag{10}$$

where

$$B=n_{12}^2(1-n_{23}^2)(n_{12}^2-1)\sinh^2 u-(\sin^2\theta_1-n_{12}^2)[2\sin^2\theta_1-n_{12}^2n_{23}^2-1]$$

$$C=2(\sin^2\theta_1-n_{12}^2)\cos\theta_1\sqrt{n_{12}^2n_{23}^2-\sin^2\theta_1}$$

and the reflectance for the parallel component is given by

$$R_p=\frac{A'_{1p}A'^{*}_{1p}}{A_{1p}^2}=\frac{D+E}{D-E} \tag{11}$$

where

$$D=\frac{(\sin^2\theta_1-n_{12}^2)}{n_{23}^2}[n_{12}^2n_{23}^2(1+n_{12}^2n_{23}^2)-\sin^2\theta_1(1+n_{12}^4n_{23}^4)]$$

$$+\frac{\sinh^2 u}{n_{23}^2}[\sin^2\theta_1(1-n_{12}^4)+n_{12}^2(n_{12}^2-1)][(n_{23}^4-1)\sin^2\theta_1+n_{12}^2n_{23}^2(1-n_{23}^2)]$$

$$E=-2n_{12}^2\cos\theta_1(\sin^2\theta_1-n_{12}^2)\sqrt{n_{12}^2n_{23}^2-\sin^2\theta_1}.$$

When the frustrating medium has a complex refractive index, i.e., when $\mu_3=n(1-i\alpha)$ where n is the refractive index and α is the absorption index, n_{23} and $\cos\theta_3$ become complex and eqs (8) and (9) must be modified. From eq (2),

$$\cos\theta_3=\frac{-1}{n_{12}n_{23}}\sqrt{n_{12}^2n_{23}^2-\sin^2\theta_1}\ ^{3}$$

and

$$n_{23}=\frac{n(1-i\alpha)}{\mu_2}.$$

---

[2] The sign of $\cos\theta_2$ is chosen negative as this results in a dampening of the electric vector E_2 as it progresses in the film medium in a negative z direction.

[3] The sign of $\cos\theta_3$ is chosen negative as this results in a dampening of the electric vector E_3 as it progresses in the frustrating medium in a negative z direction.

Applying these expressions to eqs (8) and (9), one obtains for the perpendicular polarization,

$$\frac{-A'_{1s}}{A_{1s}}=\frac{\left[\begin{array}{l}\sinh u\left[\sin^2\theta_1-n_{12}^2-\rho^{1/2}\cos\theta_1\cos\frac{\phi}{2}\right]-\rho^{1/2}(\sin^2\theta_1-n_{12}^2)^{1/2}\sin\frac{\phi}{2}\cosh u\\ -i\left[\rho^{1/2}\cos\theta_1\sin\frac{\phi}{2}\sinh u-(\sin^2\theta_1-n_{12}^2)^{1/2}\left(\cos\theta_1+\rho^{1/2}\cos\frac{\phi}{2}\right)\cosh u\right]\end{array}\right]}{\left[\begin{array}{l}\sinh u\left[\sin^2\theta_1-n_{12}^2+\rho^{1/2}\cos\theta_1\cos\frac{\phi}{2}\right]-\rho^{1/2}(\sin^2\theta_1-n_{12}^2)^{1/2}\sin\frac{\phi}{2}\cosh u\\ +i\left[\rho^{1/2}\cos\theta_1\sin\frac{\phi}{2}\sinh u-(\sin^2\theta_1-n_{12}^2)^{1/2}\left(\cos\theta_1-\rho^{1/2}\cos\frac{\phi}{2}\right)\cosh u\right]\end{array}\right]} \tag{12}$$

and for the parallel polarization,

$$\frac{A'_{1p}}{A_{1p}}=\frac{\left[\begin{array}{l}\left[n_{12}^2\mu_2^2\rho^{1/2}\cos\theta_1\cos\frac{\phi}{2}-n^2(1-\alpha^2)(\sin^2\theta_1-n_{12}^2)\right]\sinh u\\ +\left[\mu_2^2\rho^{1/2}\sin\frac{\phi}{2}-2n_{12}^2n^2\alpha\cos\theta_1\right](\sin^2\theta_1-n_{12}^2)^{1/2}\cosh u\\ +i\left\{\sinh u\left[n_{12}^2\mu_2^2\rho^{1/2}\cos\theta_1\sin\frac{\phi}{2}+2n^2\alpha(\sin^2\theta_1-n_{12}^2)\right]\right.\\ \left.-\cosh u\left[\mu_2^2\rho^{1/2}\cos\frac{\phi}{2}+n_{12}^2n^2(1-\alpha^2)\cos\theta_1\right][\sin^2\theta_1-n_{12}^2]^{1/2}\right\}\end{array}\right]}{\left[\begin{array}{l}\left[n_{12}^2\mu_2^2\rho^{1/2}\cos\theta_1\cos\frac{\phi}{2}+n^2(1-\alpha^2)(\sin^2\theta_1-n_{12}^2)\right]\sinh u\\ -\left[\mu_2^2\rho^{1/2}\sin\frac{\phi}{2}+2n_{12}^2n^2\alpha\cos\theta_1\right][\sin^2\theta_1-n_{12}^2]^{1/2}\cosh u\\ +i\left\{\sinh u\left[n_{12}^2\mu_2^2\rho^{1/2}\cos\theta_1\sin\frac{\phi}{2}-2n^2\alpha(\sin^2\theta_1-n_{12}^2)\right]\right.\\ \left.+\cosh u\left[\mu_2^2\rho^{1/2}\cos\frac{\phi}{2}-n_{12}^2n^2(1-\alpha^2)\cos\theta_1\right][\sin^2\theta_1-n_{12}^2]^{1/2}\right\}\end{array}\right]} \tag{13}$$

where,

$$\rho=+\sqrt{\left[\frac{n_{12}^2n^2(1-\alpha^2)}{\mu_2^2}-\sin^2\theta_1\right]^2+\frac{4n_{12}^4n^4\alpha^2}{\mu_2^4}}$$

$$\sin\phi=-\frac{2n_{12}^2n^2\alpha}{\mu_2^2\rho}$$

$$\cos\phi=\frac{n_{12}^2n^2(1-\alpha^2)-\mu_2^2\sin\theta_1}{\mu_2^2\rho}.$$

Equations (12) and (13) may be used to determine the magnitude and phase of the reflected electric vector when the frustrating medium has a complex refractive index, e.g., a metallic material. Reflectance equations similar to eqs (10) and (11), but for the case where μ_3 is complex are given by eqs (14) and (15).

$$R_s=\frac{A'_{1s}A'^{*}_{1s}}{A_{1s}^2} \tag{14}$$

$$R_p=\frac{A'_{1p}A'^{*}_{1p}}{A_{1p}^2}. \tag{15}$$

Numerical calculations of reflectance can be obtained by evaluating eqs (12) and (13) and multiplying by the numerical complex conjugate.

For an all-dielectric system where $\mu_1=\mu_3=1.72$; $\mu_2=1.38$; $\theta=60°$; the reflectance relationship to film thickness as calculated from eqs (10) and (11) is identical to that calculated by Vasicek [6]. The solid curves of figure 3 are also calculated from eq (10). They show the theoretical relationships of reflectance to film thickness of air between the surfaces of glass having a refractive index of 1.5. The abscissa indicates the film thickness in microinches and the ordinate represents the percentage of perpendicularly polarized mercury green light reflected. Curves for parallel-polarized light, calculated from eq (11), have the same form but exhibit somewhat better sensitivity at larger angles of incidence. For instance, as the film increases from 0 to 0.2 μin. the intensity of the reflected light incident at 80° increases from 0 to 10 percent.

The broken curve of figure 3 results from calculation of eq (14). The curve shows the theoretical relationship between reflectance of perpendicular polarized light and a film thickness of air existing between a "totally reflecting" glass surface and a steel surface. Curves for angles of incidence less than 80° intercept the ordinate axis at lower values of reflectance but do not change their slope to any significant degree.

Curves derived from calculations of eq (15) are much more interesting. Figure 4 shows, for different angles of incidence, theoretical relationships between reflectance of parallel polarized light and a film thickness of air existing between a "totally reflecting" glass surface and a steel surface. Of significance, is the formation of a minimum occurring at a film thickness dependent upon the angle of incidence. Furthermore, there is indicated a sensitivity in the reflectance to film thickness relationship that essentially equals the sensitivity obtained in the dielectric case. Unlike the dielectric case, a considerable increase in reflectance is obtained as the film thickness approaches zero. The form of the curves shows theoretically that a measurement of reflectance to 1 percent could indicate the thickness of a very thin film of air to an accuracy of 20 billionths of an inch.

From the form of the curves in figure 4 it is apparent that for a very thin film of varying thickness a pattern of minimum reflectance should be obtained resembling an interference fringe of equal thickness. Unlike an interference fringe pattern, only one minimum should be obtained, corresponding to a thickness of film dependent upon the angle of incidence. Therefore no ambiguity concerning the order of interference should exist. Another important difference arises from the sharpness of the reflectance dip obtained for larger angles of incidence. For instance, the half width of a conventional two-beam interference fringe corresponds to approximately 5 millionths of an inch variation in film thickness whereas the half width of these dips can be less than 1 millionth of an inch.[4]

[4] Defining the half width of an unsymmetrical dip is somewhat arbitrary. In this instance the half width is defined as the width of the dip at that reflectance equal to the minimum reflectance plus one-half the difference in reflectance between the minimum value and the value at zero film thickness.

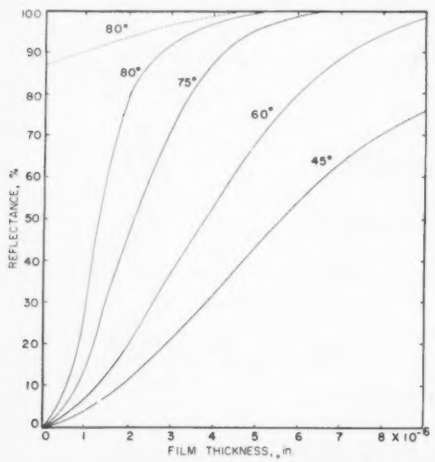

FIGURE 3. *Variation of reflectance with film thickness of air at various angles of incidence of perpendicular polarized light.*

Solid lines are calculated from eq (10) for an all dielectric case. The dotted line obtained from eq (14) is for the case where μ_3 is a steel surface of complex index.

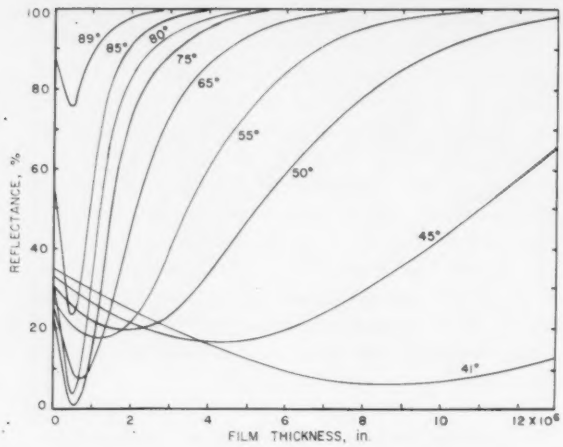

FIGURE 4. *Variation of reflectance with film thickness of air at various angles of incidence of parallel polarized light for the case where μ_3 is of complex index.*

The curves are calculated from eq (15). Note the unique minima obtained in the reflectance.

The film thicknesses at which the minima are obtained can be calculated from the following equation.

$$d=\frac{-\lambda_0}{4\pi\mu_1(\sin^2\theta_1-n_{12}^2)^{1/2}}\cdot\ln\left[\frac{(AE-BD)\pm\sqrt{(BD-AE)^2-[F(A+B)-C(D+E)][F(B-A)+C(D-E)]}}{F(A+B)-C(D+E)}\right] \quad (16)$$

where

$$A=(a-b)^2+(c-\delta)^2+(e+f)^2+(g+h)^2$$

$$B=2[(a-b)(c-\delta)-(e+f)(g+h)]$$

$$C=(c-\delta)^2+(g+h)^2-(a-b)^2-(e+f)^2$$

$$D=(a+b)^2+(c+\delta)^2+(e-f)^2+(g-h)^2$$

$$E=2[(e-f)(g-h)-(a+b)(c+\delta)]$$

$$F=(c+\delta)^2+(g-h)^2-(a+b)^2-(e-f)^2$$

where

$$a=n_{12}^2\mu_2^2\rho^{1/2}\cos\frac{\phi}{2}\cos\theta_1$$

$$b=n^2(1-\alpha^2)(\sin^2\theta_1-n_{12}^2)$$

$$c=\mu_2^2\rho^{1/2}\sin\frac{\phi}{2}(\sin^2\theta_1-n_{12}^2)^{1/2}$$

$$\delta=2n_{12}^2n^2\alpha\cos\theta_1(\sin^2\theta_1-n_{12}^2)^{1/2}$$

$$e=n_{12}^2\mu_2^2\rho^{1/2}\sin\frac{\phi}{2}\cos\theta_1$$

$$f=2n^2\alpha(\sin^2\theta_1-n_{12}^2)$$

$$g=\mu_2^2\rho^{1/2}\cos\frac{\phi}{2}(\sin^2\theta_1-n_{12}^2)^{1/2}$$

$$h=n_{12}^2n^2(1-\alpha^2)\cos\theta_1(\sin^2\theta_1-n_{12}^2)^{1/2}.$$

Equation 16 is derived by differentiating eq (15) with respect to the function u. Setting the differential to zero, solving for u and applying eq (7) to the expression for u in eq (4), one obtains eq (16).

By varying the constants μ_1, μ_2, μ_3, λ in eq (13) the location of the minimum is changed as is indicated in figures 5, 6, 7, 8.[5] Variation of μ_3 and λ does not significantly change the location of the minimum and no major increase in sensitivity is noticed. However, with an increase in the optical constant, μ_1, or the ratio $\frac{\mu_1}{\mu_2}$, the minimum forms at smaller values of d and the sensitivity significantly increases as there is a larger change in reflectance with changes in d.

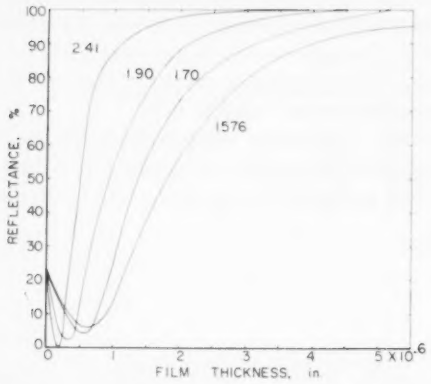

FIGURE 5. *Variation of reflectance with film thickness of air for increasing values of index of μ_1 as calculated from eq (15).*

The angle of incidence of parallel polarized light is 65°.

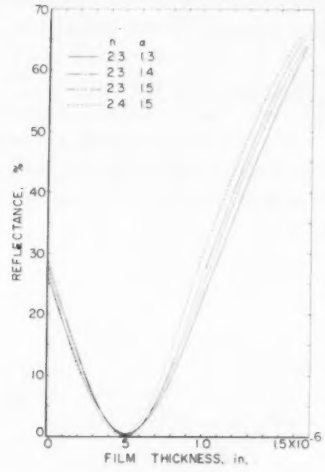

FIGURE 7. *Variation of reflectance with film thickness of air for various values of index of μ_3.*

The angle of incidence is 65°.

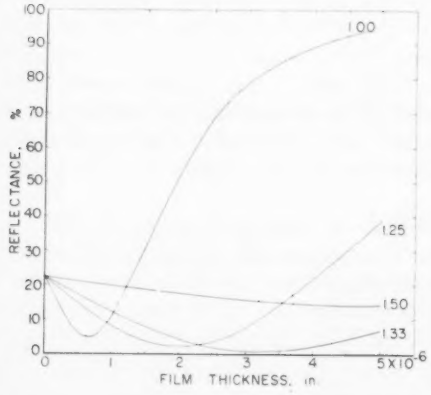

FIGURE 6. *Variation of reflectance with film thickness for increasing value of index of the film for parallel polarized light.*

The angle of incidence is 65°.

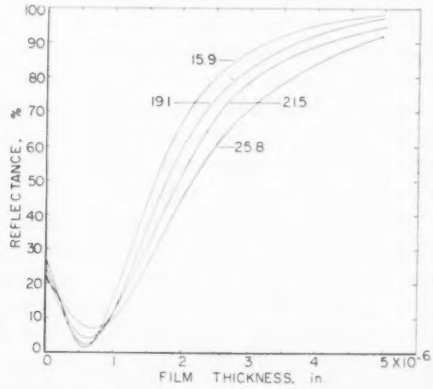

FIGURE 8. *Variation of reflectance with film thickness of air for various values of wavelength given in microinches.*

The angle of incidence is 65°.

[5] In calculations for varying wavelength, μ_1, and μ_3 were changed to account for dispersion of glass and steel.

3. Experimental Procedure

To experimentally verify the theoretical eqs (14), (15), and (16) the arrangement drawn in plane view in figure 9 was employed. A variable prism, consisting of a half cylinder of glass with two planoconcave cylindrical lenses of the same refractive index ($\mu_g = 1.576$) contacted to the surface with glycerine, was positioned on a lapped steel table of a spectrometer. The spectrometer rested on a table surface whose normal could be inclined through small angles from the vertical. The autocollimating telescope and the divided circle of the spectrometer were employed to aline each of the planoconcave cylindrical lenses so that the plane surfaces of the lenses formed included angles with the reflecting surface of the prism equal to the desired angle of incidence, θ. The prism assembly was then rotated so that the entrance window of the prism assembly was normal to a beam of plane polarized, collimated white light filtered with a mercury-green interference filter. Using the tilt table supporting the spectrometer, the normal to the spectrometer table was inclined one degree from the vertical in such a direction as to fall in the plane defined by the vertical axis and the normal to the reflecting surface of the prism. A lapped S.A.E. 52100 steel ball of 1 in. diam and having a mass known to 1 percent was positioned on the spectrometer table. This platform served as an inclined plane holding the ball against the reflecting surface of the prism with a computed contact load of 0.1 g.

The telescope of the spectrometer was replaced with a calibrated microscope having a 32 mm objective and a 10X filar eyepiece. The microscope was positioned to receive the reflected beam and was focused on the totally reflecting surface of the prism at the point where the ball made contact.

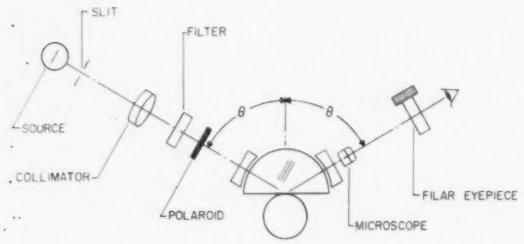

FIGURE 9. *Schematic outline of setup used in experimental verification of theory.*

The basic equipment consists of a spectrometer with the vertical axis of rotation being perpendicular to the plane of the paper. The prism, end caps, and ball rests on the spectrometer table with the ball held against the prism by a 0.1 g force due to a 1 deg tilt in the table.

4. Results

With the incident light perpendicularly polarized a slight diminishing in intensity of the reflected beam at and surrounding the point of contact was observed. This qualitatively verified the result indicated by eq (14) (see the broken line curve of figure 3). No minima were observed for this condition.

With the incident light parallel polarized, minima such as those predicted by eq (15) were obtained. Figure 1, B, C, D illustrates typical patterns observed at different angles of incidence larger than the critical angle. These elliptical patterns, having major diameters as small as 0.0015 in., were all obtained at the same magnification as that used for the Newton Ring pattern shown in figure 1A. The film thickness at which the minimum occurs is proportional to the second power of the diameter as measured along the major axis of the elliptical ring. The existence of a unique mimimum rather than the cyclic pattern shown in figure 1A, and the effect of increasing angle of incidence upon ring size, sharpness, and contrast qualitatively verify eq (15) as represented by the calculated curves shown in figure 4. The irregularities of the ring pattern for 45°, shown in figure 1B, are considered to be the effect of surface irregularity of the steel ball. This same surface finish appears to have less effect on the minima obtained at larger angles of incidence.

A quantitative verification of eqs (15) and (16) was obtained by comparing the experimental determinations of film thickness at which the minima are formed with results derived from calculations of eq (16). To experimentally determine the film thickness x, the major diameters, $2y$, of the elliptical rings formed at known angles of incidence were measured with the calibrated filar eyepiece of the microscope. These measured values were applied to the sagittal equation

$$x=R-(R^2-y^2)^{1/2},$$

where R is the radius of the steel ball.

The experimental results are compared in table 1 with the theoretical results as determined by eq (16). The experimental results and the estimated error associated with the particular measurement indicate clearly the close agreement of experiment with theory. In every case except one the theory falls within the experimental error. The amount of error indicates primarily the ability of the observer to set a crosshair on the minimum ring. With increasing angle of incidence the pattern becomes sharper and therefore easier to set on.

TABLE 1. *Comparison between experimental and theoretical determinations of film thickness*

θ_1	Exp. values	Theor. values	Diff.
Degrees	*Microinches*	*Microinches*	*Microinches*
41	6.6±1.2	7.0	0.4
45	2.58±.24	2.60	.02
55	1.13±.15	.98	.15
65	.47±.12	.63	.16
75	.49±.09	.49	.00

In the theoretical determination no factor was used to compensate for the surface finish of the ball. However, agreement between theoretical and experimental values was essentially 0.1 μin. The predominant scratch depth of the ball was approximately 2 μin. This indicates the phenomena are practically independent of surface finish.

5. Conclusions

Preliminary investigation and results indicate the method of frustrated total reflection applicable to the precise measurement of thin films such as those existing between a dielectric and conductor. Significant in this investigation are that the measurements are independent of any phase change due to surface finish and the minimum obtained is single valued, eliminating the necessity of establishing an order as with fringes.

6. References

[1] C. F. Bruce and B. S. Thornton, J. Appl. Phys. **27,** 853 (1956).
[2] A. M. Dexter, ASTE **59,** Tech. Paper 195 (1959).
[3] F. H. Rolt and H. Barrell, Proc. Royal Soc. **A116,** 401 (1927).
[4] R. W. Ditchburn, Light, Interscience Publishers, Inc., N.Y., 434 (1955).
[5] E. E. Hall, Phys. Rev. **15,** 73 (1902).
[6] A. Vasicek, Optics of Thin Films, Trans. by Mrs. H. Watney-Kaczer, North Holland Pub. Company Amsterdam. Interscience Publishers, New York (1960).

(Paper 67A2–199)

JOURNAL OF RESEARCH of the National Bureau of Standards—A. Physics and Chemistry
Vol. 67A, No. 2, March–April 1963

Quantitative Metallography With a Digital Computer: Application to a Nb-Sn Superconducting Wire

G. A. Moore and L. L. Wyman

(November 20, 1962)

Accurate quantitative data pertinent to the structure of solid materials at the micro size level, which are difficult or prohibitive to obtain by traditional manual measurements, are now obtained directly by a digital computer which uses a photomicrograph as the information input. The history of picture interpretation experiments at the National Bureau of Standards is reviewed. The fundamental computer operations are illustrated, together with a description of 24 image processing routines now functional at a practical level.

A micrograph of a specimen of Nb-Sn superconductor wire is exhaustively analyzed. This specimen is found to contain approximately 70 percent Nb_3Sn, nearly all of which is mutually interconnected. It is also found that in this specimen the mean free path in the Nb_3Sn superconducting phase is only 26.5 microns. This small value results from the spongy structure of the material and numerous interruptions caused by voids and by particles of four other solid phases. The comparative importance of the several types of interruptions is measured. It is determined that small voids are the most important single cause of the short mean free path, and deduced that these voids appear to have formed mainly from the reaction during heat treatment.

1. Introduction

In any attempt to relate the fundamental structure of a solid material to its useful mechanical and physical properties, one is forced to recognize three basic levels of organization. At the smallest level, beginning at about 10^{-8} cm, atoms are organized into crystals of varying regularity and order, which may or may not contain molecular entities, and which usually incorporate imperfections such as vacancies, dislocations, and various larger defects. The properties of such individual crystals can be quantitatively determined by numerous measurements in the realm of physics, but frequently bear little direct relation to the gross properties of useful aggregates.

At the opposite end of the size scale, the properties of a useful piece of material are again quantitatively measured by the well standardized instruments of the engineer, and to some extent correlated with the gross chemical analysis and with semiquantitative parameters classed as the "material history." On the basis of such engineering properties, the material is incorporated into a structure or machine, within which it usually functions as expected.

Between these extreme levels of organization there falls the level of organization on the micro scale, in which dimensions will usually fall between 10^{-4} and 10^{-1} cm. At this level, individual particles, usually crystals, of one chemical identity or "phase," are orientated and joined to other similar particles or, more frequently, dispersed between particles of other phases. In the resulting aggregate, the physical and mechanical properties of the individual particles are combined in a very nonlinear manner to produce the engineering properties of the whole. A common analogy can be found in the fact that the strength of a masonry wall depends more on the skill with which the stones are cemented together than on the actual strength of either the stones or the cement. For inorganic materials, studies at this level fall into the closely parallel specialities of metallography and petrography, which use many techniques closely related to those of biological microscopy.

The traditional tool of the metallographer is the light microscope, which has in recent years been supplemented by the electron microscope for use on more minute structures, and the X-ray microscope for three dimensional studies. Elegant specialized methods have been developed for measuring some properties of individual particles; for example microspot spectrochemical analysis, microspot diffraction of X-rays or electrons, and micro-scale testing arrangements. Average crystal orientation data are obtained by X-ray diffraction and expressed in quantitative maps called "pole figures."

The use of the optical microscope for analysis of the phase systems in metallic materials offers certain specific advantages over the newer and more specialized methods. First, information is obtained on the shape and size distribution of the "grains" or phase particles, which information is very difficult to obtain by any other method. Second, optical examination includes a larger area than other

670682—63——4

methods, and thus more truly studies the whole material, as evidenced in part by the fact that the particles examined by specialized methods are usually first selected optically.

A cardinal rule of metallography requires that any *recorded* micrograph (photomicrograph) must be a true representation of the structural constituents of the whole material unless specifically stated to represent a special case. This assurance of validity can be achieved only by the critical examination of large areas of the specimen, or of several specimens, during which the metallographer accumulates a mental picture of an "average area," followed by the recording of one or several areas statistically representative of this average. An experienced metallographer, when examining a familiar structure or one in which the identity and nature of the phases is known, can deduce a good qualitative estimate of the properties of the material. With the aid of carefully prepared comparison standards, semiquantitative values can be obtained, but, unless numerous actual measurements are made on each micrograph, it is not feasible to obtain numerical data of a quality comparable with that of the specialized measurements on specific areas.

In most cases, the effort necessary to obtain a quantitative or mathematical description of the information displayed in a micrograph has been considered prohibitive. Thus while "there is no substitute for seeing" (Lucas), the information supplied by visual examination is under the best of circumstances only semiquantitative, and may sometimes prove to be misleading. The metallurgist has of necessity been forced to be satisfied with information not much better than a qualitative opinion based on accumulated experience or on visual comparison with a few laboriously measured "standard" micrographs.

Many aspects of the problems and methods of quantitative interpretation of micrographic information will be found reviewed in detail in the book "Quantitative Metallography" [1].[1] The basic mathematical principles have long been known; for example, the Delesse Principle (1852) which states that the ratio of areas of phases on a random sliced surface is equal to the ratio of volumes of phases in the mass, and the methods of Rosiwal (1898) and Glagoleff (1933) which equate these volume ratios to the ratios of line intercept lengths and of point counts respectively.

The laws of the binomial distribution may be used to set *minimum* requirements for the amount of information to be processed to attain any desired potential degree of accuracy [1,11]. If one wishes to obtain a phase analysis with an accuracy comparable to the usual chemical analysis, one must process, irrespective of method used, nearly one million "binary bits" of information. Treating black and white micrographs with a useful resolution of 100 lines per inch or 40 lines per centimeter (=10,000 bits per in.^{2} or 1600 bits per cm^2), an 8 $\times$ 10 in. (or 20 $\times$ 25 cm) print, totally analyzed, approximately fills the purely statistical requirement. A separate determination will be necessary to decide whether one such print, or an equal area of smaller prints, is in fact representative of the material. When an 8 step or 16 step grey scale can be usefully treated, the required area may be reduced by a factor of 3 or 4; or alternately, a full scale print may yield up to twice the accuracy of a black and white print of the same size.

Hand measurements at this level of detail imply an expenditure of time of the order of hundreds of hours per specimen. Much progress has been made in devising mechanical aids of several varieties which considerably reduce the labor requirement, but it has now become abundantly clear that the only practical tool for making high accuracy quantitative metallography an everyday process must be a digital computer system which directly accepts suitable photomicrographs, either in photographic or electrically recorded form, and prints out the desired statistical information. Such a program has been shown to be feasible, and has been described in detail in the chapter mentioned [1].

2. Development of Computer Methods

A number of laboratories have experimented with systems in which a computer "looks at" paper material *originally designed for visual interpretation by the human eye* [2], producing therefrom some numerical result. Some of these experiments have been closely related to metallographic measurement, but no general program suitable for micrographic analysis has been disclosed. It is believed that others are working along somewhat analogous lines.

Experiments generally using the same class of viewing and computing "hardware" fall in two distinct classes.

(A) *Character recognition* in which the computer is asked to "see" a hand-drawn or printed character and recognize the character by recording the equivalent code character. Such problems range from the recognition of numbers on bank checks to the translation of Russian script or Chinese ideographs into English.

(B) *Picture interpretation;* in which the visual material might be

1. Aerial or satellite photographs of the nature of a map or weather pattern.
2. Astronomical photographs.
3. Drawings, as for example, organic chemistry structure diagrams.
4. Photomicrographs, mainly
   (a) Metallographic,
   (b) Biological,
   (c) Petrographic.

In all of these cases, the computer may be asked to state the frequency, size, location, or total occurrence (area) of one or more classes of objects ("blobs") which can be recognized by some topological rule. In general, program systems developed for any problem in Class B have some application

[1] Figures in brackets indicate the literature references at the end of this paper.

to all of the problems in this group, but programs are not interchangeable with the A problems.

The National Bureau of Standards experiments on picture interpretation problems were initiated in 1956 by Kirsch, Cahn, Ray, and Urban [2], using the SEAC (Standards Electronic Automatic Computer) and translating black and white pictures into binary machine data by means of the scanner SADIE (Scanning Analogue to Digital Input Equipment) shown in figure 1. A cathode ray tube display of the picture in the SEAC memory was added in 1957. The first experiments were directed toward diagram recognition problems related to the Patent Office "HAYSTAQ" literature searching program, but experiments have also been conducted with star photographs and in the mapping field. A few typical metallurgical micrographs were processed for area at this time.

During 1958, R. B. Thomas, with G. H. Urban and L. C. Ray, compiled a "library" of routines, STRIP–2 (Standard Taped Routines for Image Processing) generally useful for all problems in the picture interpretation class. These routines are supplied to the computer from a magnetic sound tape, and are commanded in any desired combination by typing in seven-letter code words in shorthand English. This "library" has recently been augmented by the addition of two routines specifically composed for metallographic purposes. Additional programs are being composed to complete the statistical analysis of metallographic grain size distributions.

The present size limitation of "SADIE" (17.64 cm^2 or approximately 3 $in.^2$) and the speed and memory limitations of SEAC limit present experiments to an accuracy much lower than that eventually desired. As a consequence of this, the present experiments serve primarily to develop logic which will shortly be translated for use on the new NBS computer, PILOT, where a combination of more powerful logical operations, much faster operation, and greatly expanded memory is expected to permit processing 80 $in.^2$ (500 cm^2) pictures in less time than is now required for the small sections on SEAC. Input equipment giving resolutions up to 80 lines per centimeter, areas up to 500 cm^2 and an eight step grey scale is under construction for use with PILOT, or alternately with a commercial computer when appropriate.

A future version of the system is anticipated to include a directly connected reader, composed of matrices of solid state photoluminescent and photosensitive elements, whereby a transparency (as a micrographic negative) will serve directly as the primary image memory and further reduce the machine time required for picture processing. Alternately, encoded picture tapes can be prepared on a slow mechanical scanner, or on a scanning microscope, and the tape supplied to the computer in place of the original picture.

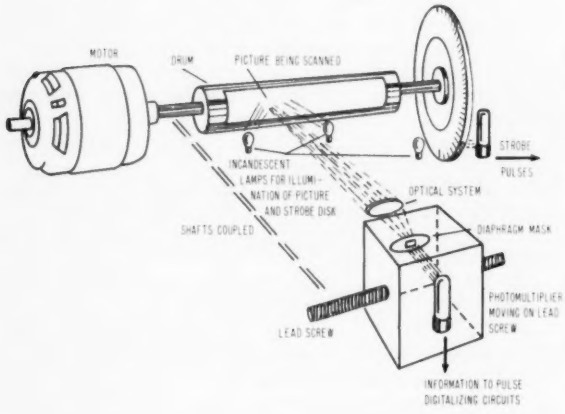

FIGURE 1. *"SADIE" (Scanning Analogue to Digital Input Equipment) by which a picture is inserted into the computer memory.*

3. Elements of Computer Processing Programs

SEAC is a three address computer operating at a bit-rate of one megacycle, in serial processing mode, with a memory capacity of 2,048 words. The average computation rate is somewhat over 1,000 complete operations per second. The SEAC word consists of a string of 48 binary bits, of which the first 3 are dummies for machine control and the last is the sign; thus leaving 44 bits of actual information. This word may be interpreted in 5 ways:

1. A binary number of 44 places.
2. 44 independent Boolean statements.
3. A hexadecimal number (0, 1—9, A—F), of 11 places, each using 4 bits.
4. An alpha-numeric word of 7 letters, each using 6 bits.
5. An order, normally entered in hexadecimal, but actually interpreted as five independent binary numbers. Since the word interpretation is optional, an order can be treated as any other number, and thus incremented by addition to operate in succession on all, or on a selected portion, of the words in any specified block of the memory.

The logical ability is limited to 16 basic orders, viz:

Four operational—Read, Write (or "Dump"), Rewind source, and "File."

Six basic arithmetic—Add, Subtract, Multiply (major and minor portions of product) and Divide.

Three logical choices of program route by comparing or equating specified numbers.

One boolean operation—"And."

One pseudo-boolean operation—"Logical transfer."

One lateral displacement of word—"Shift."

The ability of SEAC to perform picture interpretation lies in the existence of the last three orders listed. Through the "Boolean And," 44 bit sections

of two different images can be compared to produce a word showing *only* those spots where the images match or agree. The Logical Transfer order is a peculiar but powerful operation which may be likened to silk screen printing, or to the simultaneous printing of two negatives on to a single sheet of photographic paper. The information (1's and 0's) in Boolean word α is projected through the 1's in Boolean word β to be copied into Boolean word γ, which at the same time is unchanged where the mask word, β, shows zeros. The equivalent Boolean function is: $\gamma^1 = (\beta \textit{ and } \alpha) \textit{ or } (\text{not } \beta \textit{ and } \gamma)$. Thus, projecting an α of 44 zeros through a word β which is part of a picture, into a γ, which is originally 44 ones, produces the complement (photographic reversal) of the image β. In another application, an α word from the original picture may be projected through a β word which comes from a copy image, containing some small portion of a single grain, to make a new copy. If β masks are obtained by shifting operations, using successively the eight adjacent image points of a square array, the copy will be enlarged by one ring of image points, but cannot acquire points absent from the original, and cannot grow through a boundary line of zeros. By many repetitions of this controlled copying, the image of some single "blob"—for example, a metallurgical grain—can be separately copied out—or transferred to a second image storage which is otherwise blank, and there measured in any desired manner.

By appropriate combinations of these elementary orders into routines varying in length from a few dozen to a few hundred order words, including instructions to apply the series in turn to each word of the entire picture, nearly any rigorously defined alteration or analysis of the picture can be accomplished.

4. Present Operational Program

To allow convenient use of computer operations for such purposes as quantitative metallography, it is first necessary to devise a series of specific routines, each of which will accomplish some specific and useful operation on a picture. Second, it is necessary to arrange that the operator can, in some simple manner, command the performance of specific selected routines whenever these are useful to the problem in hand.

This is accomplished by first feeding a "master routine" into a small part of the computer memory. The function of the master routine is to cause the machine to ask for a list of instructions, (which are in the form of English words); to store these, and then to carry them out in the listed sequence. To perform an instruction, the computer first searches along the order tape until it finds the matching title, then reads in the routine of detailed orders, and finally executes this set of orders. Thus, by typing in a few words in "English," the operator will cause the machine to read in and to execute some thousands of specific orders in the machine language. For routine use, the selected list of instructions can itself be prepared in advance—as on punched paper tape—and simply fed into a reading unit of the computer.

The present experiments are being performed with a specific "library" of routines, "STRIP–2B." As originally put into service in January 1959 (superseding less complete libraries) STRIP–2 had the capabilities shown in table 1. The original capabilities include all the necessary manipulations to put a picture into the computer, select a portion (as one phase) of the picture, perform minor repairs or corrections, determine the area of the phase and count the number of particles shown. This list is adequate to perform elementary forms of quantitative metallography, such as to treat cases where the particles can be considered spherical.

In addition to the functions originally available, the following new analytical functions were composed during 1961.

(5c) LINE—This operation performs a complete lineal analysis for both image and background separately; treating the image as if it were wrapped into a cylinder. Histograms of line lengths, by $\sqrt{2}$ class increments, are generated together with statistical summaries of the histograms.

(5d) "BLTR"—Blob Transfer and Record: This operation abstracts one blob (or grain) at a time from the image, measures it, enumerates it, and states its area, location in the image and dimensions. This is a faster and more complete form of the BLOB operation, primarily designed for determining grain size distributions. Grains cut by the border are identified by the location parameters.

TABLE 1. *Original functional capabilities of "STRIP-2"*

(1) *Input—Output functions:*

(a) SCAN—Operates the device SADIE and supplies the computer with one picture 44 mm^2 recorded as 704 words. This is stored in either of 2 Image Spaces, "A" or "B" in the memory. *Black* picture objects are recorded as computer *1's*, which will be displayed white on the output scope. A blank border, 1 mm (4 bits) wide is masked onto the picture. The gross picture area is 30976 bits and the net usable area inside the border is 28224 bits (17.64 cm^2 or approximately 2.82 in.^{2}).

(b) READ—A previously scanned and electrically recorded picture is read back into the machine.

(c) DISPLAY—One image is exhibited on the cathode ray (TV) tube.

(d) DUMP—An image in the machine is electrically recorded on wire or tape.

(e) PUNCH—An image is recorded as coded characters on a paper tape (can be used to transfer the image to a different computer).

(2) *Program sequencing functions:*

(a) ITERATION (Repeat series of operations).

(b) TRAC (Transfer to different operation on "Clear 0" signal from Console).

(c) TRAZ (Transfer Operation if Area=Zero).

(d) TRA (Transfer Operation, Unconditional).

These operations permit recycling the machine through selected portions of the listed orders, or repeating the entire list on successive pictures without retyping the list of orders.

(3) *Picture shifting functions:*

(a) ROTATE—Picture is turned 90 or 180 deg, as may be necessary for a directional interpretation.

(b) COPY—One image is duplicated in the 2d image space, permitting further transformation without loss of the original.

(c) SWAP—Two images are interchanged.

(4) *Image modification functions:*

(a) COMPLEMENT—Photographic Reversal.

(b) AND—Shows image features (ones) common to each of 2 images.

(c) OR—Combines features (ones) existing in either of 2 images.

(d) M2S—Modulo-2 Superposition: Shows features (ones) existing in either one of 2 images but *not* in both.

(e) ERASE—Destroys one image.

(f) NOISE—Inserts a specified proportion of "dust" similar to "snow" in a television program. This permits experiments on how to clean a dirty image.

(g) CUSTER—This operation wipes out the internal area of each image spot (or blob) saving only the outline. One application is to use this information to estimate the grain boundary area of the phase represented in the image.

(h) BITOP—This is a general Boolean operation on one entire image, producing a new image in which the nature of each new image point C' is specified by any desired Boolean function of the original point value C, and of the values of the eight nearest neighbors A, B, D, E, and 1, 2, 3, 4.

1	*A*	2
B	*C*	*D*
3	*E*	4

Point array for BITOP

Boolean functions are written: AB (A and B); $A+B$ (A or B); $A-B$ (A and not B) etc.

Some of the useful BITOP functions which may be written are:

"Etch": $C'=ABCD1234$ which will discard the border line (custer) and save the solid center of each blob. It has been used (ref. 1) to separate and correctly count powder particles which were clustered in a micrograph.

"Plate": $C'=A+B+C+D+E+1+2+3+4$ will restore the original image after etching, except that blobs originally less than 9 bits in area, or lines less than 3 bits thick will have vanished.

"Clean": $C'=C+ABCD1234$ will eliminate all single blank points existing within an image.

More complex BITOP functions could be used to erase scratches which might appear in a micrograph of a poorly polished specimen, or to repair small defects in the etching of grain boundaries.

(5) *Analytical functions:*

(a) AREA—This operation counts the number of image points in the image. Division of area by the appropriate total (30976 or 28224) gives the percentage of the phase represented by the image.

(b) BLOB—This operation enumerates the individual separate areas, or blobs, (which in the metallographic case would usually be the grains) and states the area of each. Tabulation of these data will give a grain size distribution.

5. Experimental Illustrations

In the previously mentioned report [1], illustrations of computer interpretation are given for three types of cases. The central section of one of the ASTM grain size charts was measured, with results in close agreement with the stated value. A group of powder particles, containing a few clusters, was separated by use of the "Etch" Bitop function, and the particles counted and measured. A three-phase dendritic structure was analyzed for the area of the three phases, using scans at two levels of grey sensitivity, and the M2S function to obtain an image of the grey phase alone.

Recently, analyses have been made of the numbers and sizes of carbide particles found in aging gage block steels. These will be reported on a future occasion when they can be related to the changes which occur in such blocks. Analyses have also been made of a number of graphitic type structures of interest in establishing standards for cast iron. [14]

There is currently very widespread interest and activity concerned with the superconductor material Nb_3Sn. Since the current knowledge of the physical metallurgy of this material can be increased by quantitative metallographic determinations within the accuracy range obtainable from the present small picture format, experiments are at present being conducted with micrographs of this material. The structure of this material is typically so complex that simple relationships between various geometrical parameters are not applicable, hence each desired parameter must be measured directly.

6. Niobium-Tin Superconductor

Magnetic fields more powerful than can in practice be obtained in any other manner can be created by the use of solenoids of superconducting wire operated at liquid helium temperature [3, 4]. Such fields have many potential applications, including nuclear fusion devices [5].

Niobium and tin are both elemental superconductors, and this property occurs in at least two of the intermediate phases of the alloy system. Within the past few years, considerable interest has been shown in the compound Nb_3Sn for its

possible application to the fabrication of superconducting solenoids. Unfortunately, Nb_3Sn is very brittle and can not be processed by normal metallurgical methods. If, however, a stoichiometric mixture of Nb and Sn powders is compressed within a niobium tube, the duplex tube containing the moderately ductile mixture can be cold worked to wire, wound into coils, and finally the core converted to the Nb_3Sn phase by appropriate heat treatment.

However, it has been found that wires prepared in this manner may have properties which differ significantly from specimen to specimen, particularly with respect to the retention of superconductivity in high magnetic fields or with high current densities. It is presently thought that the differences in the behavior of various specimens may reflect differences in the form and distribution of the Nb_3Sn phase which is produced by the heat treatment accorded the mechanical mixture of Nb and Sn powders in the niobium sheath.

7. Superconductor "Quality"

In the absence of an agreed upon quantitative measure of the concept of superconductor quality, it is necessary to establish some working hypothesis covering the factors which may be involved. Given a superconducting material, the superconducting state can be destroyed either by an increase in temperature, a high magnetic field, or by excessive current. These three influences cooperate in a complex manner, and a high test value for one factor does not necessarily guarantee an equally high value for the other two.

Thus, in practice, a high quality superconductor is one which, at the intended service temperature, successfully resists a high magnetic field and simultaneously carries a current sufficient to establish this field.[2]

Metallurgical reasoning toward improving superconductor quality may emphasize the current carrying factor as appearing to be somewhat less obscure than the others. Subject to certain limitations, those metallurgical changes which would increase the *normal* conductivity of a specific material may be expected to be of at least some benefit to its superconducting quality. However, at least two distinct types of superconductor materials are recognized. In the "ideal" or "soft" superconductor (viz, pure tin) the superconductive current appears to be largely confined to the surface. In a "hard" superconductor, such as niobium-tin, the critical current appears to be approximately proportional to cross-sectional area, hence the superconductive current appears to flow in the volume. A possible intermediate condition is one in which the current follows "internal surfaces" whose nature has not yet been definitely specified.

The most obvious metallurgical factors which may bear on the performance of various Nb_3Sn wires fabricated as previously indicated are (1) the mean, or the minimum, effective area of superconducting phase in a cross section perpendicular to the current flow, and (2) continuity of superconducting phase along the length of the wire.[3] An additional factor which might be involved in determining the overall performance of a wire is the anisotropy of grain shape. In particular, long or fibrous grains alined along the wire axis might be a desirable structure.

Other factors relating to the stoichiometry and lattice perfection within individual grains are probably also quite important. However, these factors are best investigated by diffraction methods and will not be further considered at this time. Factors 1 and 2 and the question of grain shape and orientation are matters which can be evaluated by quantitative metallography.

Methods will be illustrated for obtaining measurements of the volume fraction of the superconducting phase and of its continuity, of the mechanical mean free path, and of the sizes and shapes of the particles of the various phases present.

8. Niobium-Tin Alloy System

The specimens presently under investigation by quantitative metallography are part of a series of diffusion specimens and reacted powder mixtures which have been under investigation by a number of methods in an effort to establish the phase diagram of the Nb–Sn system and to determine the most effective method of preparing the Nb_3Sn phase [8].

Specimens are polished normally and are then anodized, without etching, by the method of M. L. Picklesimer [9] to develop characteristic colors on each of the phases.

The colors produced on different metallographic constituents vary somewhat with the degree of anodization, and can be deliberately varied to aid in distinguishing phase areas. On the basis of microspot spectrochemical analyses of characteristic areas, the constituents in the microstructures have been tentatively identified [8] as shown in table 2.

TABLE 2.—*Tenative identification of metallographic constituents in Niobium-Tin alloys*

(1) Niobium metal, which may contain up to about 10 percent tin in solid solution. The charac-

[2] If alternating current or pulsed applications are planned [5], additional factors may be involved in the concept of quality. Thus it may be required that the superconducting material must not introduce sources of non-ohmic impedances, viz: inductances, capacitances, or rectifying junctions. It has been shown [6] that at least one porous, or distended, alloy structure (Pd-H_2) has capacitive properties. In the presence of particles of several phases, the possibility of accidentally creating diode junctions cannot be ignored. The possibility of such "microelectronic" effects may further restrict the range of acceptable metallographic structures.

[3] Values for the electronic mean free path are commonly computed from conductivity data, and may run from the order of 100 A at room temperature to the order of a millimeter or more in good conductors near absolute zero. The high value at low temperature, where the effect of thermal vibrations has vanished, is referred to as "residual electronic mean free path" (L_r). The "reciprocal residual mean free path" ($1/L_r$) is the average number of interruptions per centimeter of electron travel due to residual impurities and mechanical imperfections. Hagedorn [7] reports that L_r corresponds to the observed grain size in superconducting high purity tin films, and proposes that the superconducting transition temperature of poor films is lowered by an amount ΔT_c, proportional to ($1/L_r$). The number of interruptions here considered should be the sum of the microscale interruptions measured by the mechanical mean free path and of the atomic scale interruptions due to impurities and crystal imperfections.

teristic color is in the light blue range, viz: "Light Beryl Blue" in the Maerz Dictionary of Color [10].

(2) Phase, nominally Nb_4Sn, with a composition range of around 6 atomic percent. This phase is believed to melt congruently not far below the melting point of Nb metal. The color is consistently a more brilliant blue than Nb; "Calamine Blue." This phase has been reported to be a superconductor of moderately good quality.

(3) Phase of nominal composition Nb_3Sn, probably of fixed composition. This phase is generally believed to be one of the best superconductors now known. The characteristic color is darker than the Nb_4Sn, and more reddish, ranging from "Orient" (blue) to magenta (process red) according to anodizing treatment. This phase is presently thought to decompose by a peritectoid reaction (to $Nb_4Sn + Nb_2Sn_3$) around 730 °C.

(4) Phase of nominal composition Nb_2Sn, which is characteristically more red than Nb_3Sn, viz: "Purple Aster" when Nb_3Sn is "Orient." The phase has been tentatively equated with areas which are greenish when Nb_3Sn is anodized to magenta. This phase is presently believed to decompose by a peritectoid reaction (to $Nb_3Sn + Nb_2Sn_3$) around 690 °C.

(5) Phase of nominal composition Nb_2Sn_3, which is very dense and brittle. The color range is in the brownish yellows, viz, "Burnt Sienna" to yellow. This phase appears to decompose by peritectic reaction to Nb_4Sn and liquid at about 863 °C. The formation of this structure has been associated with the formation of porosity.

(6) Sn or quenched supersaturated solution of Nb in Sn. The tin side of the system appears to be occupied by a low melting eutectic mixture. The high tin material is more yellow than any of the other constituents, viz: "Chrome Yellow" or golden.

(7) Impurities: The impurity most often recognized is Salmon Pink in color and may perhaps be niobium nitride.

(8) Porosity: Reacted powder mixtures characteristically show considerable porosity, even when the powders were fully compacted. The amount of this porosity generally increases with the amount of tin incorporated, and is high for mixtures of the Nb_2Sn_3 ratio. The blackness of the pores is partly obscured by reflections of yellow or green light from high tin material coating their inner surfaces. Pores deliberately filled with acrylic plastic are white under polarized light.

9. Low Quality Nb_3Sn Wire

If high quality superconducting devices are to be manufactured on a reliable basis, it will be necessary to relate the superconducting quality of Nb_3Sn materials to the details of the complex phase structures which may be formed under various fabricating treatments. To this end, the balance of this report is devoted to a detailed quantitative analysis of a microstructure which is believed to represent a quality somewhat below an acceptable level, and thus should illustrate the types of defects which should be eliminated.

An original color micrograph, of which a general print is shown in figure 2, was supplied by Dr. M. L. Picklesimer of the Oak Ridge National Laboratory. This comes from a section of commercial core wire which was given only a minimum heat treatment of 2 hours at 1,000 °C, and was selected as a low quality area by virtue of higher-than-usual electrical resistance at room temperature. Other sections, more completely heat-treated, had normal quality for the period (July 1961).

The color transparency was copied in the photographic laboratory to produce 4 color-separation negatives similar to ones which would normally be made for ink reproduction. From these, high-contrast black-and-white prints were made for the computer input. These prints were then cut in sets of matching areas to produce three separate series for computer analysis, as shown in figure 3. By comparison with specimens made for the diagram study, and with other transparencies supplied by Dr. Picklesimer, the separations are judged to contain the following materials:

Black—holes or voids

Blue (actually cyan or blue-green)—Niobium with some tin in solid solution, together with a lesser amount of Nb_4Sn not clearly seen in this particular micrograph.

Yellow—Nb_2Sn_3

Magenta (purple or "Process Red")—The presumed superconducting phase Nb_3Sn.

The magenta area of the original contained numerous "dots" of various colors, not all of which were successfully reproduced in the black and yellow separations. It is believed that a small amount of extraneous material, mainly Nb_2Sn, has been included in the magenta separation.

In selecting the three areas to be shown to the computer, sections 1 and 2 were logical cuts of the left and right portions of the original, while section 3 was deliberately chosen to try to make the material look as good as possible. This allowed a statistical evaluation of the possible effect on the computer results of nonobjectivity on the part of the metallographer. It may be seen, in the results to follow, that this attempt to deceive the computer was statistically unsuccessful; hence the results from the three cuts have been combined in the total analyses.

The prints shown were analyzed on a number of occasions during the perfection of the LINE and BLTR routines with results in overall agreement with each other. However, results are reported only for analyses obtained after the routines were fully corrected. The total (SEAC) computer time used in obtaining the reported data for 12 pictures was 129 min.

10. Area and Material Balance

The area values obtained by the AREA order, and duplicated exactly in the LINE analyses are shown

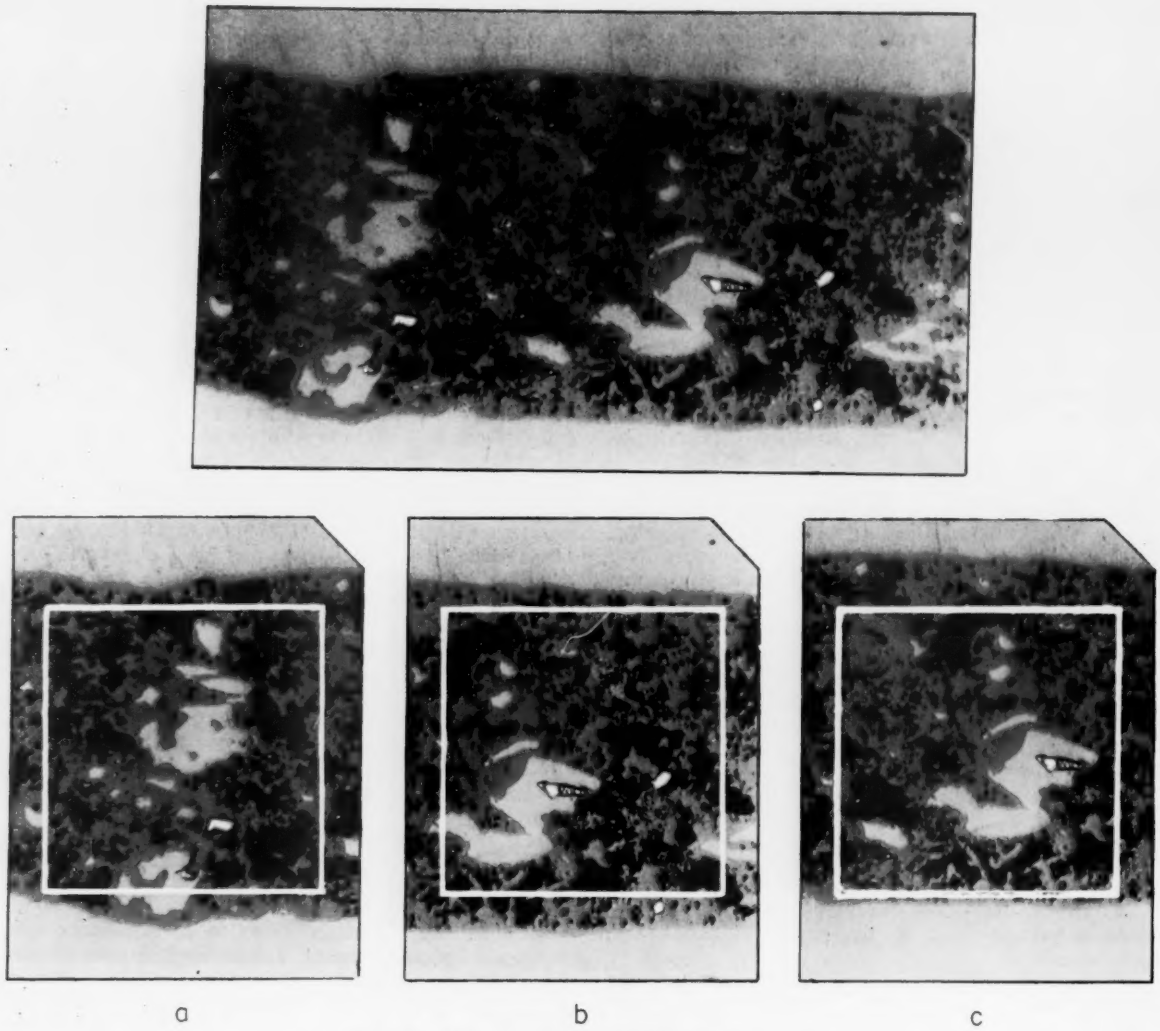

FIGURE 2. *General view of low quality* Nb_3Sn *core wire.*

Grey: Nb_3Sn phase (magenta)
Black: Voids
Light: Nb solid solution + Nb_6Sn (blue)
Light: Nb_2Sn_3 phase (yellow)
From Color Micrograph #CY 468 (250X), courtesy of
Dr. M. L. Picklesimer (Oak Ridge National Laboratory)
Areas of micrograph used for computer analysis
(a) Cut 1 (b) Cut 2 (c) Cut 3

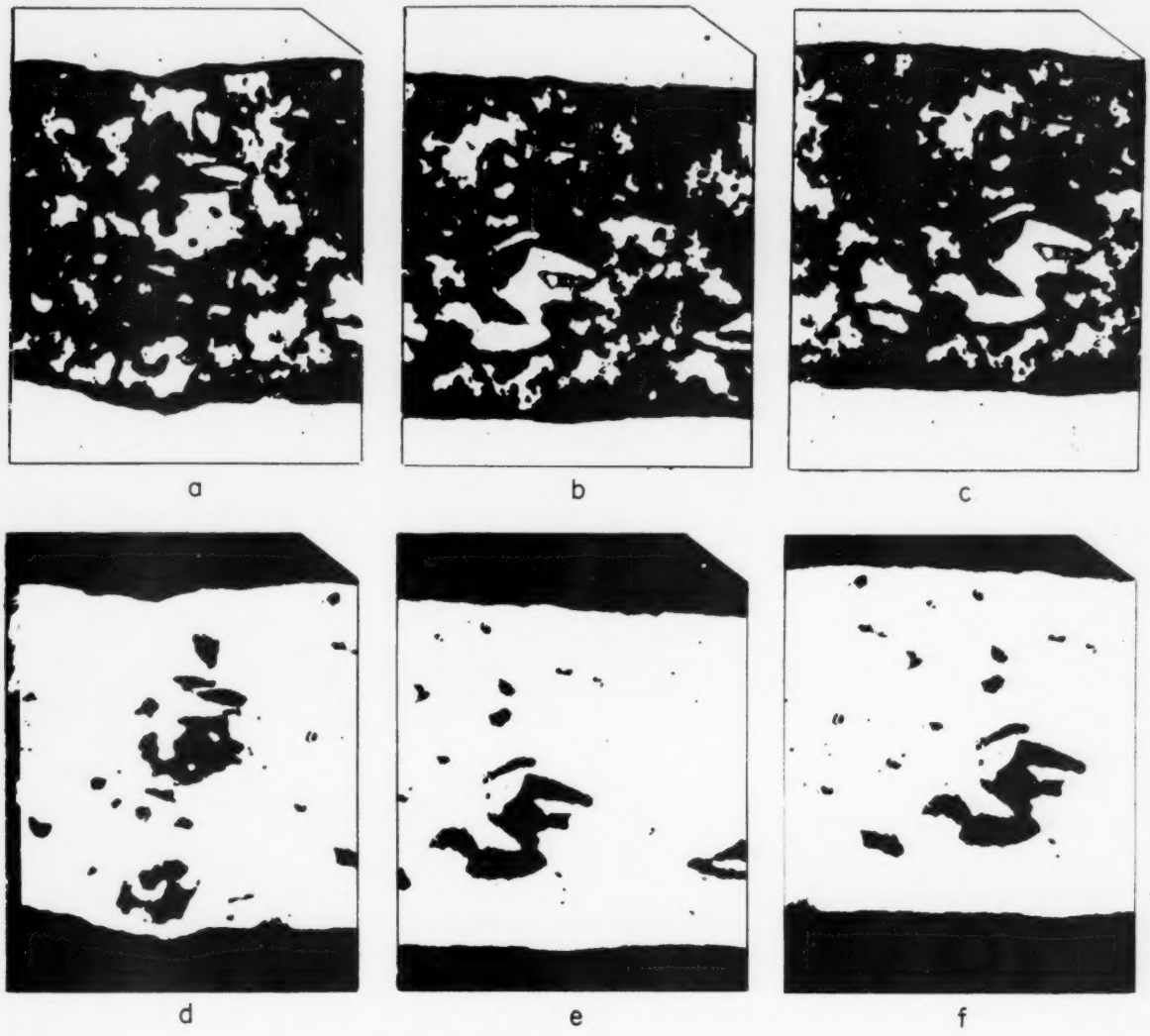

FIGURE 3. *Micrographs used for computer analysis.*

Magenta separations (Nb_3Sn phase) of the same color micrograph
(a) Cut 1 (b) Cut 2 (c) Cut 3
Blue separations ($Nb+Nb_3Sn$) of the same color micrograph
(d) Cut 1 (e) Cut 2 (f) Cut 3

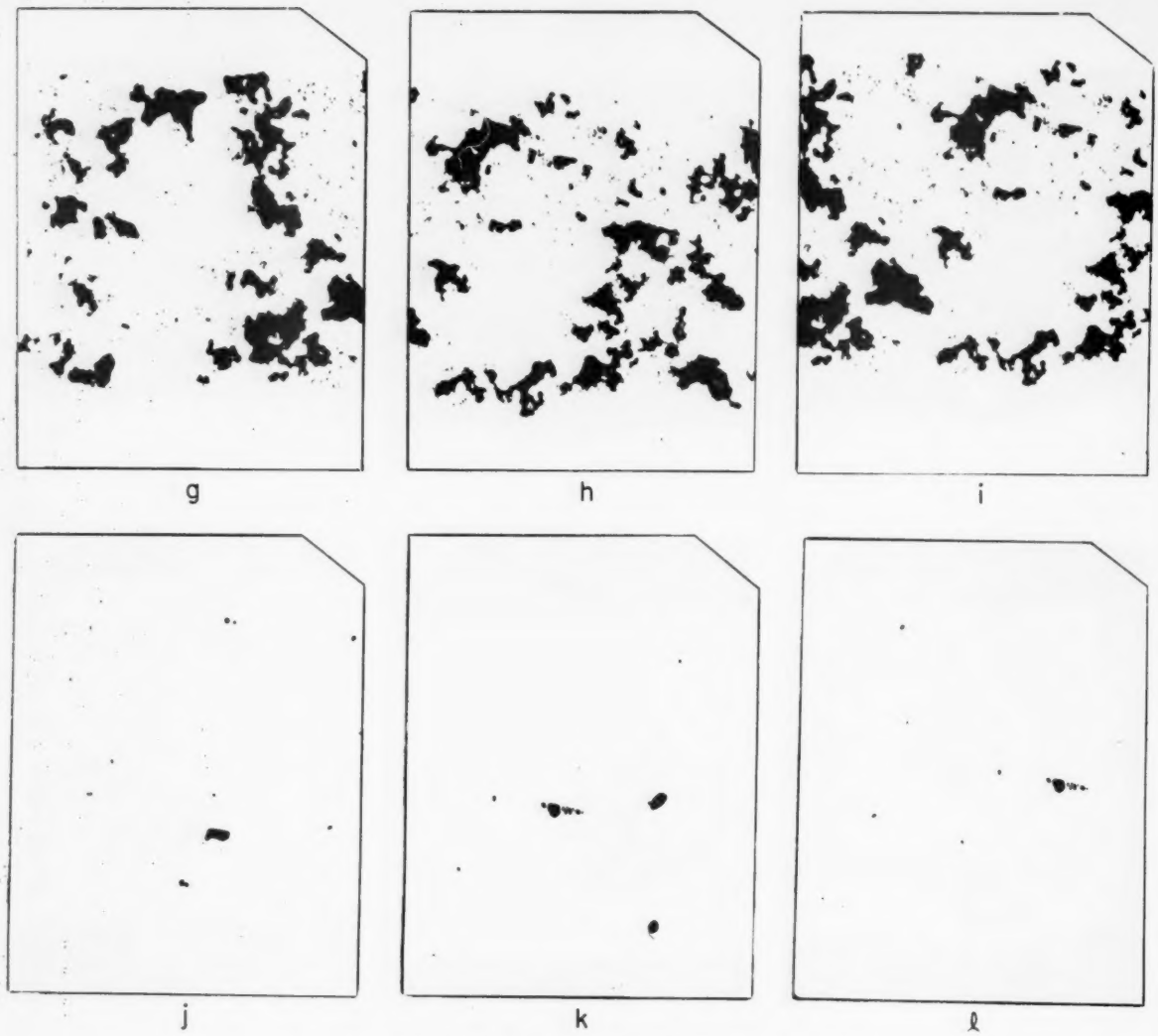

FIGURE 3. *Micrographs used for computer analysis*—Continued

Black separations (Voids) of same (Con't)
(g) Cut 1 (h) Cut 2 (i) Cut 3
Yellow separations (Nb_3Sn_3) of the same
(j) Cut 1 (k) Cut 2 (l) Cut 3

in table 3. Due to the tendency of high contrast prints to show slight enlargement of black areas, together with a photocell setting which probably slightly favored image detection, the four prints of a set add up to slightly more than the theoretical area of 28224 units. The actual totals, rather than the theoretical values, are therefore used to obtain the percentage by volume of the constituents, on the assumption that the reading error may be proportional to the area actually read. As the micrograph is at ×250, and 1 computer unit=0.25 mm on the print, one computer unit is 0.001 mm (1μ) in actual length and 10^{-6} mm^2 in actual area.

TABLE 3. *Areas and material balance in low quality* Nb_3Sn *wire specimen*

1 unit=0.000001 mm^2

Item	Cut 1	Cut 2	Cut 3	Total
Magenta	20055	21082	21349	62486
Blue area	3327	3014	3235	9576
Black area	5878	4948	5010	15836
Yellow area	306	301	293	900
Total area	29566	29345	29887	88798
Ideal total	28224	28224	28224	84672
Σ4 errors	1342	1121	1663	4126
As percentage of total readings				
	%	%	%	%
Σ4 reading errors	4.54	3.82	5.56	4.65
Holes (black)	19.88	16.86	16.76	17.83
Phases as percentage of total solid				
Solid area	23688	24397	24877	72962
	%	%	%	%
Magenta	84.66	86.41	85.82	85.64
Blue	14.05	12.35	13.00	13.12
Yellow	1.29	1.23	1.18	1.23

Material balance, assuming Nb_3Sn mixture in original

	Nb	Sn	Nb	Sn	Nb	Sn	Nb	Sn
Original (at %)	75.00	25.00	75.00	25.00	75.00	25.00	75.00	25.00
Blue (at 10% Sn)	12.64	1.41	11.11	1.24	11.70	1.30	11.81	1.31
Nb_3Sn_2 (yellow)	1.03	1.55	0.98	1.48	0.94	1.42	0.98	1.48
Apparent magenta	61.33	22.04	62.91	22.28	62.36	22.28	62.21	22.21
Magenta, normalized	73.56	26.44	73.85	26.15	73.68	26.32	73.69	26.31

Assuming the statistics of the binomial distribution to be applicable to the measuring process used, one may expect [11] for a sample size of 28224 units, a standard deviation of about 74 units (=0.26% of the gross) in estimating a value of about 21000 units, which would decrease to about 5 units (=0.02% of the gross) when measuring 1 percent of the area; that is a maximum error (3σ) of less than 1 percent on any area measurement. The discrepancies between the three cuts in table 3 are somewhat larger than predicted in this manner, except for the yellow phase which conforms exactly. The (RMS) average deviation of the 12 area readings from their respective averages is 366 units, or 1.30 percent. Thus the nonrepresentative nature of the small micrographs appears to introduce errors about four times as great as those inherent in the sample size itself. However, the table shows that cut 3 does not exhibit the greatest deviation from the mean in any of the four measurements, hence the attempt to deliberately select a statistically invalid area was unsuccessful.

It may be noted from the area values that the magenta area, presumably the desired superconductor, accounts for only about 70 percent of the total core area. Of the remainder, almost 60 percent is occupied by voids, with the balance being occupied by unreacted niobium (with some Nb_4Sn) except for about 1 percent occupied by high tin material (Nb_2Sn_3).[4]

If it may be assumed that the original powder mixture was actually 75 atomic percent niobium and 25 percent tin, these materials may be allocated to the phases found, although the simple balance rule of a two phase system is not applicable here. To minimize the effect of errors, it is appropriate to assign the material first to the minor phases, and determine the apparent content of the major phase by difference. The densities of the phases are needed for an accurate evaluation. All intermediate phases apparently are denser than the mixed elements. As specimens consisting mainly of Nb_2Sn_3 show around 50 percent voids, the relative density of Nb_2Sn_3 is assumed to be 2. The density of the blue material is assumed not to be significantly different from that of Nb_3Sn, for the present purpose. As the blue particles appear to include some Nb_4Sn, they are assumed to average somewhat higher in tin than the saturated niobium and assigned an arbitrary composition of 10 percent Sn.

On these assumptions, the magenta material appears to have a composition slightly above 26 atomic percent tin, and must be primarily Nb_3Sn. The data certainly do not justify assuming that this phase departs from the stoichiometric ratio, and the accuracy of the estimate probably does not demand an explanation of the discrepancy. Nevertheless, the magenta area is thought to contain a little Nb_2Sn, which could rise the average tin content by a fraction of 1 percent, and it appears entirely reasonable that the reacting mixture may have dissolved around 3 percent of niobium from the sheath material.

11. Lineal Analysis

The Lineal Analysis routine (LINE) makes a *total* lineal analysis of one computer image in one specific (Horizontal) direction which, in the present examples, is made the axis of the wire. The picture is treated as if wrapped into a vertical cylinder; that is, the edges are jumped so that a totally black image would be seen as one continuous helical line 28224

[4] *Brittle Behavior of* Nb_3Sn. Edelson and Baldwin [12] report that the tensile ductility of powder metallurgy copper alloys falls off rapidly as a function of the total volume fraction of holes and foreign particles, irrespective of the nature of these particles, their size, or the mean free path in the copper. More than 70 percent of the original ductility is lost at 5 volume percent noncopper, and nearly all at 30 volume percent. As the ductility of pure Nb is of the same order as that of copper, a core which contains only 70 percent Nb_3Sn might be very brittle purely as a result of its interrupted structure, without necessarily requiring that Nb_3Sn would be brittle in pure form.

units long. Each uninterrupted traverse in black (1's) or white (0's) is measured, added into the total (area), looked up in a class distribution table, and tallied as one occurrence of a line of the appropriate class.

A typical computer print-out is shown in table 4, which gives the analysis for the magenta phase of cut 1 of the wire micrograph. In this print, the three lines following "LIST" are the instructions inserted by the operator, with all other printing done by the machine. The "CLEAR O" instructions from the machine *to* the operator represent options to record the table in either of the two number systems. Fractions of a computer unit are dropped in the mean free path (M.F.P.) values and the two standard deviations, but can be retrieved from the total lines, area, and variance values.

TABLE 4. PHOTOCOPY OF LINE PRINT-OUT FOR CY468-1-MAGENTA

```
LIST:


LINE A
LINE B
END
LINE A

CLEAR 0 TO DUMP TABLE TO TAPE 0C (hex)

LENGTH    ONES   ZEROS
     1      32      64
     2      30      75
     3      36      66
     4      48      64
   5-6      63     111
   7-8      61      87
  9-11      78     107
 12-16      92      97
 17-22      86      83
 23-32      73      49
 33-45      89      24
 46-64      77       1
 65-90      48       0
91-128      12       0
TO 180       4       0
TO 256       0       0
TO 360       0       0
LONGER       0       0
ΣLINES     829     828
AREA     20055    8169
M.F.P.      24       9
VAR:       603      90
STD.DV      24       9
SD.MFP       0       0
CLEAR 0 TO DUMP TABLE TO TAPE 0C (dec)
LINE B
```

While particle area distributions can be deduced from lineal analyses, such operations require assumptions which would be invalid in the present case. Area distributions are obtained directly in the BLTR routine.

The significance of lineal analysis in the present case lies in the determination of a value for the mechanical mean free path in the superconducting phase in the axial direction. This value, of course, takes no cognizance of possible disturbances of regularity on the atomic scale, but as previously noted (footnote 3), the mechanical and electrical values of the mean free path may be expected to be similar for sufficiently pure materials at very low temperatures.

The line length class distributions for the three cuts of the magenta (Nb_3Sn) pictures are plotted in figure 4. The bars of this histogram have been

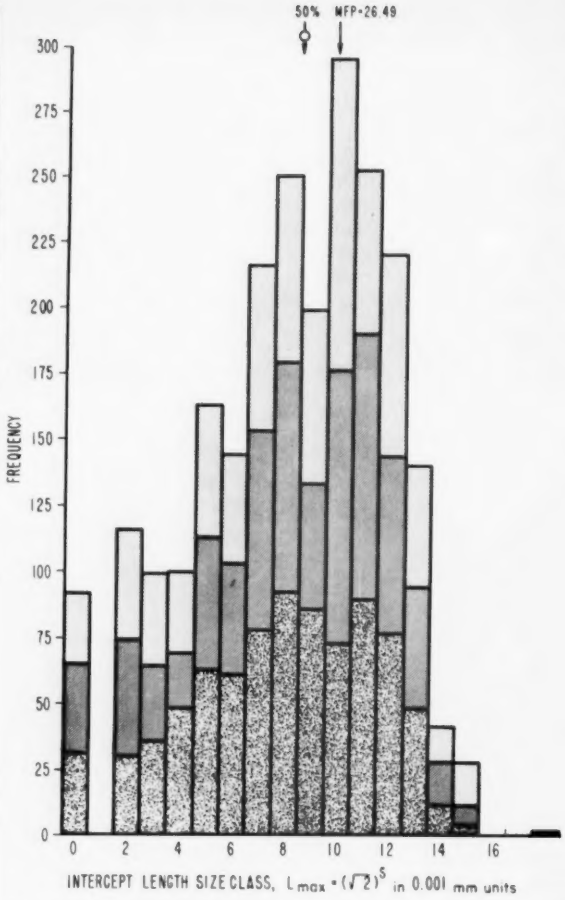

FIGURE 4. *Histogram of line length distribution in the magenta phase* (Nb_3Sn).

divided to show the contributions from each of the three cuts, which will be observed to be of similar magnitude in each case. The class size interval for all distributions has been obtained by multiplying the next lower size interval by $\sqrt{2}$. For convenience in labeling, plots are shown as frequency of occurrence versus a class size number "S" such that L max$=(\sqrt{2})^S$. Thus the maximum length included in "Class 10" is L max$=(\sqrt{2})^{10}=2^5$, which is 32 units in decimal notation, or 20 in the hexadecimal notation of the computer. Limits which would have fractional values are rounded to the next higher integer. Class 0 ($L=1$) actually starts with a minimum value of 0.51 units, the lowest value seen by the computer (read as 1). Class 1, for which L would be the unmeasurable value of 1.4, is nonexistent in the present data. Thus classes "0" and "2" will contain some tallies which should properly belong in the nonexistent classes -1 and $+1$, and should appear somewhat more populous than they

would appear in a distribution obtained at higher resolution. The limits of all classes are given in both the decimal and hexadecimal notation in table 5.

TABLE 5. *Size limits for class distributions*

Class No. (S)	Decimal values		Hexadecimal values	
	Min	Max	Min	Max
0	(0.51)	1	(0.81)	1
1	nonexistent in the present data			
2	(1.01)	2	(1.01)	2
3	2+	3	2+	3
4	3+	4	3+	4
5	5	6	5	6
6	7	8	7	8
7	9	11	9	B
8	12	16	C	10
9	17	22	11	16
10	23	32	17	20
11	33	45	21	2D
12	46	64	2E	40
13	65	90	41	5A
14	91	128	5B	80
15	129	181	81	B5
16	182	256	BA	100
17	257	362	101	16A
18	363	512	16B	200
19	513	724	201	2D4
20	725	1024	2D5	400
21	1025	1448	401	5A8
22	1449	2048	5A9	800
23	2049	2898	801	B50
24	2899	4096	B51	1000
25	4097	5790	1001	169E
26	5791	8192	169F	2000
27	8183	11575	2001	2D37
28	11576	16384	2D38	4000
29	16385	23150	4001	5A82
30	23151	32768	5A83	8000

NOTE: Hexadecimal integers are: 0, 1, 2, 3, 4, 5, 6, 7, 8, 9, A, B, C, D, E, F, 10.

To interpret the line histogram in figure 4, it is first necessary to recognize that the line intercepts of regular areas have a broader distribution than the sizes of the particles. For example, the intercepts of a circle whose caliper diameter is at the top of a size class are so distributed that only 70.5 percent are in the same size class as the diameter, while 29.5 percent are distributed among smaller size classes. The intercept distribution for a group of circles, all having diameters within one size class, is somewhat flatter. Such a distribution, obtained by the computer for circles in diameter class 10, is illustrated in figure 5.

In this light, it may be seen that the distribution of path length in the Nb_3Sn phase (fig. 4) results from intercepting a wide range of Nb_3Sn particle sizes. The occurrence of the 50 percentile point and of the average at positions close to the modal value indicates an essentially random nature for the distribution.

The summary statistics for the path lengths in Nb_3Sn are shown in table 6. The significant finding is that the mechanical mean free path averages only 26.5 μ, corresponding to 377 interruptions per centimeter. This value indicates a very large number of potential disturbances of orderly electron flow in a useful length of wire (footnote 3, p. 132). Also significant is the fact that the standard deviation of lengths is somewhat greater than the average length, which is to say that the distribution is very broad as compared with the usual chance distribution (such as Poisson and Binomial cases). This would imply that there is a good probability that the smaller particle sizes, or shorter paths, could be eliminated by more effective metallurgical treatment.

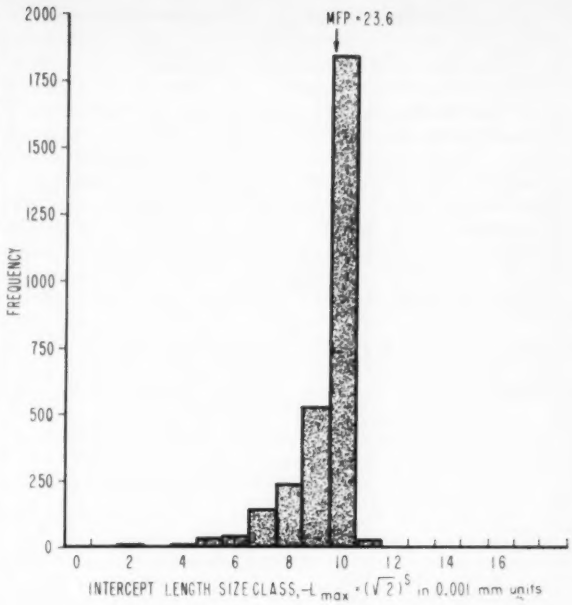

FIGURE 5. *Histogram for comparison: distribution of line lengths for 100 circles whose caliper diameters are distributed over size class 10 (23 to 32 units).*

TABLE 6. *Summary statistics for lineal analysis of magenta images* (Nb_3Sn *phase*)

1 unit = 0.001 mm on specimen

Item	Cut 1	Cut 2	Cut 3	All
Total lines	829	769	760	2358
Area (= total length)	20055	21082	21349	62468
Mean free path, M.F.P. (average L)	24.19	27.41	28.09	26.49
Variance of L	603	1141	1106	943.91
Standard deviation of L	24.56	33.78	33.26	30.72
Standard deviation of M.F.P.	0.85	1.22	1.21	0.63
Reciprocal M.F.P. interruptions/cm	413.4	364.8	356.0	377.5

12. Nature of the Interruptions

The additional lineal data obtained from the 12 images may be examined primarily with the objective of evaluating the nature of the 2358 interruptions tallied along a line length of 62.5 mm in the Nb_3Sn phase.

A line distribution for all nonmagenta material (including holes) is shown in figure 6. It may be seen that this distribution is more populous in the short length classes than that for the Nb_3Sn (fig. 4) and that the whole background histogram lies about 3 classes to the left of the histogram for the magenta image; that is, that background intercepts are generally only about ⅓ the length of Nb_3Sn intercepts. The line intercept histograms for the Blue (high Nb) particles and for the Black holes are shown in figures 7 and 8. It may be seen that the holes account for a majority of the interruptions. The summary statistics for these distributions are given in table 7.

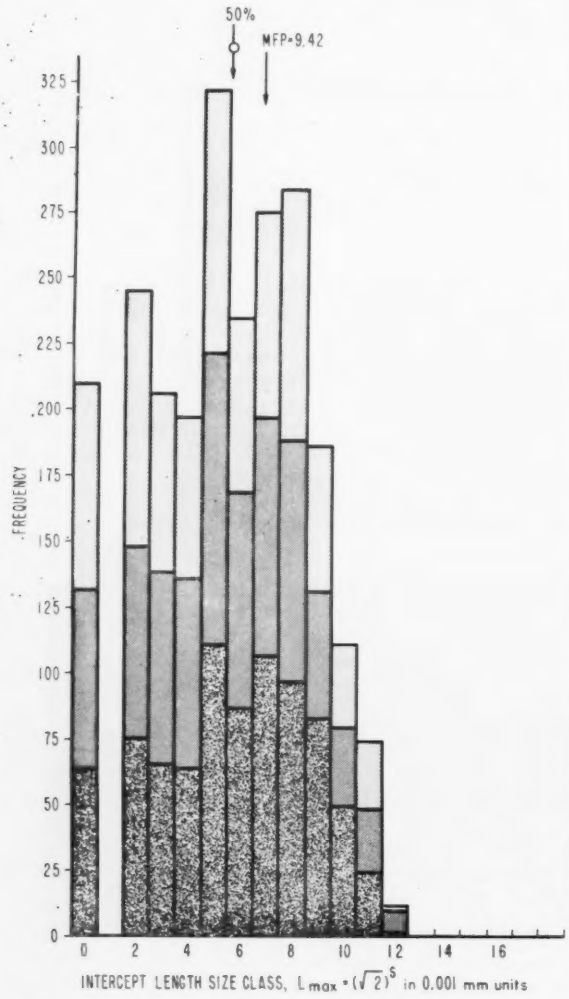

FIGURE 6. *Histogram of line length distribution in the Nonmagenta (background) material.*

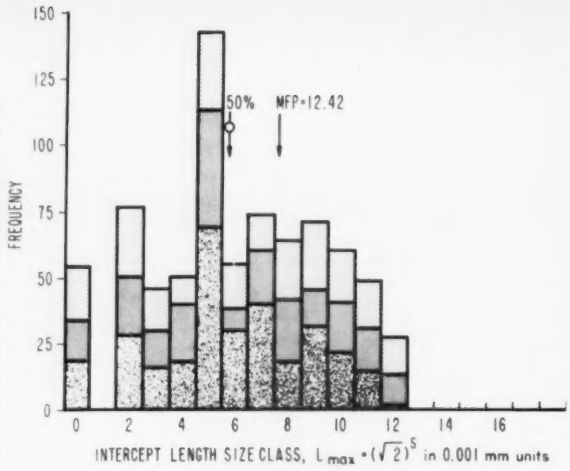

FIGURE 7. *Histogram of line length distribution in the blue material* ($Nb + Nb_4Sn$).

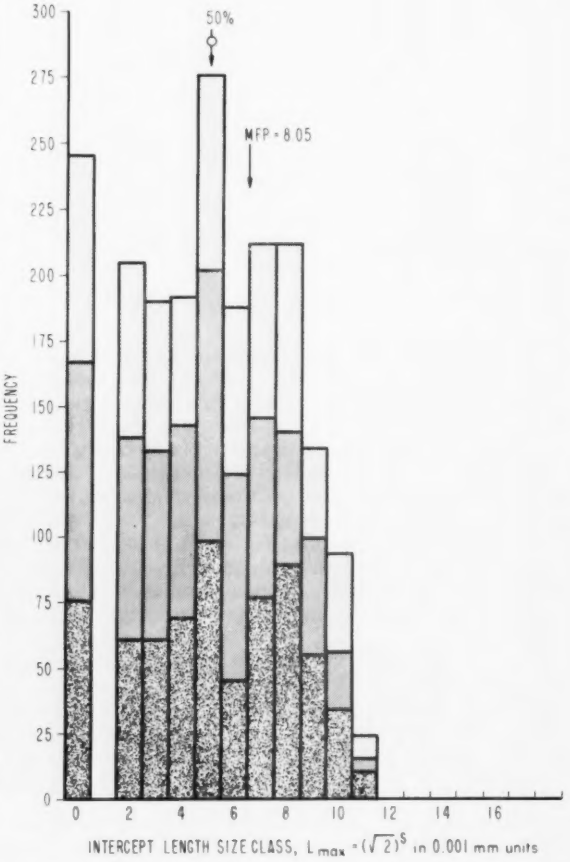

FIGURE 8. *Histogram of line length distribution in the black voids.*

In only 3 of the 12 cases did the actual differences between the 3 determinations slightly exceed the 3σ limit determined from the internal variance values, hence the slightly nonrepresentative nature of the 3 cuts is ignored and only the total of 3 runs considered.

TABLE 7. *Summary statistics for lineal analysis of background, and of areas not Nb_3Sn*

1 unit =0.001 mm on specimen

Item	Background of magenta	All blues	All blacks	All yellows	Total not magenta
Total lines	2355	771	1967	242	2980
Area (total length)	22186	9576	15836	900	26312
MFP=Average length, $\bar{L}$	9.42	12.42	8.05	3.72	8.83
Variance of L	86.95	170.93	61.84	10.84	91.76
Standard deviation of L	9.32	13.07	7.86	3.29	9.58
Standard deviation of average	0.19	0.47	0.18	0.11	0.18
Interruptions, percent		25.87	66.01	8.12	100.
Background area, percent		36.39	60.18	3.42	100.
$1/\bar{L}$=interruptions/cm of path in this material	1061.5	805.1	1242.1	2688.9	1132.6

It may be noted in table 7 that there were 625 cases (2980–2355) when the line trace passed from one nonmagenta area to a different nonmagenta area without first returning to the Nb_3Sn. The (4%) excess in the area readings of the 4 sets of pictures now is found distributed among the minor constituents, with the compensating effect that the average line length is nearly the same in the direct background determination and in the sum of the three individual determinations.

It may be concluded from table 7 that the most important cause of interruptions of the Nb_3Sn continuity is the voids. As many of these are small, they are more important than their share of the area would indicate. This disproportionate effect also is shared by the yellow Nb_2Sn_3 particles; however, these make only a minor contribution to the total effect. The blue Nb particles being on the average large, cause proportionally less interruption than their share of the area, and would presumably be regarded as less objectionable than the holes and Nb_2Sn_3 particles.

13. Area Analysis

The term "blob," is used in our computer terminology to designate any coherent object, no matter how complicated its shape, provided that some path, at least one computer unit wide, can be found from any one point in the blob to any other point in the same blob. No limit is placed on the complexity or length of the connecting path. So far as can be determined, no complication of the shape will itself result in a false identification. Although the computer may take a long time to find and transfer all of a complex shape, it will not report the blob until no additional connective area can be found.

Thus a blob can be a single metal grain, provided the grain boundary is completely etched; or it can be a cluster of adhering grains of the same phase if the material is unetched, or if the grain boundaries are incompletely developed. As the specimen under study is anodized *without* etching, the second blob definition applies in the present case.

A typical BLTR print-out, again for Magenta Cut 1, is shown in table 8. As in table 4, five lines following "LIST": are the instructions from the operator *to* the computer, while all statements following "END" are the computers statements of progress and instructions by the computer to the operator concerning options and format. The BLTR output represents data in an intermediate form, intended for further statistical treatment by additional routines, hence is given in machine words and in hexadecimal notation. For economy, 11 items of information are incorporated into 4 words The positions of the hexadecimal point for each item have been indicated.

TABLE 8. PHOTOCOPY OF BLTR PRINT-OUT FOR CY 468-1-MAGENTA

```
 CY-468-1....RED

 STRIP2B
 LIST:
 READA14
 AREA A
 BLTRA--
 TRAC-03
 END

 READA14
 AREA A

      20055
 BLTRA--

 CLEAR COUNTER 0 TO DUMP IMAGE B ON TAPE 0A NOW OR NEVER :
 START AS REQUIRED
 CLEAR COUNTER 0 TO DUMP IMAGE A ON TAPE 0A
 AT ANY FLEX PRINT BREAKPOINT
 Set flex to 4 COLUMNS:

 NO..    AREA   YminYmax Ht   XminXmax Wd   Ln. Th. L/T

 0001|0004DAD| □ 004|00A|00A8| □ 004|00A|00A8|  0CA|006|2|00|20
 0002|0000003| * 004|0005|0001|   03F|004|2|0003|  003|0001|00|30
 0003|0000001|   00C|000D|0001|   087|0088|0001|  001|0001|00|10
 0004|0000003|   01A|001C|0002|   01E|0021|0003|  003|0001|00|30
 0005|0000005|   01D|0020|0003|   06F|0072|0003|  003|0001|00|1C
 0006|0000003|   044|0046|0002|   06A|006C|0002|  002|0001|00|15
 0007|0000020|   045|004C|0007|   052|0058|0006|  008|0004|00|20
 0008|0000002|   052|0053|0001|   058|005A|0002|  002|0001|00|20
 0009|000001A|   059|005E|0005|   03F|0048|0009|  00A|0002|00|3D
 000A|000002C|   08F|0097|0008|   05C|0067|000B|  00C|0003|00|34
 000B|0000003|   09A|009C|0002|   07A|007C|0002|  002|0001|00|15
 000C|0000001|   09E|009F|0001|   042|0043|0001|  001|0001|00|10
 000D|0000001|   09F|00A0|0001|   00D|000E|0001|  001|0001|00|10
 000E|000002A| *0A5|00AC|0007| *0A4|00AC|0008|  009|0004|00|1E
 000F|0000004| *0AA|00AC|0002|   059|005C|0003|  003|0001|00|24
 BLOBS CLEAR
 TRAC-03
 CLEAR 0 TO TRANSFER
```

The first magenta cut is found to contain F=15 "blobs." Of these, blob number 1 has an area of 4DAD=19885 units, which is 99.15 percent of the total magenta area of 20055 units. The minimum and maximum addresses in Y (vertical, down) and X (horizontal, to right) are found to be the known edge addresses, 004 and 0AC, respectively, hence this blob extends over the entire height and width of the image, but surrounds other small blobs to which it is not connected in the plane of the micrograph. It may also be noted that blobs numbered

2. E and F also show one or two edge addresses, and thus touch some edge of the image. It should be presumed that their area of 49 units would have been found connected to the main blob if the cut had been made in a different position. The remaining 11 small blobs, containing 0.6 percent of the Nb_3Sn area, cannot be proved to be connected to the main area, but very likely are so connected some place in the unseen volume.

The connectivity data for the three magenta cuts are summarized in table 9. As the three cuts overlap in the original micrograph, the three large blobs are all parts of one larger blob, which encompasses 99.6 percent of the observed Nb_3Sn area, and occupies 70 percent of the volume observed. Thus, at least one convoluted but continuous path can be traced between two points at least 140 mm apart in the picture (560μ in specimen). There is every reason to presume that at least one such continuous path would extend (in volume) through the length of the wire even if the observable path should be found to terminate somewhere on the particular plane examined. Therefore, if the magenta phase is in fact a good superconductor, and this micrograph represents a low quality superconductor, the cause of this low quality must be presumed to lie in the short *linear* paths (or in restricted cross sections), not in lack of connectivity in the absolute sense.

TABLE 9. *Connectivity of Nb_3Sn phase; magenta images—complex paths*

1 area unit = 1×10^{-6} mm² on original

Item	Cut 1	Cut 2	Cut 3	Total
Area of phase	20055	21082	21349	62486
Area, main blob	19885	20882	21294	62061
Main blob, %	99.15	99.05	99.74	99.32
Number edge blobs	3	5	3	11
Area in edge blobs	49	143	8	200
In edge blobs, %	0.24	0.68	0.04	0.32
Presumed connective, %	99.40	99.73	99.78	99.64
No. disconnected blobs	11	11	8	30
Area, disconnected	121	57	47	225
Disconnected, %	0.60	0.27	0.22	0.36
Total volume connective, %	67.42	71.65	71.28	70.12

14. Particle Size Distributions

A further statistical description of the nature of the areas which interrupt the Nb_3Sn phase can be obtained by constructing histograms of the additional parameters given by the BLTR analyses. Since the machine coding for these operations has not been completed, the tallies were made manually from the BLTR print-out in the same manner as performed by the machine in the LINE operation. These tallies thus may also serve to determine the utility which may be expected from the next phase of the computer programming.

The distributions of blue, black, and yellow blobs according to area classes are shown in figures 9–11. Since, on logarithmic classes, a blob having height in class 7 and a width in class 5 should have an area in class 12, the scale of the abscissa is now reduced by a factor of two. Peaks due to the same groups of particles will thus fall in the same physical position on the graphs in both area and length plots.

The "raw" distributions are obtained by tallying the blob areas stated by the computer, without regard to the fact that some blobs have been cut by the edges of the pictures, and are therefore larger than stated. In the "edge corrected" distributions blobs which had edge addresses were tallied as half blobs twice as large (two classes larger), and corner blobs as quarter blobs four classes larger. This treatment has essentially the same effect as the half grain convention normally used with the Jeffries method of grain size determination.[5]

Both forms of the area distributions show essentially similar patterns, the average area being increased only a fraction of one class by edge correction. The displacements between the 50 percentile points, modes, and averages show these distributions to be abnormal. This is due to the presence of concentrations of very small areas, the presence of which was not entirely obvious in the line distributions. In the case of the black voids, a very high concentration of unit areas (class 0; area = 10^{-6} mm²) is the most prominent feature of the histograms.

[5] The circular format used in the Jeffries method [13] is advantageous in manual counting, since a circle of exactly known area is easily constructed. Establishing a circular border in the computer would be a complex operation involving greater error than that due to the $4/\pi$ increase in border length due to the square format; hence the square format is dictated for computer use.

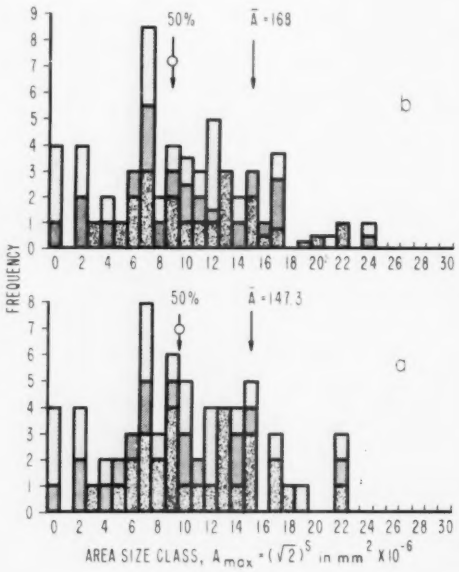

FIGURE 9. *Histogram of area class distribution for blue particles* (Nb + Nb Sn).

(a) Raw data.
(b) Data corrected for edge cutting.

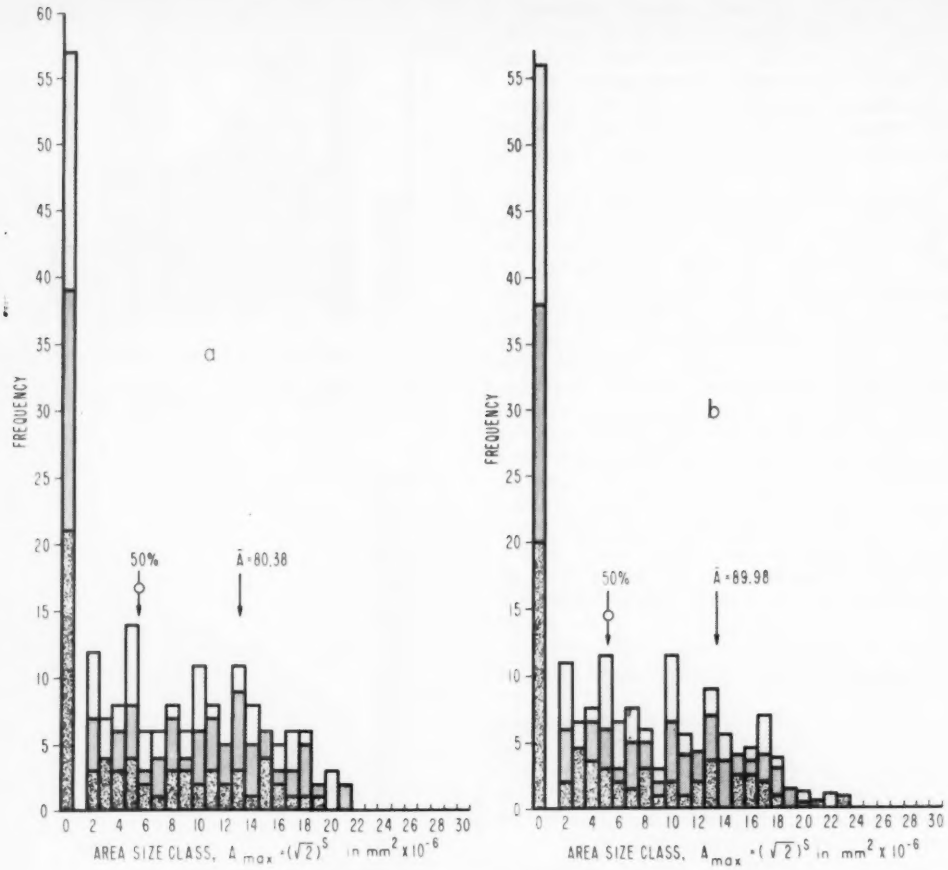

FIGURE 10. *Histogram of area class distribution for black voids.*

(a) Raw data.
(b) Data corrected for edge cutting.

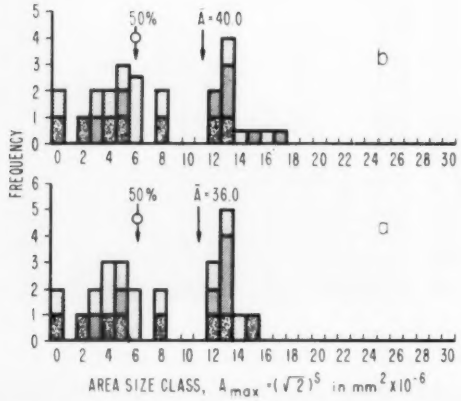

FIGURE 11. *Histogram of area class distribution for yellow particles* (Nb_2Sn_2).

(a) Raw data.
(b) Data corrected for edge cutting.

If one ascribes all of the unit areas to spherical voids of unit volume (a crude approximation) it may be estimated that 1 mm^3 of the core material contains 6.6×10^5 such voids of average volume $= 10^{-9}$ mm^3, as compared with about 25000 voids of volume class 15 (V max$=181\times10^{-9}$ mm^3), which are mainly responsible for the mode at class 5 in the lineal analysis.

If nearly a million voids per cubic millimeter were caused by improper packing—that is by failure of tin to fill the spaces between the original niobium particles, than a majority of these particles would have had to be in diameter class 7 (9 to 11 μ). Such an assumption is contradicted by the presence of blue residues in area class 22 and height and width classes 12 and 13 (figs 12 and 14). It would thus seem apparent that the original niobium powder was of the common 200 mesh grade (diameter class 12) and therefore consisted of only around 5000 grains/mm^3. Since there are apparently more than 100 small voids per original niobium grain, it must be assumed that these small voids must have resulted from the Nb-Sn diffusion reaction and not from poor packing. Metallurgically, this might result either from decomposition of some compound of niobium and a gas, or from the Kirkendall effect in the diffusion.

15. Height, Width, and Length

The parameter "height" in the BLTR routine output is the calliper dimension of a particle in the vertical dimension of the image as seen by the computer. In the present pictures, height is perpendicular to the axis of the wire. Histograms for this parameter are shown in figures 12 and 13.

"Width" is the corresponding caliper dimension in a direction parallel to the wire axis. Histograms are shown in figures 14 and 15. These two sets of histograms share some of the properties of the area histograms, in that the abnormal abundance of small holes can be more clearly detected than in the lineal analysis, where the multiple traces from larger particles overshadow the single traces from the smallest particles.

The height and width histograms can be compared to detect preferred orientation or elongation of particles. In the case of the blue (niobium) material, the mean width, 14.16 μ, exceeds the mean height, 10.69 μ, by almost a factor of $\sqrt{2}$, which is a strong indication that the niobium particles were *rotated* in the soft tin matrix during the production of the wire. However, if the niobium grains had themselves been appreciably cold-worked, they would then be expected to have been elongated to an extent approaching the final length/diameter ratio attained by a hypothetical cube of metal from the original niobium sheath; which ratio is computed as 3815, (for a diameter reduction of 15.6 times). As actual width to height ratios of at least 100 can be observed in an etched micrograph of the sheath, it is apparent that the niobium grains remaining in the core were not subject to any significant amount of

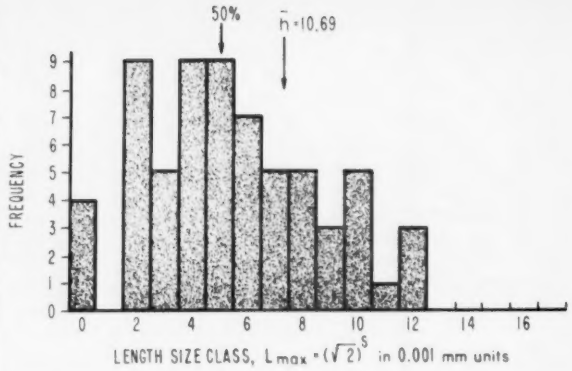

FIGURE 12. *Histogram of height distribution for blue particles (Nb+Nb$_3$Sn).*

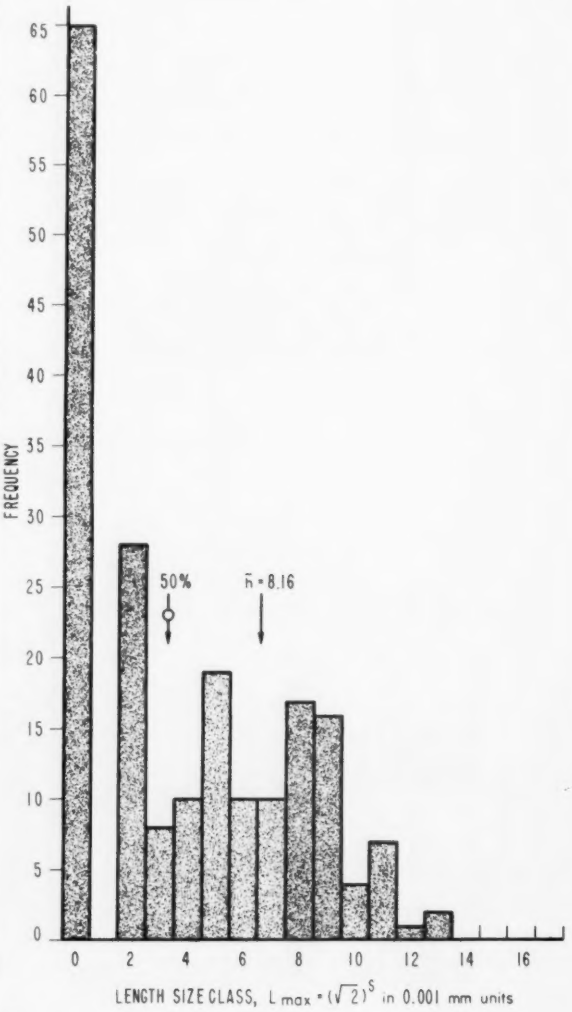

FIGURE 13. *Histogram of height distribution for black voids.*

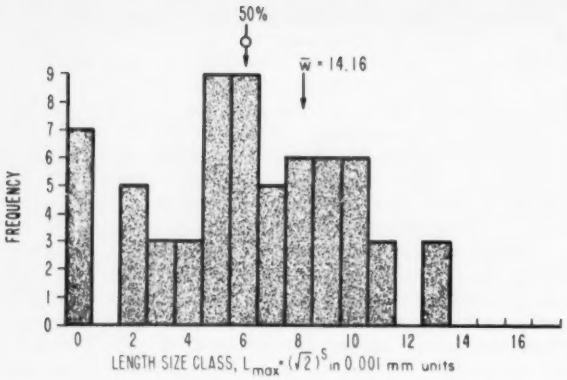

FIGURE 14. *Histogram of width distribution for blue particles* ($Nb+Nb_4Sn$).

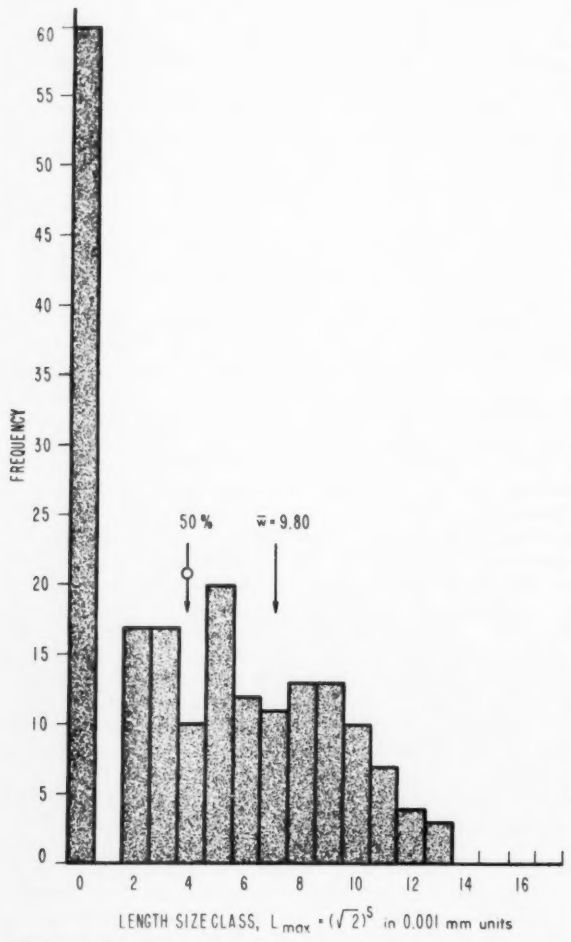

FIGURE 15. *Histogram of width distribution for black voids.*

coldwork, and that the anisotropy of dimensions is probably only that existing in the original niobium powder.

The average ratio of width to height for voids is 9.80 to 8.16 or 1.20; hardly a significant departure from symmetry. Voids which resulted from incomplete packing of the original powders would have been elongated even more easily than the particles of soft tin. Thus it again appears clear that the observed voids are not held over from the packing of the powders.

"Length" is an estimated value taken as the average of the longer of the two measured dimensions and the maximum diagonal of the circumscribed rectangle. The approximation is adequate to place the largest dimension of the section in the correct size class, with a maximum error of ½ class. Length histograms are shown in figures 16 and 17. These are somewhat more regular than the corresponding height or width histrograms, but do not appear to disclose any new information in the present case. The increase of average length over average width is only that inherent in the computation.

The division of blob area by estimated length gives a value for the estimated mean thickness. The ratio of the length to this thickness gives a shape factor whose values lie from 1 1/16 to 2 for equiaxed particles. High values indicate a complex shape, and are mainly useful to permit the computer to recognize blobs which are in fact clustered grains which should be subdivided in computing a standard grain size distribution. Histograms of this factor show only that many of the blue grains and holes are not equiaxed. Such histograms are therefore omitted from this report.

16. Summary

Methods have been developed whereby a metallurgical micrograph can be shown to the digital computer SEAC, which may then be instructed to determine a number of useful parameters in the fields of lineal analysis and of particle size measurements. The elementary computer processes which make such measurements possible have been described, together with an outline of the manner in which many elementary operations can be combined into practical working routines. Such working routines can thereafter be applied to practical problems by operators who are not required to be familiar with the details of the actual computer program.

To illustrate routines already operating at the practical level, and to explore the possible significance of the data produced, the authors have chosen to show a detailed analysis of a color micrograph of what is believed to be a low quality specimen of the superconductor Nb_3Sn. In addition to its possible significance in the problem of producing higher quality superconducting devices, this micrograph presents analytical problems considerably greater than those which have normally been encountered in micrographic sections of other, and usually less complex, materials which have been quantitatively analyzed by hand methods.

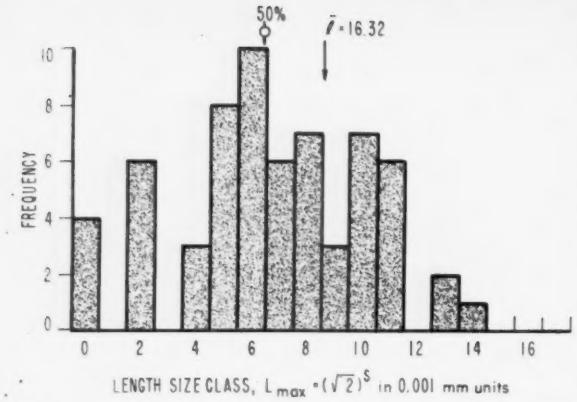

FIGURE 16. *Histogram of length distribution for blue particles (Nb+Nb_4Sn).*

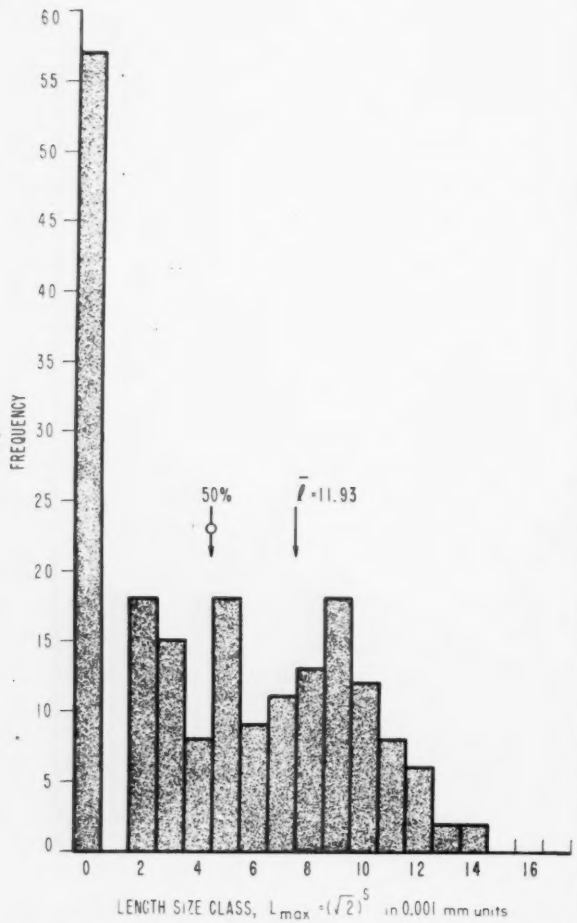

FIGURE 17. *Histogram of length distribution for black voids.*

The micrograph analyzed actually showed evidence of five solid constituents in addition to voids. Inasmuch as two of these constituents were in very small concentration, it was considered sufficient to make four color-separations, each showing one of the four major constituents. Three separate areas of each color were analyzed, with one being deliberately chosen to look "better" than the others. This "best" area proved, however, not to be significantly different from the others on a statistical basis.

The relative amounts of the four constituents were determined within a precision of about 1 percent, and the composition of the Nb_3Sn phase was computed with good agreement among the three tests and an absolute value within 1.3 percent of the stoichiometric value. Computations of variance indicate that differences between the sections of the micrograph are responsible for errors approximately four times as great as those inherent in the point sampling process used (as computed from the binomial distribution).

Parameters of possible significance in defining a high quality superconductor were measured, viz, the mechanical mean free path in each constituent, and the distributions of particle area, height, width, and length in each. The poor material was found to contain 70 percent by volume of the Nb_3Sn phase, of which 99.6 percent was interconnected by one or more paths (often complex). It does not appear reasonable to expect that an additional increase in absolute connectivity by a fraction of 1 percent would appreciably improve the superconducting quality.

The mechanical mean free path in the Nb_3Sn phase was found to be only 26.5μ. This represents an upper limit to the electronic mean free path in this phase, and a value low in the range which has been reported for good superconductors.

The interruptions of this mean free path are assigned mainly to the voids in the structure, with lesser portions due to residual high-niobium particles, and a small part due to high-tin material. The high-niobium particles are found to have been rotated during the working of the wire, but not to have themselves been significantly elongated or cold worked. The voids do not show evidence of elongation, and are found to exist in numbers of the order of 100 times the abundance which might reasonably be assigned to inadequate packing of the original mixture. The voids thus may be presumed to have originated in the reaction between tin and niobium, either by the Kirkendall effect or perhaps by decomposition of some compound of niobium and a gas.

It must however be emphasized that the actual role of the observed defects in the superconducting process must remain hypothetical until there are available, for quantitative metallographic analysis, micrographs of actual sections from good and bad wires, whose superconducting quality has been accurately measured. When numerical correlations can be made between a numerical index of superconducting quality and the various measurable micrographic parameters, it will be possible to determine which of these parameters are in fact significant.

With the presently available computer methods, data comparable to those illustrated in this report are no longer prohibitive to obtain. The present data were obtained in slightly over 2 hr of actual computer operation, at a nominal computer charge of less than $200. In this analysis, the computer performed around 8 million individual arithmetical and logical operations. As some of the necessary data processing steps had not yet been coded for the computer, an estimated 20 thousand equivalent elementary operations were performed by hand, at a cost of around 100 man hours. Based on these estimates, the cost of acquiring quantitative metallographic information by computer may be less than 1 percent of the cost to perform the same processes with equal accuracy by hand.

Programming is in process for a "slice" analysis to determine variations in cross sections, and for a more accurate measurement of grain circumferences, as well as for the computation of the histograms for the particle size analysis. Means are available for the direct machine plotting of the histograms from the computer output. When all steps of the analytical process have been mechanized, it will be entirely feasible to deliver completed diagrams of the distributions of the desired parameters within minutes of the delivery to the computer of suitable photomicrographs. Once all parts of this programming have been worked out on the present size scale, the routines are expected to be duplicated for a larger computer (PILOT) where work can be done on the 8 × 10 in. (20 × 25 cm) scale with an expected accuracy in the 0.1 percent range.

While the present illustration has been taken from the field of optical metallography, the computer processes are in no way dependent on the actual nature of the original material, or on the magnification or kind of microscope used. The same computer programs may be applied directly to petrographic subjects, and to many similar biological problems, and, on any size scale, to any similar counting or measuring problem in which the original information can be represented in a suitable photograph. Further exploration may be expected to show many useful applications for geometrical parameters which have heretofore been neglected because of the labor required for measuring such parameters by hand methods.

Sincere thanks are extended to Dr. M. L. Picklesimer of the Oak Ridge National Laboratory for supplying color micrographs of actual Nb-Sn superconductor wires.

Mr. R. B. Thomas of the NBS Data Processing Systems Division compiled the basic library of image processing routines used and has supplied valuable advice and help in composing additional analytical routines.

Mr. H. M. Joseph has assisted in the composition of the new routines and in the operation of the computer during the present study.

17. References

[1] Quantitative Metallography, F. N. Rhines (Ed.) (McGraw-Hill Book Co., Inc., New York, N.Y., in Press). Chapter 15: Comments on the possibilities of performing quantitative metallographic analyses with a digital computer, G. A. Moore, L. L. Wyman, and H. M. Joseph.

[2] R. A. Kirsch, Processing pictorial information with digital computers, A.I.E.E., CP 57–878 (1957). R. A. Kirsch, L. Cahn, C. Ray, and G. H. Urban, Experiments in processing pictorial information with a digital computer, p. 221, Proc. Eastern Joint Computer Conference (1957).

[3] (a) B. T. Matthias, T. H. Geballe, S. Geller, and E. Covenzwit, Superconductivity of Nb_3Sn, Phys. Rev. **95,** 1435 (1954). (b) J. E. Kunzler, E. Buchler, F. S. L. Hso, and J. H. Wernick, Superconductivity in Nb_3Sn at high current density in a magnetic field of 88 Kgauss, Phys. Rev. Letters **6,** 89 (1961).

[4] V. D. Arp, R. H. Kropschot, and J. H. Wilson, Superconductivity of Nb_3Sn in pulsed fields of 185 kilogauss, Phys. Rev. Letters **6,** (9) 452 (1961).

[5] (a) R. McFee, Applications of superconductivity to the generation and distribution of electric power, Electrical Engineering 81/2 (2/62) 122–129. (b) F. Bitter, Strong magnets, International Science and Technology 1/4 (Apr. 1962) 58–64.

[6] G. A. Moore, The comportment of the palladium-hydrogen system toward alternating electric current, Journal of Electrochem. Soc. **75,** 237–267 (1939).

[7] F. B. Hagedorn, Dependence of superconducting—transition temperature on residual, electronic mean free path in tin thin films, Bul. Am. Phys. Soc. **11,** 7/3 p. 175 (Mar. 26, 1962).

[8] L. L. Wyman, J. R. Cuthill, G. A. Moore, J. J. Park, and H. Yakowitz, Intermediate phases in superconducting niobium-tin alloys, Journal of Research of the NBS 66A (Phys. and Chem.) No. 4, 351–363 (July–Aug. 1962).

[9] M. L. Picklesimer, Anodizing as a metallographic technique for zirconium base alloys, U.S. Atomic Energy Commission, ORNL 2296 13 p. (1957).

[10] A. Maerz and M. R. Paul, Dictionary of Color (McGraw-Hill Book Company, Inc., New York, New York 1930).

[11] Welding Handbook, 3d Edition, Am. Welding Society, 1950, Table p. 1023.

[12] B. I. Edelson and W. M. Baldwin, Jr., The Effect of second phases on the mechanical properties of alloys, Trans. Am. Soc. Met. **55** [1] 230–250 (Mar. 1962).

[13] ASTM Designation E112–61, Standard methods for estimating the average grain size of metals.

[14] L. L. Wyman and G. A. Moore, Quantitative metallographic evaluations of graphitic microstructures—modern castings **43** [1] 7–16 (Jan. 1963).

(Paper 67A2–200)

JOURNAL OF RESEARCH of the National Bureau of Standards—A. Physics and Chemistry
Vol. 67A, No. 2, March–April 1963

Moiré Fringes Produced by a Point Projection X-ray Microscope

Sanford B. Newman

(November 30, 1962)

Moiré fringes produced by soft X-rays passing through crossed gratings of fine wire mesh are demonstrated. Regular systems of bands appearing superimposed on radiomicrographs of oriented cellulosic structures may also be moiré fringes. These fringes could be formed by fibrillate structures acting as crossed diffraction gratings.

1. Introduction

In the simplest and most familiar case moiré fringes are observed when two parallel, fairly coarse, bar and slit gratings of different pitch are held between the eye and an extended source. When the gratings overlap, the wide bars shown in figure 1a appear. Superimposed gratings of equal pitch will also produce a moiré pattern when given an angular displacement about the normal to the plane of the gratings as shown in figure 1b. There are, of course, many types of gratings whose fringes cannot be observed in this way, especially if the gratings are of fine pitch. Moreover, moiré patterns containing contributions from both of these basic types are often encountered as well as complexities arising from grating irregularities and angular displacements other than those mentioned previously. The designation, moiré, is derived from the effect produced by the fabric of the same name when two layers are in contact.

Rayleigh [1] [1] was probably the first to record observations on a simple arrangement for producing moiré fringes and to indicate the relationship between the spacing of the primary gratings, the spacing of the parallel bars, and the mutual inclination of the two gratings of the set. In recent years these fringes have been studied intensively as part of the diffraction grating development program at the National Physical Laboratory, and characteristics and applications have been presented in great detail by Guild [2]. Electron microscopists have also been

[1] Figures in brackets indicate the literature references at the end of this paper.

FIGURE 1a. *Moiré fringes in the upper right quadrant formed by superimposing two Ronchi rulings of different pitch, (upper left and lower right quadrant).*

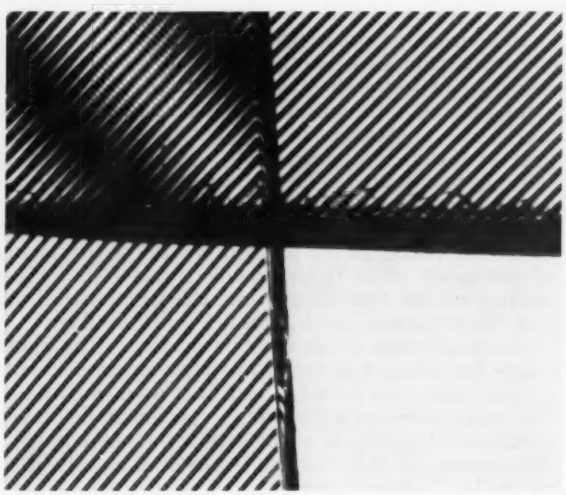

FIGURE 1b. *Moiré fringes in the upper left quadrant formed by slight rotation of two Ronchi rulings of the same pitch, (upper right and lower left) about normal to the plane of the gratings.*

able to utilize moiré fringes in the determination of crystal lattice parameters. Overlapping thin crystals act as the gratings to produce fringes, which may be examined and measured at high magnification [3].

Moiré fringes produced by X-rays, however, do not appear to have been noted or utilized in X-ray optics. This paper demonstrates their formation and their similarity to fringes produced by light with the same gratings. The use of such fringes for elucidating structure in point projection X-ray microscopy is also indicated.

2. Equipment and Materials

The first practical X-ray point projection microscopes were produced over a decade ago [4] but their availability has been extremely limited until the last few years. All of the observations to be described here were made using electromagnetic microfocus tubes. An instrument designed by Long [5] having only an objective lens was used in the early work. A commercially produced, two-lens, X-ray microscope was used for the subsequent examinations. Both instruments were fitted with copper and aluminum targets and operated at about 15 kv and at not more than 20 μa.

The fibers were obtained from the collection of the U.S. Department of Agriculture, Bureau of Plant Industry, through the courtesy of Elton G. Nelson.

3. Observations

To determine the practicability of forming moiré fringes by means of X-rays, some coarse gratings were observed in the X-ray point projection microscope. A piece of electrodeposited silver fabric having 1000 wires to the inch was folded on itself so that the wires in both directions were nearly parallel. This grating system when examined with a low power light microscope produced the broad moiré pattern of crossed bars shown in figure 2a. The folded fabric was then placed a short distance from the target of a microfocus tube and the projected image of the fabric was photographed. Broad fringes again appear in the image produced by the X-ray beam as seen in figure 2b. The pattern was visible using either copper or aluminum radiation but the contrast in the radiograph was higher with the latter. Small differences in the pattern are due to displacing of the mesh while it was being transferred for recording of the two images but the general outlines and dimensions of the fringes are quite similar.

A phenomenon which may be related to the moiré fringe formation was noted in specimens of tula istlé (*Agave lecheguilla* Torr.), a leaf fiber used in cordage. The radiomicrographs of many specimens displayed transverse banding of a surprisingly regular nature. The increment between the bands was usually close to the limit of resolution of the microscope—some 2 or 3 μ. Bands were not present uniformly over the entire fiber bundle but would appear in patches often hundreds of square microns in extent. The indi-

FIGURE 2a. *Silver mesh (1000 wires/in.) folded double.*

The wires of the two layers are displaced sufficiently to produce the moiré pattern shown when viewed in white light.

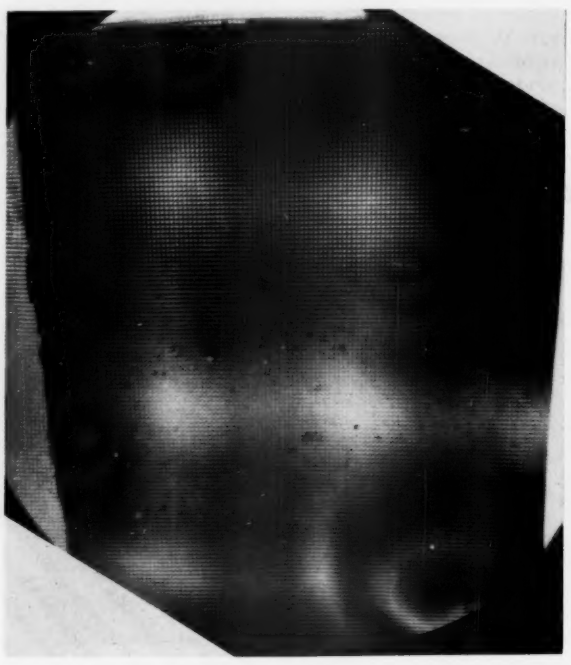

FIGURE 2b. *The same specimen as in 2a.*

The radiograph was made at slightly higher magnification using an aluminum target at 15 kv. Slight changes in the pattern are caused mainly by manipulating the specimen in transferring it between instruments.

vidual bands seemed to have only a rather nebulous relationship with single fibers in the bundle and usually extended over the diameters of several of these components as shown in figures 3a and 3b.

The structure of the cell walls of higher plants are well known due to the work of Bailey [6], Kerr [7], and Hock [8], as well as a host of others too numerous to cite here. From these studies it would appear that the only structure which could be correlated with these parallel bars are the spiral windings that form one of the outer layers of the cell wall. This winding consists of a fibrillate thread, a few tenths of a micron in diameter, and make a steep angle with the fiber axis. Since the winding could not be resolved directly by either instrument it might be assumed that windings in opposite sides of fibers or windings on adjacent fibers were acting as gratings to produce the effect.

An alternative source of the bars could be gratings consisting of the fibrillae parallel to the fiber axis yielding rotation moiré. Because of the variables inherent in such a grating system, however, it would be difficult to determine the importance of each of the basic patterns in the fringe formation.

The bars were not exhibited by fibers such as flax (*Linum usitatissimum* L.) and ramie (*Boehmeria nivea* (L.) Gaud.) which possess two windings spiralling in different directions. Spacings were observed in a number of agaves, in hemp (*Cannabis sativa* L.) and in fiber from a luffa sponge (*Luffa* sp), all of which have only a single peripheral winding.

Staining the fiber structure by precipitating gold or silver did not contribute to the resolution of the bands. As far as can be determined instrumentally the metal is deposited fairly homogeneously in the matrix.

4. Summary

Moiré fringes are readily formed by a broad beam of X-rays. These fringes may be an aid in revealing structure below the projection imaging power of the X-ray microscope.

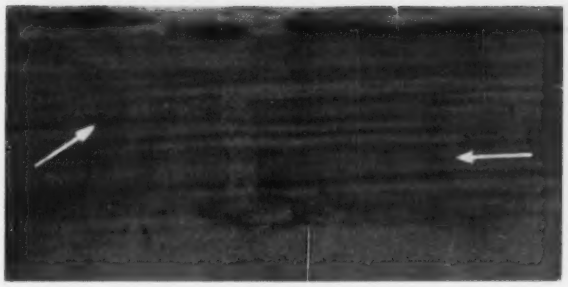

FIGURE 3a. *Transverse bands in microradiographs of the fibers of the fruit of* Luffa.

Copper target, 15 kv.

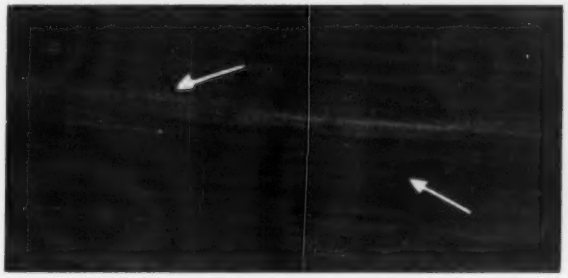

FIGURE 3b. *Transverse bands in microradiograph of leaf fibers of* Agave lecheguilla *Torr.*

Copper target, 15 kv.

5. References

[1] Lord Rayleigh, Phil. Mag. **47,** 81 (1874).
[2] Guild J., Interference Systems of Crossed Diffraction Gratings, Oxford University Press, London (1956).
[3] Menter, J., Advances in Physics **1,** 299 (1958).
[4] Cosslett, V. E. and Nixon, W. C., Nature **168,** 24 (1951).
[5] Long, J. V. P., Ph. D. Thesis, Cambridge (1959).
[6] Bailey, I. W., Ind. Eng. Chem. **30,** 40 (1938).
[7] Kerr, T., Protoplasma **27,** 229 (1937).
[8] Hock, C., J. Research NBS **29,** 41 (1942).

(Paper 67A2–201)

JOURNAL OF RESEARCH of the National Bureau of Standards—A. Physics and Chemistry
Vol. 67A, No. 2, March–April 1963

Cyclic Polyhydroxy Ketones. I. Oxidation Products of Hexahydroxybenzene (Benzenehexol)

Alexander J. Fatiadi, Horace S. Isbell, and William F. Sager*

(December 11, 1962)

Reliable procedures are given for the preparation and purification of hexahydroxybenzene (benzenehexol), tetrahydroxy-*p*-benzoquinone, rhodizonic acid, triquinoyl (cyclohexanehexone), croconic acid, and leuconic acid (cyclopentanepentone). Certain derivatives and color tests, as well as infrared and ultraviolet spectra, are reported for their identification.

1. Introduction

On oxidation, cyclohexanehexols (inositols) yield keto derivatives which, by successive enolization and elimination reactions, can be transformed to polyhydroxybenzenes [1–5].[1] In progressing from cyclohexane derivatives through cyclic olefinic intermediates to aromatic compounds, reactions and materials are encountered which are eminently suited for the study of reaction mechanisms and basic concepts of theoretical organic chemistry [6].

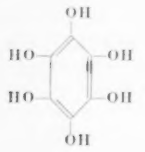

I

Hexahydroxybenzene (Benzenehexol)

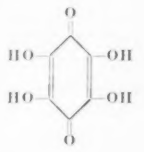

II

Tetrahydroxy-*p*-benzoquinone

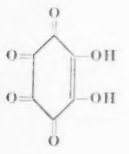

III

Rhodizonic acid

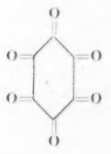

IV

Triquinoyl (Cyclohexanehexone)

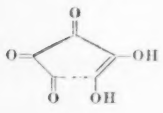

V

Croconic acid

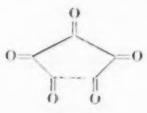

VI

Leuconic acid (Cyclopentanepentone)

Hexahydroxybenzene (benzenehexol, I) can be prepared from inositols (cyclohexanehexols) and from tetrahydroxy-*p*-benzoquinone (II, obtained by self-condensation of glyoxal in alkaline solution). Oxidation of I yields II, which is further oxidized to rhodizonic acid (III), and this is oxidized to triquinoyl (cyclohexanehexone, IV). Tetrahydroxy-*p*-benzoquinone and rhodizonic acid are not only interesting in their own right, but also serve as intermediates in the preparation of croconic acid (V), a dihydroxy triketone having a five-carbon ring. Oxidation of croconic acid yields leuconic acid (VI). Because these compounds, needed as model substrates in a study of antioxidant and oxygen-carrier properties, were not available in a suitable state of purity, the methods reported in the experimental part were developed for their synthesis and purification.

2. Hexahydroxybenzene (Benzenehexol, I) [7]

2.1. Discussion

Hexahydroxybenzene (I), the enolic form of the trihydroxytriketocyclohexanes, can be prepared by the self-condensation of potassium carbonyl followed by hydrolysis [8, 9], by nitration of di-*O*-acetylhydroquinone followed by reduction and hydrolysis [10], by oxidation of *myo*-inositol followed by enolization [11], and by reduction of tetrahydroxy-*p*-benzoquinone (II) by means of stannous chloride [12].

2.2 Preparation of Hexahydroxybenzene [13][2]

Stannous chloride dihydrate (100 g, 0.44 mole) is added in one portion to a boiling, mechanically stirred solution of 10 g (0.058 mole) of tetrahydroxy-*p*-benzoquinone (II) in 200 ml of 2.5-*N* hydrochloric acid. In a few minutes, the red color of II disappears and long, needle-like crystals of hexa-

* The George Washington University, Washington, D. C.

[1] Figures in brackets indicate the literature references at the end of this paper.

[2] This procedure was developed in 1959 by one of us (A.J.F.), under the direction of Dr. William F. Sager at George Washington University [13], and was briefly described by Fieser and Fieser [14].

hydroxybenzene (I) begin to form. Concentrated hydrochloric acid (250 ml; specific gravity 1.08) is added, and the stirred suspension is heated to boiling, mixed with 600 ml of concentrated hydrochloric acid, cooled in ice, and filtered with suction on a fritted-glass filter. As much solvent as possible is removed by suction, without exposure to air, by covering the filter with an inverted funnel and introducing nitrogen, and by using a polyethylene dam to remove the final traces of the solvent.

For purification, the crude product is dissolved in 450 ml of hot 2.5-*N* hydrochloric acid containing 3 g of stannous chloride dihydrate. Decolorizing carbon is added, the hot suspension is filtered, the insoluble matter is washed with 75 ml of hot water, and the combined filtrate and washings are mixed with 1 liter of concentrated hydrochloric acid and cooled in ice. The resulting crystals are collected on a fritted-glass filter, in an atmosphere of nitrogen, washed with 100 ml of a cold, 1:1 mixture of ethanol and concentrated hydrochloric acid, and dried over sodium hydroxide in a vacuum desiccator to give 7 to 8 g (about 75%) of colorless crystals which do not melt[3] when placed on a hot plate at 310 ° C. Infrared and ultraviolet absorption spectra are recorded on pages 158 and 160.

Hexahydroxybenzene can also be recrystallized from 2-methoxyethanol by the addition of benzene; the crystals are separated, washed with acetone, and dried in a vacuum desiccator. The yield is about the same as in the previous method.

Characteristic derivatives of hexahydroxybenzene are the hexaacetate, mp 203 to 205 °C [10, 15], the hexabenzoate, mp 323 to 325 °C [9], and the hexamethyl ether, mp 81 °C [16].

The following convenient color tests may be used for identification of hexahydroxybenzene:

(a) (Developed in this laboratory.) A solution of ferric chloride in 1:1 aqueous methanol is slowly added dropwise to a stirred, aqueous solution of hexahydroxybenzene under a stream of nitrogen. As addition of the ferric chloride proceeds, the color of the solution passes successively through the following characteristic series, representing oxidation steps: magenta or cherry red (II); green (III); and, finally, a stable, deep blue (presumably a mixture of III and IV). When the solution is cooled in ice for several hours, colorless crystals of the octahydrate of IV gradually separate.

(b) [9] One ml of a concentrated, aqueous solution of barium chloride is mixed with 0.5 ml of a dilute, aqueous solution of ferric chloride containing one or two drops of acetic acid (or of dilute hydrochloric acid). To the mixed solution are added one or two drops of an aqueous solution of hexahydroxybenzene. A bright-red precipitate of barium rhodizonate results.

(c) [9] One ml of a dilute, aqueous solution of hexahydroxybenzene is mixed with 1 ml of a saturated, aqueous solution of magnesium nitrate, and a few drops of dilute ammonia are added. A carmine-red precipitate results.

3. Tetrahydroxy-*p*-benzoquinone (II) [17]

3.1. Discussion

The preparation of tetrahydroxy-*p*-benzoquinone is based on the self-condensation of glyoxal in the presence of sodium sulfite, air, and a base. The procedure was originated by Homolka [15], and has been studied and modified by subsequent workers [18, 19, 20]. Presumably, hexahydroxybenzene is formed initially; this is oxidized to tetrahydroxy-*p*-benzoquinone, and this, in turn, to rhodizonic acid. As shown by Fatiadi and Sager [13], when sodium bicarbonate is used as a buffer, the disodium salt of tetrahydroxy-*p*-benzoquinone is formed in a yield of 8 to 11 percent. When the reaction mixture is highly alkaline, substantial quantities of disodium rhodizonate and disodium croconate are formed, in addition to the disodium salt of tetrahydroxy-*p*-benzoquinone.

3.2. Preparation of the Disodium Salt of Tetrahydroxy-*p*-benzoquinone [13]

A solution of 400 g (3.17 moles) of anhydrous sodium sulfite and 150 g (1.79 moles) of sodium bicarbonate in 3 liters of water is placed in a 5-liter, three-necked flask fitted with a thermometer, an air inlet tube (1-cm diam), and a tube connected to a water aspirator. The solution is heated to 40 to 45 °C, and 600 g of a 30-percent, aqueous solution of glyoxal (3.1 moles) is added. A brisk stream of air is drawn through the solution for 1 hr without heating, after which the mixture is gradually heated to 90 °C. Aeration is then stopped, and the mixture is heated to incipient boiling and cooled to room temperature. The resulting, crystalline disodium salt of II is removed by filtration, washed successively with 50 ml of cold, 50-percent, aqueous methanol and 50 ml of methanol, and dried in a vacuum desiccator. The yield (22 to 24 g) corresponds to about 10 percent of the theoretical, based on the glyoxal used. The product can be used without purification for the preparation of tetrahydroxybenzene, rhodizonic acid, or croconic acid. It is sensitive to oxidation by air and, if stored in a loosely stoppered bottle, is completely oxidized to disodium rhodizonate in several months. Tetrahydroxy-*p*-benzoquinone is, however, relatively stable in air.

3.3. Preparation of Tetrahydroxy-*p*-benzoquinone

The crude disodium salt of II (20 g) is dissolved in 220 ml of 2.5-*N* hydrochloric acid by heating. On cooling, the solution yields glistening, black crystals of tetrahydroxy-*p*-benzoquinone which are collected by filtration, washed with ice water, and dried in a vacuum desiccator; wt, 12 to 15 g. The product is recrystallized from warm, 2-*N* hydro-

[3] Unless the product is thoroughly washed, it may contain traces of tin salts. The presence of tin can be determined by dissolving a sample in nitric acid, evaporating the solution, and igniting the residue. When the recrystallization is conducted properly, this test does not provide any appreciable final residue. Use of stannous chloride in the recrystallization prevents the formation of undesired oxidation products.

chloric acid to give lustrous, dark crystals [8]; alternatively, it may be recrystallized from acetone by the addition of petroleum ether to give small, dark crystals. Spectrograms are given on pages 158 and 160.

4. Rhodizonic Acid (III) [21]

4.1. Discussion

Heretofore, rhodizonic acid (III), the oxidation product of II, has been prepared by oxidation of *myo*-inositol with nitric acid [11], by reduction of IV with sulfurous acid [10, 16, 20], and by synthesis from glyoxal [15]. Described below are the preparation of ammonium rhodizonate [21] from glyoxal, and of rhodizonic acid from the disodium salt of II by oxidation in air.

4.2. Preparation of Tetrahydroxy-*p*-benzoquinone and Ammonium Rhodizonate from Glyoxal

Aqueous glyoxal (600 g of a 30-percent solution) is self-condensed in the presence of sodium sulfite, oxygen, and sodium bicarbonate as described in section 3.2. After 1 hr of aeration, 100 g of sodium hydroxide is added. The alkaline solution (*p*H 10) is heated, with aeration, to incipient boiling, and cooled to room temperature. The mixture of crystalline sodium salts of II and III is filtered off and washed successively with 50 ml of cold, 50-percent aqueous methanol and 50 ml of methanol. The air-dried salts (24 to 26 g) are dissolved in 200 ml of 2.5-*N* hydrochloric acid by boiling, and the solution is immediately cooled in ice.[4] The resulting crystalline II (8 to 9 g) is separated by filtration, washed with 20 ml of ice water, and dried.

The ice-cold, dark-red filtrate is brought to *p*H 5.5 to 6.5 with ammonia. The resulti g, dark-blue, crystalline ammonium rhodizonate is separated by filtration, washed with 25 ml of ice water, and air-dried; wt, 7 to 8 g. It is recrystallized from 750 ml of hot water.

4.3. Preparation of Rhodizonic Acid from the Disodium Salt of II

The disodium salt of II (40 g), prepared as described in section 3.2, is placed in a large, flat-bottomed dish and heated in an oven at 170 to 180 °C for 24 hr. The residue is suspended, with mechanical stirring, in 200 ml of warm, 2.5-*N* hydrochloric acid, and after several minutes, 1 g of decolorizing carbon is added; the solution is cooled in ice and filtered through a filter paper precoated with paper pulp. The brownish-yellow solution is concentrated under diminished pressure at 35 °C to a semicrystalline mass, and the aqueous hydrochloric acid is removed by successive addition and evaporation of three 50-ml portions of a 1:1 mixture of benzene and acetone. The residue is triturated with 50 ml of acetone, the suspension is filtered, and the insoluble product is washed with sufficient cold acetone to remove all colored impurities. The crystalline residue, consisting of sodium chloride and crude rhodizonic acid dihydrate, is air-dried and pulverized, and the powder is added to 200 ml of dioxane preheated to 80 °C. The suspension is stirred for 5 min and then filtered through a filter paper precoated with decolorizing carbon. The insoluble matter is washed with 50 ml of warm dioxane, and the slightly colored filtrate is cooled to about 20 °C. Pentane (about 150 ml) is added to incipient turbidity, and crystallization of rhodizonic acid dihydrate is induced by scratching the inside walls of the container with a glass rod. The mixture is cooled in ice for about 30 min, the suspension is filtered, and the crystals are washed with 50 ml of a cold, 1:1 mixture of dioxane and pentane, and air-dried; wt, 25 to 35 g.

The crude rhodizonic acid dihydrate is recrystallized from warm dioxane by the addition of pentane and ether; by concentration of the filtrate, an additional crop is obtained. The air-dried product, which still contains dioxane, is dried for 48 hr in a vacuum desiccator over sulfuric acid; total yield, about 21 g (60%) of colorless crystals. Measurements of infrared and ultraviolet absorption are reported on pages 158 and 160.

The purity of the product may be determined by titration with iodine [20]; 155 mg of rhodizonic acid dihydrate consume 14.97 ml of 0.1-*N* I_3^- solution; found, 15.07 ml.

If subjected to a high vacuum (0.1 mm) at room temperature the compound is converted into the scarlet-red crystals of anhydrous rhodizonic acid in as little as 5 min. The same transformation can be accomplished at higher temperatures by vacuum sublimation [20]. Rhodizonic acid gives a colorless solution in 2.5-*N* hydrochloric acid, whereas tetrahydroxy-*p*-benzoquinone gives a cherry-red solution.

5. Triquinoyl (Cyclohexanehexone, IV) [23]

5.1. Discussion

In 1862, Lerch [24] obtained a product, now known as triquinoyl, by oxidation of either hexahydroxybenzene (I) or tetrahydroxy-*p*-benzoquinone (II) with nitric acid or chlorine. The substance has been characterized by Nietzki and coworkers [8, 10, 25], and studied by Henle [26], Bergel [27], and Eistert and coworkers [20, 22]. The procedure described here is based on the original work of Lerch and of Nietzki. Because some workers have experienced difficulty in the preparation and purification of IV, the procedures are given in detail.

5.2. Preparation of Triquinoyl Octahydrate

Recrystallized tetrahydroxy-*p*-benzoquinone (10 g) is added in small increments during 5 min to a mechanically stirred solution of 100 ml of concentraten nitric acid and 25 ml of water kept at 10 °C. The reaction is continued for an additional 5 min, 25 ml of water is added, and the mixture is cooled in ice for 15 min. The crystalline triquinoyl octahydrate that separates is filtered off, washed successively with 20 ml of ice water and 30 ml of an ice-cold,

[4] Prolonged heating causes disproportionation [22].

1:1 mixture of acetone and ether, and air-dried; wt, 12 to 12.5 g; mp 96 to 97 °C.

The substance is recrystallized in the following manner: The octahydrate (5 g) is suspended in 50 ml of methanol containing 3 ml of concentrated nitric acid, and the suspension is heated to 55 to 60 °C, with stirring. When dissolution is complete, about 200 mg of decolorizing carbon is added, the suspension is filtered, and the insoluble matter is washed with 25 ml of water. The combined filtrate and washings are evaporated under diminished pressure to about 25 ml, and the solution is cooled in ice until crystallization begins, and then gradually diluted with 20 ml of acetone. The crystals are collected on a filter, washed successively with 10 ml of cold 1:1 acetone-water mixture and 20 ml of cold acetone, and air-dried; wt, 2.1 g. By concentration of the mother liquor, additional material (0.6 g) is obtained. The octahydrate consists of colorless, lustrous plates or prisms, mp 99 to 100 °C (decomposition). Infrared and ultraviolet absorption spectra are recorded on pages 159 and 161.

A characteristic color test [26] for IV involves heating the compound with a saturated, aqueous solution of barium chloride; bright-red barium rhodizonate is precipitated, following disproportionation [8, 22].

6. Croconic Acid (V) [28]

6.1. Discussion

Croconic acid (V) is one of the first enediolic acids to have been reported. Since its discovery by Gmelin [29] in 1825, it has engaged the attention of many workers [10, 30–39]. As pointed out by Hirata and coworkers [36], the anion has an unusual resonance structure. Croconic acid is formed from a variety of polyhydroxybenzene derivatives by oxidation followed by a rearrangement of the benzylic acid type. It can be efficiently prepared by oxidation of tetrahydroxy-*p*-benzoquinone or rhodizonic acid with manganese dioxide. In the process, the benzene ring is degraded, with elimination of carbon dioxide. The reaction was discovered by Nietzki [32] and has since been used by many workers. The procedure given here resembles one described by Yamada and Hirata [40], and differs from prior methods in that it starts with the crude mixture of sodium salts obtained from the condensation of glyoxal (instead of with pure sodium rhodizonate) and uses a special type [41] of active manganese dioxide as the oxidant.

6.2. Preparation of Active Manganese Dioxide

Commercial manganese carbonate (500 g) in a flat-bottomed tray or dish is heated in an oven at 295 to 310°C for 12 to 18 hr. After being cooled, the product is treated with sufficient aqueous nitric acid (15 to 20 ml of concentrated acid per 100 ml of solution) to decompose any residual carbonate and to give a strongly acid solution. After 30 to 45 min, the manganese dioxide is filtered off, thoroughly washed with water, and dried at 150 to 160 °C for 18 to 24 hr. After its recovery from reaction mixtures, active manganese dioxide can be used repeatedly if it is redried at 150 to 160 °C for 18 to 24 hr. Manganese dioxide prepared by other methods proved to be less satisfactory.

6.3. Barium Croconate Hydrate

To a solution of 40 g of sodium hydroxide in 1.2 liters of water are added, with stirring, 21 g (0.1 mole) of crude disodium tetrahydroxy-*p*-benzoquinone (see section 3.2) and 55 g of active manganese dioxide. After 5 min, the mixture is heated to boiling, refluxed for 45 min, and filtered, and the manganese dioxide is washed with 800 ml of hot water. The combined filtrate and washings are treated with about 210 ml of concentrated hydrochloric acid in portions, giving a bright-yellow solution. To this is added a hot solution of 50 g of barium chloride dihydrate in 150 ml of water, with stirring; the mixture is heated to 85 to 90 °C, cooled, and kept at room temperature. The resulting, lustrous, yellow plates of barium croconate monohydrate are collected on a filter, washed successively with water and ethanol, and air-dried; wt, 22 to 23 g.

6.4. Conversion of Barium Croconate to Sodium Croconate

Barium croconate (17.5 g; 0.06 mole) is added in small portions, with stirring, to 150 ml of a 10-percent aqueous solution of anhydrous sodium carbonate. The mixture is boiled for 5 min and filtered; the barium carbonate is washed with 30 ml of hot water, and the combined yellow filtrate and washings are diluted with 20 ml of glacial acetic acid, heated to boiling, and cooled in ice. Disodium croconate trihydrate separates in long, yellow crystals, which are collected on a filter, washed with 40 ml of ice water, and air-dried; wt, about 10 g. A second crop (2.5 to 3.5 g) is obtained by adding about 200 ml of 95-percent ethanol to the mother liquor and cooling the solution.

Dipotassium croconate may be prepared similarly.

6.5. Croconic Acid Trihydrate

Barium croconate (55 g) is added in small portions to 200 ml of mechanically stirred, aqueous sulfuric acid (containing 20 ml of concentrated acid) at 55 to 60 °C; stirring is continued for 30 to 45 min. The barium sulfate is separated by filtration, washed with 25 ml of hot water, and discarded. The combined filtrate and washings are evaporated to dryness under diminished pressure, the residue is dissolved in a hot solution of 25 ml of absolute ethanol and 150 ml of dioxane, and the solution is treated with a small quantity of decolorizing carbon and filtered. The filtrate is concentrated under diminished pressure at 40 °C until crystallization begins, and the mixture is diluted with benzene to incipient turbidity and cooled.

After several hours, the resulting crystals are separated by filtration, washed with benzene, and dried in a vacuum desiccator. By concentration of the mother liquor, additional crystals are obtained; the combined yield of croconic acid trihydrate is about 20 g. Infrared and ultraviolet absorption spectra are recorded on pages 159 and 161.

Anhydrous croconic acid is prepared by heating the trihydrate at 120 °C for 2 to 4 hrs; it slowly decomposes above 150 °C. Croconic acid may be characterized as the dimethyl ether, mp 113 °C [35].

Small quantities of croconic acid may be prepared by passing a solution of 5 g of disodium croconate in 300 ml of water through 80 ml of a cation-exchange resin (Amberlite 120–H^+), concentrating the effluent under diminished pressure, and crystallizing the product from dioxane with the addition of ether, benzene, or pentane.

6.6. Preparation of Manganese Croconate Trihydrate

A solution of 5 g of croconic acid trihydrate in 50 ml of hot water is treated, with stirring, with a hot, saturated, aqueous solution of manganous acetate until a precipitate forms. The mixture is cooled to room temperature, and the resulting greenish-yellow crystals are separated by filtration. The product is recrystallized from water by the addition of acetone; the yield is almost quantitative.

Analysis: Calculated for $C_5MnO_5 \cdot 3H_2O$: C, 24.1; H, 2.41. Found: C, 24.0; H, 2.5.

6.7. Analysis of Croconic Acid

The purity of samples of croconic acid may be determined by titration with a standard solution of potassium permanganate (see eq (1)).

$$12\ KMnO_4 + 23\ H_2SO_4 + 5\ Na_2C_5O_5 \rightarrow 6\ K_2SO_4 + 12\ MnSO_4 + 25\ CO_2 + 5\ Na_2SO_4 + 23\ H_2O \quad (1)$$

A 50-mg sample of disodium croconate, previously dried at 120 °C for 1 hr, is transferred to a 250-ml Erlenmeyer flask with 25 to 50 ml of water. Sulfuric acid (50 ml of 3.6 *N*) is added, and the solution is heated to 80 °C and rapidly titrated with 0.1-*N* potassium permanganate to the complete disappearance of the original yellow color. Then 5 ml of a 5-percent solution of zinc chloride is added, and the addition of permanganate is continued dropwise with swirling, until a faint pink color, stable for about 1 min, is produced. A 50-mg sample of disodium croconate monohydrate consumed 29.20 ml of 0.1-*N* potassium permanganate; calculated for $Na_2C_5O_5 \cdot H_2O$: 29.40 ml.

7. Leuconic Acid (Cyclopentanepentone, VI) [42]

7.1. Discussion

Leuconic acid was first prepared by Will [43] in 1861. Particularly noteworthy investigations were made by Nietzki [32], Homolka [44], and Eistert and coworkers [22]. The procedure given in the present paper is a modification of that of Nietzki.

7.2. Preparation of Leuconic Acid Pentahydrate

Purified anhydrous croconic acid (2 g), or an equivalent amount of the trihydrate, is added in portions, with stirring, to 20 ml of ice-cold, concentrated nitric acid during 3 min, and the mixture is stirred until evolution of nitrogen dioxide ceases (about 10 min). Then 20 ml of ice-cold methanol is added, and the mixture is stirred while crystallization of leuconic acid pentahydrate occurs; after 10 min, the crystals are separated by filtration, washed with methanol, and air-dried; wt, about 2.7 g.

For recrystallization, the compound is dissolved in the minimal quantity of water; the solution is treated with decolorizing carbon and filtered, and the filtrate is concentrated under diminished pressure at 40 °C to about 5 ml. After the addition of several drops of concentrated nitric acid, the solution, on cooling, yields colorless crystals of leuconic acid pentahydrate. Infrared and ultraviolet absorption spectra are given on pages 159 and 161.

Crystalline leuconic acid pentahydrate may be isolated from concentrated, aqueous solution by adding a 1:1 mixture of 2-propanol and ethanol; this product is devoid of nitric acid.

The pentahydrate melts with dehydration at 115 to 118 °C, followed by slow decomposition at 158 to 162 °C. Leuconic acid may be characterized as the pentaoxime [32], mp 172 °C. In the present study, it has been found that the oxime may conveniently be recrystallized from *N*,*N*-dimethylformamide.

When a saturated solution of sodium carbonate is added to an aqueous solution of leuconic acid, a pink color is produced, followed by deposition of a difficultly soluble, white precipitate of the sodium salt of mesoxalic acid [44].

8. Spectrophotometric Measurements

Figure 1 reports infrared spectrograms for the freshly prepared, crystalline compounds in Nujol mulls. The measurements were made with a Perkin-Elmer Infracord Model 137 (double beam) spectrophotometer equipped with a prism of sodium chloride for the 2- to 15-μ range.

The ultraviolet absorption measurements given in figure 2 were made with a Beckman DK–2 spectrophotometer with matched, 1-cm quartz cells and the appropriate solvent as the reference standard. In the course of time, the spectra for some of the compounds change, presumably from oxidation reactions. To minimize oxidation, freshly boiled solvents were used, but complete exclusion of oxygen was not attempted.

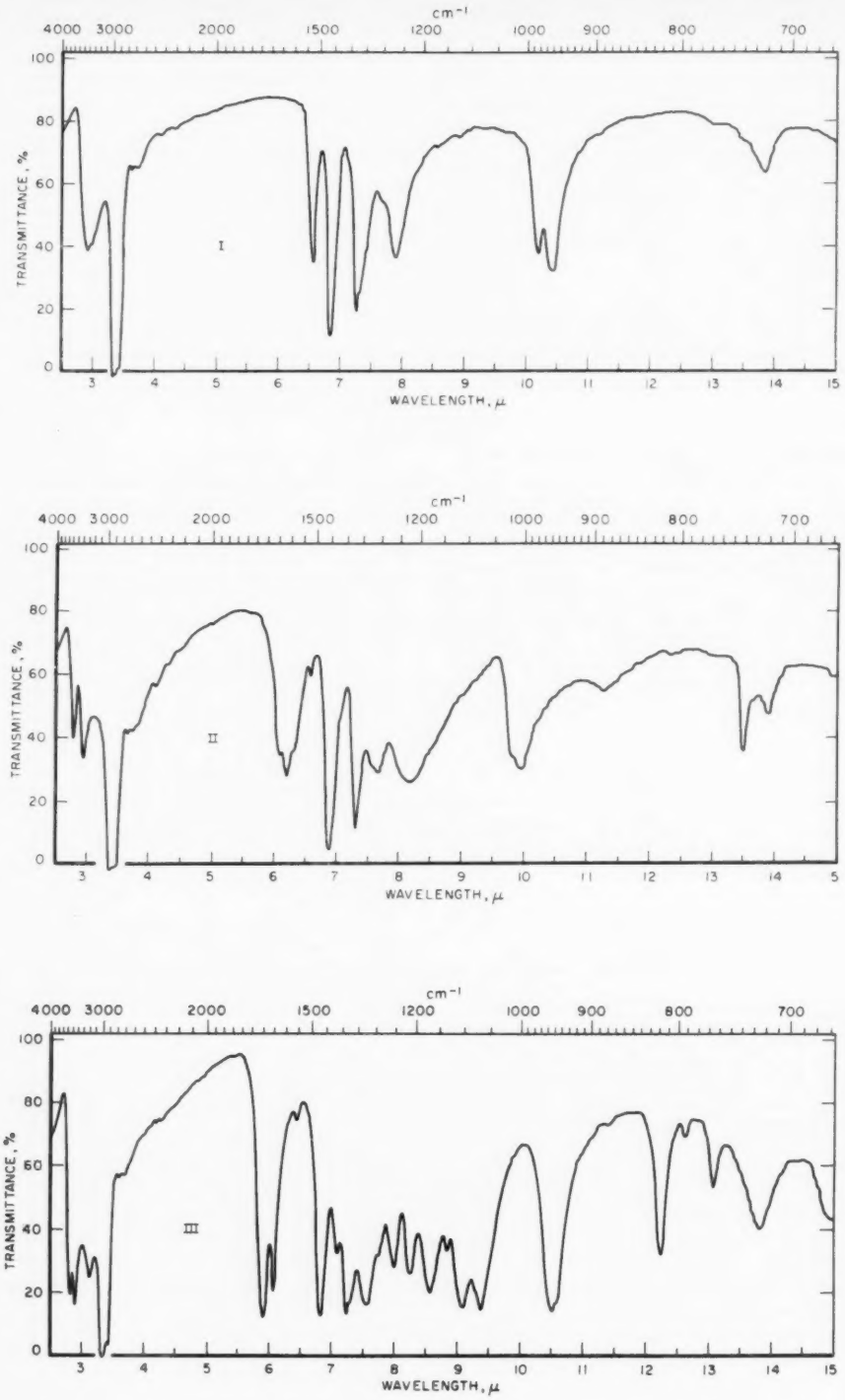

FIGURE 1. *Infrared spectrograms of materials in Nujol mulls.*

I, Hexahydroxybenzene; II, tetrahydroxyquinone; III, rhodizonic acid dihydrate.

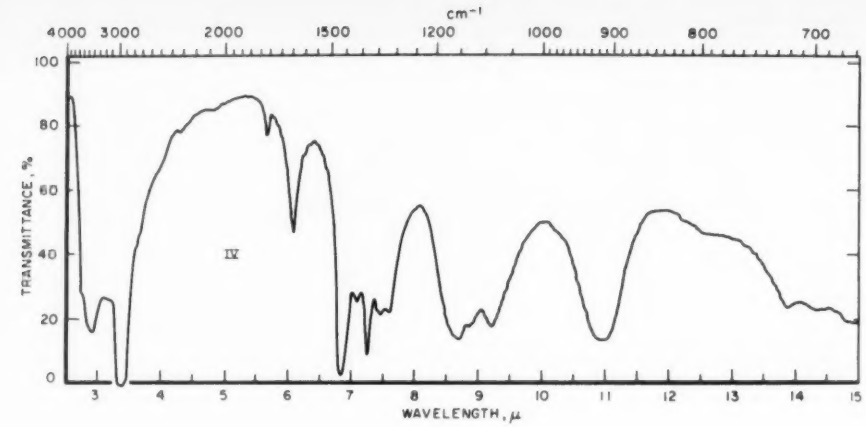

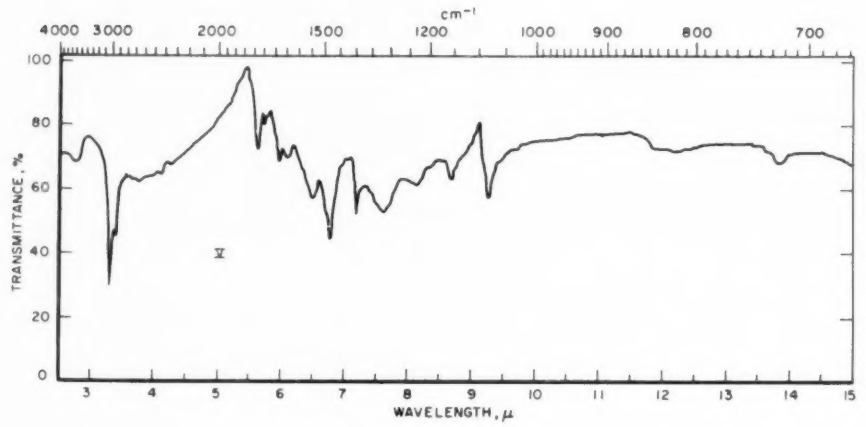

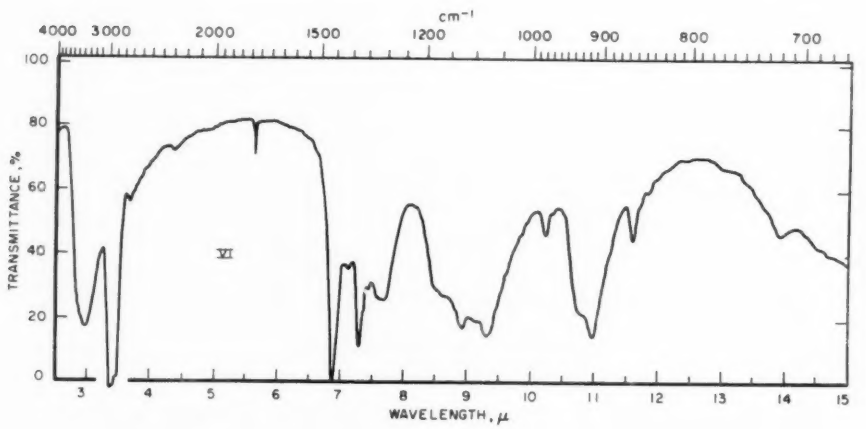

FIGURE 1. *Infrared spectrograms of materials in Nujol mulls*—Continued

IV, Triquinoyl octahydrate; V, croconic acid trihydrate; VI, leuconic acid pentahydrate.

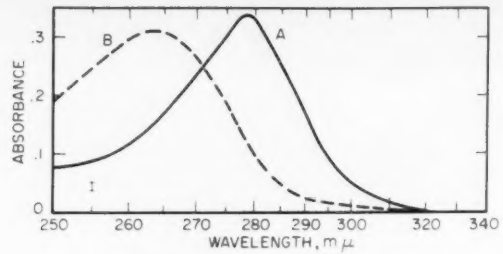

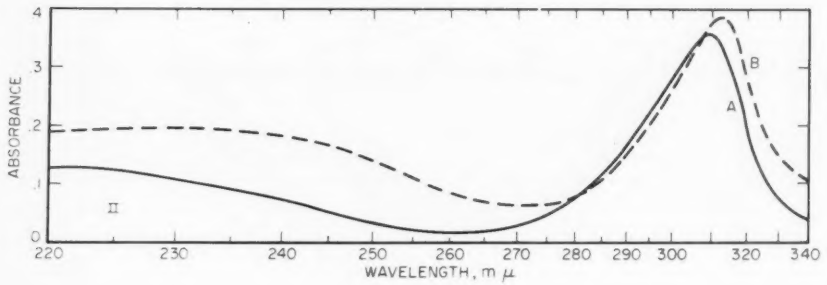

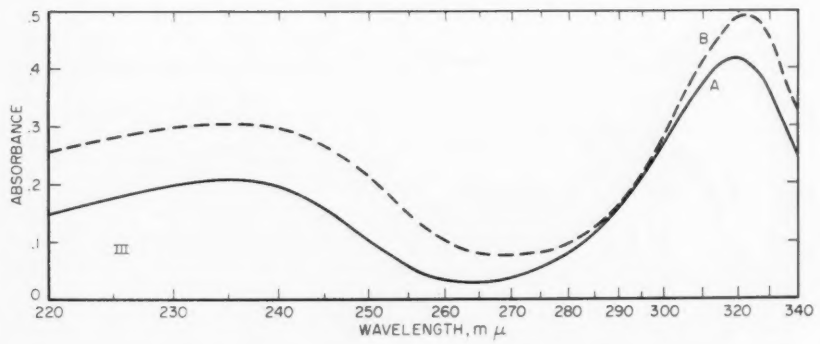

FIGURE 2. *Ultraviolet spectrograms of materials.*

I. Hexahydroxybenzene. Curve A, 7.39 mg of I in 100 ml of 6*N* HCl in methanol, 3 min after dissolution; λ_{max} at 278 mμ. Curve B, 67 mg of the hexaacetate of I in 200 ml of glacial acetic acid, 10 min after dissolution; λ_{max} at 283 mμ.
II. Tetrahydroxyquinone. Curve A, 3.82 mg of II in 1000 ml of 2*N* aqueous HCl, 24 hr after dissolution; λ_{max} at 308 mμ. Curve B, 7 mg of II in 1000 ml of methanol, 30 min after dissolution; λ_{max} at 312 mμ.
III. Rhodizonic acid dihydrate. Curve A, 6.87 mg of III in 1000 ml of 2*N* aqueous HCl 24 hr after dissolution; λ_{max} at 235 mμ and at 319 mμ. Curve B, 8.58 mg of III in 1000 ml of methanol, 5 min after dissolution; λ_{max} at 235 mμ and at 323 mμ. In the visible region, III shows absorption at 443 mμ and at 487 mμ (sh).

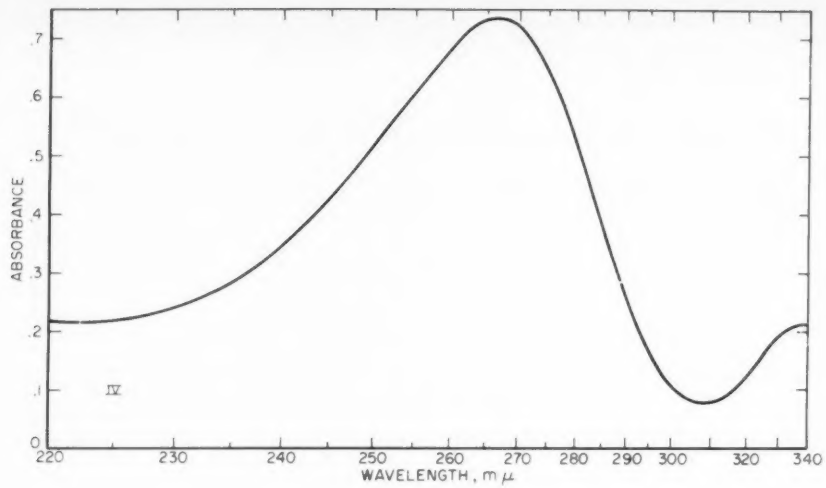

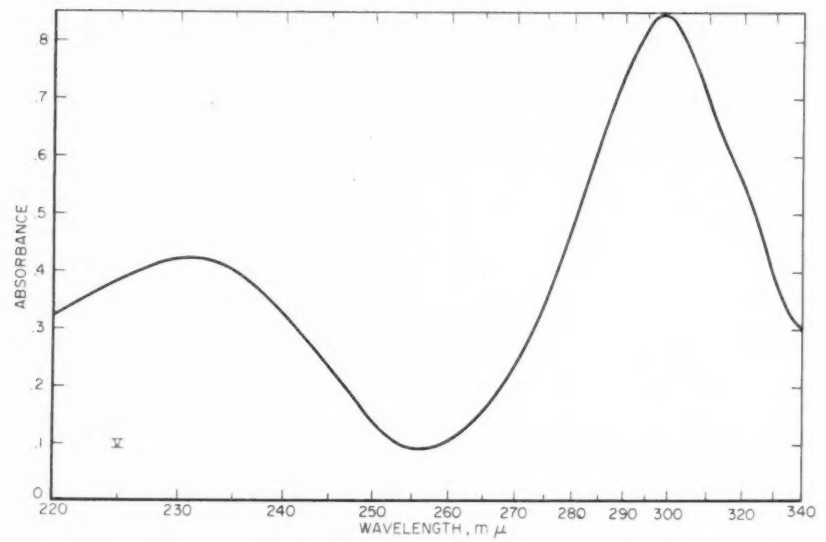

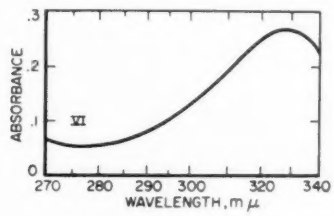

FIGURE 2. *Ultraviolet spectrograms of materials*—Continued.

IV. Triquinoyl octahydrate. 3.24 mg of IV in 100 ml of 2*N* aqueous NaCl 1.5 hr after dissolution; λ_{max} at 267 mμ. In the visible region, IV shows marked absorption at 363 mμ, 440 mμ (sh) and 480 mμ.

V. Croconic acid trihydrate. 5.87 mg of V in 100 ml of 2*N* aqueous HCl, 10 min after dissolution; λ_{max} at 231 mμ and at 298 mμ.

VI. Leuconic acid pentahydrate. 156.45 mg of VI in 50 ml of water, 5 min after dissolution; λ_{max} at 328 mμ.

9. References

[1] T. Posternak, Helv. Chim. Acta **19,** 1333 (1936); **24,** 1045 (1941).
[2] T. Posternak and J. Deshusses, Helv. Chim. Acta **44,** 2089 (1961).
[3] N. Z. Stanacev and M. Kates, J. Org. Chem. **26,** 912 (1961).
[4] H. S. Isbell, Ann. Rev. Biochem. **12,** 213 (1943).
[5] H. S. Isbell, J. Research NBS **32,** 45 (1944).
[6] R. West and Hsien-Ying Niu, J. Am. Chem. Soc. **84,** 1324 (1962); Chem. Eng. News **40,** 40 (1962).
[7] Beilsteins Handb. Org. Chemie **6,** 1198, Springer, Berlin (1923).
[8] R. Nietzki and T. Benckiser, Ber. **18,** 1833 (1885).
[9] A. J. Fatiadi (with W. F. Sager), M. S. Thesis, 1959, The George Washington University, Washington, D.C.
[10] R. Nietzki and T. Benckiser, Ber. **18,** 499 (1885).
[11] P. W. Preisler and L. Berger, J. Am. Chem. Soc. **64,** 67 (1942).
[12] R. C. Anderson and E. S. Wallis, J. Am. Chem. Soc. **70,** 2931 (1948).
[13] A. J. Fatiadi and W. F. Sager, Org. Syntheses **42,** (a)66, (b)90 (1962).
[14] Louis F. Fieser and Mary Fieser, Advanced Organic Chemistry, p. 757 (Reinhold Publ. Corp., New York, N.Y., 1961).
[15] B. Homolka, Ber. **54,** 1393 (1921).
[16] R. Robinson and C. Vasey, J. Chem. Soc. 1941, 660.
[17] Beilsteins Handb. Org. Chemie **8,** 534, Springer, Berlin (1925).
[18] H. J. Backer and S.v.d. Baan, Rec. Trav. Chim. **56,** 1161 (1937).
[19] R. Kuhn, G. Quadbeck, and E. Rohm, Ann. **565,** 1 (1949).
[20] B. Eistert and G. Bock, Angew. Chem. **70,** 595 (1958).
[21] Beilsteins Handb. Org. Chemie **8,** 535, Springer, Berlin (1925).
[22] B. Eistert, G. Bock, E. Kosch, and F. Spalink, Chem. Ber. **93,** 1451 (1960).
[23] Beilsteins Handb. Org. Chemie **7,** 907, Springer, Berlin (1925).
[24] J. Lerch, Ann. **124,** 34 (1862).
[25] R. Nietzki and F. Kehrman, Ber. **20,** 322 (1887).
[26] F. Henle, Ann. **350,** 330 (1906).
[27] F. Bergel, Ber. **62,** 490 (1929).
[28] Beilsteins Handb. Org. Chemie **8,** 489, Springer, Berlin (1925).
[29] L. Gmelin, Ann. Phys. **4,** 31 (1825).
[30] J. Liebig, Ann. **11,** 182 (1834).
[31] R. Nietzki and T. Benckiser, Ber. **19,** 293 (1886).
[32] R. Nietzki, Ber. **20,** 1617 (1887).
[33] R. Nietzki, Ber. **23,** 3136 (1890).
[34] O. Gelormini and E. Artz, J. Am. Chem. Soc. **52,** 2483 (1930).
[35] R. Malachowski and S. Prebendowski, Ber. **71,** 2241 (1938).
[36] Y. Hirata, K. Inukai, and T. Tsujiuchi, J. Chem. Soc. Japan **69,** 63 (1948); C. A. **47,** 5902 (1953).
[37] F. Arcamone, C. Prevost, and P. Souchay, Bull. Soc. Chim. France 1953, 891.
[38] S. Ruthkowski, Rocz. Chem. **36,** 169 (1962).
[39] B. Carlquist and D. Dyrssen, Acta Chem. Scand. **16,** 94 (1962).
[40] K. Yamada and Y. Hirata, Bull. Chem. Soc. Japan **31,** 550 (1958).
[41] M. Harfenist, A. Barley, and W. A. Lazier, J. Org. Chem. **19,** 1608 (1954).
[42] Beilsteins Handb. Org. Chemie **7,** 905, Springer, Berlin (1925).
[43] H. Will, Ann. **118,** 177 (1861).
[44] B. Homolka, Ber. **55,** 1310 (1922).

(Paper 67A2–202)

JOURNAL OF RESEARCH of the National Bureau of Standards—A. Physics and Chemistry
Vol. 67A, No. 2, March–April 1963

Effect of Pressure and Temperature on the Refractive Indices of Benzene, Carbon Tetrachloride, and Water

R. M. Waxler and C. E. Weir

(October 31, 1962)

An interferometer for measuring change in index of refraction with pressure is described. Absolute indices of refraction are reported to five decimals for benzene, carbon tetrachloride, and water at pressures as high as 1100 bars over a small temperature range. The results of replicate measurements agree to within ± 0.0001. Various equations relating index and specific volume show systematic deviations in all cases. At constant specific volume, the index of carbon tetrachloride increases with increasing temperature, while the index of water decreases with increasing temperature. The refractive index of benzene shows no effect due solely to temperature within the experimental error. Possible explanations for this behavior are discussed.

1. Introduction

Recently there has been great interest in studying optical properties of materials at high pressure as a method of examining short range molecular interactions, the present emphasis being confined largely to spectroscopic measurements. To a large extent index of refraction measurements have been neglected in these studies, although it would appear that index studies with their inherent precision might be of assistance in interpreting spectroscopic data. Index-density studies on condensed phases have been made previously, but the objectives of the previous experiments were usually to determine the applicability of index-density relationships or the usefulness of index as a measure of volume change. Most of the data published have been given to about the fourth decimal, and although such precision is excellent for many measurements, it is not particularly good for index of refraction. The present work was undertaken in an attempt to increase the precision of index measurements at elevated pressures. For these studies an interferometer for use at high pressures has been developed, and this report contains the results of measurements on three liquids at pressures up to about 1000 bars.

Poulter, Ritchey, and Benz [1] [1] used the minimum deviation method for studying the refractive indices of liquids to 13,600 atm. The windows [2] of their pressure vessel were mounted at an angle of 30° to each other and with the enclosed liquid constituted a 30° prism. Poulter and Benz [3] discussed the errors arising from distortion of the windows. Rosen [4] used a similar method for studying water to 1800 bars. This equipment as described by Lyons and Poindexter [5] utilized windows forming a prism with a 51° angle. These workers estimated the errors arising from distortion to be of the order of 0.0003 in index but concluded that this error was less than other experimental errors. Gibson and Kincaid [6] used the immersion method for studying the index of benzene. In these studies glass particles were immersed in benzene and pressure was used to match the index of the benzene to that of the glass. A sensitivity of 0.00004 is reported for index but the data are reported to the fourth decimal in index. In these studies the index of the glass was known at 1 bar but its value at elevated pressure was calculated.

As early as 1857, Jamin [7] described the use of an interferometer for measuring change in refractive index of fluids under pressure. Most subsequent work has been done on gases, the most notable being that of Michels and Hamers [8]. The windows limit the pressure range of interference methods. The present report describes an interferometer which is completely enclosed in the pressure vessel so that distortion of the windows at elevated pressure has a negligible effect on the interference pattern. In the present experiments, change in refractive index was measured with a sensitivity of 0.00001 and estimated limits of reproducibility, expressed as twice the standard deviations about the mean, of the order of ± 0.0001. With modifications it is believed that both the precision and the pressure range can be extended by at least one order of magnitude. It is also apparent that the principle can be used to obtain precise data on PVT behavior of solids.

2. Apparatus and Experimental Method

2.1. Interferometer Construction

The interferometer, figure 1, was constructed using a stainless steel bar, A, which was about 130 mm long and 13 mm square. The optical portion consisted of two optical flats separated by a steel spacer.

[1] Figures in brackets indicate the literature references at the end of this paper.

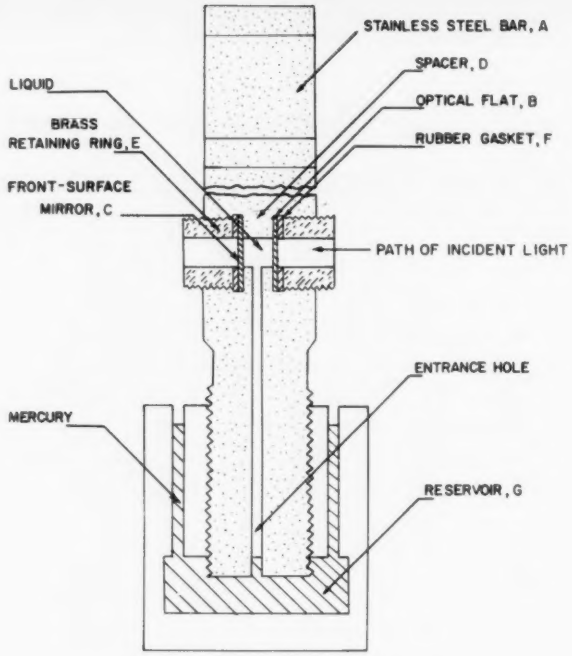

FIGURE 1. *Cross section of the interferometer.*

Recesses 11 mm in diameter to accommodate the flats were made in opposite sides near one end of the bar. The recesses were of such depth as to leave a web, D, of steel about 3 mm thick in the center of the bar. The steel web served as a seat and spacer for the optical flats and was machined so that its surfaces were parallel. The flats were held firmly against the web by threaded brass rings, E, screwed into the upper threaded portion of the recesses. A small neoprene rubber gasket, F, under each ring was used to seal the cell against leakage and to prevent cracking of the flat. It was necessary to silver both flats to produce bright fringes because they were in contact with liquids having indices of refraction not appreciably different from that of the glass. Thus the front flat, B, was half-silvered on its rear surface and the back plate, C, was a front surface mirror, the light being incident from the right as shown in figure 1. The small glass flats 11 mm in diameter were cut from larger optical flats obtained commercially.

A small hole 3 mm in diameter drilled through the web served as the interferometer chamber. To permit introduction of liquid into the chamber, a small axial hole about 1.5 mm in diameter connected the chamber with the lower end of the bar. This end of the bar was threaded and screwed into a stainless steel reservoir, G, containing mercury to separate the liquid under study from the oil used as a pressure-transmitting medium. A small hole was drilled into the reservoir to permit transmission of pressure. The upper end of the bar was slotted to facilitate alinement of the interferometer inside the pressure vessel before applying pressure.

2.2. Pressure Vessel

The pressure vessel was mounted on a large optical bench with the associated optical equipment. This vessel was the one used by Gibson [9] in his classic experiments on liquids. The heavy-walled steel container was fitted with two heavy plate glass windows. The windows were supported by hardened optically flat steel plugs of a design proposed by Poulter [2]. The windows provided an aperture of 8 mm which was adequate for viewing the fringes in the 3 mm interferometer chamber placed opposite the windows inside the vessel. The pressure vessel was thermostatted by means of a temperature-controlled oil bath capable of control to within ± 0.02 °C. To obtain temperatures below room temperature, the bath was cooled with the immersion coil of a portable refrigerator.

In studying each liquid, the oil bath was brought to constant temperatures of 25, 35, and 55 °C. In the case of water, additional experiments were conducted where the bath was brought to temperatures of 2 and 8 °C. By probing with a calibrated thermocouple it was discovered that temperature gradients existed within the pressure vessel itself. A cali-

brated thermocouple was fastened to the interferometer at a position very close to the liquid under study to determine the actual temperatures at which the experiments were conducted.

Pressures were measured to ± 0.3 bar with a thermostatted manganin pressure gage mounted in the oil line external to the pressure vessel. The pressure gage was calibrated at the freezing point of benzene as reported by Gibson [10].

2.3. Optics

The optical system was similar to the one described by Saunders [11] and the measurements were made photographically. The light source was a helium discharge tube used in conjunction with a constant deviation prism to permit isolation of individual helium lines for illumination. In these studies the 5875.62 A line was used because it was found to produce fringes best suited for photographing. The optical design permitted visual observation of the interference fringes while photographing, and incorporated a right-angle prism so that the observer was out of direct line of the windows in the pressure vessel. This right-angle prism was turned 90° from its normal position [11] so that all the elements of the optical system were in a horizontal plane. In these experiments one window of the pressure vessel and the oil used to transmit pressure were in the path. They were not expected to affect the fringe pattern even when the window became distorted at elevated pressures. To check this prediction, a thin microscope cover glass (0.015 mm thick) was placed in the vessel. The surfaces of the cover glass were sufficiently flat and parallel to produce internal interference, while the glass was so thin that a negligible change in thickness would be produced by a pressure change of 1000 bars. No change in the fringe system was detected at pressures between 1 bar and 1000 bars and it was concluded that distortion of the windows would have no appreciable effect on the measurements.

3. Experimental Technique

A typical experiment was performed as follows: The interferometer was assembled and adjusted to produce a fringe system. The instrument was then filled with the liquid under study. In order to remove air and to ensure that air bubbles were not formed at elevated temperatures it was found necessary to fill the interferometer under vacuum with freshly boiled liquid. The fringe system was rechecked and the interferometer placed inside the pressure vessel and alined. After waiting for about 20 min for attainment of thermal equilibrium, the pressure was raised to some value between 1 bar and 1000 bars and an interval of about 20 min permitted for dissipation of the heat generated by compression. The pressure was then decreased slowly to 1 bar and the fringes photographed as they passed a reference mark on one of the flats. Another 20 min interval was allowed for restoration of thermal equilibrium at 1 bar. Each measurement, therefore, represented an independent experiment between an elevated pressure and 1 bar. Pressure intervals were chosen to give essentially four measurements between 1 bar and 1000 bars.

4. Materials

Measurements were made on benzene, carbon tetrachloride, and water at approximately 25, 35, and 55 °C. Additional measurements were made on water at approximately 2 and 8 °C. The water was freshly distilled while the organic liquids were commercially available materials of high purity used with no further purification. In all cases the purity was corroborated by determination of the index of refraction as described later.

5. Index Calculation

The change in index under pressure was calculated from the equation

$$\Delta\mu = \Delta n\lambda/2t \sin\theta, \tag{1}$$

where $\Delta\mu$ is the change in refractive index, Δn—the number of fringes passing the reference mark, t—the spacing between the optical flats and θ—the angle of incidence of the light. In these experiments $\theta = 90°$, $\lambda = 5875.62$A, and $t = 0.2664$ cm; so that

$$\Delta\mu = 1.1028 \times 10^{-4} \Delta n. \tag{2}$$

Therefore, a shift of one interference fringe represents a change of approximately 1 in the fourth decimal place of refractive index. Estimates of fractional fringes were made to one-tenth of a fringe so that the measurements were made to approximately 1×10^{-5} in the index. With this sensitivity it was necessary to correct for the compressibility of the steel spacer. The volume compressibility of the steel was taken to be 0.59×10^{-6}/bar [12] with the linear compressibility being one-third of this value. At 1000 bars the correction for the compression of the steel was approximately 3 fringes.

It was feared that unequal differential compressions might cause tilting of the interferometer plates and introduce an error in the fringe count. The error from this source was largely eliminated by counting the number of fringes in the field and noting the fringe orientation before and after each run. In some experiments changes were noted in number or orientation of fringes and these data were discarded. Only those experiments showing no changes in the fringe system were considered acceptable.

6. Initial Index Measurement

In order to ascertain the purity of the materials, the indices were first measured to the fourth decimal place with an Abbé refractometer using sodium light. Refractive indices for the 5875.62 A He line were calculated from these results and published dispersion data on the liquids [13, 14, 15].

To use the data of the present investigation for change in index it was necessary to know the initial indices to five decimals. For benzene and water, refractive indices to the fifth decimal were taken from published data on dispersion over a range of temperatures [13, 14]. The initial refractive index of carbon tetrachloride was determined by the method of minimum deviation, the liquid being enclosed in a hollow glass prism [14].

For benzene and carbon tetrachloride the initial refractive indices were only known at temperatures very close to 25 °C. The refractive index at other temperatures of interest was determined in a manner completely analogous to the pressure measurements. In these experiments it was necessary to correct for the expansivity of the steel spacer. This expansivity was determined by experiment using air in the interferometer to be 14.9×10^{-6}/°C.

It may be noted that all changes in refractive index as determined with the interferometer were absolute values. The initial measurements of refractive index referred to air but were converted to absolute values from a knowledge of the refractive index of air at various temperatures [16].

7. Results and Discussion

The experimental results are given in tables 1 to 4. Tables 1 to 3 include specific volumes in addition to the indices of refraction, while table 4 shows only the index data. Specific volumes given in columns 3 of tables 1 to 3 were computed from values of the constants of the Tait equation given by Gibson and his coworkers [6, 17] who studied these liquids over the same pressure and temperature range. Data of equal precision do not appear to be available for water at 1.56 and 7.64 °C. The data of several workers [18] who studied water at the lower temperatures were compared with the results of Gibson at higher temperatures where there was overlapping of experimental conditions. Although most of the data agreed reasonably well it was considered that the agreement was not sufficiently close to permit calculations involving specific volumes from different sources to be compared. Consequently only index data are reported for water at 1.56 and 7.64 °C and no further discussion of these data are contemplated at this time.

TABLE 1. *Effect of temperature and pressure upon the refractive index and specific volume of benzene*

Pressure	Absolute refractive index	Specific volume
24.80 °C		
Bars		*ml/g*
1.0	1.49859	1.14433
250.1	1.51031	1.11973
489.0	1.51982	1.10057
666.1.	1.52593	1.08828
34.50 °C		
1.0	1.49221	1.15805
246.2	1.50438	1.13187
484.8	1.51445	1.11138
757.2	1.52418	1.09192
1107.7	1.53489	1.07112
54.34 °C		
1.0	1.47910	1.18757
274.5	1.49422	1.15350
484.4	1.50382	1.13305
770.2	1.51478	1.11014
1124.5	1.52633	1.08705

TABLE 2. *Effect of temperature and pressure upon the refractive index and specific volume of carbon tetrachloride*

Pressure	Absolute refractive index	Specific volume
24.80 °C		
Bars		*ml/g*
1.0	1.45791	0.63093
276.9	1.47089	.61486
523.6	1.48037	.60347
797.4	1.48934	.59299
1116.7	1.49847	.58276
34.50 °C		
1.0	1.45197	0.63855
255.4	1.46481	.62234
480.9	1.47426	.61094
756.1	1.48381	.59948
1119.9	1.49441	.58710
54.34 °C		
1.0	1.44067	0.65496
248.7	1.45493	.63623
452.7	1.46428	.62423
751.9	1.47616	.61006
1059.2	1.48617	.59830

TABLE 3. *Effect of temperature and pressure upon the refractive index and specific volume of water*

Pressure	Absolute refractive index	Specific volume
24.80 °C		
Bars		*ml/g*
1.0	1.33293	1.00288
259.6	1.33652	.99152
463.6	1.33942	.98318
762.8	1.34322	.97180
1108.6	1.34747	.95973
34.50 °C		
1.0	1.33177	1.00580
259.3	1.33531	.99463
480.9	1.33832	.98572
799.2	1.34228	.97385
1110.0	1.34588	.96318
54.34 °C		
1.0	1.32866	1.01415
241.6	1.33192	1.00372
489.7	1.33517	.99371
785.1	1.33883	.98267
1127.7	1.34274	.97089

TABLE 4. *Effect of temperature and pressure upon the refractive index of water at two lower temperatures*

Pressure	Absolute refractive index
1.56 °C	
Bars	
1.0	1.33439
269.5	1.33859
507.4	1.34213
768.5	1.34581
1049.7	1.34948
7.64 °C	
1.0	1.33423
256.1	1.33805
497.8	1.34161
730.7	1.34495
1088.9	1.34929

7.1. Internal Consistency of the Data

Several replicate measurements were made where the interferometer was completely disassembled and refilled with liquid before each measurement. In each experiment the system was brought to the same pressure as nearly as possible, and then small interpolations were made in order to compare the data directly. On the basis of two experiments of five and four determinations each, the standard deviation was computed to be 0.00005 in refractive index, corresponding to limits of reproducibility of measurements of ± 0.0001, or twice the standard deviation about the mean. Inspection of large scale graphs of index versus pressure, figures 2 and 3, shows that the points lie on a smooth curve with random deviations in the fifth decimal. As a matter of interest, it may be noted that the pressure measurement although assumed exact in this discussion may be subject to a greater relative error than the measurement of index. Of the present data those for water and benzene appear to be slightly more consistent than those for carbon tetrachloride.

7.2. Comparison With Other Data

For purposes of comparing the present data there appear to be only two previously published sets of data, those of Gibson and Kincaid on benzene [6] and those of Rosen on water [4]. Gibson and Kincaid covered essentially the same pressure and temperature range as the present experiments, but Rosen restricted his measurements to 25 °C. Gibson and Kincaid used the immersion method of determining index while Rosen employed the minimum deviation method. Both sets of data are reported to four decimals. Both authors made measurements for more than one wavelength, all differing from the wavelength used here. These data may best be compared with the data of the present investigation by plotting change in refractive index versus pressure. If allowance is made for dispersion, temperature, and vacuum corrections, it is found that the present data agree with the data of Gibson and Kincaid [6] and Rosen [4] exactly to the third decimal with maximum deviations of two or three units in the fourth decimal or last significant figure reported by these authors.

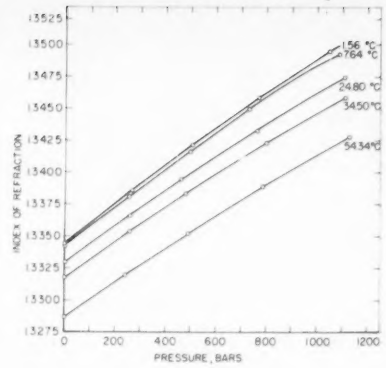

FIGURE 2. *Pressure dependence of index of refraction of water.*

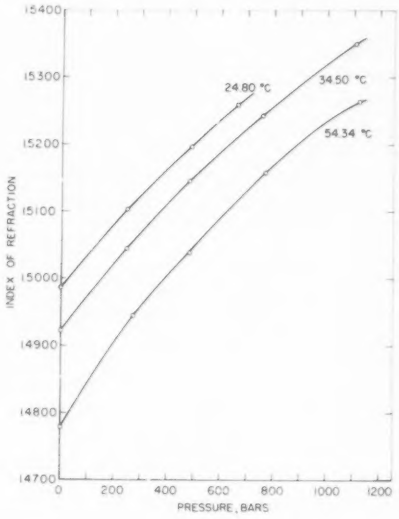

FIGURE 3. *Pressure dependence of index of refraction of benzene.*

A similar approach was followed in comparing the data of the present investigation for change of refractive index with temperature at 1 bar with that of Pesce for benzene [19]. Pesce found the change in absolute refractive index in going from 24.80 to 54.34 °C to be −0.01934. The measurement from the present study over the same temperature range was −0.01949.

7.3. Variation of Index at Constant Volume

In the case of the present data, a graph of index versus specific volume is of considerable interest.

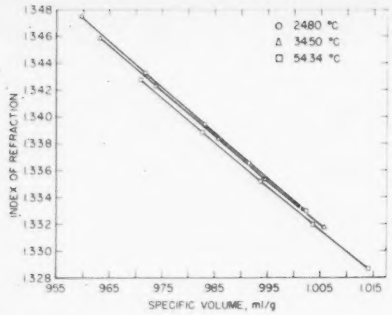

FIGURE 4. *Index of refraction-specific volume relationship in water.*

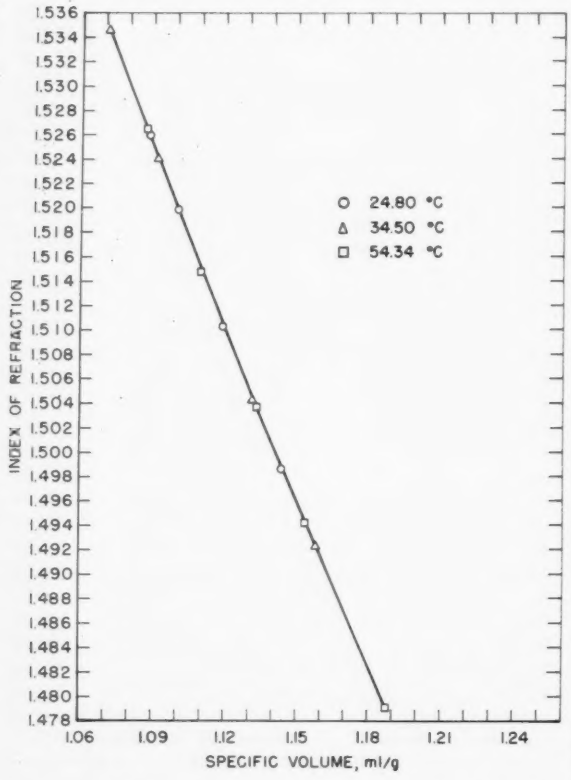

FIGURE 5. *Index of refraction-specific volume relationship in benzene.*

These graphs are given in figures 4, 5, and 6 for water, benzene, and carbon tetrachloride. The relationship is not linear but rather that of a curve convex to the specific volume axis with a very large radius of curvature. In the case of water, the refractive index decreases with increasing temperature at constant specific volume, while in carbon

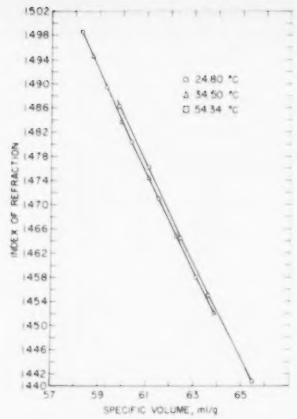

FIGURE 6. *Index of refraction-specific volume relationship in carbon tetrachloride.*

tetrachloride the refractive index increases with increasing temperature, the changes in index in both cases being small—of the order of a few parts in the fourth decimal for a temperature change of 10 °C. It appears that, in the case of benzene, there is no significant dependence of refractive index upon temperature at constant volume, although a larger scale graph of the data shows a separation into three curves of constant temperature with the refractive index decreasing with increase of temperature at the same specific volume. For each liquid there appears to be a tendency for the refractive index to vary less with temperature at higher specific volumes.

These results show that in a liquid where specific volume is held constant, it does not necessarily follow that the refractive index is constant. Despite the fact that this appears to be the first report of this effect, it is not completely unexpected. Gibson and Loeffler [20] observed a shift in the absorption band of solutions of chromophoric materials with temperature at constant volume. Oksengorn [21, 22] has demonstrated a shift of the ultraviolet absorption band of C_6H_6 to longer wavelengths with increasing temperature at constant volume. Robertson [23] has given analogous data for solutions of organic materials in an inert solvent. Gibson and Loeffler [20] attributed the shift to the fact that at higher temperatures the molecules spend a greater fraction of time at close distances to their neighbors. The increased perturbation arising in the close approaches would produce a shift in position of the electronic levels and shift the band. Robertson [23], although attributing the shift with changing specific volume at constant temperature to perturbations arising from Van der Waal forces, believes the shift with temperature at constant volume arises from changes in band shape as a result of increased population of the higher vibrational levels at high temperatures. It is well known that band shapes vary when pressure and temperature are changed [24, 25, 26].

Inasmuch as this represents the first report of change in index at constant volume, as far as can be ascertained, it is of some importance to inquire whether the effect is real or might arise from experimental errors. In order to produce coincidence in the curves for water a maximum shift of the order of 0.0006 in index, or a shift of 0.002 in specific volume or some combination of these two is required. According to the estimates of precision in index the value 0.0006 lies far outside the experimental precision and the value of 0.002 in specific volume is not comparable with the precision of ± 0.00005 in specific volume claimed by Gibson [9]. There remains the additional possibility that the temperatures reported here might be in error sufficiently to produce the observed spread in figures 4 and 6. Temperatures were measured using both a thermocouple and platinum resistance thermometer, with a maximum difference over the temperature range of 0.11 °C. This maximum uncertainty cannot attribute appreciably to the observed separation of the data. In addition, all measurements were performed in exactly the same manner at identical temperatures. The fact that the shifts for water and C Cl_4 are in opposite directions, while C_6H_6 shows no shift within experimental error, plus the estimates of errors involved requires the conclusion that the shifts of index at constant volume are real for H_2O and C Cl_4.

From the previous discussion it is concluded that at constant volume the position and shape of the absorption bands change with temperature. For the liquids studied here data at constant volume appear to be available only for benzene which was studied by Oksengorn [21, 22]. The frequency used here is on the low frequency tail of the uv absorption band as shown by the dispersion data of Gibson and Kincaid [6]. The shift in the uv band with increasing temperature at constant volume is toward lower frequencies and, at the frequency of measurement used here, a higher index should result from this shift.

If it is assumed that the shift in absorption frequency with temperature at constant volume is equivalent to a change in frequency of measurement at constant temperature and pressure, the available data can be combined to calculate the change in index resulting from the shift in the absorption band. This assumption specifically requires that the shape of the absorption band be unchanged by the shift. At a specific volume of 1.10 cm^3/g, Oksengorn's data show a shift $\Delta\nu/\Delta T \approx -1.5$ $cm^{-1}/°C$. Gibson and Kincaid report a frequency dependence $\Delta\mu/\Delta\nu \approx 2.5 \times 10^{-6}/cm^{-1}$ at 1 atm and 25 °C. Therefore, the change in index at constant volume would be $\Delta\mu/\Delta T \approx 3.7 \times 10^{-6}/°C$ with the change in sign resulting from the fact that shift of the absorption band is of opposite sense to the change in index. The calculated change in index in increasing the temperature from 24.80 to 54.34 °C, at constant volume is 1.1×10^{-4}. Considering the several measurements required for the experimental determination of change in index at constant volume, i.e., change in index with pressure at various temperatures, change in index with temperature at 1 bar and expansivity and compressibility of the interferometer, it appears that the predicted change in index of 1.1×10^{-4} would most probably not be detected. The results of the present study do not indicate any significant change in refractive index with temperature at constant specific volume for benzene.

The shift of an absorption band in the ultraviolet region of the spectrum is not the only possible explanation for change in index with temperature at constant volume. Since the dispersion of benzene is large, the index would be very sensitive to changes in band contour. According to Robertson [23] at constant volume an enhancement of the low frequency tail of the absorption band with increasing temperature is to be expected. The results of the present study do not appear to be in accordance with this expectation. Measurements of index at different wavelengths might provide a sensitive method for studying changes in contour of the band tail.

No comparable data at constant volume appear to be available for C Cl_4 or H_2O. The magnitude of the change in index of C Cl_4 with temperature at a constant volume of 0.60 ml/g is about $4.8 \times 10^{-5}/°C$. This result might be explained by a shift of the uv band to longer wavelengths with increasing temperature at constant volume. Alternatively, changes in band contour might cause the observed changes in refractive index.

The data for H_2O show a decrease in index with increasing temperature of magnitude $2.6 \times 10^{-5}/°C$ at a constant volume of 0.97 ml/g. From dispersion data on H_2O [14] it is apparent that the frequency used here is on the tail of the uv absorption band near 1800 A [27]. Therefore, it would appear that the data on index might be explained by a shift of the uv band to shorter wavelengths with increasing temperature at constant volume. It is not clear that shifts in this direction occur since no data at constant volume are available, and data of Collins [28] on the near infrared absorption of water to 5000 atm show no appreciable shifts or intensity changes in this region. However, an appropriate change in contour without a shift of the center of gravity of the band would also produce the observed result. It is possible that the effect observed in water with temperature at constant volume is due to small changes in the hydrogen binding.

7.4. Refractive Index Formulas

Various equations have been proposed which express a relationship between refractive index and specific volume in such a way that the relationship is independent of temperature. The following equations may be mentioned: the Gladstone-Dale [29], $(\mu-1)V=$constant, the Lorentz-Lorenz [30, 31], $(\mu^2-1/\mu^2+2)V=$constant, the Newton [32], $(\mu^2-1)V=$constant and the Eykman [33], $(\mu^2-1/\mu+0.4)V=$constant, where μ represents the index of refraction and V the specific volume. Upon fitting the data of the present investigation to the various

equations it was found, in agreement with the earlier conclusion of Gibson [6], that the Eykman equation for benzene gives a satisfactory fit to four significant figures. However, none of the formulations give satisfactory agreement for each liquid over the range of temperature and pressure employed. This observation is not new [4, 6, 34] and a considerable amount of work has been done, particularly on the Clausius-Mosotti equation, the dielectric analog of the Lorentz-Lorenz equation with the dielectric behavior of both gases and liquids at elevated pressures. Danforth [35] who measured the dielectric constant of liquids up to 12,000 bars believed that his data indicated both a change of polarizability and a failure of the Clausius-Mosotti equation at elevated pressures. A comprehensive survey of much of this work is given by Ten Seldam [36]. More recently it has been realized that the intermolecular forces may be investigated directly by spectroscopic studies at elevated pressures and a survey of current work in this field is available [24].

By using a more refined approximation of the local field acting upon a molecule Böttcher [37] gives as an improved form of the Lorentz-Lorenz equation

$$\frac{\mu^2}{(\mu^2-1)(2\mu^2+1)V}=\frac{m}{12\pi N_A}\left\{\frac{1}{\alpha}-\frac{1}{a^3}\left(\frac{2\mu^2-2}{2\mu^2+1}\right)\right\} \quad (3)$$

where m is the molecular weight, N_A is Avogadro's number, α is the polarizability of the molecule and a is the effective radius of the molecule. It can be seen that by plotting

$$\frac{\mu^2}{(\mu^2-1)(2\mu^2+1)V} \text{ vs } \frac{(2\mu^2-2)}{(2\mu^2+1)}$$

a straight line results with an intercept involving α and a slope involving a. The data for water, benzene, and carbon tetrachloride were plotted according to eq (3) and the graphs are shown in figures 7, 8, and 9. Values of α and a determined by least squares are given in table 5.

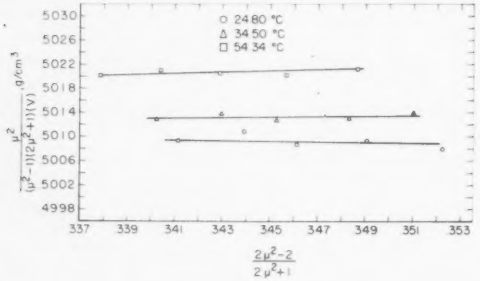

FIGURE 7. *Relationship between* $\frac{2\mu^2-2}{2\mu^2+1}$ *and* $\frac{\mu^2}{(\mu^2-1)(2\mu^2+1)V}$ *for the water molecule.*

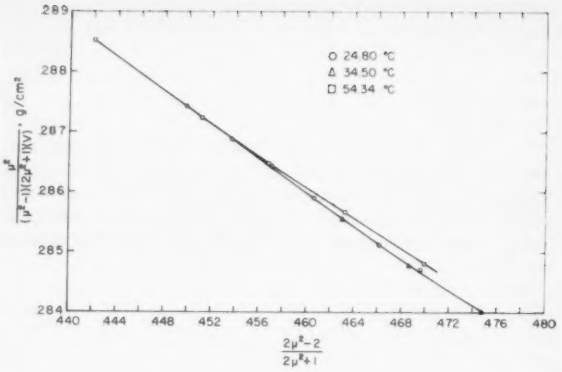

FIGURE 8. *Relationship between* $\frac{2\mu^2-2}{2\mu^2+1}$ *and* $\frac{\mu^2}{(\mu^2-1)(2\mu^2+(1)V}$ *for the benzene molecule.*

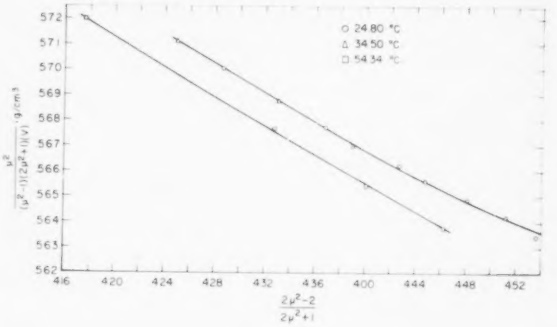

FIGURE 9. *Relationship between* $\frac{2\mu^2-2}{2\mu^2+1}$ *and* $\frac{\mu^2}{(\mu^2-1)(2\mu^2+1)V}$ *for the carbon tetrachloride molecule.*

TABLE 5. *Polarizabilities and molecular radii as determined from Böttcher's equation*

Molecule	Temperature	Polarizability, α	Average polarizability, α	Molecular radius, a	Average molecular radius, a
	°C	A^3	A^3	A	A
Water	24.80	1.57	1.58	3.77	3.77
	34.50	1.59			
	54.34	1.59			
Benzene	24.80	9.86	9.86	2.93	2.93
	34.50	9.83		2.92	
	54.34	9.90		2.95	
Carbon tetrachloride	24.80	9.93	9.88	2.96	2.93
	34.50	9.93		2.96	
	54.34	9.79		2.87	

Böttcher used as his model a spherical molecule whose polarizability and radius were independent of temperature and pressure. It can be seen from the figures that, of the three liquids, benzene fits this model best, but even with benzene an increasing curvature is apparent at the right-hand side of the graph. This region corresponds to the physical situation of the liquid being under greater pressure. It may be inferred, therefore, that polarizability and/or radius of the benzene molecule is not completely independent of pressure.

This curvature may also be observed for carbon tetrachloride in figure 9. There is here, in addition, a lateral displacement of the isotherms. The fact that both the intercept and the slope of the lines representing the data for 24.80 and 54.34 °C are distinctly different indicates that both polarizability and radius are not independent of temperature (as well as pressure) for $C Cl_4$.

Böttcher's formula, eq (3), was developed for a nonpolar dielectric, and figure 7 shows that water fits Böttcher's model least well of the liquids studied. Despite some scattering of points there appears to be a definite separation of the isotherms. A meaningful estimate of molecular radius, a, may only be had for the data at 24.80 °C, because the slope of the curve at this temperature is negative as is necessary for the calculation. The slopes of the curves at the two higher temperatures are slightly positive.

For each liquid average values of α and a over the temperature range involved are shown in table 5. For carbon tetrachloride it was found that $\alpha=9.88$ A^3 and $a=2.93$ A. Böttcher calculated $\alpha=9.07$ A^3 and $a=2.42$ A by applying his equation to a series of mixtures of carbon disulfide and carbon tetrachloride. Average values of a for water, carbon tetrachloride, and benzene were found to be 3.77 A, 2.93 A, and 2.93 A, respectively. From molar volume data for these liquids over the same temperature range, corresponding values of a were found to be 1.94 A, 3.33 A, and 3.40 A. The large difference in the case of water is again presumed to be due to the fact that water is a polar liquid.

The authors are indebted to R. E. Gibson, Director of the Applied Physics Laboratory of the Johns Hopkins University, for the use of the pressure vessel in which the experiments were conducted. The authors also thank I. Malitson of the Refractometry Section of the National Bureau of Standards for his initial measurements of the refractive index of carbon tetrachloride.

8. References

[1] T. C. Poulter, C. Ritchey, and C. A. Benz, Phys. Rev. **41,** 366 (1932).
[2] T. C. Poulter, Phys Rev. **40,** 860 (1932).
[3] T. C. Poulter and C. A. Benz, Phys. Rev. **40,** 872 (1932).
[4] J. S. Rosen, J. Opt. Soc. Am. **37,** 932 (1947).
[5] W. J. Lyons and F. E. Poindexter, J. Opt. Soc. Am. **26,** 146 (1936).
[6] R. E. Gibson and J. F. Kincaid, J. Am. Chem. Soc. **60,** 511 (1938).
[7] J. Jamin, Compt. rend **45,** 892 (1857).
[8] A. Michels and J. Hamers, Physica **4,** 995 (1937).
[9] R. E. Gibson, J. Am. Chem. Soc. **59,** 1521 (1937).
[10] R. E. Gibson, J. Am. Chem. Soc. **57,** 284 (1935).
[11] J. B. Saunders, J. Research NBS **35,**157 (1945) RP1668.
[12] P. W. Bridgman, The Physics of High Pressure (G. Bell & Sons Ltd., London 1949).
[13] A. F. Forziati, J. Research NBS **44,** 373 (1950) RP2085.
[14] L. W. Tilton and J. K. Taylor, J. Research NBS **20,** 419 (1939) RP1085.
[15] Smithsonian Physical Tables, 9th ed. (Washington, D.C., 1954).
[16] A. Pérard, Travaux et Memoires du Bureau International des Poids et Mesures **19** (1932).
[17] R. E. Gibson and O. H. Loeffler, J. Am. Chem. Soc. **63,** 898 (1941).
[18] N. E. Dorsey, Properties of Ordinary Water Substance (Reinhold Publ. Corp., New York, N.Y., 1940).
[19] B. Pesce, Gazz. Chim. ital. **65,** 440 (1935).
[20] R. E. Gibson and O. H. Loeffler, J. Am. Chem. Soc. **62,** 1324 (1940).
[21] B. Oksengorn, Compt. rend. **242,** 2324 (1956).
[22] Ref. 24 p. 323.
[23] W. W. Robertson, J. Chem. Phys. **33,** 362 (1960).
[24] Colloques Internationaux du Centre National de la Recherche Scientifique Proprietes Optiques et Acoustiques des Fluides Comprimes et Actions Intermoleculaires (Centre National de la Recherche Scientifique, Paris, 1959).
[25] A. Kronenberger and P. Pringsheim, Z. Physik **40,** 75 (1926).
[26] E. Fishman and H. G. Drickamer, J. Chem. Phys. **24,** 548 (1956).
[27] K. Watanabe and M. Zelikoff, J. Opt. Soc. Am. **43,** 753 (1953).
[28] J. R. Collins, Phys. Rev. **36,** 305 (1930).
[29] J. H. Gladstone and T. P. Dale, Phil. Trans. **153,** 337 (1863).
[30] H. A. Lorentz, Ann. Physik **9,** 641 (1880).
[31] L. Lorenz, Ann. Physik **11,** 70 (1880).
[32] R. A. Houstoun, A Treatise on Light (Longmans, Green & Co., New York, 1938).
[33] J. F. Eykman, Rec. Trav. Chim. **14,** 177 (1895).
[34] F. E. Poindexter and L. E. James, Phys. Rev. **42,** 910 (1932).
[35] W. E. Danforth, Phys. Rev. **38,** 1224 (1931).
[36] C. A. Ten Seldam, Dissertation Univ. of Utrecht, March 1953 (Van Gorcum & Co., N. V., Assen, Netherlands, 1953).
[37] C. J. F. Böttcher, Theory of Electric Polarization (Elsevier Publishing Co., Amsterdam, 1952).

(Paper 67A2–203)

JOURNAL OF RESEARCH of the National Bureau of Standards—A. Physics and Chemistry
Vol. 67A, No. 2, March–April 1963

Pressure-Density-Temperature Relations of Fluid Para Hydrogen From 15 to 100 °K at Pressures to 350 Atmospheres*

Robert D. Goodwin, Dwain E. Diller, Hans M. Roder, and Lloyd A. Weber

(May 29, 1962)

Experimental data are presented at closely spaced intervals of temperature and density. The range of experimental densities is from 0.064 to 2.8 times the critical density. There are presented, in addition, tables interpolated uniformly in arguments density and temperature, and also in pressure and temperature.

1. Introduction

Very few data exist on the compressibility (PVT) behavior of 20 °K-equilibrium (i.e., "para") hydrogen in compressed liquid and dense fluid states [1–5].[1] The low-density PVT differences between normal and para hydrogen are known to be small in the neighborhood of 20 °K [6].

The purpose of this report is to place on record our experimental PVT observations on para hydrogen at high densities, together with useful interpolations to uniform values of all variables. Experimental second and third virial coefficients were reported in the apparatus publication supporting the present results [7]. Smoothing and representation of the temperature-dependence of these coefficients is in progress.

Data of this report are the basis for several related properties of para hydrogen. The observed vapor pressures have been represented analytically and compared with earlier data [8]. The derived orthobaric liquid-vapor densities have been reported [9, 10]. An empirical representation of the pressure-temperature relation at melting [11] has been used to obtain densities of liquid at freezing [12]. An equation of state, adjusted to the present PVT data, has been used to obtain a provisional set of thermodynamic functions [13]. These functions have been extended by others to lower temperatures and pressures [14].

2. Symbols, Dimensions and Constants

The term "parahydrogen" is employed for brevity here to mean 20 °K-equilibrium hydrogen [1]. Confirmation of para hydrogen in the piezometer has been described [7].

Pressures, P, are in standard atmospheres [17]. Temperatures, T, are on the NBS 1955 low-temperature scale, obtained by subtracting 0.01 °C from temperatures on the NBS 1939 scale of Hoge and Brickwedde [16]. Densities, ρ, are in gram moles per cubic centimeter. These derive from use of the gas constant, R, in conjunction with experimental quantities. Determination of the amount of sample as gas at normal conditions is based upon compressibility data of normal hydrogen with $R=82.057$ cm^3 atm/g mol deg [7, 15]. Representations of isotherms of $(Pv\text{-}RT)v$ are based upon $R=82.0597$ cm^3 atm/g mol deg, corresponding to the recent international temperature scale [17].

The largest experimental errors occur in density. Accuracy and precision in this variable have been estimated at 0.1 and 0.02 percent respectively [7].

3. Data Tables

Experimental data in table 1 result from the laboratory observations and computer program described for computation of apparatus adjustments [7]. They are arranged in the sequence of increasing densities, except as noted below. Each set of four columns represents an experimental "run" of increasing temperature at nearly constant density. Each run is identified by the first two digits in the fourth column.

The slight decrease of density with increasing pressure in each run is due to expulsion of fluid from the piezometer into the pressure gage diaphragm cell. Since temperatures are reproduced accurately from run to run, these data yield isotherms. Absence of an entry for density indicates that two phases coexist.

The last three runs in table 1 give closely spaced vapor pressures and densities in the critical region.

Table 2 presents the PVT data interpolated to isochores, that is to uniform densities at the experimental temperatures. Table entries are pressures in atmospheres.

*Supported in part by the National Aeronautics and Space Administration.

[1] Figures in brackets indicate the literature references at the end of this paper

Table 1 Temperature-Pressure-Density Observations on Para Hydrogen

T, °K	P, atm	ρ, g mol/cc	Ident.	T, °K	P, atm	ρ, g mol/cc	Ident.	T, °K	P, atm	ρ, g mol/cc	Ident
22	1.612		9401	23	2.069		9301	25	3.246		9201
23	1.783	.0010849	9402	24	2.459	.0014969	9302	26	3.644	.0021611	9202
24	1.878	.0010848	9403	25	2.592	.0014967	9303	27	3.843	.0021608	9203
25	1.972	.0010847	9404	26	2.726	.0014966	9304	28	4.040	.0021606	9204
26	2.066	.0010845	9405	27	2.858	.0014964	9305	29	4.235	.0021603	9205
27	2.160	.0010844	9406	28	2.990	.0014962	9306	30	4.430	.0021601	9206
28	2.254	.0010843	9407	29	3.121	.0014961	9307	31	4.624	.0021599	9207
29	2.347	.0010842	9408	30	3.251	.0014959	9308	32	4.817	.0021596	9208
30	2.440	.0010841	9409	31	3.382	.0014958	9309	33	5.010	.0021594	9209
31	2.533	.0010840	9410	32	3.513	.0014956	9310	34	5.203	.0021591	9210
32	2.626	.0010839	9411	33	3.643	.0014954	9311	35	5.395	.0021589	9211
33	2.719	.0010837	9412	34	3.773	.0014953	9312	36	5.587	.0021586	9212
34	2.812	.0010836	9413	35	3.903	.0014951	9313	37	5.779	.0021584	9213
35	2.904	.0010835	9414	36	4.032	.0014949	9314	38	5.970	.0021581	9214
36	2.997	.0010834	9415	37	4.162	.0014947	9315	39	6.161	.0021578	9215
37	3.089	.0010833	9416	38	4.291	.0014946	9316	40	6.352	.0021576	9216
38	3.181	.0010831	9417	39	4.421	.0014944	9317	42	6.732	.0021570	9217
39	3.273	.0010830	9418	40	4.550	.0014942	9318	44	7.111	.0021565	9218
40	3.366	.0010829	9419	42	4.807	.0014939	9319	46	7.489	.0021560	9219
42	3.550	.0010826	9420	44	5.064	.0014935	9320	48	7.867	.0021555	9220
44	3.733	.0010824	9421	46	5.320	.0014931	9321	50	8.244	.0021549	9221
46	3.916	.0010821	9422	48	5.576	.0014928	9322	55	9.184	.0021536	9222
48	4.099	.0010819	9423	50	5.832	.0014924	9323	60	10.119	.0021523	9223
50	4.282	.0010816	9424	55	6.471	.0014915	9324	65	11.054	.0021510	9224
55	4.738	.0010810	9425	60	7.106	.0014906	9325	70	11.984	.0021497	9225
60	5.193	.0010803	9426	65	7.741	.0014897	9326	75	12.912	.0021484	9226
65	5.648	.0010797	9427	70	8.375	.0014889	9327	80	13.839	.0021471	9227
70	6.101	.0010790	9428	75	9.005	.0014880	9328	85	14.763	.0021458	9228
75	6.553	.0010784	9429	80	9.635	.0014871	9329	90	15.687	.0021445	9229
80	7.005	.0010777	9430	85	10.265	.0014862	9330	95	16.608	.0021431	9230
85	7.457	.0010771	9431	90	10.894	.0014853	9331	100	17.526	.0021418	9231
90	7.907	.0010764	9432	95	11.521	.0014843	9332				
95	8.356	.0010758	9433	100	12.146	.0014834	9333				
100	8.805	.0010751	9434								

T, °K	P, atm	ρ, g mol/cc	Ident.	T, °K	P, atm	ρ, g mol/cc	Ident.	T, °K	P, atm	ρ, g mol/cc	Ident
26	3.983		9101	27	4.829		9001	28	5.792		8901
27	4.364	.0025668	9102	28	5.505	.0033328	9002	29	6.509	.0039818	8902
28	4.603	.0025666	9103	29	5.825	.0033324	9003	30	6.901	.0039813	8903
29	4.840	.0025663	9104	30	6.142	.0033320	9004	31	7.287	.0039808	8904
30	5.076	.0025660	9105	31	6.457	.0033316	9005	32	7.673	.0039803	8905
31	5.311	.0025657	9106	32	6.770	.0033312	9006	33	8.056	.0039798	8906
32	5.544	.0025654	9107	33	7.082	.0033308	9007	34	8.436	.0039793	8907
33	5.777	.0025651	9108	34	7.393	.0033304	9008	35	8.816	.0039788	8908
34	6.009	.0025648	9109	35	7.703	.0033300	9009	36	9.193	.0039783	8909
35	6.242	.0025645	9110	36	8.012	.0033296	9010	37	9.570	.0039778	8910
36	6.473	.0025641	9111	37	8.321	.0033291	9011	38	9.945	.0039773	8911
37	6.704	.0025638	9112	38	8.628	.0033287	9012	39	10.319	.0039768	8912
38	6.934	.0025635	9113	39	8.934	.0033283	9013	40	10.692	.0039763	8913
39	7.164	.0025632	9114	40	9.240	.0033279	9014	42	11.436	.0039752	8914
40	7.393	.0025629	9115	42	9.849	.0033271	9015	44	12.177	.0039742	8915
42	7.851	.0025623	9116	44	10.457	.0033262	9016	46	12.914	.0039732	8916
44	8.308	.0025616	9117	46	11.062	.0033254	9017	48	13.650	.0039722	8917
46	8.763	.0025610	9118	48	11.666	.0033245	9018	50	14.385	.0039712	8918
48	9.217	.0025604	9119	50	12.269	.0033237	9019	55	16.213	.0039687	8919
50	9.670	.0025597	9120	55	13.771	.0033217	9020	60	18.031	.0039662	8920
55	10.800	.0025582	9121	60	15.265	.0033196	9021	65	19.845	.0039637	8921
60	11.924	.0025566	9122	65	16.755	.0033175	9022	70	21.651	.0039613	8922
65	13.047	.0025550	9123	70	18.240	.0033155	9023	75	23.448	.0039588	8923
70	14.166	.0025535	9124	75	19.718	.0033134	9024	80	25.245	.0039563	8924
75	15.280	.0025519	9125	80	21.194	.0033114	9025	85	27.031	.0039538	8925
80	16.393	.0025504	9126	85	22.666	.0033093	9025	90	28.821	.0039513	8926
85	17.505	.0025488	9127	90	24.136	.0033072	9026	95	30.600	.0039487	8927
90	18.615	.0025472	9128	95	25.601	.0033051	9028	100	32.369	.0039462	8928
95	19.720	.0025456	9129	100	27.059	.0033030	9029				
100	20.821	.0025440	9130								

T, °K	P, atm	ρ, g mol/cc	Ident.	T, °K	P, atm	ρ, g mol/cc	Ident.	T, °K	P, atm	ρ, g mol/cc	Ident
29	6.886		8801	31	9.502		8701	32	10.946	.0083120	8601
30	7.803	.0049650	8802	32	10.266	.0067855	8702	33	11.878	.0083107	8602
31	8.309	.0049644	8803	33	10.989	.0067845	8703	34	12.794	.0083095	8603
32	8.808	.0049637	8804	34	11.702	.0067836	8704	35	13.699	.0083083	8604
33	9.303	.0049631	8805	35	12.411	.0067826	8705	36	14.597	.0083071	8605
34	9.794	.0049624	8806	36	13.114	.0067816	8706	37	15.489	.0083059	8606
35	10.283	.0049618	8807	37	13.814	.0067807	8707	38	16.378	.0083046	8607
36	10.771	.0049611	8808	38	14.511	.0067798	8708	39	17.261	.0083035	8608
37	11.256	.0049604	8809	39	15.206	.0067788	8709	40	18.142	.0083023	8609
38	11.738	.0049598	8810	40	15.896	.0067779	8710	42	19.894	.0082999	8610
39	12.220	.0049591	8811	42	17.271	.0067760	8711	44	21.639	.0082976	8611
40	12.700	.0049585	8812	44	18.640	.0067742	8712	46	23.377	.0082952	8612
42	13.656	.0049572	8813	46	20.003	.0067723	8713	48	25.110	.0082929	8613
44	14.606	.0049559	8814	48	21.360	.0067705	8714	50	26.839	.0082906	8614
46	15.554	.0049546	8815	50	22.714	.0067686	8715	55	31.138	.0082848	8615
48	16.498	.0049533	8816	55	26.087	.0067641	8716	60	35.414	.0082791	8616
50	17.443	.0049520	8819	60	29.435	.0067596	8717	65	39.673	.0082735	8617
55	19.788	.0049488	8820	65	32.775	.0067551	8718	70	43.911	.0082679	8618
60	22.120	.0049456	8821	70	36.097	.0067507	8719	75	48.125	.0082623	8619
65	24.446	.0049425	8822	75	39.398	.0067462	8720	80	52.326	.0082566	8620
70	26.760	.0049393	8823	80	42.694	.0067417	8721	85	56.514	.0082511	8621
75	29.062	.0049362	8824	85	45.978	.0067372	8722	90	60.691	.0082455	8622
80	31.360	.0049330	8825	90	49.262	.0067328	8723	95	64.846	.0082398	8623
85	33.653	.0049298	8826	95	52.518	.0067283	8724	100	68.980	.0082342	8624
90	35.941	.0049267	8827	100	55.759	.0067239	8725				
95	38.217	.0049234	8828								
100	40.483	.0049202	8829								

Table 1. Temperature-Pressure-Density Observations on Para Hydrogen - Continued

T, °K	P, atm	ρ, g mol/cc	Ident.	T, °K	P, atm	ρ, g mol/cc	Ident.	T, °K	P, atm	ρ, g mol/cc	Ident.
33	12.473	.0101447	8501	33	12.709	.0118152	8401	34	14.502	.0141333	8301
34	13.644	.0101431	8502	34	14.114	.0118133	8402	35	16.202	.0141310	8302
35	14.797	.0101415	8503	35	15.497	.0118115	8403	36	17.908	.0141287	8303
36	15.942	.0101400	8504	36	16.870	.0118096	8404	37	19.614	.0141264	8304
37	17.078	.0101384	8505	37	18.239	.0118078	8405	38	21.321	.0141241	8305
38	18.209	.0101369	8506	38	19.603	.0118059	8406	39	23.029	.0141218	8306
39	19.337	.0101354	8507	39	20.963	.0118041	8407	40	24.740	.0141195	8307
40	20.465	.0101339	8508	40	22.322	.0118023	8408	42	28.158	.0141150	8308
42	22.699	.0101309	8509	42	25.035	.0117987	8409	44	31.578	.0141104	8309
44	24.929	.0101279	8510	44	27.737	.0117951	8410	46	35.000	.0141059	8310
46	27.151	.0101249	8511	46	30.436	.0117915	8411	48	38.421	.0141013	8311
48	29.369	.0101219	8512	48	33.129	.0117879	8412	50	41.837	.0140969	8312
50	31.581	.0101190	8513	50	35.820	.0117843	8413	55	50.362	.0140858	8313
55	37.090	.0101116	8514	55	42.520	.0117755	8414	60	58.850	.0140748	8314
60	42.570	.0101044	8515	60	49.190	.0117668	8415	65	67.315	.0140641	8315
65	48.028	.0100973	8516	65	55.841	.0117582	8416	70	75.730	.0140534	8316
70	53.458	.0100902	8517	70	62.457	.0117496	8417	75	84.096	.0140428	8317
75	58.856	.0100831	8518	75	69.030	.0117411	8418	80	92.423	.0140322	8318
80	64.238	.0100760	8519	80	75.580	.0117327	8419	85	100.714	.0140218	8319
85	69.609	.0100689	8520	85	82.108	.0117241	8420	90	108.972	.0140114	8320
90	74.951	.0100619	8521	90	88.610	.0117157	8421	95	117.166	.0140010	8321
95	80.263	.0100548	8522	95	95.070	.0117074	8422	100	125.316	.0139907	8322
100	85.547	.0100477	8523	100	101.491	.0116990	8423				

T, °K	P, atm	ρ, g mol/cc	Ident.	T, °K	P, atm	ρ, g mol/cc	Ident.	T, °K	P, atm	ρ, g mol/cc	Ident.
32	11.051		5101	34	14.798	.0163960	8201	33	12.841	.0181179	8101
33	12.801	.0151286	5102	35	16.833	.0163932	8202	34	15.098	.0181148	8102
34	14.630	.0151261	5103	36	18.891	.0163904	8203	35	17.432	.0181116	8103
35	16.477	.0151236	5104	37	20.962	.0163876	8204	36	19.792	.0181084	8104
36	18.332	.0151211	5105	38	23.043	.0163849	8205	37	22.175	.0181052	8105
37	20.192	.0151185	5106	39	25.132	.0163821	8206	38	24.583	.0181020	8106
38	22.061	.0151160	5107	40	27.227	.0163793	8207	39	26.990	.0180988	8107
39	23.930	.0151135	5108	42	31.430	.0163737	8208	40	29.413	.0180956	8108
40	25.800	.0151110	5109	44	35.648	.0163681	8209	42	34.280	.0180892	8109
42	29.549	.0151061	5110	46	39.835	.0163627	8210	44	39.153	.0180828	8110
44	33.305	.0151011	5111	48	44.054	.0163573	8211	46	44.039	.0180764	8111
46	37.060	.0150961	5112	50	48.269	.0163517	8212	48	48.928	.0180701	8112
48	40.816	.0150913	5113	55	58.797	.0163381	8213	50	53.820	.0180638	8113
50	44.576	.0150865	5114	60	69.274	.0163248	8214	55	66.031	.0180481	8114
55	53.945	.0150742	5115	65	79.725	.0163117	8215	60	78.193	.0180329	8115
60	63.286	.0150622	5116	70	90.114	.0162988	8216	65	90.304	.0180180	8116
65	72.593	.0150505	5117	75	100.433	.0162859	8217	70	102.345	.0180032	8117
70	81.854	.0150388	5118	80	110.701	.0162733	8218	75	114.296	.0179886	8118
75	91.053	.0150272	5119	85	120.913	.0162607	8219	80	126.175	.0179743	8119
80	100.208	.0150157	5120	90	131.078	.0162482	8220	85	137.978	.0179601	8120
85	109.316	.0150043	5121	95	141.168	.0162359	8221	90	149.739	.0179460	8121
90	118.392	.0149930	5122	100	151.191	.0162236	8222	95	161.397	.0179322	8122
95	127.405	.0149817	5123					100	172.960	.0179183	8123
100	136.361	.0149706	5124								

T, °K	P, atm	ρ, g mol/cc	Ident.	T, °K	P, atm	ρ, g mol/cc	Ident.	T, °K	P, atm	ρ, g mol/cc	Ident.
32	11.051		5001	33	13.216	.0207027	8001	33	13.595	.0216206	7901
33	12.999	.0198034	5002	34	16.041	.0206989	8002	34	16.665	.0216165	7902
34	15.605	.0197998	5003	35	18.932	.0206950	8003	35	19.794	.0216122	7903
35	18.284	.0197961	5004	36	21.862	.0206910	8004	36	22.961	.0216080	7904
36	21.002	.0197925	5005	37	24.820	.0206871	8005	37	26.153	.0216037	7905
37	23.749	.0197888	5006	38	27.794	.0206831	8006	38	29.359	.0215995	7906
38	26.514	.0197852	5007	39	30.782	.0206792	8007	39	32.582	.0215953	7907
39	29.283	.0197815	5008	40	33.781	.0206752	8008	40	35.810	.0215911	7908
40	32.064	.0197778	5009	42	39.802	.0206674	8009	42	42.290	.0215826	7909
42	37.661	.0197703	5010	44	45.837	.0206595	8010	44	48.779	.0215742	7910
44	43.268	.0197632	5011	46	51.876	.0206518	8011	46	55.273	.0215660	7911
46	48.887	.0197557	5012	48	57.920	.0206440	8012	48	61.770	.0215576	7912
48	54.512	.0197485	5013	50	63.961	.0206364	8013	50	68.258	.0215496	7913
50	60.131	.0197415	5014	55	79.026	.0206175	8014	55	84.439	.0215294	7914
55	74.156	.0197239	5015	60	94.015	.0205991	8015	60	100.505	.0215098	7915
60	88.108	.0197065	5016	65	108.922	.0205812	8016	65	116.494	.0214907	7916
65	101.998	.0196896	5017	70	123.721	.0205635	8017	70	132.353	.0214720	7917
70	115.808	.0196730	5018	75	138.375	.0205462	8018	75	148.062	.0214536	7918
75	129.495	.0196567	5019	80	152.940	.0205291	8019	80	163.658	.0214358	7919
80	143.069	.0196405	5020	85	167.419	.0205123	8020	85	179.153	.0214182	7920
85	156.597	.0196246	5021	90	181.791	.0204957	8021	90	194.540	.0214006	7921
90	170.024	.0196090	5022	95	196.038	.0204793	8022	95	209.772	.0213835	7922
95	183.348	.0195938	5023	100	210.149	.0204631	8023	100	224.862	.0213665	7923
100	196.571	.0195781	5024								

Table 1 Temperature-Pressure-Density Observations on Para Hydrogen Continued

T, °K	P, atm	ρ, g mol/cc	Ident.	T, °K	P, atm	ρ, g mol/cc	Ident.	T, °K	P, atm	ρ, g mol/cc	Ident.
32	11.052		7801	32	11.875	.0238327	7701	31	9.499		4901
33	14.346	.0227217	7802	33	15.564	.0238277	7702	32	13.272	.0248963	4902
34	17.741	.0227171	7803	34	19.309	.0238227	7703	33	17.345	.0248908	4903
35	21.185	.0227125	7804	35	23.091	.0238176	7704	34	21.451	.0248853	4904
36	24.663	.0227079	7805	36	26.897	.0238125	7705	35	25.585	.0248798	4905
37	28.154	.0227033	7806	37	30.716	.0238075	7706	36	29.726	.0248744	4906
38	31.658	.0226986	7807	38	34.549	.0238024	7707	37	33.895	.0248690	4907
39	35.175	.0226940	7808	39	38.390	.0237975	7708	38	38.064	.0248634	4908
40	38.701	.0226894	7809	40	42.236	.0237925	7709	39	42.232	.0248580	4909
42	45.770	.0226803	7810	42	49.930	.0237828	7710	40	46.402	.0248527	4910
44	52.837	.0226712	7811	44	57.631	.0237728	7711	42	54.745	.0248422	4911
46	59.911	.0226622	7812	46	65.318	.0237631	7712	44	63.089	.0248316	4912
48	66.981	.0226533	7813	48	72.996	.0237535	7713	46	71.393	.0248210	4913
50	74.039	.0226445	7814	50	80.666	.0237440	7714	48	79.692	.0248109	4914
55	91.632	.0226229	7815	55	99.733	.0237209	7715	50	87.939	.0248008	4915
60	109.074	.0226018	7816	60	118.642	.0236983	7716	55	108.542	.0247761	4916
65	126.409	.0225814	7817	65	137.417	.0236766	7717	60	128.920	.0247518	4917
70	143.603	.0225615	7818	70	155.999	.0236556	7718	65	149.132	.0247290	4918
75	160.617	.0225421	7819	75	174.400	.0236347	7719	70	169.131	.0247063	4919
80	177.512	.0225227	7820	80	192.631	.0236143	7720	75	188.926	.0246846	4920
85	194.271	.0225039	7821	85	210.738	.0235947	7721	80	208.507	.0246628	4921
90	210.905	.0224853	7822	90	228.692	.0235749	7722	85	227.963	.0246421	4922
95	227.380	.0224671	7823	95	246.449	.0235557	7723	90	247.262	.0246214	4923
100	243.695	.0224491	7824	100	264.040	.0235368	7724	95	266.278	.0246015	4924
								100	285.168	.0245811	4925

T °K	P, atm	ρ, g mol/cc	Ident	T, °K	P, atm	ρ, g mol/cc	Ident.	T, °K	P, atm	ρ, g mol/cc	Ident.
31	10.210	.0255512	7601	31	11.524	.0262244	7501	30	8.628	.0269624	7401
32	14.476	.0255454	7602	32	16.044	.0262184	7502	31	13.404	.0269559	7402
33	18.783	.0255396	7603	33	20.594	.0262122	7503	32	18.222	.0269495	7403
34	23.122	.0255339	7604	34	25.170	.0262061	7504	33	23.056	.0269429	7404
35	27.483	.0255280	7605	35	29.765	.0262001	7505	34	27.908	.0269365	7405
36	31.848	.0255223	7606	36	34.370	.0261940	7506	35	32.765	.0269301	7406
37	36.221	.0255165	7607	37	38.981	.0261880	7507	36	37.630	.0269238	7407
38	40.599	.0255109	7608	38	43.589	.0261820	7508	37	42.499	.0269176	7408
39	44.974	.0255053	7609	39	48.197	.0261762	7509	38	47.362	.0269113	7409
40	49.356	.0254997	7610	40	52.805	.0261704	7510	39	52.222	.0269051	7410
42	58.116	.0254886	7611	42	62.000	.0261586	7511	40	57.076	.0268990	7411
44	66.848	.0254776	7612	44	71.169	.0261473	7512	42	66.763	.0268869	7412
46	75.566	.0254668	7613	46	80.330	.0261360	7513	44	76.419	.0268749	7413
48	84.267	.0254560	7614	48	89.445	.0261248	7514	46	86.038	.0268631	7414
50	92.929	.0254455	7615	50	98.529	.0261139	7515	48	95.622	.0268515	7415
55	114.456	.0254199	7616	55	121.075	.0260872	7516	50	105.176	.0268401	7416
60	135.767	.0253951	7617	60	143.396	.0260616	7517	55	128.858	.0268124	7417
65	156.903	.0253715	7618	65	165.485	.0260369	7518	60	152.275	.0267858	7418
70	177.808	.0253481	7619	70	187.342	.0260130	7519	65	175.469	.0267601	7419
75	198.459	.0253255	7620	75	208.921	.0259894	7520	70	198.386	.0267354	7420
80	218.934	.0253032	7621	80	230.298	.0259666	7521	75	221.003	.0267116	7421
85	239.206	.0252820	7622	85	251.477	.0259448	7522	80	243.406	.0266877	7422
90	259.343	.0252608	7623	90	272.480	.0259229	7523	85	265.594	.0266648	7423
95	279.231	.0252400	7624	95	293.213	.0259015	7524	90	287.572	.0266425	7424
100	298.903	.0252193	7625	100	313.736	.0258803	7525	95	309.280	.0266203	7425
								100	330.750	.0265987	7426

T °K	P, atm	ρ, g mol/cc	Ident.	T, °K	P, atm	ρ, g mol/cc	Ident.	T, °K	P, atm	ρ, g mol/cc	Ident.
30	10.564	.0276407	7301	28	5.785		4801	28	6.096	.0293118	7201
31	15.630	.0276340	7302	29	8.051	.0284479	4802	29	11.854	.0293039	7202
32	20.728	.0276272	7303	30	13.426	.0284406	4803	30	17.617	.0292963	7203
33	25.829	.0276204	7304	31	18.812	.0284334	4804	31	23.372	.0292886	7204
34	30.940	.0276136	7305	32	24.239	.0284262	4805	32	29.138	.0292810	7205
35	36.055	.0276069	7306	33	29.649	.0284162	4806	33	34.899	.0292735	7206
36	41.170	.0276003	7307	34	35.069	.0284119	4807	34	40.653	.0292660	7207
37	46.279	.0275937	7308	35	40.490	.0284048	4808	35	46.400	.0292586	7208
38	51.383	.0275872	7309	36	45.910	.0283979	4809	36	52.149	.0292513	7209
39	56.478	.0275808	7310	37	51.314	.0283911	4810	37	57.874	.0292441	7210
40	61.570	.0275744	7311	38	56.712	.0283842	4811	38	63.600	.0292368	7211
42	71.715	.0275618	7312	39	62.099	.0283773	4812	39	69.307	.0292297	7212
44	81.818	.0275493	7313	40	67.480	.0283708	4813	40	74.991	.0292228	7213
46	91.889	.0275372	7314	42	78.209	.0283577	4814	42	86.331	.0292091	7214
48	101.916	.0275251	7315	44	88.893	.0283448	4815	44	97.610	.0291953	7215
50	111.909	.0275133	7316	46	99.520	.0283319	4816	46	108.831	.0291822	7216
55	136.662	.0274846	7317	48	110.097	.0283193	4817	48	120.008	.0291693	7217
60	161.135	.0274572	7318	50	120.628	.0283075	4818	50	131.123	.0291568	7218
65	185.348	.0274309	7319	55	146.709	.0282775	4819	55	158.655	.0291252	7219
70	209.268	.0274054	7320	60	172.441	.0282486	4820	60	185.821	.0290956	7220
75	232.871	.0273806	7321	65	197.902	.0282211	4821	65	212.670	.0290671	7221
80	256.235	.0273559	7322	70	223.023	.0281950	4822	70	239.174	.0290401	7222
85	279.383	.0273329	7323	75	247.840	.0281685	4823	75	265.294	.0290138	7223
90	302.286	.0273097	7324	80	272.351	.0281443	4824	80	291.120	.0289880	7224
95	324.948	.0272872	7325	85	296.625	.0281200	4825	85	316.681	.0289627	7225
				90	320.697	.0280966	4826	90	341.943	.0289386	7226
				95	344.394	.0280727	4827				

Table 1. Temperature-Pressure-Density Observations on Para Hydrogen - Continued

T, °K	P, atm	ρ, g mol/cc	Ident.
27	4.832		7101
28	10.553	.0301765	7102
29	16.676	.0301683	7103
30	22.802	.0301602	7104
31	28.917	.0301521	7105
32	35.025	.0301441	7106
33	41.134	.0301362	7107
34	47.229	.0301284	7108
35	53.324	.0301206	7109
36	59.402	.0301130	7110
37	65.463	.0301055	7111
38	71.518	.0300979	7112
39	77.545	.0300905	7113
40	83.573	.0300833	7114
42	95.571	.0300690	7115
44	107.495	.0300546	7116
46	119.346	.0300409	7117
48	131.139	.0300275	7118
50	142.862	.0300144	7119
55	171.896	.0299818	7120
60	200.511	.0299514	7121
65	228.784	.0299218	7122
70	256.676	.0298938	7123
75	284.157	.0298666	7124
80	311.342	.0298403	7125
85	338.184	.0298145	7126

T, °K	P, atm	ρ, g mol/cc	Ident.
24	7.464	.0332321	4601
25	14.929	.0332219	4602
26	22.366	.0332120	4603
27	29.775	.0332024	4604
28	37.161	.0331928	4605
29	44.525	.0331835	4606
30	51.889	.0331743	4607
31	59.230	.0331652	4608
32	66.583	.0331558	4609
33	73.901	.0331467	4610
34	81.220	.0331376	4611
35	88.528	.0331288	4612
36	95.813	.0331203	4613
37	103.070	.0331118	4614
38	110.316	.0331030	4615
39	117.533	.0330941	4616
40	124.716	.0330861	4617
42	139.026	.0330704	4618
44	153.257	.0330545	4619
46	167.364	.0330390	4620
48	181.403	.0330233	4621
50	195.374	.0330089	4622
55	229.844	.0329740	4623
60	263.806	.0329398	4624
65	297.292	.0329080	4625
70	330.271	.0328780	4626

T, °K	P, atm	ρ, g mol/cc	Ident.
21	5.063	.0349781	6701
22	13.171	.0349669	6702
23	21.288	.0349559	6703
24	29.416	.0349452	6704
25	37.544	.0349347	6705
26	45.662	.0349244	6706
27	53.768	.0349143	6707
28	61.862	.0349042	6708
29	69.939	.0348943	6709
30	77.994	.0348846	6710
31	86.033	.0348748	6711
32	94.065	.0348653	6712
33	102.087	.0348556	6713
34	110.085	.0348461	6714
35	118.068	.0348369	6715
36	126.044	.0348279	6716
37	133.981	.0348188	6717
38	141.906	.0348100	6718
39	149.803	.0348014	6719
40	157.684	.0347927	6720
42	173.343	.0347758	6721
44	188.912	.0347593	6722
46	204.384	.0347433	6723
48	219.720	.0347279	6724
50	235.012	.0347126	6725
55	272.753	.0346759	6726
60	309.912	.0346408	6727
65	346.529	.0346075	6728

T, °K	P, atm	ρ, g mol/cc	Ident.
26	3.978		4701
27	10.446	.0311387	4702
28	17.005	.0311299	4703
29	23.542	.0311212	4704
30	30.056	.0311127	4705
31	36.565	.0311043	4706
32	43.062	.0310960	4707
33	49.542	.0310877	4708
34	55.999	.0310795	4709
35	62.469	.0310712	4710
36	68.921	.0310634	4711
37	75.361	.0310557	4712
38	81.768	.0310475	4713
39	88.164	.0310398	4714
40	94.554	.0310322	4715
42	107.271	.0310176	4716
44	119.910	.0310025	4717
46	132.469	.0309879	4718
48	144.966	.0309736	4719
50	157.384	.0309603	4720
55	188.112	.0309271	4721
60	218.355	.0308951	4722
65	248.202	.0308648	4723
70	277.642	.0308358	4724
75	306.644	.0308080	4725
80	335.370	.0307810	4726

T, °K	P, atm	ρ, g mol/cc	Ident.
23	6.803	.0338769	6901
24	14.495	.0338664	6902
25	22.179	.0338561	6903
26	29.860	.0338460	6904
27	37.532	.0338361	6905
28	45.199	.0338263	6906
29	52.849	.0338167	6907
30	60.484	.0338072	6908
31	68.103	.0337978	6909
32	75.710	.0337884	6910
33	83.311	.0337791	6911
34	90.886	.0337699	6912
35	98.448	.0337609	6913
36	105.994	.0337522	6914
37	113.505	.0337435	6915
38	121.011	.0337346	6916
39	128.467	.0337261	6917
40	135.927	.0337179	6918
42	150.730	.0337016	6919
44	165.460	.0336852	6920
46	180.076	.0336697	6921
48	194.608	.0336545	6922
50	209.055	.0336396	6923
55	244.738	.0336031	6924
60	279.879	.0335690	6925
65	314.532	.0335363	6926
70	348.644	.0335040	6927

T, °K	P, atm	ρ, g mol/cc	Ident.
20	5.797	.0355896	4501
21	14.033	.0355780	4502
22	22.336	.0355670	4503
23	30.629	.0355561	4504
24	38.933	.0355454	4505
25	47.248	.0355348	4506
26	55.598	.0355244	4507
27	63.936	.0355143	4508
28	72.275	.0355040	4509
29	80.590	.0354940	4510
30	88.918	.0354840	4511
31	97.211	.0354743	4512
32	105.470	.0354649	4513
33	113.758	.0354548	4514
34	122.001	.0354447	4515
35	130.226	.0354357	4516
36	138.441	.0354265	4517
37	146.633	.0354174	4518
38	154.790	.0354087	4519
39	162.914	.0353996	4520
40	171.038	.0353911	4521
42	187.185	.0353746	4522
44	203.196	.0353578	4523
46	219.173	.0353410	4524
48	234.980	.0353244	4525
50	250.743	.0353086	4526
55	289.612	.0352724	4527
60	327.894	.0352373	4528

T, °K	P, atm	ρ, g mol/cc	Ident.
25	4.544	.0321463	7001
26	11.525	.0321367	7002
27	18.484	.0321273	7003
28	25.442	.0321181	7004
29	32.380	.0321091	7005
30	39.308	.0321002	7006
31	46.221	.0320913	7007
32	53.126	.0320826	7008
33	60.019	.0320738	7009
34	66.902	.0320652	7010
35	73.773	.0320566	7011
36	80.633	.0320483	7012
37	87.476	.0320400	7013
38	94.290	.0320319	7014
39	101.083	.0320238	7015
40	107.858	.0320159	7016
42	121.324	.0320004	7017
44	134.704	.0319848	7018
46	148.006	.0319700	7019
48	161.240	.0319554	7020
50	174.384	.0319412	7021
55	206.870	.0319067	7022
60	238.882	.0318738	7023
65	270.474	.0318423	7024
70	301.616	.0318125	7025
75	332.300	.0317841	7026

T, °K	P, atm	ρ, g mol/cc	Ident.
22	5.565	.0344165	6801
23	13.444	.0344057	6802
24	21.343	.0343950	6803
25	29.236	.0343846	6804
26	37.123	.0343744	6805
27	45.005	.0343644	6806
28	52.873	.0343544	6807
29	60.747	.0343447	6808
30	68.592	.0343351	6809
31	76.432	.0343255	6810
32	84.238	.0343160	6811
33	92.055	.0343064	6812
34	99.844	.0342972	6813
35	107.628	.0342879	6814
36	115.389	.0342789	6815
37	123.110	.0342702	6816
38	130.820	.0342612	6817
39	138.496	.0342527	6818
40	146.150	.0342442	6819
42	161.389	.0342274	6820
44	176.510	.0342112	6821
46	191.540	.0341951	6822
48	206.486	.0341800	6823
50	221.330	.0341646	6824
55	258.022	.0341280	6825
60	294.102	.0340935	6826
65	329.732	.0340607	6827
70	364.785	.0340293	6828

T, °K	P, atm	ρ, g mol/cc	Ident.
19	7.950	.0362396	6601
20	16.429	.0362277	6602
21	24.943	.0362163	6603
22	33.484	.0362052	6604
23	42.048	.0361943	6605
24	50.613	.0361835	6606
25	59.189	.0361729	6607
26	67.760	.0361624	6608
27	76.335	.0361521	6609
28	84.911	.0361418	6610
29	93.471	.0361318	6611
30	102.019	.0361217	6612
31	110.561	.0361117	6613
32	119.081	.0361019	6614
33	127.601	.0360919	6615
34	136.104	.0360823	6616
35	144.590	.0360728	6617
36	153.059	.0360636	6618
37	161.494	.0360545	6619
38	169.924	.0360452	6620
39	178.314	.0360365	6621
40	186.682	.0360278	6622
42	203.326	.0360102	6623
44	219.858	.0359936	6624
46	236.294	.0359775	6625
48	252.629	.0359617	6626
50	268.867	.0359460	6627
55	308.982	.0359089	6628
60	348.454	.0358731	6629

Table 1. Temperature-Pressure-Density Observations on Para Hydrogen - Continued

T, °K	P, atm	ρ, g mol/cc	Ident.
18	11.609	.0369239	5201
19	20.292	.0369121	5202
20	28.980	.0369006	5203
21	37.715	.0368894	5204
22	46.489	.0368784	5205
23	55.308	.0368671	5206
24	64.145	.0368562	5207
25	72.982	.0368454	5208
26	81.818	.0368348	5209
27	90.655	.0368245	5210
28	99.492	.0368139	5211
29	108.318	.0368039	5212
30	117.132	.0367938	5213
31	125.947	.0367835	5214
32	134.739	.0367737	5215
33	143.508	.0367635	5216
34	152.244	.0367538	5217
35	161.014	.0367444	5218
36	169.727	.0367351	5219
37	178.440	.0367257	5220
38	187.119	.0367164	5221
39	195.753	.0367076	5222
40	204.388	.0366986	5223
42	221.554	.0366813	5224
44	238.585	.0366645	5225
46	255.583	.0366481	5226
48	272.411	.0366325	5227
50	289.171	.0366173	5228
55	330.613	.0365789	5229

T, °K	P, atm	ρ, g mol/cc	Ident.
15	5.158	.0379143	5301
16	13.920	.0379020	5302
17	22.778	.0378903	5303
18	31.706	.0378784	5304
19	40.695	.0378665	5305
20	49.723	.0378551	5306
21	58.821	.0378438	5307
22	67.940	.0378328	5308
23	77.082	.0378216	5309
24	86.248	.0378109	5310
25	95.424	.0378003	5311
26	104.612	.0377895	5312
27	113.801	.0377789	5313
28	122.995	.0377686	5314
29	132.172	.0377586	5315
30	141.349	.0377481	5316
31	150.498	.0377380	5317
32	159.653	.0377279	5318
33	168.785	.0377181	5319
34	177.928	.0377084	5320
35	187.050	.0376984	5321
36	196.148	.0376889	5322
37	205.224	.0376799	5323
38	214.267	.0376711	5324
39	223.309	.0376615	5325
40	232.318	.0376527	5326
42	250.222	.0376357	5327
44	268.012	.0376182	5328
46	285.747	.0376017	5329
48	303.334	.0375859	5330
50	320.866	.0375706	5331

T, °K	P, atm	ρ, g mol/cc	Ident.
15	23.735	.0386924	5401
16	32.741	.0386809	5402
17	41.832	.0386693	5403
18	50.986	.0386571	5404
19	60.202	.0386456	5405
20	69.491	.0386344	5406
21	78.826	.0386232	5407
22	88.207	.0386121	5408
23	97.622	.0386012	5409
24	107.048	.0385904	5410
25	116.497	.0385796	5411
26	125.957	.0385689	5412
27	135.417	.0385583	5413
28	144.866	.0385475	5414
29	154.350	.0385371	5415
30	163.799	.0385271	5416
31	173.249	.0385175	5417
32	182.698	.0385071	5418
33	192.113	.0384974	5419
34	201.563	.0384866	5420
35	210.968	.0384775	5421
36	220.361	.0384684	5422
37	229.733	.0384593	5423
38	239.058	.0384505	5424
39	248.430	.0384407	5425
40	257.721	.0384318	5426
42	276.283	.0384145	5427
44	294.709	.0383976	5428
46	312.999	.0383812	5429
48	331.256	.0383652	5430

T, °K	P, atm	ρ, g mol/cc	Ident.
16	51.884	.0393822	5501
17	61.151	.0393704	5502
18	70.498	.0393593	5503
19	79.930	.0393477	5504
20	89.407	.0393362	5505
21	98.957	.0393250	5506
22	108.542	.0393141	5507
23	118.167	.0393033	5508
24	127.814	.0392924	5509
25	137.501	.0392818	5510
26	147.177	.0392712	5511
27	156.898	.0392602	5512
28	166.586	.0392504	5513
29	176.285	.0392397	5514
30	185.984	.0392300	5515
31	195.683	.0392195	5516
32	205.371	.0392102	5517
33	215.082	.0391988	5518
34	224.770	.0391896	5519
35	234.435	.0391799	5520
36	244.089	.0391705	5521
37	253.743	.0391617	5522
38	263.364	.0391529	5523
39	272.951	.0391438	5524
40	282.538	.0391352	5525
42	301.610	.0391175	5526
44	320.581	.0391007	5527
46	339.416	.0390842	5528

T, °K	P, atm	ρ, g mol/cc	Ident.
16	70.191		5601
17	80.524	.0400112	5602
18	89.882	.0399999	5603
19	99.626	.0399882	5604
20	109.313	.0399770	5605
21	119.068	.0399663	5606
22	128.858	.0399556	5607
23	138.692	.0399444	5608
24	148.557	.0399336	5609
25	158.454	.0399231	5610
26	168.368	.0399124	5611
27	178.294	.0399019	5612
28	188.237	.0398913	5613
29	198.158	.0398812	5614
30	208.095	.0398703	5615
31	218.021	.0398609	5616
32	227.936	.0398509	5617
33	237.806	.0398409	5618
34	247.801	.0398306	5619
35	257.693	.0398210	5620
36	267.620	.0398113	5621
37	277.513	.0398025	5622
38	287.371	.0397938	5623
39	297.230	.0397852	5624
40	307.045	.0397754	5625
42	326.594	.0397587	5626
44	346.053	.0397423	5627

T, °K	P, atm	ρ, g mol/cc	Ident.
17	100.092	.0405981	5701
18	109.767	.0405866	5702
19	119.534	.0405758	5703
20	129.390	.0405649	5704
21	139.304	.0405543	5705
22	149.274	.0405435	5706
23	159.301	.0405323	5707
24	169.390	.0405209	5708
25	179.412	.0405108	5709
26	189.508	.0405003	5710
27	199.671	.0404903	5711
28	209.801	.0404795	5712
29	219.930	.0404696	5713
30	230.060	.0404597	5714
31	240.224	.0404501	5715
32	250.354	.0404406	5716
33	260.518	.0404315	5717
34	270.648	.0404205	5718
35	280.812	.0404110	5719
36	290.946	.0404019	5720
37	301.074	.0403927	5721
38	311.103	.0403832	5722
39	321.167	.0403741	5723
40	331.228	.0403646	5724
42	351.221	.0403473	5725

T, °K	P, atm	ρ, g mol/cc	Ident.
18	129.341	.0411268	5801
19	139.278	.0411156	5802
20	149.277	.0411047	5803
21	159.339	.0410940	5804
22	169.469	.0410835	5805
23	179.660	.0410724	5806
24	189.880	.0410618	5807
25	200.134	.0410510	5808
26	210.411	.0410405	5809
27	220.711	.0410310	5810
28	231.035	.0410202	5811
29	241.346	.0410095	5812
30	251.681	.0409996	5813
31	261.976	.0409902	5814
32	272.316	.0409806	5815
33	282.673	.0409711	5816
34	292.986	.0409614	5817
35	303.344	.0409520	5818
36	313.622	.0409430	5819
37	323.923	.0409341	5820
38	334.225	.0409252	5821
39	344.492	.0409168	5822

T, °K	P, atm	ρ, g mol/cc	Ident.
19	159.487	.0416369	5901
20	169.617	.0416257	5902
21	179.815	.0416148	5903
22	190.115	.0416041	5904
23	200.415	.0415938	5905
24	210.816	.0415831	5906
25	221.252	.0415723	5907
26	231.654	.0415622	5908
27	242.158	.0415520	5909
28	252.697	.0415420	5910
29	263.201	.0415317	5911
30	273.706	.0415221	5912
31	284.235	.0415121	5913
32	294.716	.0415025	5914
33	305.255	.0414927	5915
34	315.794	.0414834	5916
35	326.300	.0414744	5917
36	336.840	.0414657	5918
37	347.312	.0414571	5919

T, °K	P, atm	ρ, g mol/cc	Ident.
19	179.205	.0421111	6001
20	189.505	.0421005	6002
21	199.838	.0420911	6003
22	210.240	.0420803	6004
23	220.744	.0420693	6005
24	231.316	.0420589	6006
25	241.865	.0420489	6007
26	252.494	.0420383	6008
27	263.135	.0420285	6009
28	273.810	.0420180	6010
29	284.449	.0420083	6011
30	295.112	.0419984	6012
31	305.764	.0419892	6013
32	316.473	.0419797	6014
33	327.149	.0419709	6015
34	337.824	.0419615	6016
35	348.500	.0419524	6017

Table 1. Temperature-Pressure-Density Observations on Para Hydrogen - Continued

T, °K	P, atm	ρ, g mol/cc	Ident.	T, °K	P, atm	ρ, g mol/cc	Ident.	T, °K	P, atm	ρ, g mol/cc	Ident.
20	211.053	.0425775	6101	21	241.686	.0430003	6201	21	263.293	.0434403	6301
21	221.489	.0425677	6102	22	252.326	.0429902	6202	22	274.103	.0434307	6302
22	232.026	.0425578	6103	23	263.069	.0429797	6203	23	284.982	.0434207	6303
23	242.665	.0425461	6104	24	273.812	.0429696	6204	24	295.928	.0434096	6304
24	253.306	.0425363	6105	25	284.690	.0429596	6205	25	306.909	.0433992	6305
25	264.015	.0425262	6106	26	295.535	.0429499	6206	26	317.991	.0433897	6306
26	274.757	.0425164	6107	27	306.448	.0429404	6207	27	329.040	.0433806	6307
27	285.534	.0425064	6108	28	317.428	.0429312	6208	28	340.124	.0433715	6308
28	296.311	.0424967	6109	29	328.340	.0429226	6209	29	351.242	.0433624	6309
29	307.155	.0424874	6110	30	339.320	.0429137	6210				
30	317.966	.0424782	6111	31	350.301	.0429046	6211				
31	328.811	.0424691	6112								
32	339.656	.0424598	6113								
33	350.502	.0424511	6114								

T, °K	P, atm	ρ, g mol/cc	Ident.	T, °K	P, atm	ρ, g mol/cc	Ident.
22	293.888	.0438020	6401	22	312.227		6501
23	304.767	.0437923	6402	23	324.091	.0441553	6502
24	315.748	.0437820	6403	24	335.208	.0441461	6503
25	326.762	.0437731	6404	25	346.427	.0441359	6504
26	337.879	.0437633	6405				
27	348.995	.0437540	6406				

T, °K	P, atm	ρ, g mol/cc	Ident.	T, °K	P, atm	ρ, g mol/cc	Ident.	T, °K	P, atm	ρ, g mol/cc	Ident.
30.0	8.117		9601	30.0	8.117		9701	30.0	8.116		9501
30.5	8.789		9602	30.5	8.789		9702	30.5	8.787		9502
31.0	9.500		9603	31.0	9.500		9703	31.0	9.503		9503
31.5	10.254		9604	31.5	10.254		9704	31.5	10.253		9504
32.0	11.052		9605	32.0	11.052		9705	32.0	11.050		9505
32.5	11.898		9606	32.5	11.899		9706	32.5	11.899		9506
32.6	12.074		9607	32.6	12.075		9707	32.6	12.075		9507
32.7	12.252		9608	32.7	12.254		9708	32.7	12.253		9508
32.8	12.433		9609	32.8	12.435		9709	32.8	12.433		9509
32.9	12.619		9610	32.9	12.618		9710	32.9	12.617		9510
33.0	12.794	.0140986	9611	33.0	12.804	.0155239	9711	33.0	12.807	.0163976	9511
33.1	12.966	.0140983	9612	33.1	12.991	.0155236	9712	33.1	13.003	.0163973	9512
33.2	13.137	.0140981	9613	33.2	13.178	.0155234	9713	33.2	13.200	.0163970	9513
33.3	13.308	.0140979	9614	33.3	13.365	.0155231	9714	33.3	13.397	.0163967	9514
33.4	13.478	.0140977	9615	33.4	13.552	.0155229	9715	33.4	13.596	.0163965	9515
33.5	13.648	.0140976	9616	33.5	13.740	.0155226	9716	33.5	13.795	.0163962	9516
34.0	14.497	.0140963	9617	34.0	14.683	.0155213	9717	34.0	14.799	.0163948	9517
35.0	16.194	.0140940	9618	35.0	16.583	.0155188	9718	35.0	16.832	.0163921	9518
36.0	17.892	.0140917	9619	36.0	18.498	.0155162	9719	36.0	18.886	.0163893	9519
37.0	19.593	.0140894	9620	37.0	20.422	.0155136	9720	37.0	20.955	.0163866	9520
38.0	21.294	.0140871	9621	38.0	22.353	.0155110	9721	38.0	23.035	.0163837	9521
39.0	22.997	.0140848	9622	39.0	24.289	.0155084	9722	39.0	25.123	.0163809	9522
40.0	24.699	.0140826	9623	40.0	26.228	.0155058	9723	40.0	27.216	.0163782	9523

Experimental isotherm functions $(Pv-RT)v$, where v is molal volume, were represented by polynomial expansions in density [18], using least-squares methods [19] and an electronic computer with eleven digits. The number of terms in each polynomial was selected by trial as the minimum number required to give deviations within experimental precision [7]. This number increases from five terms at 100 °K to fifteen terms at 33 °K. From 32 through 24 °K, data for both vapor and compressed liquid were represented simultaneously by single isotherm polynomials of nine terms. From 23 through 17 °K, data for the compressed liquid were represented with six terms.

Differences between experimental and calculated results were averaged for each run and converted to an assumed error in experimental determination of density (amount of sample) for that run. Fixed adjustments to the density throughout certain runs were applied for smoothing, as given in table 2A. These are within the experimental precision. A final set of polynomial representations of isotherms, obtained as above, then represents all pressures within the experimental precision. The first derivatives of pressure with respect to density, obtained from these polynomials, are smooth; the second derivatives are smooth and monotonically increasing. These representations were used to calculate pressures at the uniform densities in table 2. Some entries in table 2 are extrapolated beyond the maximum experimental pressure of 350 atm.

Table 2. Pressures in Atmospheres at Integral Densities and Temperatures

DENSITY MOL/CC	TEMPERATURE DEGREES K 17.000	18.000	19.000	20.000	21.000	22.000	23.000	24.000	25.000	26.000	27.000	28.000	29.000
.0005								.929	.972	1.014	1.056	1.098	1.140
.0010								1.750	1.836	1.923	2.009	2.095	2.181
.0015								2.462	2.597	2.730	2.863	2.996	3.127
.0020										3.438	3.620	3.801	3.981
.0025											4.283	4.515	4.745
.0030												5.139	5.422
.0035												5.677	6.015
.0040													6.526
.0285													8.317
.0290													10.400
.0295												6.950	12.833
.0300												9.543	15.645
.0305											6.210	12.545	18.867
.0310											9.444	15.988	22.531
.0315										6.349	13.145	19.905	26.667
.0320									3.327	10.337	17.349	24.327	31.309
.0325									7.625	14.861	22.088	29.288	36.489
.0330								5.059	12.500	19.956	27.398	34.820	42.240
.0335							2.688	10.320	17.986	25.658	33.314	40.959	48.596
.0340							8.364	16.232	24.118	32.001	39.870	47.738	55.592
.0345						6.732	14.743	22.830	30.929	39.021	47.102	55.191	63.262
.0350					5.379	13.615	21.851	30.146	38.454	46.754	55.047	63.355	71.641
.0355				4.452	12.799	21.250	29.719	38.217	46.730	55.237	63.741	72.264	80.764
.0360			3.880	12.456	21.026	29.678	38.378	47.076	55.791	64.505	73.219	81.954	90.668
.0365		3.784	12.501	21.285	30.094	38.942	47.862	56.761	65.675	74.596	83.519	92.463	101.389
.0370	4.207	13.087	22.027	30.998	40.038	49.081	58.207	67.306	76.418	85.546	94.679	103.827	112.964
.0375	14.275	23.360	32.491	41.642	50.895	60.134	69.451	78.751	88.060	97.394	106.734	116.084	125.430
.0380	25.354	34.619	43.927	53.261	62.703	72.138	81.635	91.133	100.639	110.177	119.724	129.273	138.825
.0385	37.468	46.885	56.368	65.888	75.499	85.130	94.797	104.492	114.195	123.934	133.685	143.431	153.187
.0390	50.640	60.185	69.848	79.557	89.323	99.146	108.982	118.869	128.768	138.704	148.657	158.599	168.556
.0395	64.891	74.555	84.403	94.294	104.214	114.223	124.230	134.305	144.399	154.527	164.678	174.815	184.970
.0400	80.240	90.036	100.067	110.131	120.212	130.397	140.583	150.843	161.129	171.442	181.787	192.120	202.468
.0405	96.705	106.680	116.878	127.100	137.357	147.707	158.084	168.523	178.998	189.490	200.024	210.554	221.092
.0410		124.549	134.872	145.244	155.688	166.193	176.772	187.389	198.046	208.711	219.429	230.156	240.879
.0415			154.088	164.614	175.246	185.898	196.686	207.477	218.312	229.146	240.041	250.965	261.870
.0420			174.564	185.280	196.067	206.869	217.860	228.826	239.831	250.835	261.901	273.019	284.103
.0425				207.333	218.189	229.157	240.327	251.465	262.636	273.817	285.050	296.354	307.616
.0430					241.649	252.819	264.111	275.418	286.753	298.132	309.527	321.004	332.443
.0435					266.479	277.921	289.235	300.699	312.202	323.816	335.374	346.996	358.619
.0440						304.534	315.711	327.308	338.994	350.903	362.630	374.358	386.174

Table 2. Pressures in Atmospheres at Integral Densities and Temperatures - Continued

DENSITY MOL/CC	TEMPERATURE DEGREES K												
	30.000	31.000	32.000	33.000	34.000	35.000	36.000	37.000	38.000	39.000	40.000	42.000	44.000
.0005	1.182	1.223	1.265	1.307	1.349	1.391	1.433	1.475	1.517	1.559	1.600	1.684	1.767
.0010	2.267	2.352	2.438	2.524	2.609	2.695	2.780	2.866	2.951	3.036	3.121	3.291	3.461
.0015	3.259	3.390	3.521	3.652	3.783	3.914	4.044	4.175	4.305	4.435	4.565	4.825	5.084
.0020	4.160	4.339	4.518	4.696	4.874	5.051	5.229	5.406	5.583	5.759	5.936	6.288	6.639
.0025	4.975	5.203	5.431	5.658	5.884	6.111	6.336	6.562	6.787	7.011	7.235	7.683	8.129
.0030	5.704	5.984	6.263	6.541	6.818	7.095	7.370	7.645	7.920	8.194	8.468	9.013	9.557
.0035	6.352	6.685	7.017	7.348	7.677	8.006	8.333	8.660	8.986	9.311	9.635	10.282	10.927
.0040	6.920	7.309	7.697	8.083	8.465	8.848	9.229	9.608	9.987	10.364	10.741	11.492	12.240
.0045	7.412	7.859	8.305	8.747	9.186	9.624	10.059	10.493	10.926	11.358	11.788	12.646	13.500
.0050	7.831	8.339	8.844	9.344	9.842	10.336	10.828	11.318	11.807	12.293	12.779	13.747	14.709
.0055		8.751	9.319	9.879	10.436	10.989	11.539	12.086	12.632	13.175	13.718	14.798	15.872
.0060		9.101	9.732	10.354	10.972	11.584	12.194	12.801	13.404	14.006	14.607	15.801	16.990
.0065		9.392	10.087	10.773	11.454	12.127	12.797	13.464	14.128	14.789	15.449	16.761	18.066
.0070			10.388	11.140	11.884	12.620	13.352	14.081	14.805	15.527	16.248	17.680	19.105
.0075			10.638	11.458	12.266	13.066	13.862	14.653	15.440	16.224	17.006	18.561	20.108
.0080			10.842	11.730	12.605	13.470	14.330	15.185	16.035	16.882	17.727	19.407	21.080
.0085			11.003	11.961	12.903	13.834	14.759	15.679	16.593	17.505	18.414	20.221	22.022
.0090				12.155	13.164	14.162	15.153	16.138	17.119	18.096	19.070	21.006	22.938
.0095				12.314	13.392	14.458	15.516	16.567	17.615	18.658	19.698	21.767	23.832
.0100				12.442	13.590	14.725	15.850	16.969	18.083	19.194	20.301	22.505	24.706
.0105				12.544	13.762	14.966	16.159	17.345	18.528	19.708	20.883	23.225	25.564
.0110				12.622	13.912	15.184	16.445	17.700	18.953	20.202	21.446	23.928	26.409
.0115				12.681	14.041	15.382	16.712	18.037	19.359	20.679	21.995	24.620	27.244
.0120				12.724	14.154	15.564	16.963	18.358	19.752	21.143	22.531	25.303	28.073
.0125				12.754	14.252	15.731	17.200	18.666	20.132	21.596	23.058	25.979	28.900
.0130				12.775	14.339	15.886	17.427	18.965	20.504	22.042	23.580	26.654	29.727
.0135				12.787	14.417	16.033	17.645	19.256	20.871	22.485	24.099	27.329	30.559
.0140				12.795	14.488	16.172	17.858	19.544	21.235	22.926	24.619	28.010	31.400
.0145				12.799	14.554	16.308	18.068	19.831	21.600	23.370	25.144	28.699	32.254
.0150				12.800	14.617	16.442	18.278	20.120	21.968	23.820	25.677	29.400	33.124
.0155				12.801	14.679	16.578	18.491	20.414	22.345	24.280	26.222	30.118	34.017
.0160				12.803	14.743	16.717	18.711	20.717	22.732	24.753	26.783	30.857	34.935
.0165				12.806	14.811	16.863	18.940	21.032	23.135	25.245	27.364	31.622	35.885
.0170				12.811	14.886	17.019	19.182	21.364	23.557	25.759	27.971	32.418	36.872
.0175				12.821	14.970	17.189	19.442	21.717	24.004	26.301	28.608	33.250	37.902
.0180				12.837	15.068	17.377	19.724	22.095	24.480	26.875	29.282	34.124	38.980
.0185				12.864	15.183	17.588	20.033	22.504	24.990	27.488	29.997	35.047	40.114
.0190				12.904	15.321	17.827	20.375	22.950	25.542	28.146	30.761	36.026	41.310
.0195				12.963	15.487	18.100	20.755	23.439	26.141	28.856	31.581	37.068	42.577
.0200				13.047	15.687	18.414	21.181	23.978	26.795	29.625	32.464	38.182	43.923
.0205				13.164	15.929	18.775	21.661	24.577	27.513	30.462	33.420	39.375	45.356
.0210				13.322	16.221	19.193	22.202	25.242	28.302	31.376	34.457	40.658	46.886
.0215				13.533	16.573	19.677	22.816	25.984	29.174	32.376	35.585	42.041	48.523
.0220				13.806	16.995	20.237	23.511	26.814	30.137	33.473	36.815	43.535	50.279
.0225				14.155	17.498	20.885	24.300	27.742	31.205	34.678	38.159	45.151	52.165

Table 2. Pressures in Atmospheres at Integral Densities and Temperatures - Continued

DENSITY MOL/CC	TEMPERATURE DEGREES K												
	30.000	31.000	32.000	33.000	34.000	35.000	36.000	37.000	38.000	39.000	40.000	42.000	44.000
.0230			11.170	14.594	18.095	21.633	25.195	28.782	32.388	36.004	39.628	46.902	54.194
.0235			11.552	15.137	18.801	22.494	26.209	29.946	33.701	37.465	41.236	48.801	56.379
.0240			12.046	15.799	19.629	23.483	27.356	31.249	35.157	39.074	42.998	50.862	58.735
.0245			12.669	16.599	20.597	24.617	28.653	32.707	36.773	40.847	44.929	53.101	61.276
.0250			13.440	17.552	21.721	25.911	30.116	34.335	38.565	42.800	47.044	55.533	64.020
.0255		10.116	14.377	18.677	23.020	27.385	31.764	36.153	40.550	44.951	49.361	58.177	66.983
.0260		11.041	15.501	19.994	24.513	29.057	33.614	38.178	42.747	47.319	51.899	61.049	70.182
.0265		12.172	16.832	21.522	26.222	30.948	35.687	40.430	45.175	49.922	54.675	64.168	73.639
.0270	8.718	13.530	18.394	23.283	28.167	33.080	38.004	42.931	47.856	52.781	57.712	67.555	77.371
.0275	10.115	15.140	20.208	25.299	30.371	35.474	40.588	45.701	50.811	55.919	61.031	71.231	81.401
.0280	11.783	17.024	22.298	27.592	32.859	38.155	43.462	48.766	54.064	59.357	64.653	75.218	85.749
.0285	13.751	19.209	24.691	30.187	35.654	41.148	46.650	52.147	57.637	63.120	68.602	79.540	90.440
.0290	16.046	21.721	27.412	33.112	38.784	44.478	50.178	55.872	61.557	67.233	72.904	84.219	95.497
.0295	18.695	24.587	30.487	36.391	42.274	48.172	54.072	59.965	65.849	71.720	77.584	89.283	100.944
.0300	21.727	27.836	33.946	40.055	46.153	52.257	58.360	64.454	70.539	76.609	82.668	94.756	106.807
.0305	25.173	31.495	37.817	44.133	50.449	56.761	63.069	69.367	75.656	81.927	88.184	100.667	113.113
.0310	29.061	35.597	42.131	48.655	55.191	61.715	68.230	74.733	81.229	87.703	94.160	107.043	119.889
.0315	33.423	40.172	46.919	53.655	60.410	67.147	73.870	80.581	87.285	93.965	100.626	113.912	127.162
.0320	38.290	45.251	52.213	59.164	66.137	73.088	80.022	86.941	93.857	100.744	107.611	121.306	134.962
.0325	43.694	50.868	58.046	65.214	72.403	79.570	86.716	93.846	100.973	108.069	115.146	129.253	143.317
.0330	49.668	57.056	64.451	71.840	79.241	86.625	93.984	101.326	108.665	115.973	123.261	137.785	152.257
.0335	56.244	63.850	71.461	79.074	86.685	94.284	101.859	109.413	116.966	124.485	131.989	146.932	161.814
.0340	63.456	71.282	79.112	86.948	94.766	102.582	110.373	118.141	125.907	133.639	141.360	156.725	172.018
.0345	71.339	79.387	87.436	95.496	103.520	111.551	119.559	127.542	135.522	143.468	151.407	167.196	182.901
.0350	79.929	88.201	96.468	104.751	112.981	121.225	129.451	137.649	145.842	154.003	162.160	178.376	194.494
.0355	89.261	97.758	106.242	114.745	123.182	131.640	140.083	148.497	156.901	165.278	173.653	190.296	206.829
.0360	99.371	108.092	116.792	125.506	134.159	142.829	151.489	160.119	168.734	177.327	185.917	202.988	219.941
.0365	110.298	119.239	128.152	137.077	145.947	154.828	163.704	172.550	181.374	190.184	198.985	216.484	233.860
.0370	122.078	131.234	140.357	149.492	158.582	167.673	176.762	185.824	194.857	203.884	212.891	230.817	248.622
.0375	134.750	144.113	153.443	162.776	172.098	181.400	190.700	199.977	209.216	218.460	227.669	246.020	264.259
.0380	148.353	157.915	167.448	176.988	186.534	196.045	205.553	215.043	224.488	233.949	243.357	262.130	280.806
.0385	162.924	172.676	182.410	192.161	201.925	211.647	221.359	231.059	240.711	250.386	259.993	279.185	298.297
.0390	178.502	188.439	198.372	208.320	218.309	228.242	238.155	248.063	257.921	267.809	277.623	297.230	316.768
.0395	195.124	205.244	215.376	225.536	235.727	245.870	255.982	266.095	276.161	286.256	296.295	316.316	336.255
.0400	212.830	223.135	233.468	243.842	254.218	264.569	274.882	285.196	295.471	305.766	316.070	336.503	356.794
.0405	231.655	242.154	252.691	263.280	273.824	284.380	294.899	305.411	315.898	326.382	337.016	357.864	378.424
.0410	251.635	262.343	273.085	283.862	294.590	305.344	316.084	326.789	337.490	348.147	359.218	380.492	
.0415	272.806	283.734	294.680	305.640	316.560	327.505	338.489	349.386	360.304	371.108	382.782		
.0420	295.202	306.349	317.483	328.635	339.783	350.906	362.177	373.264	384.400	395.318			
.0425	318.859	330.186	341.467	352.805	364.303	375.596	387.215	398.495					
.0430	343.810	355.205	366.546	378.247	390.168								
.0435	370.092	381.308	392.547										
.0440	397.745												

Table 2. Pressures in Atmospheres at Integral Densities and Temperatures - Continued

DENSITY MOL/CC	TEMPERATURE DEGREES K												
	46.000	48.000	50.000	55.000	60.000	65.000	70.000	75.000	80.000	85.000	90.000	95.000	100.000
.0005	1.851	1.934	2.018	2.226	2.434	2.643	2.851	3.059	3.267	3.475	3.683	3.891	4.098
.0010	3.631	3.800	3.970	4.393	4.816	5.238	5.661	6.082	6.504	6.927	7.348	7.769	8.190
.0015	5.343	5.601	5.859	6.504	7.148	7.791	8.434	9.075	9.716	10.358	11.000	11.640	12.279
.0020	6.990	7.340	7.690	8.563	9.433	10.304	11.173	12.039	12.907	13.774	14.641	15.506	16.369
.0025	8.574	9.019	9.463	10.571	11.676	12.779	13.881	14.979	16.078	17.176	18.275	19.371	20.464
.0030	10.100	10.642	11.183	12.533	13.878	15.221	16.561	17.897	19.234	20.570	21.905	23.238	24.567
.0035	11.570	12.211	12.852	14.451	16.042	17.632	19.217	20.798	22.378	23.957	25.536	27.112	28.682
.0040	12.986	13.730	14.474	16.327	18.172	20.014	21.851	23.683	25.513	27.341	29.170	30.995	32.813
.0045	14.352	15.201	16.050	18.165	20.270	22.372	24.467	26.556	28.643	30.727	32.812	34.892	36.963
.0050	15.670	16.628	17.584	19.967	22.339	24.708	27.068	29.420	31.771	34.117	36.465	38.806	41.137
.0055	16.944	18.012	19.080	21.737	24.383	27.024	29.656	32.279	34.900	37.516	40.133	42.741	45.338
.0060	18.176	19.358	20.539	23.478	26.404	29.326	32.236	35.136	38.034	40.926	43.820	46.701	49.571
.0065	19.369	20.667	21.964	25.192	28.405	31.614	34.810	37.995	41.176	44.352	47.529	50.690	53.840
.0070	20.527	21.944	23.360	26.883	30.391	33.894	37.382	40.858	44.330	47.797	51.264	54.712	58.148
.0075	21.652	23.191	24.728	28.553	32.363	36.168	39.956	43.730	47.500	51.265	55.029	58.771	62.501
.0080	22.748	24.411	26.073	30.208	34.326	38.439	42.535	46.614	50.690	54.761	58.829	62.872	66.903
.0085	23.818	25.608	27.396	31.848	36.283	40.712	45.123	49.514	53.904	58.289	62.668	67.019	71.358
.0090	24.864	26.784	28.702	33.479	38.238	42.990	47.723	52.435	57.146	61.852	66.549	71.218	75.872
.0095	25.890	27.943	29.994	35.103	40.194	45.277	50.341	55.382	60.421	65.455	70.479	75.472	80.450
.0100	26.900	29.088	31.275	36.725	42.155	47.577	52.980	58.357	63.733	69.103	74.461	79.787	85.096
.0105	27.896	30.223	32.549	38.347	44.125	49.895	55.644	61.366	67.087	72.801	78.501	84.169	89.817
.0110	28.882	31.351	33.820	39.974	46.109	52.234	58.339	64.414	70.488	76.554	82.605	88.623	94.618
.0115	29.861	32.476	35.090	41.609	48.110	54.599	61.068	67.506	73.941	80.368	86.777	93.154	99.505
.0120	30.838	33.601	36.364	43.258	50.132	56.995	63.838	70.647	77.453	84.247	91.023	97.769	104.485
.0125	31.815	34.731	37.646	44.923	52.181	59.427	66.652	73.843	81.027	88.199	95.351	102.474	109.564
.0130	32.797	35.869	38.940	46.610	54.261	61.900	69.517	77.099	84.671	92.229	99.766	107.276	114.748
.0135	33.787	37.019	40.251	48.324	56.377	64.419	72.438	80.421	88.391	96.343	104.275	112.181	120.044
.0140	34.790	38.186	41.582	50.068	58.535	66.989	75.421	83.815	92.193	100.549	108.885	117.196	125.461
.0145	35.810	39.374	42.939	51.849	60.739	69.618	78.473	87.288	96.083	104.854	113.604	122.330	131.005
.0150	36.851	40.589	44.327	53.671	62.996	72.311	81.599	90.847	100.069	109.265	118.439	127.589	136.685
.0155	37.919	41.834	45.750	55.541	65.313	75.074	84.807	94.498	104.158	113.789	123.398	132.982	142.508
.0160	39.018	43.116	47.214	57.464	67.694	77.914	88.104	98.249	108.358	118.435	128.491	138.517	148.484
.0165	40.154	44.439	48.726	59.446	70.148	80.839	91.496	102.107	112.677	123.212	133.725	144.203	154.621
.0170	41.333	45.811	50.292	61.495	72.680	83.855	94.993	106.081	117.123	128.127	139.109	150.050	160.929
.0175	42.560	47.237	51.916	63.618	75.300	86.971	98.601	110.179	121.704	133.191	144.653	156.065	167.417
.0180	43.842	48.723	53.607	65.822	78.014	90.195	102.330	114.409	126.431	138.412	150.366	162.260	174.094
.0185	45.186	50.278	55.373	68.114	80.831	93.535	106.189	118.781	131.311	143.800	156.259	168.645	180.973
.0190	46.600	51.909	57.221	70.504	83.760	97.001	110.186	123.305	136.356	149.366	162.341	175.230	188.063
.0195	48.091	53.623	59.160	73.000	86.810	100.602	114.332	127.989	141.575	155.119	168.624	182.026	195.375
.0200	49.668	55.431	61.197	75.612	89.991	104.348	118.637	132.846	146.980	161.071	175.117	189.045	202.921

67082-63--7

Table 2. Pressures in Atmospheres at Integral Densities and Temperatures - Continued

DENSITY MOL/CC	TEMPERATURE DEGREES K												
	46.000	48.000	50.000	55.000	60.000	65.000	70.000	75.000	80.000	85.000	90.000	95.000	100.000
.0205	51.340	57.340	63.344	78.349	93.313	108.249	123.111	137.885	152.581	167.232	181.832	196.298	210.714
.0210	53.117	59.361	65.610	81.222	96.786	112.317	127.766	143.119	158.391	173.615	188.781	203.798	218.764
.0215	55.009	61.505	68.005	84.241	100.423	116.562	132.614	148.559	164.420	180.232	195.976	211.558	227.086
.0220	57.027	63.783	70.542	87.420	104.234	120.998	137.667	154.218	170.683	187.094	203.430	219.590	235.692
.0225	59.184	66.207	73.231	90.769	108.233	125.637	142.938	160.109	177.192	194.216	211.154	227.908	244.597
.0230	61.491	68.789	76.087	94.303	112.432	130.491	148.440	166.246	183.962	201.610	219.163	236.527	253.813
.0235	63.962	71.544	79.122	98.033	116.846	135.576	154.187	172.643	191.006	209.290	227.470	245.461	263.356
.0240	66.612	74.485	82.351	101.976	121.488	140.905	160.195	179.316	198.339	217.272	236.092	254.724	273.241
.0245	69.456	77.628	85.790	106.146	126.374	146.495	166.478	186.279	205.978	225.570	245.042	264.332	283.483
.0250	72.510	80.989	89.454	110.559	131.520	152.360	173.052	193.550	213.937	234.201	254.338	274.302	294.098
.0255	75.791	84.584	93.360	115.231	136.942	158.518	179.935	201.145	222.235	243.182	263.997	284.650	305.102
.0260	79.316	88.432	97.526	120.180	142.657	164.987	187.143	209.081	230.888	252.531	274.039	295.392	316.513
.0265	83.105	92.551	101.970	125.426	148.685	171.785	194.696	217.377	239.914	262.267	284.483	306.546	328.347
.0270	87.177	96.962	106.713	130.986	155.044	178.930	202.611	226.052	249.332	272.409	295.351	318.129	340.623
.0275	91.554	101.683	111.775	136.881	161.755	186.443	210.909	235.126	259.162	282.981	306.667	330.162	353.358
.0280	96.256	106.738	117.176	143.132	168.837	194.345	219.609	244.617	269.423	294.004	318.456	342.661	366.572
.0285	101.307	112.148	122.940	149.761	176.314	202.656	228.734	254.548	280.137	305.503	330.747	355.648	380.283
.0290	106.731	117.937	129.089	156.791	184.208	211.400	238.305	264.938	291.324	317.506	343.571	369.141	394.512
.0295	112.551	124.128	135.647	164.246	192.542	220.599	248.345	275.811	303.006	330.040	356.961	383.162	
.0300	118.793	130.748	142.640	172.149	201.340	230.277	258.877	287.188	315.207	343.136	370.954	397.731	
.0305	125.483	137.821	150.093	180.528	210.629	240.459	269.927	299.092	327.950	356.829	385.592		
.0310	132.649	145.374	158.031	189.408	220.433	251.169	281.519	311.546	341.258	371.154			
.0315	140.319	153.435	166.484	198.815	230.779	262.432	293.680	324.572	355.156	386.151			
.0320	148.520	162.032	175.477	208.777	241.694	274.276	306.437	338.196	369.670				
.0325	157.281	171.193	185.040	219.323	253.205	286.725	319.816	352.439	384.826				
.0330	166.634	180.948	195.201	230.479	265.337	299.805	333.848	367.326					
.0335	176.607	191.327	205.990	242.275	278.119	313.544	348.560	382.880					
.0340	187.232	202.361	217.436	254.738	291.574	327.965	363.984	399.124					
.0345	198.539	214.079	229.570	267.896	305.726	343.095	380.151						
.0350	210.559	226.513	242.420	281.775	320.600	358.956	397.090						
.0355	223.324	239.694	256.018	296.400	336.212	375.571							
.0360	236.865	253.653	270.393	311.795	352.581	392.961							
.0365	251.213	268.422	285.574	327.981	369.718								
.0370	266.399	284.032	301.590	344.977	387.629								
.0375	282.452	300.514	318.469	362.795									
.0380	299.403	317.898	336.239	381.446									
.0385	317.282	336.214	354.926										
.0390	336.115	355.493	374.554										
.0395	355.932	375.762	395.148										
.0400	376.757	397.049											
.0405	398.616												

Table 2-A. Density Adjustments for Smoothing
(In sequence of increasing densities of runs.)

Run No.	$\Delta\rho \cdot 10^6$	Run No.	$\Delta\rho \cdot 10^6$	Run No.	$\Delta\rho \cdot 10^6$
94	-0.04	50	+0.20	67	+5.01
93	+.29	80	+2.20	45	-2.25
92	-.40	79	+1.55	66	+3.34
91	-.41	78	+0.19	52	-0.76
90	+.02	77	-1.99	53	-2.53
89	+.66	49	-1.02	54	+1.39
88	+1.17	76	+0.36	55	+0.85
87	-0.92	75	+1.01	56	-1.32
86	-1.90	74	+1.08	57	+0.46
85	+0.68	73	+2.35	58	+1.90
84	+2.36	48	-10.33	59	-2.01
96	0.00	72	+2.31	60	-1.98
83	-2.21	71	+1.59	61	+3.67
51	+1.38	47	+2.47	62	-1.26
97	0.00	70	+0.18	63	-1.97
95	.00	46	+2.15	64	0.00
82	-.89	69	-6.09	65	.00
81	-1.79	68	-3.07		

Table 3 presents the data interpolated to isobars, that is to uniform pressures at the experimental temperatures. Table entries are densities in gram moles per cubic centimeter, multiplied by 1000. An iterative computer program was applied to locate these densities corresponding to assigned pressures on each isotherm, represented by the polynomial expansion described above.

The above polynomial representations of isotherms provide a smoothing in one of the two independent variables only. The interpolated isochores of table 2 have been given polynomial representations for the purpose of computing changes in thermodynamic functions. Comparison of the interpolated isochore data with these representations shows a behavior which is smooth within the precision of pressure measurements [7]. Entries in the tables of this report may contain more than an experimentally significant number of digits. These are useful in smoothed data for obtaining derivatives by numerical methods.

Table 3. Densities in g mol/cc x 10^3, at Integral Pressures and Temperatures

PRESSURE ATM	TEMPERATURE DEGREES K												
	17.000	18.000	19.000	20.000	21.000	22.000	23.000	24.000	25.000	26.000	27.000	28.000	29.000
1.0	36.8295	36.3394	35.8205	35.2681				.5408	.5155	.4930	.4723	.4536	.4363
2.0	36.8833	36.3977	35.8836	35.3364	34.7530	34.1221		1.1672	1.1020	1.0453	.9949	.9501	.9097
3.0	36.9365	36.4553	35.9459	35.4037	34.8275	34.2046	33.5291	32.7862	1.7974	1.6825	1.5860	1.5026	1.4297
4.0	36.9892	36.5122	36.0073	35.4702	34.9009	34.2857	33.6211	32.8915	32.0828	31.1707	2.2782	2.1329	2.0116
5.0	37.0413	36.5684	36.0680	35.5359	34.9730	34.3653	33.7110	32.9940	32.2025	31.3146	30.2928	2.8822	2.6809
6.0	37.0928	36.6239	36.1278	35.6007	35.0440	34.4436	33.7990	33.0940	32.3185	31.4529	30.4649	29.2953	3.4868
7.0	37.1438	36.6788	36.1870	35.6646	35.1139	34.5205	33.8852	33.1916	32.4312	31.5862	30.6288	29.5104	28.1349
8.0	37.1943	36.7330	36.2454	35.7278	35.1828	34.5962	33.9696	33.2869	32.5408	31.7150	30.7853	29.7117	28.4162
9.0	37.2442	36.7867	36.3031	35.7901	35.2507	34.6707	34.0524	33.3800	32.6474	31.8395	30.9354	29.9014	28.6731
10.0	37.2937	36.8397	36.3602	35.8518	35.3176	34.7440	34.1337	33.4712	32.7512	31.9602	31.0795	30.0809	28.9100
11.0	37.3427	36.8922	36.4165	35.9126	35.3835	34.8162	34.2135	33.5605	32.8525	32.0773	31.2183	30.2516	29.1305
12.0	37.3913	36.9441	36.4723	35.9728	35.4486	34.8873	34.2918	33.6479	32.9514	32.1910	31.3521	30.4143	29.3372
13.0	37.4394	36.9955	36.5274	36.0322	35.5128	34.9574	34.3688	33.7337	33.0480	32.3017	31.4815	30.5701	29.5318
14.0	37.4870	37.0464	36.5820	36.0910	35.5762	35.0264	34.4445	33.8178	33.1425	32.4094	31.6068	30.7195	29.7162
15.0	37.5342	37.0968	36.6359	36.1491	35.6388	35.0945	34.5190	33.9003	33.2350	32.5145	31.7283	30.8631	29.8914
16.0	37.5810	37.1467	36.6893	36.2065	35.7005	35.1617	34.5923	33.9814	33.3255	32.6169	31.8461	31.0016	30.0585
17.0	37.6274	37.1961	36.7422	36.2634	35.7615	35.2279	34.6645	34.0610	33.4142	32.7170	31.9607	31.1353	30.2184
18.0	37.6734	37.2451	36.7945	36.3195	35.8218	35.2933	34.7356	34.1393	33.5012	32.8148	32.0723	31.2646	30.3718
19.0	37.7189	37.2936	36.8463	36.3751	35.8814	35.3578	34.8057	34.2163	33.5865	32.9104	32.1809	31.3899	30.5193
20.0	37.7641	37.3416	36.8976	36.4301	35.9403	35.4215	34.8747	34.2920	33.6703	33.0041	32.2868	31.5114	30.6614
22.0	37.8534	37.4365	36.9986	36.5384	36.0560	35.5465	35.0099	34.4400	33.8333	33.1856	32.4912	31.7443	30.9313
24.0	37.9413	37.5297	37.0978	36.6445	36.1693	35.6685	35.1415	34.5835	33.9909	33.3602	32.6865	31.9650	31.1845
26.0	38.0278	37.6213	37.1953	36.7486	36.2801	35.7877	35.2698	34.7229	34.1434	33.5284	32.8736	32.1750	31.4232
28.0	38.1130	37.7115	37.2909	36.8506	36.3886	35.9042	35.3949	34.8585	34.2912	33.6907	33.0533	32.3755	31.6494
30.0	38.1969	37.8002	37.3850	36.9507	36.4951	36.0182	35.5170	34.9905	34.4347	33.8478	33.2264	32.5675	31.8646
32.0	38.2796	37.8876	37.4775	37.0491	36.5994	36.1297	35.6363	35.1192	34.5742	33.9999	33.3934	32.7518	32.0699
34.0	38.3612	37.9736	37.5685	37.1456	36.7018	36.2390	35.7530	35.2447	34.7100	34.1475	33.5548	32.9291	32.2664
36.0	38.4417	38.0584	37.6581	37.2406	36.8023	36.3461	35.8673	35.3673	34.8422	34.2909	33.7110	33.1001	32.4550
38.0	38.5210	38.1421	37.7463	37.3339	36.9011	36.4512	35.9791	35.4872	34.9712	34.4303	33.8624	33.2653	32.6364
40.0	38.5993	38.2245	37.8331	37.4257	36.9982	36.5543	36.0888	35.6044	35.0970	34.5660	34.0094	33.4251	32.8113
42.0	38.6767	38.3058	37.9187	37.5161	37.0936	36.6555	36.1963	35.7191	35.2200	34.6982	34.1523	33.5800	32.9801
44.0	38.7530	38.3861	38.0031	37.6050	37.1875	36.7549	36.3017	35.8315	35.3401	34.8273	34.2914	33.7303	33.1434
46.0	38.8285	38.4653	38.0862	37.6926	37.2799	36.8527	36.4053	35.9416	35.4577	34.9532	34.4268	33.8764	33.3016
48.0	38.9030	38.5435	38.1683	37.7789	37.3708	36.9487	36.5070	36.0496	35.5729	35.0763	34.5589	34.0184	33.4551
50.0	38.9766	38.6207	38.2492	37.8639	37.4604	37.0432	36.6069	36.1556	35.6856	35.1967	34.6877	34.1567	33.6042
55.0	39.1571	38.8097	38.4470	38.0713	37.6785	37.2730	36.8495	36.4123	35.9581	35.4866	34.9972	34.4877	33.9595
60.0	39.3327	38.9933	38.6386	38.2719	37.8891	37.4942	37.0825	36.6581	36.2182	35.7624	35.2902	34.7999	34.2928
65.0	39.5037	39.1718	38.8247	38.4661	38.0927	37.7076	37.3069	36.8942	36.4672	36.0255	35.5689	35.0956	34.6074
70.0	39.6705	39.3456	39.0054	38.6545	38.2899	37.9139	37.5234	37.1214	36.7062	36.2774	35.8349	35.3769	34.9054
75.0	39.8333	39.5149	39.1813	38.8376	38.4812	38.1135	37.7326	37.3405	36.9363	36.5192	36.0894	35.6454	35.1890

Table 3. Densities in g mol/cc x 10^3, at Integral Pressures and Temperatures - Continued

PRESSURE ATM	TEMPERATURE DEGREES K												
	17.000	18.000	19.000	20.000	21.000	22.000	23.000	24.000	25.000	26.000	27.000	28.000	29.000
80.0	39.9925	39.6801	39.3527	39.0156	38.6670	38.3072	37.9352	37.5522	37.1581	36.7518	36.3337	35.9024	35.4597
85.0	40.1481	39.8413	39.5197	39.1890	38.8477	38.4952	38.1315	37.7572	37.3723	36.9760	36.5687	36.1491	35.7188
90.0	40.3005	39.9989	39.6828	39.3581	39.0236	38.6780	38.3221	37.9558	37.5796	37.1925	36.7951	36.3863	35.9675
95.0	40.4498	40.1529	39.8422	39.5231	39.1950	38.8559	38.5074	38.1486	37.7805	37.4020	37.0138	36.6150	36.2068
100.0	40.5961	40.3036	39.9979	39.6842	39.3622	39.0293	38.6877	38.3360	37.9755	37.6050	37.2254	36.8359	36.4374
105.0	40.7397	40.4511	40.1504	39.8418	39.5254	39.1984	38.8633	38.5183	38.1649	37.8020	37.4304	37.0495	36.6601
110.0		40.5956	40.2996	39.9960	39.6849	39.3635	39.0345	38.6959	38.3491	37.9933	37.6292	37.2565	36.8755
115.0		40.7372	40.4458	40.1470	39.8409	39.5248	39.2016	38.8689	38.5286	38.1794	37.8224	37.4572	37.0842
120.0		40.8760	40.5892	40.2949	39.9936	39.6826	39.3648	39.0379	38.7034	38.3607	38.0102	37.6523	37.2867
125.0		41.0122	40.7298	40.4399	40.1431	39.8370	39.5243	39.2028	38.8741	38.5373	38.1932	37.8419	37.4834
130.0		41.1458	40.8679	40.5822	40.2896	39.9881	39.6804	39.3640	39.0407	38.7096	38.3714	38.0266	37.6746
135.0		41.2770	41.0034	40.7218	40.4332	40.1363	39.8331	39.5217	39.2035	38.8778	38.5453	38.2065	37.8608
140.0		41.4058	41.1366	40.8589	40.5742	40.2815	39.9827	39.6760	39.3627	39.0423	38.7151	38.3820	38.0422
145.0			41.2675	40.9935	40.7125	40.4240	40.1294	39.8272	39.5186	39.2030	38.8810	38.5533	38.2192
150.0			41.3963	41.1258	40.8483	40.5638	40.2732	39.9753	39.6712	39.3604	39.0432	38.7207	38.3920
155.0			41.5230	41.2559	40.9818	40.7011	40.4143	40.1206	39.8207	39.5144	39.2020	38.8844	38.5608
160.0			41.6476	41.3838	41.1130	40.8361	40.5528	40.2631	39.9673	39.6654	39.3574	39.0445	38.7258
165.0			41.7703	41.5096	41.2420	40.9687	40.6888	40.4029	40.1111	39.8134	39.5097	39.2013	38.8872
170.0			41.8912	41.6335	41.3690	41.0991	40.8225	40.5403	40.2523	39.9586	39.6590	39.3549	39.0453
175.0			42.0103	41.7553	41.4939	41.2274	40.9539	40.6753	40.3909	40.1011	39.8055	39.5055	39.2002
180.0			42.1277	41.8753	41.6169	41.3536	41.0832	40.8080	40.5271	40.2411	39.9493	39.6532	39.3520
185.0				41.9934	41.7381	41.4779	41.2104	40.9384	40.6610	40.3786	40.0904	39.7981	39.5009
190.0				42.1098	41.8575	41.6003	41.3356	41.0668	40.7926	40.5137	40.2291	39.9404	39.6470
195.0				42.2244	41.9751	41.7208	41.4589	41.1931	40.9221	40.6465	40.3654	40.0802	39.7904
200.0				42.3373	42.0911	41.8396	41.5803	41.3175	41.0496	40.7772	40.4994	40.2176	39.9313
210.0				42.5583	42.3184	42.0721	41.8179	41.5607	41.2986	41.0324	40.7609	40.4854	40.2059
220.0				42.7730	42.5396	42.2982	42.0489	41.7969	41.5403	41.2799	41.0143	40.7447	40.4715
230.0					42.7553	42.5183	42.2738	42.0267	41.7752	41.5203	41.2602	40.9961	40.7288
240.0					42.9658	42.7328	42.4929	42.2504	42.0038	41.7539	41.4990	41.2402	40.9784
250.0					43.1713	42.9420	42.7067	42.4685	42.2265	41.9813	41.7314	41.4774	41.2208
260.0					43.3722	43.1461	42.9155	42.6814	42.4436	42.2028	41.9577	41.7083	41.4566
270.0						43.3454	43.1196	42.8893	42.6556	42.4189	42.1782	41.9332	41.6861
280.0						43.5401	43.3193	43.0926	42.8627	42.6298	42.3933	42.1525	41.9098
290.0						43.7306	43.5148	43.2916	43.0653	42.8358	42.6034	42.3666	42.1280
300.0						43.9168	43.7064	43.4865	43.2635	43.0373	42.8086	42.5757	42.3411
310.0						44.0992	43.8943	43.6776	43.4578	43.2344	43.0094	42.7801	42.5492
320.0							44.0787	43.8651	43.6481	43.4274	43.2058	42.9802	42.7528
330.0							44.2597	44.0492	43.8349	43.6165	43.3982	43.1760	42.9520
340.0							44.4377	44.2302	44.0183	43.8019	43.5867	43.3680	43.1470
350.0							44.6126	44.4081	44.1984	43.9837	43.7716	43.5561	43.3382

Table 3. Densities in g mol/cc x 10^3, at Integral Pressures and Temperatures - Continued

PRESSURE ATM	TEMPERATURE DEGREES K												
	30.000	31.000	32.000	33.000	34.000	35.000	36.000	37.000	38.000	39.000	40.000	42.000	44.000
1.0	.4204	.4057	.3920	.3792	.3673	.3561	.3457	.3358	.3265	.3177	.3094	.2941	.2803
2.0	.8729	.8395	.8086	.7802	.7538	.7294	.7066	.6853	.6654	.6466	.6289	.5965	.5674
3.0	1.3650	1.3069	1.2543	1.2064	1.1624	1.1221	1.0847	1.0500	1.0177	.9875	.9592	.9076	.8618
4.0	1.9074	1.8159	1.7348	1.6623	1.5965	1.5367	1.4819	1.4314	1.3848	1.3415	1.3011	1.2281	1.1637
5.0	2.5165	2.3779	2.2583	2.1537	2.0604	1.9766	1.9008	1.8317	1.7683	1.7099	1.6557	1.5586	1.4736
6.0	3.2208	3.0107	2.8367	2.6885	2.5598	2.4460	2.3445	2.2530	2.1699	2.0939	2.0241	1.8998	1.7919
7.0	4.0764	3.7447	3.4880	3.2786	3.1026	2.9503	2.8169	2.6983	2.5917	2.4953	2.4074	2.2523	2.1192
8.0	5.2291	4.6396	4.2423	3.9413	3.6996	3.4966	3.3228	3.1710	3.0364	2.9159	2.8071	2.6171	2.4558
9.0	27.1088	5.8469	5.1568	4.7053	4.3666	4.0947	3.8687	3.6754	3.5068	3.3578	3.2247	2.9950	2.8023
10.0	27.4623	25.4290	6.3695	5.6218	5.1284	4.7587	4.4631	4.2170	4.0068	3.8237	3.6620	3.3869	3.1593
11.0	27.7759	25.9797	8.4901	6.8014	6.0275	5.5091	5.1173	4.8028	4.5408	4.3166	4.1213	3.7940	3.5274
12.0	28.0591	26.4298	23.9583	8.5927	7.1458	6.3786	5.8477	5.4419	5.1143	4.8400	4.6047	4.2174	3.9071
13.0	28.3183	26.8151	24.7272	19.7426	8.6788	7.4227	6.6778	6.1463	5.7342	5.3982	5.1152	4.6584	4.2993
14.0	28.5580	27.1546	25.3100	22.2921	11.3328	8.7465	7.6434	6.9323	6.4092	5.9962	5.6558	5.1185	4.7044
15.0	28.7813	27.4597	25.7879	23.3835	17.6605	10.5749	8.8006	7.8222	7.1501	6.6399	6.2301	5.5990	5.1232
16.0	28.9907	27.7378	26.1972	24.1344	20.6298	13.3863	10.2381	8.8457	7.9698	7.3361	6.8421	6.1017	5.5564
17.0	29.1883	27.9940	26.5576	24.7211	22.0056	16.9414	12.0760	10.0406	8.8841	8.0925	7.4959	6.6279	6.0047
18.0	29.3754	28.2322	26.8810	25.2090	22.9256	19.3244	14.3387	11.4443	9.9092	8.9169	8.1959	7.1793	6.4686
19.0	29.5534	28.4551	27.1754	25.6299	23.6276	20.7778	16.6267	13.0600	11.0572	9.8161	8.9459	7.7572	6.9486
20.0	29.7233	28.6648	27.4463	26.0021	24.2007	21.7969	18.4487	14.7932	12.3248	10.7936	9.7482	8.3626	7.4452
22.0	30.0420	29.0516	27.9327	26.6427	25.1135	23.2218	20.8204	17.8783	15.0425	12.9522	11.5051	9.6564	8.4882
24.0	30.3367	29.4026	28.3622	27.1856	25.8357	24.2362	22.3172	20.0189	17.4958	15.1974	13.4046	11.0513	9.5954
26.0	30.6115	29.7250	28.7484	27.6598	26.4387	25.0320	23.4021	21.5099	19.3861	17.2258	15.2981	12.5153	10.7573
28.0	30.8693	30.0238	29.1004	28.0828	26.9596	25.6912	24.2558	22.6293	20.8142	18.8921	17.0232	13.9928	11.9558
30.0	31.1125	30.3027	29.4247	28.4659	27.4200	26.2569	24.9623	23.5219	21.9318	20.2292	18.5020	15.4187	13.1645
32.0	31.3429	30.5646	29.7258	28.8168	27.8340	26.7541	25.5672	24.2645	22.8417	21.3175	19.7419	16.7402	14.3523
34.0	31.5621	30.8119	30.0074	29.1411	28.2111	27.1991	26.0976	24.9014	23.6071	22.2247	20.7847	17.9306	15.4908
36.0	31.7714	31.0463	30.2721	29.4432	28.5580	27.6026	26.5709	25.4600	24.2672	22.9985	21.6736	18.9871	16.5592
38.0	31.9716	31.2693	30.5223	29.7263	28.8798	27.9725	26.9991	25.9582	24.8479	23.6718	22.4432	19.9207	17.5466
40.0	32.1638	31.4822	30.7596	29.9929	29.1803	28.3145	27.3906	26.4085	25.3665	24.2672	23.1198	20.7481	18.4510
42.0	32.3487	31.6860	30.9855	30.2450	29.4626	28.6330	27.7522	26.8199	25.8357	24.8010	23.7223	21.4856	19.2758
44.0	32.5268	31.8815	31.2013	30.4845	29.7289	28.9314	28.0881	27.1991	26.2643	25.2848	24.2652	22.1481	20.0278
46.0	32.6989	32.0696	31.4079	30.7126	29.9812	29.2123	28.4021	27.5510	26.6592	25.7274	24.7589	22.7476	20.7146
48.0	32.8653	32.2509	31.6062	30.9306	30.2212	29.4779	28.6972	27.8797	27.0255	26.1355	25.2119	23.2942	21.3439
50.0	33.0264	32.4259	31.7969	31.1394	30.4500	29.7299	28.9759	28.1882	27.3675	26.5143	25.6302	23.7959	21.9228
55.0	33.4090	32.8390	32.2448	31.6265	30.9808	30.3102	29.6123	28.8872	28.1356	27.3583	26.5556	24.8938	23.1888
60.0	33.7661	33.2223	32.6575	32.0719	31.4624	30.8322	30.1794	29.5041	28.8068	28.0886	27.3494	25.8222	24.2536
65.0	34.1014	33.5804	33.0408	32.4831	31.9043	31.3078	30.6924	30.0578	29.4046	28.7340	28.0457	26.6267	25.1697
70.0	34.4181	33.9169	33.3994	32.8656	32.3135	31.7456	31.1617	30.5613	29.9447	29.3134	28.6671	27.3370	25.9725
75.0	34.7183	34.2347	33.7366	33.2238	32.6950	32.1520	31.5951	31.0238	30.4382	29.8401	29.2291	27.9736	26.6869

Table 3. Densities in g mol/cc x 10^3, at Integral Pressures and Temperatures - Continued

PRESSURE ATM	TEMPERATURE DEGREES K												
	30.000	31.000	32.000	33.000	34.000	35.000	36.000	37.000	38.000	39.000	40.000	42.000	44.000
80.0	35.0040	34.5361	34.0554	33.5610	33.0529	32.5317	31.9983	31.4522	30.8933	30.3236	29.7428	28.5510	27.3305
85.0	35.2767	34.8231	34.3579	33.8801	33.3904	32.8885	32.3757	31.8517	31.3161	30.7711	30.2164	29.0797	27.9165
90.0	35.5379	35.0972	34.6461	34.1832	33.7100	33.2253	32.7310	32.2265	31.7115	31.1881	30.6562	29.5678	28.4547
95.0	35.7886	35.3597	34.9214	34.4720	34.0139	33.5447	33.0668	32.5798	32.0831	31.5789	31.0672	30.0214	28.9525
100.0	36.0298	35.6118	35.1852	34.7482	34.3036	33.8486	33.3855	32.9142	32.4339	31.9470	31.4533	30.4455	29.4160
105.0	36.2623	35.8544	35.4386	35.0129	34.5808	34.1386	33.6890	33.2320	32.7665	32.2951	31.8176	30.8439	29.8497
110.0	36.4869	36.0883	35.6825	35.2673	34.8466	34.4162	33.9789	33.5348	33.0830	32.6257	32.1626	31.2198	30.2577
115.0	36.7040	36.3142	35.9177	35.5122	35.1020	34.6826	34.2566	33.8244	33.3849	32.9405	32.4907	31.5759	30.6429
120.0	36.9144	36.5328	36.1449	35.7485	35.3480	34.9387	34.5231	34.1019	33.6738	33.2411	32.8035	31.9143	31.0079
125.0	37.1185	36.7447	36.3649	35.9772	35.5854	35.1855	34.7795	34.3684	33.9509	33.5291	33.1025	32.2369	31.3550
130.0	37.3167	36.9502	36.5780	36.1983	35.8148	35.4236	35.0267	34.6250	34.2172	33.8055	33.3892	32.5452	31.6860
135.0	37.5095	37.1499	36.7849	36.4127	36.0369	35.6539	35.2654	34.8724	34.4738	34.0714	33.6645	32.8406	32.0024
140.0	37.6971	37.3441	36.9859	36.6209	36.2521	35.8769	35.4962	35.1114	34.7213	34.3276	33.9296	33.1243	32.3056
145.0	37.8800	37.5332	37.1814	36.8231	36.4611	36.0931	35.7198	35.3426	34.9605	34.5749	34.1852	33.3972	32.5967
150.0	38.0583	37.7175	37.3717	37.0200	36.6642	36.3030	35.9367	35.5566	35.1920	34.8140	34.4320	33.6603	32.8769
155.0	38.2323	37.8972	37.5573	37.2115	36.8617	36.5069	36.1472	35.7839	35.4164	35.0456	34.6709	33.9143	33.1469
160.0	38.4024	38.0727	37.7383	37.3982	37.0541	36.7054	36.3519	35.9950	35.6342	35.2701	34.9022	34.1600	33.4076
165.0	38.5686	38.2441	37.9150	37.5804	37.2416	36.8987	36.5511	36.2003	35.8458	35.4881	35.1267	34.3979	33.6596
170.0	38.7312	38.4118	38.0876	37.7583	37.4245	37.0871	36.7452	36.4001	36.0516	35.6999	35.3446	34.6285	33.9036
175.0	38.8904	38.5758	38.2564	37.9320	37.6032	37.2710	36.9344	36.5948	36.2519	35.9059	35.5565	34.8524	34.1402
180.0	39.0464	38.7363	38.4216	38.1019	37.7777	37.4505	37.1191	36.7846	36.4472	36.1066	35.7628	35.0700	34.3698
185.0	39.1993	38.8936	38.5833	38.2681	37.9484	37.6259	37.2994	36.9599	36.6376	36.3022	35.9637	35.2818	34.5929
190.0	39.3492	39.0478	38.7417	38.4309	38.1154	37.7975	37.4756	37.1509	36.8235	36.4930	36.1596	35.4880	34.8099
195.0	39.4964	39.1990	38.8970	38.5903	38.2790	37.9653	37.6480	37.3278	37.0052	36.6794	36.3508	35.6890	35.0211
200.0	39.6408	39.3473	39.0493	38.7467	38.4392	38.1297	37.8167	37.5008	37.1827	36.8614	36.5376	35.8850	35.2270
210.0	39.9221	39.6360	39.3453	39.0501	38.7503	38.4487	38.1438	37.8361	37.5264	37.2136	36.8986	36.2636	35.6237
220.0	40.1940	39.9146	39.6307	39.3426	39.0499	38.7555	38.4582	38.1580	37.8562	37.5511	37.2443	36.6254	36.0022
230.0	40.4572	40.1840	39.9065	39.6245	39.3389	39.0512	38.7610	38.4679	38.1733	37.8753	37.5762	36.9723	36.3643
240.0	40.7124	40.4449	40.1733	39.8974	39.6182	39.3368	39.0531	38.7666	38.4787	38.1875	37.8955	37.3055	36.7115
250.0	40.9602	40.6978	40.4318	40.1617	39.8885	39.6130	39.3355	39.0551	38.7735	38.4886	38.2032	37.6262	37.0452
260.0	41.2010	40.9435	40.6826	40.4177	40.1505	39.8805	39.6088	39.3342	39.0585	38.7795	38.5002	37.9355	37.3666
270.0	41.4353	41.1823	40.9262	40.6664	40.4047	40.1399	39.8736	39.6046	39.3343	39.0609	38.7873	38.2342	37.6767
280.0	41.6637	41.4147	41.1632	40.9084	40.6517	40.3919	40.1306	39.8668	39.6017	39.3336	39.0653	38.5232	37.9763
290.0	41.8863	41.6413	41.3940	41.1434	40.8919	40.6368	40.3802	40.1214	39.8612	39.5981	39.3346	38.8030	38.2663
300.0	42.1036	41.8623	41.6191	41.3728	41.1257	40.8752	40.6230	40.3689	40.1133	39.8551	39.5959	39.0743	38.5473
310.0	42.3159	42.0783	41.8388	41.5970	41.3536	41.1074	40.8593	40.6097	40.3585	40.1049	39.8496	39.3376	38.8199
320.0	42.5235	42.2894	42.0537	41.8154	41.5758	41.3337	41.0894	40.8442	40.5971	40.3481	40.0960	39.5934	39.0848
330.0	42.7265	42.4962	42.2639	42.0294	41.7927	41.5546	41.3138	41.0728	40.8297	40.5850	40.3357	39.8420	39.3424
340.0	42.9253	42.6989	42.4701	42.2384	42.0046	41.7703	41.5327	41.2957	41.0564	40.8160	40.5689	40.0838	39.5931
350.0	43.1201	42.8978	42.6724	42.4436	42.2116	41.9811	41.7464	41.5132	41.2776	41.0414	40.7960	40.3192	39.8375

Table 3. Densities in g mol/cc x 10^3, at Integral Pressures and Temperatures - Continued

PRESSURE ATM	TEMPERATURE DEGREES K											
	46.000	48.000	50.000	55.000	60.000	65.000	70.000	75.000	80.000	85.000	90.000	95.000	100.000
1.0	.2677	.2562	.2457	.2229	.2041	.1881	.1746	.1628	.1526	.1435	.1355	.1283	.1219
2.0	.5412	.5173	.4955	.4486	.4100	.3776	.3500	.3263	.3056	.2873	.2712	.2568	.2439
3.0	.8206	.7834	.7496	.6771	.6178	.5683	.5264	.4904	.4590	.4315	.4071	.3854	.3659
4.0	1.1062	1.0546	1.0079	.9083	.8275	.7604	.7037	.6551	.6129	.5759	.5432	.5141	.4880
5.0	1.3984	1.3312	1.2706	1.1424	1.0392	.9537	.8818	.8204	.7672	.7205	.6794	.6429	.6101
6.0	1.6973	1.6132	1.5378	1.3794	1.2527	1.1483	1.0608	.9863	.9218	.8655	.8158	.7717	.7323
7.0	2.0032	1.9010	1.8097	1.6193	1.4681	1.3442	1.2407	1.1528	1.0769	1.0107	.9524	.9007	.8545
8.0	2.3166	2.1946	2.0864	1.8621	1.6853	1.5413	1.4214	1.3199	1.2324	1.1561	1.0891	1.0298	.9767
9.0	2.6376	2.4943	2.3679	2.1078	1.9045	1.7396	1.6029	1.4875	1.3882	1.3018	1.2259	1.1589	1.0990
10.0	2.9666	2.8002	2.6544	2.3566	2.1255	1.9392	1.7852	1.6556	1.5443	1.4477	1.3629	1.2880	1.2213
11.0	3.3040	3.1126	2.9460	2.6083	2.3484	2.1399	1.9683	1.8242	1.7008	1.5938	1.5000	1.4173	1.3435
12.0	3.6500	3.4317	3.2428	2.8630	2.5731	2.3418	2.1521	1.9934	1.8576	1.7400	1.6372	1.5465	1.4658
13.0	4.0051	3.7576	3.5449	3.1207	2.7997	2.5449	2.3368	2.1630	2.0147	1.8865	1.7745	1.6759	1.5881
14.0	4.3696	4.0905	3.8524	3.3815	3.0281	2.7491	2.5221	2.3331	2.1721	2.0332	1.9119	1.8052	1.7104
15.0	4.7437	4.4306	4.1654	3.6453	3.2582	2.9545	2.7082	2.5036	2.3297	2.1800	2.0494	1.9346	1.8326
16.0	5.1280	4.7781	4.4839	3.9121	3.4902	3.1609	2.8949	2.6745	2.4877	2.3269	2.1869	2.0639	1.9549
17.0	5.5225	5.1330	4.8080	4.1820	3.7239	3.3684	3.0823	2.8459	2.6458	2.4740	2.3245	2.1933	2.0770
18.0	5.9277	5.4955	5.1377	4.4548	3.9594	3.5769	3.2703	3.0176	2.8042	2.6212	2.4622	2.3227	2.1992
19.0	6.3437	5.8657	5.4731	4.7305	4.1965	3.7865	3.4590	3.1897	2.9628	2.7686	2.5998	2.4521	2.3213
20.0	6.7706	6.2435	5.8141	5.0092	4.4353	3.9970	3.6482	3.3622	3.1216	2.9160	2.7376	2.5814	2.4434
22.0	7.6572	7.0221	6.5127	5.5750	4.9176	4.4208	4.0283	3.7081	3.4398	3.2111	3.0130	2.8400	2.6873
24.0	8.5863	7.8304	7.2328	6.1516	5.4059	4.8481	4.4105	4.0551	3.7585	3.5064	3.2885	3.0984	2.9310
26.0	9.5540	8.6659	7.9728	6.7382	5.8997	5.2785	4.7944	4.4031	4.0777	3.8019	3.5639	3.3566	3.1743
28.0	10.5526	9.5248	8.7304	7.3338	6.3984	5.7116	5.1799	4.7519	4.3972	4.0973	3.8391	3.6145	3.4173
30.0	11.5709	10.4015	9.5022	7.9370	6.9013	6.1471	5.5666	5.1013	4.7169	4.3927	4.1140	3.8720	3.6598
32.0	12.5944	11.2884	10.2841	8.5464	7.4077	6.5845	5.9542	5.4511	5.0366	4.6879	4.3886	4.1291	3.9018
34.0	13.6067	12.1768	11.0710	9.1602	7.9167	7.0233	6.3426	5.8011	5.3563	4.9827	4.6627	4.3858	4.1433
36.0	14.5921	13.0573	11.8573	9.7765	8.4275	7.4631	6.7313	6.1511	5.6756	5.2772	4.9364	4.6418	4.3842
38.0	15.5373	13.9208	12.6372	10.3932	8.9391	7.9034	7.1201	6.5009	5.9946	5.5711	5.2095	4.8973	4.6245
40.0	16.4331	14.7590	13.4048	11.0080	9.4504	8.3435	7.5086	6.8503	6.3131	5.8645	5.4819	5.1520	4.8641
42.0	17.2745	15.5656	14.1550	11.6189	9.9605	8.7829	7.8964	7.1991	6.6309	6.1570	5.7535	5.4061	5.1030
44.0	18.0600	16.3359	14.8834	12.2235	10.4683	9.2211	8.2833	7.5470	6.9478	6.4488	6.0244	5.6594	5.3411
46.0	18.7910	17.0675	15.5865	12.8199	10.9727	9.6575	8.6690	7.8938	7.2638	6.7396	6.2943	5.9118	5.5784
48.0	19.4702	17.7594	16.2619	13.4062	11.4728	10.0915	9.0530	8.2394	7.5786	7.0294	6.5633	6.1633	5.8149
50.0	20.1017	18.4123	16.9084	13.9807	11.9676	10.5226	9.4351	8.5834	7.8922	7.3180	6.8313	6.4138	6.0504
55.0	21.4977	19.8833	18.3961	15.3568	13.1757	11.5841	10.3796	9.4355	8.6696	8.0340	7.4962	7.0357	6.6351
60.0	22.6808	21.1521	19.7093	16.6368	14.3336	12.6167	11.3051	10.2738	9.4361	8.7408	8.1531	7.6504	7.2134
65.0	23.7000	22.2549	20.8681	17.8158	15.4333	13.6140	12.2075	11.0953	10.1897	9.4372	8.8011	8.2573	7.7846
70.0	24.5917	23.2238	21.8956	18.8963	16.4704	14.5717	13.0834	11.8976	10.9287	10.1219	9.4394	8.8556	8.3483
75.0	25.3827	24.0842	22.8132	19.8850	17.4437	15.4868	13.9300	12.6788	11.6516	10.7939	10.0671	9.4449	8.9039

Table 3. Densities in g mol/cc x 10^3, at Integral Pressures and Temperatures - Continued

PRESSURE ATM	TEMPERATURE DEGREES K												
	46.000	48.000	50.000	55.000	60.000	65.000	70.000	75.000	80.000	85.000	90.000	95.000	100.000
80.0	26.0930	24.8564	23.6390	20.7904	18.3545	16.3581	14.7458	13.4372	12.3572	11.4521	10.6835	10.0244	9.4512
85.0	26.7372	25.5557	24.3879	21.6217	19.2057	17.1856	15.5296	14.1719	13.0446	12.0959	11.2881	10.5939	9.9897
90.0	27.3266	26.1944	25.0719	22.3875	20.0014	17.9702	16.2813	14.8821	13.7130	12.7247	11.8803	11.1529	10.5192
95.0	27.8699	26.7818	25.7007	23.0956	20.7457	18.7136	17.0010	15.5677	14.3620	13.3379	12.4598	11.7011	11.0394
100.0	28.3740	27.3256	26.2823	23.7529	21.4431	19.4177	17.6895	16.2287	14.9914	13.9353	13.0262	12.2383	11.5501
105.0	28.8443	27.8319	26.8231	24.3654	22.0976	20.0850	18.3478	16.8654	15.6013	14.5167	13.5794	12.7643	12.0511
110.0	29.2852	28.3055	27.3284	24.9383	22.7134	20.7178	18.9771	17.4785	16.1917	15.0821	14.1192	13.2790	12.5425
115.0	29.7004	28.7505	27.8025	25.4760	23.2939	21.3185	19.5788	18.0685	16.7631	15.6316	14.6457	13.7825	13.0241
120.0	30.0928	29.1704	28.2490	25.9823	23.8425	21.8894	20.1544	18.6364	17.3158	16.1653	15.1588	14.2745	13.4958
125.0	30.4650	29.5678	28.6711	26.4605	24.3620	22.4327	20.7053	19.1830	17.8503	16.6836	15.6587	14.7554	13.9579
130.0	30.8191	29.9452	29.0714	26.9135	24.8550	22.9504	21.2329	19.7092	18.3673	17.1867	16.1456	15.2251	14.4102
135.0	31.1569	30.3045	29.4521	27.3437	25.3240	23.4445	21.7387	20.2160	18.8672	17.6750	16.6197	15.6838	14.8529
140.0	31.4799	30.6477	29.8150	27.7532	25.7708	23.9167	22.2239	20.7043	19.3509	18.1490	17.0814	16.1317	15.2862
145.0	31.7895	30.9760	30.1618	28.1439	26.1975	24.3686	22.6900	21.1751	19.8189	18.6092	17.5308	16.5690	15.7101
150.0	32.0868	31.2909	30.4940	28.5175	26.6056	24.8017	23.1379	21.6292	20.2718	19.0560	17.9684	16.9958	16.1248
155.0	32.3729	31.5934	30.8128	28.8754	26.9966	25.2173	23.5690	22.0676	20.7104	19.4898	18.3945	17.4125	16.5304
160.0	32.6487	31.8847	31.1193	29.2188	27.3718	25.6167	23.9842	22.4909	21.1353	19.9113	18.8094	17.8193	16.9272
165.0	32.9149	32.1655	31.4145	29.5490	27.7325	26.0010	24.3844	22.9001	21.5471	20.3209	19.2136	18.2164	17.3154
170.0	33.1723	32.4366	31.6992	29.8669	28.0795	26.3711	24.7707	23.2959	21.9464	20.7190	19.6074	18.6042	17.6952
175.0	33.4215	32.6989	31.9742	30.1734	28.4141	26.7281	25.1439	23.6790	22.3338	21.1061	19.9911	18.9828	18.0667
180.0	33.6631	32.9527	32.2403	30.4693	28.7368	27.0728	25.5046	24.0501	22.7098	21.4828	20.3652	19.3526	18.4302
185.0	33.8975	33.1989	32.4980	30.7554	29.0487	27.4059	25.8537	24.4097	23.0750	21.8493	20.7301	19.7138	18.7859
190.0	34.1253	33.4377	32.7478	31.0323	29.3504	27.7282	26.1919	24.7586	23.4298	22.2063	21.0859	20.0668	19.1340
195.0	34.3468	33.6698	32.9904	31.3007	29.6424	28.0404	26.5197	25.0972	23.7748	22.5539	21.4332	20.4117	19.4747
200.0	34.5624	33.8955	33.2261	31.5610	29.9256	28.3430	26.8377	25.4260	24.1105	22.8927	21.7721	20.7489	19.8083
210.0	34.9774	34.3293	33.6785	32.0594	30.4670	28.9216	27.4464	26.0565	24.7553	23.5453	22.4264	21.4010	20.4549
220.0	35.3726	34.7418	34.1081	32.5312	30.9785	29.4682	28.0219	26.6535	25.3674	24.1665	23.0512	22.0251	21.0753
230.0	35.7502	35.1351	34.5172	32.9791	31.4632	29.9860	28.5675	27.2203	25.9497	24.7591	23.6486	22.6230	21.6712
240.0	36.1117	35.5113	34.9080	33.4057	31.9241	30.4780	29.0861	27.7596	26.5047	25.3251	24.2207	23.1965	22.2440
250.0	36.4588	35.8719	35.2822	33.8131	32.3634	30.9467	29.5802	28.2738	27.0347	25.8666	24.7690	23.7473	22.7952
260.0	36.7927	36.2183	35.6413	34.2032	32.7833	31.3941	30.0519	28.7652	27.5417	26.3854	25.2954	24.2768	23.3261
270.0	37.1146	36.5518	35.9867	34.5775	33.1854	31.8224	30.5032	29.2356	28.0275	26.8831	25.8012	24.7865	23.8380
280.0	37.4254	36.8734	36.3195	34.9375	33.5715	32.2330	30.9358	29.6867	28.4938	27.3611	26.2878	25.2776	24.3320
290.0	37.7260	37.1842	36.6409	35.2844	33.9428	32.6275	31.3512	30.1202	28.9420	27.8208	26.7563	25.7514	24.8091
300.0	38.0171	37.4848	36.9515	35.6192	34.3007	33.0073	31.7507	30.5372	29.3734	28.2634	27.2079	26.2089	25.2704
310.0	38.2995	37.7761	37.2524	35.9430	34.6462	33.3733	32.1355	30.9392	29.7893	28.6899	27.6435	26.6511	25.7168
320.0	38.5738	38.0587	37.5441	36.2565	34.9803	33.7268	32.5067	31.3270	30.1906	29.1013	28.0640	27.0790	26.1492
330.0	38.8404	38.3332	37.8273	36.5607	35.3039	34.0686	32.8652	31.7019	30.5785	29.4985	28.4702	27.4934	26.5684
340.0	39.1000	38.6002	38.1027	36.8561	35.6178	34.3996	33.2120	32.0646	30.9537	29.8823	28.8629	27.8951	26.9751
350.0	39.3529	38.8601	38.3706	37.1433	35.9227	34.7206	33.5477	32.4159	31.3170	30.2534	29.2428	28.2849	27.3699

The self-consistency of a thermodynamic network is under investigation, using numerical methods of computation with the present data in conjunction with spectroscopic [1] and calorimetric [20, 21] specific heats.

Thomas R. Strobridge kindly gave to us his computer program [22] of the least-squares method of William B. Jones [19]. Among present authors, the preparation, examination, and interpolation of isotherm polynomials was carried through by L. A. Weber and H. M. Roder. R. J. Corruccini and R. B. Scott have given encouragement throughout this lengthy investigation.

4. References

[1] H. W. Woolley, R. B. Scott, and F. G. Brickwedde, J. Research NBS **41,** 379 (1948).
[2] H. L. Johnston and D. White, Trans. ASME **72** (6), 785 (1950).
[3] H. L. Johnston, W. F. Keller, and A. S. Friedman, J. Am. Chem. Soc. **76,** 1482 (1954).
[4] A. Michels, W. deGraff, T. Wassenaar, J. M. Levelt, and P. Louwerse, Physica **25,** 25 (1959).
[5] A. van Itterbeek and O. Verbeke, Cryogenics **2** (1), 21 (Sept. 1961).
[6] J. J. M. Beenakker, F. H. Varekamp, and H. F. P. Knapp, Physica **26,** 43 (1960).
[7] R. D. Goodwin, J. Research NBS **65C** (Engr. and Instr.) No. 4, 231 (1961).
[8] L. A. Weber, D. E. Diller, H. M. Roder, and R. D. Goodwin, Cryogenics, **2** (4), 236 (June 1962).
[9] R. D. Goodwin, D. E. Diller, H. M. Roder, and L. A. Weber, Cryogenics **2** (2), 81 (Dec. 1961).
[10] H. M. Roder, D. E. Diller, L. A. Weber, and R. D. Goodwin (On orthobaric densities, critical consts. and heats of vaporization) Cryogenics (March 1963).
[11] R. D. Goodwin, Melting pressure equation for the hydrogens, Cryogenics **2** (6), 353 (Dec. 1962).
[12] R. D. Goodwin and H. M. Roder, Pressure-density-temperature relations of freezing liquid parahydrogen to 350 Atmospheres, Cryogenics (March 1963).
[13] H. M. Roder and R. D. Goodwin, NBS Tech. Note 130 (1962).
[14] J. C. Mullins, W. T. Ziegler, and B. S. Kirk, Tech. Rpt. No. 1. Proj. No. A–593, Eng. Expt. Sta., Georgia Institute of Technology, Atlanta, Nov. 1, 1961.
[15] Joseph Hilsenrath et al., NBS Circular 564 (1955).
[16] H. J. Hoge and F. G. Brickwedde, J. Research NBS **22,** 351 (1939).
[17] H. F. Stimson, J. Research NBS **65A** (Phys. and Chem.) No. 3, 139 (1961).
[18] A. Michels, J. C. Abels, C. A. Ten Seldam, and W. deGraff, Physica **26,** 381 (1960).
[19] Wm. B. Jones and R. M. Gallet, J. Research NBS **66D** (Radio Prop.) No. 4 (July–Aug. 1962).
[20] B. A. Younglove and D. E. Diller, The specific heat of saturated liquid parahydrogen from 15° to 32° K, Cryogenics **2** (5), 283 (Sept. 1962).
[21] B. A. Younglove and D. E. Diller, The specific heat at constant volume of parahydrogen at temperatures from 15° to 90° K and pressures to 340 atmospheres, Cryogenics **2** (6), 348 (Dec. 1962).
[22] Thomas R. Strobridge, NBS Technical Note 129, PB161630, January (1962).

(Paper 67A2–204)

JOURNAL OF RESEARCH of the National Bureau of Standards—A. Physics and Chemistry
Vol. 67A, No. 2, March–April 1963

A Method for Determining the Elastic Constants of a Cubic Crystal from Velocity Measurements in a Single Arbitrary Direction; Application to $SrTiO_3$

J. B. Wachtman, Jr., M. L. Wheat,* and S. Marzullo

(December 11, 1962)

Three independent velocities of sound can be measured along any direction of propagation in a cubic crystal except the [100] and [111] directions. These three velocities suffice to determine the three elastic constants and for the [110] direction, the calculation of these constants is easy. For all other directions, the calculation is more difficult; the only existing method appears to be a perturbation technique developed by Neighbours.

The present paper presents a method using exact equations and an iterative procedure to solve these equations and to calculate both the elastic constants and their standard deviations from the sound velocities and their standard deviations. The method is illustrated with new data on $SrTiO_3$ which give $c_{11}=3.156\pm0.027$, $c_{12}=1.027\pm0.027$, $c_{44}=1.215\pm0.006\times10^{12}$ dynes/cm² at 25 °C. The importance of including covariance terms in calculations of the standard deviations is emphasized.

1. Introduction

The determination of the elastic constants of single crystals from measurements of the velocity of sound is an extensive and active field of research and several survey papers exist [*1*, *2*, *3*, *4*].[1] For any direction in a single crystal three types of sound wave may be propagated: one quasi-longitudinal and two quasi-transverse waves. The three corresponding velocities are the roots of a cubic equation, sometimes called Christoffel's equation, whose coefficients are complicated functions of the elastic constants and the direction cosines for the direction of propagation of the sound. In the case of a cubic crystal, there are only three independent elastic constants so that velocity measurements in a single direction suffice to completely determine the elastic constants provided that no two velocities are required to be equal by crystal symmetry. Such equality is required for the [100] and [111] directions so that measurements in one of these directions alone do not provide sufficient information to determine the three elastic constants. It may happen that for some other direction two of the velocities are equal; the three velocities are still independent quantities, however, and measurements in such a direction would provide sufficient information to calculate the three elastic constants. We assume that the three velocities v_1, v_2, v_3, and their standard deviations σ_1, σ_2, σ_3, have been measured for some direction which is specified by direction cosines l, m, n and which does not coincide with or closely neighbor [100] or [111]. We seek to calculate the three independent elastic constants c_{11}, c_{12}, c_{44} and their standard deviations σ_{11}, σ_{12}, σ_{44}. The theory leads to a sixth degree algebraic equation of which c_{11} must be a root. It may occur that more than one of the roots of this equation are of reasonable magnitude so that some test is needed to distinguish which of the roots is c_{11}. The direction of polarization of the quasi-transverse waves provides such a test and we therefore assume that the orientation of the transducer exciting each of the two quasi-transverse waves was also determined.

One would usually prefer to use the [110] direction for which the calculations are easy and well known and for which the present method is unnecessary. However, single crystals of many substances are available only in very limited sizes and shapes and it may occur that the only available crystals do not permit measurement along [110]. Also, even if [110] is accessible for measurement, it may be desired to check the results by measurements in other directions.

---

*Now at the University of Kansas, Lawrence, Kans.

[1] Italicized figures in brackets indicate the literature references at the end of this paper.

Neighbours and his collaborators [5, 6, 7], following a beginning by Ahrenberg [8], have developed an approximation method for calculating elastic constants from wave velocities and have applied it to the case of cubic crystals as well as several other crystal systems. In Neighbours' method, the equations relating the velocities and the elastic constants are expanded into infinite series. The first term of each equation is a simple linear combination of elastic constants and the first step in his self-consistent calculation is to solve for the elastic constants ignoring all other terms. The values so obtained are used to calculate the largest of the remaining terms of the infinite series and a second set of values of the elastic constants is then calculated considering only the elastic constants of the first term as variables. This process is repeated as often as necessary to obtain the desired degree of accuracy. Successive sets of elastic constants calculated in this manner converge to a set which satisfies the chosen finite portions of Neighbours' expanded form of the velocity equations.

Presumably the next order terms could be calculated if greater accuracy were desired, but they apparently have not been given. The present method which uses exact equations thus provides a desirable alternative to Neighbours' method. The propagation-of-error theory could presumably be applied to Neighbours' method to calculate standard deviations, but this has apparently not been worked out. The present method includes such a calculation and this is worthy of note because the calculation involves quantities which are not statistically independent and serious errors can arise if the elementary propagation-of-error equations, which do not include covariance terms, are used. Any comparison of Neighbours' method with the present work should note the great utility and generality of the former which can be applied to crystals of any symmetry (if sufficient measurements are available) while the latter is strictly limited to cubic crystals.

2. Equations for Calculating Elastic Constants

The equations relating elastic constants to wave velocities are derived in many places; see, for example, Kolsky [9] for a treatment in conventional (matrix) notation and Farnell [10] for a brief sketch in tensor notation. The resulting secular equation can be written as an equation involving a 3×3 determinant using Farnell's notation as

$$|\Gamma_{jk}-\delta_{jk}x|=0 \tag{1}$$

where

$$x=\rho v^2 \tag{2}$$

ρ = density,

v = velocity,

and

$$\Gamma_{jk}=\frac{1}{2}\sum_{i,l}\alpha_i\alpha_l(c_{ijkl}+c_{ijlk}) \tag{3}$$

In the last expression, the α_i are the direction cosines for the direction of propagation and the c_{ijkl} are the elastic constants; both are referred to the crystal axes. Assuming cubic symmetry, writing l, m, n for the direction cosines and using the conventional matrix notation for elastic constants, the Γ_{jk} become

$$\Gamma_{11}=c_{11}l^2+c_{44}(m^2+n^2) \tag{4}$$

$$\Gamma_{22}=c_{11}m^2+c_{44}(l^2+n^2) \tag{5}$$

$$\Gamma_{33}=c_{11}n^2+c_{44}(l^2+m^2) \tag{6}$$

$$\Gamma_{12}=\Gamma_{21}=(c_{12}+c_{44})lm, \tag{7}$$

$$\Gamma_{13}=\Gamma_{31}=(c_{12}+c_{44})ln, \tag{8}$$

and

$$\Gamma_{23}=\Gamma_{32}=(c_{12}+c_{44})mn. \tag{9}$$

These values can be substituted into the secular equation to give a cubic equation in x. We assume that for a given direction (l, m, n) the three velocities have been measured and the three corresponding values x_1, x_2, x_3, computed. Then for this direction the cubic equation obtained from the secular equation must factor into

$$(x-x_1)(x-x_2)(x-x_3)=0. \tag{10}$$

When this factored equation is multiplied out and the coefficients of each power of x equated to the coefficient of the same power in the secular equation three simultaneous equations are obtained. To simplify these, let

$$\alpha=c_{11}, \tag{11}$$

$$\beta=c_{44}, \tag{12}$$

$$\gamma=c_{12}+c_{44}, \tag{13}$$

$$u=x_1+x_2+x_3, \tag{14}$$

$$v=x_1x_2+x_1x_3+x_2x_3, \tag{15}$$

and

$$w=x_1x_2x_3. \tag{16}$$

The three equations are

$$u=\alpha+2\beta, \tag{17}$$

$$\begin{aligned} v=&[\alpha l^2+\beta(l^2+m^2)][\alpha m^2+\beta(l^2+n^2)]\\ &+[\alpha l^2+\beta(l^2+m^2)][\alpha n^2+\beta(l^2+m^2)]\\ &+[\alpha m^2+\beta(l^2+n^2)][\alpha n^2+\beta(l^2+m^2)]\\ &-\gamma^2(l^2m^2+l^2n^2+m^2n^2), \end{aligned} \tag{18}$$

and

$$\begin{aligned} w=&[\alpha l^2+\beta(m^2+n^2)][\alpha m^2+\beta(l^2+n^2)][\alpha n^2+\beta(l^2+m^2)]\\ &+2\gamma^3l^2m^2n^2-\gamma^2\{l^2m^2[\alpha n^2+\beta(l^2+m^2)]\\ &+l^2n^2[\alpha m^2+\beta(l^2+n^2)]+m^2n^2[\alpha l^2+\beta(m^2+n^2)]\}. \end{aligned} \tag{19}$$

The problem is to solve for α, β, and γ from a known set of values of u, v, w, l, m, and n. The procedure is to use eq (17) to eliminate β from eqs (18) and (19). Then use (18) to eliminate the γ^2 term from (19). This leaves one equation, derived from (18), which can be solved for γ^2 and one equation, derived from (19), which can be solved for γ^3. Cubing the first of these two equations and squaring the second allows the elimination of γ and gives a 6th degree equation in α. The coefficients in this equation are very long expressions when written out in full and it is much more convenient to define various functions of the starting quantities (l, m, n, u, v, w) and so simplify the algebraic manipulations. We thus define

$$l_1=1-l^2, \tag{20}$$

$$m_1=1-m^2, \tag{21}$$

$$n_1=1-n^2, \tag{22}$$

$$l_2=3l^2-1, \tag{23}$$

$$m_2=3m^2-1, \tag{24}$$

$$n_2=3n^2-1, \tag{25}$$

$$e=l^2m^2+l^2n^2+m^2n^2, \tag{26}$$

$$f=l^2m^2n_2+l^2n^2m_2+m^2n^2l_2, \tag{27}$$

$$g=l_2m_2+l_2n_2+m_2n_2, \tag{28}$$

$$h=l_2m_2n_1+l_2n_2m_1+m_2n_2l_1, \tag{29}$$

$$j=l_2m_1+l_1m_2+l_2n_1+l_1n_2+m_2n_1+m_1n_2, \tag{30}$$

$$k=l^2m^2n_1+l^2n^2m_1+m^2n^2l_1, \tag{31}$$

$$p=l_2m_1n_1+l_1m_2n_1+l_1m_1n_2, \tag{32}$$

$$q=l_1m_1+l_1n_1+m_1n_1, \tag{33}$$

$$r=2l^2m^2n^2, \tag{34}$$

$$s=l_1m_1n_1, \tag{35}$$

$$s_1=l_2m_2n_2, \tag{36}$$

$$g_1=gf/e-s_1, \tag{37}$$

$$h_1=(ugk+ujf)/e-hu, \tag{38}$$

$$j_1=(u^2jk+u^2qf-4vf)/e-u^2p, \tag{39}$$

$$k_1=uk(u^2q-4v)/e-u^3s+8w, \tag{40}$$

and

$$p_1=u^2q-4v. \tag{41}$$

When (17) is used to eliminate β, eq (18) becomes

$$v=\alpha^2g/4+\alpha uj/4+u^2q/4-\gamma^2e, \tag{42}$$

and eq (19) becomes

$$w=\alpha^3s_1/8+\alpha^2uh/8+\alpha u^2p/8+u^3s/8+r\gamma^3-\gamma^2(\alpha f+uk)/2. \tag{43}$$

Substituting for γ^2 from (42) into (43) gives

$$w=\alpha^3(s_1e-gf)/8e+\alpha^2(ueh-ugk-ujf)/8e+\alpha(u^2ep-u^2jk-u^2qf+4vf)/8e \\ +(u^3es-u^3kq+4uvk)/8e+r\gamma^3. \tag{44}$$

Computing $64r^2\gamma^6/e^3$ from (42) and equating to the same quantity computed from (44) gives

$$a_6\alpha^6+a_5\alpha^5+a_4\alpha^4+a_3\alpha^3+a_2\alpha^2+a_1\alpha+a_0=0 \tag{45}$$

where

$$a_0=r^2p_1^3/e^3-k_1^2, \tag{46}$$

$$a_1=3ur^2jp_1^2/e^3-2j_1k_1, \tag{47}$$

$$a_2=3r^2(gp_1^2+u^2j^2p_1)/e^3-2h_1k_1-j_1^2, \tag{48}$$

$$a_3=r^2(6ugjp_1+u^3j^3)/e^3-2(g_1k_1+h_1j_1), \tag{49}$$

$$a_4=3r^2(u^2gj^2+g^2p_1)/e^3-(2g_1j_1+h_1^2), \tag{50}$$

$$a_5=3ur^2g^2j/e^3-2g_1h_1, \tag{51}$$

and

$$a_6=r^2g^3/e^3-g_1^2. \tag{52}$$

The procedure for determining the elastic constants is thus as follows: Starting with the density, ρ, the velocities v_1, v_2, v_3 and the direction cosines l, m, n first compute x_1, x_2, x_3 from (2), next compute u, v, w from eqs (14) through (16), next compute the quantities defined in eqs (20) through (41), then compute the coefficients given by eqs (46) through (52). Using these coefficients plot eq (45) to determine the real, positive roots in the region of physical interest; if there is more than one such root choose the correct one, which is $\alpha=c_{11}$, as described below. Equation (45) can be plotted and the chosen root determined as accurately as desired by routine automatic computer techniques to save laborious hand computation. Then compute c_{44} from

$$c_{44}=(u-c_{11})/2. \tag{53}$$

Use eq (42) to compute $\gamma^2=(c_{12}+c_{44})^2$ and obtain γ. The sign of the square root is determined by the γ^3 term in eq (43). Then compute c_{12} from

$$c_{12}=\gamma-c_{44}. \tag{54}$$

The only ambiguity which arises in this calculation results from the fact that more than one physically reasonable root of eq (45) may occur and each such root may lead to a set of three elastic constants, none of which can be ruled out by the inequalities of Alers and Neighbours [*11*] or by any general physical argument. In this case, one can take one set and compute the polarization of each of the two quasi-transverse waves (the procedure for computing the polarization is given, for example, by Farnell [*10*]) and compare with the polarization of the transducer used to excite the waves. The results should agree for only one set of elastic constants so that the correct choice of root for c_{11} can be made in this way. A second way is to measure velocities in a second direction in the crystal and compare the elastic constants so determined. Although more than one set of elastic constants may give the correct velocities for one direction (but not the correct polarizations) only one set should give the correct velocities for both directions. This second way of choosing c_{11} avoids the need to consider the direction of polarization.

3. Equations for Computing Standard Deviations of the Elastic Constants

It is assumed that uncertainty in the density and the direction cosines may be ignored and that the principal uncertainty in the data is expressed by the three statistically independent standard deviations σ_1, σ_2, σ_3 of the velocities v_1, v_2, v_3. It is easiest to divide the calculation of the standard deviations σ_{11}, σ_{12}, σ_{44} (of c_{11}, c_{12}, c_{44} respectively) into two parts. First, propagation-of-error theory is used to calculate the variances and covariances of u, v, w. Second, these results are then used to calculate σ_{11}, σ_{12}, and σ_{13}.

The following result [12] from propagation-of-error theory is needed: Let x and y be statistically independent variables with known variances (variance=square of standard deviation). Let u and v be defined as functions of x and y and let F be defined as a function of u and v. Then

$$\sigma_F^2=\left(\frac{\partial F}{\partial u}\right)^2\sigma_u^2+\left(\frac{\partial F}{\partial v}\right)^2\sigma_v^2+2\left(\frac{\partial F}{\partial u}\right)\left(\frac{\partial F}{\partial v}\right)\mathrm{cov}\,(u,v), \tag{55}$$

where

$$\sigma_u^2=\left(\frac{\partial u}{\partial x}\right)^2\sigma_x^2+\left(\frac{\partial u}{\partial y}\right)^2\sigma_y^2, \tag{56}$$

$$\sigma_v^2=\left(\frac{\partial v}{\partial x}\right)^2\sigma_x^2+\left(\frac{\partial v}{\partial y}\right)^2\sigma_y^2, \tag{57}$$

and

$$\mathrm{cov}\,(u,v)=\left(\frac{\partial u}{\partial x}\right)\left(\frac{\partial v}{\partial x}\right)\sigma_x^2+\left(\frac{\partial u}{\partial y}\right)\left(\frac{\partial v}{\partial y}\right)\sigma_y^2. \tag{58}$$

In some textbooks it is implicitly assumed that quantities such as u and v are statistically independent so that their covariance is zero and equations such as (56) and (57) with no covariance terms are given instead of the complete eq (55). The use of the complete equation is important in the present case; the extension of these equations from two to three variables is obvious.

Application of eqs (56) through (58) gives

$$\sigma_u^2=\sigma_{x1}^2+\sigma_{x2}^2+\sigma_{x3}^2, \tag{59}$$

$$\sigma_v^2=(x_2+x_3)^2\sigma_{x1}^2+(x_1+x_3)^2\sigma_{x2}^2+(x_1+x_2)^2\sigma_{x3}^2, \tag{60}$$

$$\sigma_w^2=(x_2x_3)^2\sigma_{x1}^2+(x_1x_3)^2\sigma_{x2}^2+(x_1x_2)^2\sigma_{x3}^2, \tag{61}$$

$$\mathrm{Cov}\,(u,v)=(x_2+x_3)\sigma_{x1}^2+(x_1+x_3)\sigma_{x2}^2+(x_1+x_2)\sigma_{x3}^2, \tag{62}$$

$$\mathrm{Cov}\,(u,w)=x_2x_3\sigma_{x1}^2+x_1x_3\sigma_{x2}^2+x_1x_2\sigma_{x3}^2, \tag{63}$$

and

$$\text{Cov } (v, w) = (x_2+x_3)x_2x_3\sigma_{x1}^2 + (x_1+x_3)x_1x_3\sigma_{x2}^2 + (x_1+x_2)x_1x_2\sigma_{x3}^2, \tag{64}$$

where

$$\sigma_{x1}=2\rho v_1\sigma_1,\ \sigma_{x2}=2\rho v_2\sigma_2,\ \sigma_{x3}=2\rho v_3\sigma_3.$$

To use eq (55) for the standard deviations of the elastic constants one must compute the partial derivatives of these constants with respect to u, v, w. These partials of c_{11} can be obtained by taking derivatives of eq (45). The resulting expressions involve partials of the coefficients a_i and these in turn involve partials of the quantities defined in eqs (38) through (41). Let subscripts u, v, w denote partial differentiation with respect to u, v, w respectively. Then from eqs (38) through (41)

$$h_{1u}=(gk+jf)/e-h, \tag{65}$$

$$j_{1u}=2u[(jk+qf)/e-p], \tag{66}$$

$$k_{1u}=k(3u^2q-4v)/e-3u^2s, \tag{67}$$

$$p_{1u}=2uq, \tag{68}$$

$$j_{1v}=-4f/e, \tag{69}$$

$$k_{1v}=-4uk/e, \tag{70}$$

$$p_{1v}=-4 \tag{71}$$

$$k_{1w}=8 \tag{72}$$

and the following are all zero: h_{1v}, h_{1w}, j_{1w}, and p_{1w}. We shall next require the partial derivatives of the a_i which are given by differentiating eqs (46) through (52) with the result for the u derivatives

$$a_{0u}=3r^2p_1^2p_{1u}/e^3-2k_1k_{1u}, \tag{73}$$

$$a_{1u}=3r^2(jp_1^2+2ujp_1p_{1u})/e^3-2j_1k_{1u}-2k_1j_{1u}, \tag{74}$$

$$a_{2u}=3r^2(2gp_1p_{1u}+2uj^2p_1+u^2j^2p_{1u})/e^3-2h_1k_{1u}-2k_1h_{1u}-2j_1j_{1u}, \tag{75}$$

$$a_{3u}=r^2(6gjp_1+6ugjp_{1u}+3u^2j^3)/e^3-2(g_1k_{1u}+h_1j_{1u}+j_1h_{1u}), \tag{76}$$

$$a_{4u}=3r^2(2ugj^2+g^2p_{1u})/e^3-2g_1j_{1u}-2h_1h_{1u}, \tag{77}$$

$$a_{5u}=3r^2g^2j/e^3-2g_1h_{1u}, \tag{78}$$

and with a_{6u} equal to zero. For the v derivatives the result is

$$a_{0v}=-12r^2p_1^2/e^3-2k_1k_{1v}, \tag{79}$$

$$a_{1v}=-24r^2ujp_1/e^3-2j_1k_{1v}-2k_1j_{1v}, \tag{80}$$

$$a_{2v}=-12r^2(2gp_1+u^2j^2)/e^3-2h_1k_{1v}-2j_1j_{1v}, \tag{81}$$

$$a_{3v}=-24r^2ugj/e^3-2(g_1k_{1v}+h_1j_{1v}), \tag{82}$$

$$a_{4v}=-12r^2g^2/e^3-2g_1j_{1v}, \tag{83}$$

and with a_{5v} and a_{6v} equal to zero. For the w derivatives the result is

$$a_{0w}=-16k_1, \tag{84}$$

$$a_{1w}=-16j_1, \tag{85}$$

$$a_{2w}=-16h_1, \tag{86}$$

$$a_{3w}=-16g_1, \tag{87}$$

and with a_{4w}, a_{5w}, and a_{6w} equal to zero. Define

$$D=6a_6c_{11}^5+5a_5c_{11}^4+4a_4c_{11}^3+3a_3c_{11}^2+2a_2c_{11}+a_1 \tag{88}$$

then differentiation of eq (45) gives

$$c_{11u} = -(a_{5u}c_{11}^5 + a_{4u}c_{11}^4 + a_{3u}c_{11}^3 + a_{2u}c_{11}^2 + a_{1u}c_{11} + a_{0u})/D, \tag{89}$$

$$c_{11v} = -(a_{4v}c_{11}^4 + a_{3v}c_{11}^3 + a_{2v}c_{11}^2 + a_{1v}c_{11} + a_{0v})/D, \tag{90}$$

and

$$c_{11w} = -(a_{3w}c_{11}^3 + a_{2w}c_{11}^2 + a_{1w}c_{11} + a_{0w})/D, \tag{91}$$

where we have assumed $D \neq 0$. For the [110] direction $D=0$ and a different treatment, described below, is required. The derivatives of c_{44} are obtained from (53) and are

$$c_{44u} = (1 - c_{11u})/2, \tag{92}$$

$$c_{44v} = -c_{11v}/2, \tag{93}$$

and

$$c_{44w} = -c_{11w}/2. \tag{94}$$

The derivatives of c_{12} are obtained from eq (54) and so involve derivatives of γ. From (42) we have

$$\gamma^2 = (gc_{11}^2 + ujc_{11} + p_1)4e, \tag{95}$$

so that

$$(\gamma^2)_u = (2c_{11}gc_{11u} + jc_{11} + ujc_{11u} + p_{1u})/4e, \tag{96}$$

$$(\gamma^2)_v = (2c_{11}gc_{11v} + ujc_{11v} - 4)/4e, \tag{97}$$

and

$$(\gamma^2)_w = (2c_{11}g + uj)c_{11w}/4e. \tag{98}$$

Now use $\gamma_u = (\gamma^2)_u/2\gamma$ and eq (54) to obtain

$$c_{12u} = (\gamma^2)_u/2\gamma - c_{44u}, \tag{99}$$

$$c_{12v} = (\gamma^2)_v/2\gamma - c_{44v}, \tag{100}$$

and

$$c_{12w} = (\gamma^2)_w/2\gamma - c_{44w}. \tag{101}$$

The expression for σ_{11}^2 is then

$$\sigma_{11}^2 = c_{11u}^2\sigma_u^2 + c_{11v}^2\sigma_v^2 + c_{11w}^2\sigma_w^2 + 2c_{11u}c_{11v}\,\mathrm{cov}\,(u, v) + 2c_{11u}c_{11w}\,\mathrm{cov}\,(u, w) + 2c_{11v}c_{11w}\,\mathrm{cov}\,(v, w). \tag{102}$$

The equations for σ_{44}^2 and σ_{12}^2 are the same with the subscripts on c_{11} changed to 44 and 12 respectively.

The procedure for obtaining the desired standard deviations is thus straightforward although tedious. One begins by calculating the variances and covariances of u, v, w from eqs (59) through (64). Then compute in succession the quantities given by eqs (65) through (102).

Following eq (91) we noted that $D=0$ for the [110] direction. This can be seen as follows: For the [110] direction r is zero by eq (34) and the γ^3 term drops out of eq (43). Then eq (45) simply consists of the square of all the terms in (43) except $r\gamma^3$. Let

$$B = \alpha^3 s_1/8 + \alpha^2 uh/8 + \alpha u^2 p/8 + u^3 s/8 - \gamma^2(\alpha f + uk)/2 - w. \tag{103}$$

Then eq (45) for the [110] direction is $B^2=0$, and D is then $D = 2B\dfrac{dB}{d\alpha}$, and therefore $D=0$.

The foregoing statistical treatment thus fails for any direction for which c_{11} is a double root of eq (45). This appears to be true only for the [110] direction (we have already noted that the [100] and [111] directions are not suitable for the method of this paper) but the writers have not been able to construct a proof.

For the [110] direction the following results are well known and easily obtained from the treatment of Kolsky [9], for example. If x_1 corresponds to the longitudinal wave, x_2 to the transverse wave with displacement parallel to [001], and x_3 to the transverse wave with displacement parallel to [110], then

$$c_{11}=x_1-x_2+x_3, \tag{104}$$

$$c_{12}=x_1-x_2-x_3, \tag{105}$$

and

$$c_{44}=x_2. \tag{106}$$

These give

$$\sigma_{11}^2=\sigma_{12}^2=\sigma_{x1}^2+\sigma_{x2}^2+\sigma_{x3}^2, \tag{107}$$

and

$$\sigma_{44}=\sigma_{x2}. \tag{108}$$

We have assumed throughout this paper that errors in thickness and density can be neglected in comparison with errors in transit time t. If standard deviations were assigned to the thickness and density as well, the quantities x_i would not be statistically independent and two modifications of the foregoing treatment would be required. First, eqs (56) through (58) would have to be used with the thickness, density, and transit times as independent variables to give the variances and covariances of u, v, w. The calculations using eqs (65) through (102) would then go as before. Second, eqs (107) and (108) would have to be replaced by appropriate expressions in terms of the standard deviations of the thickness, density, and transit times derived from (56) through (58) and (104) through (106). No attempt has been made to allow for uncertainties in the orientation; such allowance should probably be made but appears to be an exceedingly difficult problem.

4. Procedure for Computing the Elastic Compliances and Their Standard Deviations

The foregoing results form a complete unit, giving the elastic constants, c_{ij}, and their standard deviations. The present section may be skipped unless it is desired to put the results in terms of the elastic compliances, s_{ij}. The calculation of the s_{ij} from the c_{ij} is trivial but the calculation of the standard deviations of the s_{ij} is more difficult and serious errors can result if the covariance terms are not taken into account. There appears to be no discussion of this problem in the literature on elastic constants, so we present the method for the cubic case.

The well-known equations for the elastic compliances of a cubic crystal in terms of the elastic constants are

$$s_{11}=(c_{11}+c_{12})/c, \tag{109}$$

$$s_{12}=-c_{12}/c, \tag{110}$$

and

$$s_{44}=1/c_{44}, \tag{111}$$

where

$$c=(c_{11}-c_{12})(c_{11}+2c_{12}). \tag{112}$$

To compute the standard deviations of the s_{ij} one can apply eq (55) which requires the covariances of the c_{ij}. To compute these covariances one might try to use eq (58) which would be wrong because x and y were assumed to be statistically independent. We require the more general formula

$$\operatorname{cov}(F,G)=\frac{\partial F}{\partial u}\frac{\partial G}{\partial u}\sigma_u^2+\frac{\partial F}{\partial v}\frac{\partial G}{\partial v}\sigma_v^2+\left(\frac{\partial F}{\partial u}\frac{\partial G}{\partial v}+\frac{\partial F}{\partial v}\frac{\partial G}{\partial u}\right)\operatorname{cov}(u,v) \tag{113}$$

for the covariance [12] of F and G which are defined in terms of quantities u and v which are not statistically independent. Writing cov (11, 12) for the covariance of c_{11} and c_{12} we have

$$\text{cov}\ (11, 12)=c_{11u}c_{12u}\sigma_u^2+c_{11v}c_{12v}\sigma_v^2+c_{11w}c_{12w}\sigma_w^2+(c_{11u}c_{12v}+c_{11v}c_{12u})\ \text{cov}\ (u, v)$$
$$+(c_{11u}c_{12w}+c_{11w}c_{12u})\ \text{cov}\ (u, w)+(c_{11v}c_{12w}+c_{11w}c_{12v})\ \text{cov}\ (v, w) \tag{114}$$

The expressions for cov (11, 44) and cov (12, 44) are identical except for the appropriate changes of subscripts, but we shall not need to calculate these latter two covariances. Writing $s_{11,11}$ for $\frac{\partial s_{11}}{\partial c_{11}}$ and similarly for other partials we have

$$s_{11,11}=c-\frac{(c_{11}+c_{12})(2c_{11}+c_{12})}{c^2}, \tag{115}$$

$$s_{11,12}=c+\frac{(c_{11}+c_{12})(4c_{12}+c_{11})}{c^2}, \tag{116}$$

$$s_{12,11}=\frac{c_{12}(2c_{11}+c_{12})}{c^2}, \tag{117}$$

$$s_{12,12}=-\frac{(c_{11}+c_{12})(4c_{12}-c_{11})}{c^2}, \tag{118}$$

$$s_{44,44}=-1/c_{44}^2, \tag{119}$$

and with $s_{11,44}$, $s_{12,44}$, $s_{44,11}$, $s_{44,12}$ all zero. Letting σs_{11} represent the standard deviation of s_{11} and similarly for the other s_{ij},

we have

$$\sigma_{s_{11}}^2=s_{11,11}^2\sigma_{11}^2+s_{11,12}^2\sigma_{12}^2+2s_{11,11}s_{11,12}\ \text{cov}\ (11, 12) \tag{120}$$

$$\sigma_{s_{12}}^2=s_{12,11}^2\sigma_{11}^2+s_{12,12}^2\sigma_{12}^2+2s_{12,11}s_{12,12}\ \text{cov}\ (11, 12), \tag{121}$$

and

$$\sigma_{s_{44}}=\sigma_{44}/c_{44}^2. \tag{122}$$

For the [110] direction the covariances of c_{11} and c_{12} is best calculated directly from (104) and (105) using (58). The result is

$$\text{cov}\ (11, 12)=\sigma_{x1}^2+\sigma_{x2}^2+\sigma_{x3}^2. \tag{123}$$

Thus, the procedure for calculating the standard deviation of the s_{ij} for any direction, including the [100] and [111], is to use eqs (120) through (122) evaluating the partial derivations from eqs (115) through (119). The situation considered in the present paper, using only information obtainable from measurements in a single direction, compels us to exclude [100] and [111] from the present considerations. For [110] cov (11, 12) is given by (123); for any other direction, it is given by (114).

5. Measurements on $SrTiO_3$

The writers carried out a series of measurements on a boule of strontium titanate, kindly supplied by the National Lead Company, to check the method. The density value [*13*] of 5.116 g/cm^3 was used. Flats were first ground to give the maximum thickness between parallel faces permitted by the shape of the crystal. A series of measurements was taken and analyzed. The crystal was then recut normal to the [110] direction and a second series of measurements was then made. The measurements were all made with 10 Mc/s X-cut and AC-cut quartz crystals 0.25 in. in diameter. A commercial pulsed oscillator was used to drive these transducers. The echoes were observed on a dual trace oscilloscope simultaneously with a 1 Mc/s standard frequency signal. The results are sumarized in table 1.

TABLE 1. *Data on* $SrTiO_3$ *at 25° C*

Parameter	Symbol	First direction	Second direction, [110]
Direction Cosines	l	0.67905	0.70711
	m	.27160	.70711
	n	.68200	.00000
Length, cm		5.3045	4.5670
Transit times, 10^{-6} sec	t_1	13.15±0.10	11.36±0.05
	t_2	22.08±.05	18.71±.07
	t_3	23.15±.07	20.92±.09
x_i, 10^{12} dyne/cm^2	x_1	3.330±.051	3.308±.029
	x_2	1.181±.005	1.219±.009
	x_3	1.074±.006	1.064±.010

6. Results

The data are summarized in table 1. The calculation of c_{11} by the method of eqs (20) through (52) was programmed for an automatic computer using an iterative procedure of solving eq (45) which gives the real roots to four places in the interval 0.0 to 5.0×10^{12} dynes/cm^2. For the first direction, there is a single root at $\alpha=3.162$ and a single root at $\alpha=3.497\times10^{12}$ dynes/cm^2. For the second direction there is a double root at $\alpha=3.153$ and a double root at $\alpha=3.462\times10^{12}$ dynes/cm^2. A complete set of elastic constants was computed for each of these possible choices of c_{11} and the results are compared in table 2. The choice of 3.497 and 3.462 leads to a disagreement in c_{12} which is outside the experimental error. The choice of 3.162 and 3.153 gives consistent sets of constants. The latter choice is also known to be correct because 3.153 is obtained from eq (104) when x_2 and x_3 are properly distinguished by the polarization of the corresponding sound waves.

For the first direction, the standard deviations of the c_{ij} were determined by the method of eqs (59) through (102) using an automatic computer. Equations (107) and (108) were used for the second direction. The final values for the c_{ij} were computed by averaging the results for the two directions weighted by the reciprocals of the squares of the standard deviations. The s_{ij} values were then computed from eqs (109) through (112) and their standard deviations from eqs (113) through (123).

TABLE 2. *Comparison of possible sets of elastic constants*

Constants	First direction	Second direction
Computed from correct choice of root for c_{11}		
c_{11}	3.162±0.052	3.153±0.032
c_{12}	1.035± .052	1.024± .032
c_{44}	1.212± .007	1.219± .009
Computed from incorrect choice of root for c_{11}		
c_{11}	3.497	3.462±0.032
c_{12}	1.200	1.024± .032
c_{44}	1.044	1.064± .010

The c_{11} and c_{12} values of Bell and Rupprecht [*14*] agree within experimental error with the results of the present work as shown in table 3; the c_{12} value of Poindexter and Giardini [*15*] also agrees within experimental error, but their c_{11} value differs from the present result by much more than twice the standard deviation and so is significantly different from our result. The other workers' c_{44} values lie on either side by slightly more than twice the standard deviation of our value, but are probably within the combined experimental error of their determination and ours. The writers feel that the c_{11} values of Poindexter and Giardini should be rejected and that the remaining data show reasonable agreement.

The anisotropy of a cubic crystal depends on the quantity δ defined by

$$\delta=2s_{11}-2s_{12}-s_{44}. \tag{124}$$

The Young's modulus, Y_f, and shear modulus, G_f, are given as a function of the usual spherical polar angles by

$$\frac{1}{Y_f}=s_{11}-\delta \sin^2\theta \cos^2\theta-(\delta/4)\sin^4\theta \sin^2 2\phi, \tag{125}$$

and

$$\frac{1}{G_f}=s_{44}+2\delta \sin^2\theta \cos^2\theta+(\delta/2)\sin^4\theta \sin^2 2\phi. \tag{126}$$

These quantities are plotted in figure 1 which shows that $SrTiO_3$ comes close to being isotropic; Young's modulus varies by only 10 percent and the shear modulus by 5 percent.

TABLE 3. *Comparison with elastic constants of $SrTiO_3$ at 25°C determined by other workers*

Constants	Poindexter and Giardini [a]	Bell and Rupprecht [b]	Present work [b]	Percent difference, last two columns
c_{11}	3.48	3.181	3.156±0.027	0.79
c_{12}	1.01	1.025	1.027± .027	0.19
c_{44}	1.19	1.236	1.215± .006	1.73
s_{11}	3.3	3.729	3.772± .023	1.14
s_{12}	−0.74	−0.909	−0.926± .010	1.84
s_{44}	8.4	8.091	8.233± .040	1.73

All c_{ij} in units of 10^{12} dyne/cm^2; s_{ij} in units of 10^{-12} cm^2/dyne.
[a] s_{ij} determined by resonance method and c_{ij} by matrix inversion.
[b] c_{ij} determined by pulse velocity method and s_{ij} by matrix inversion.

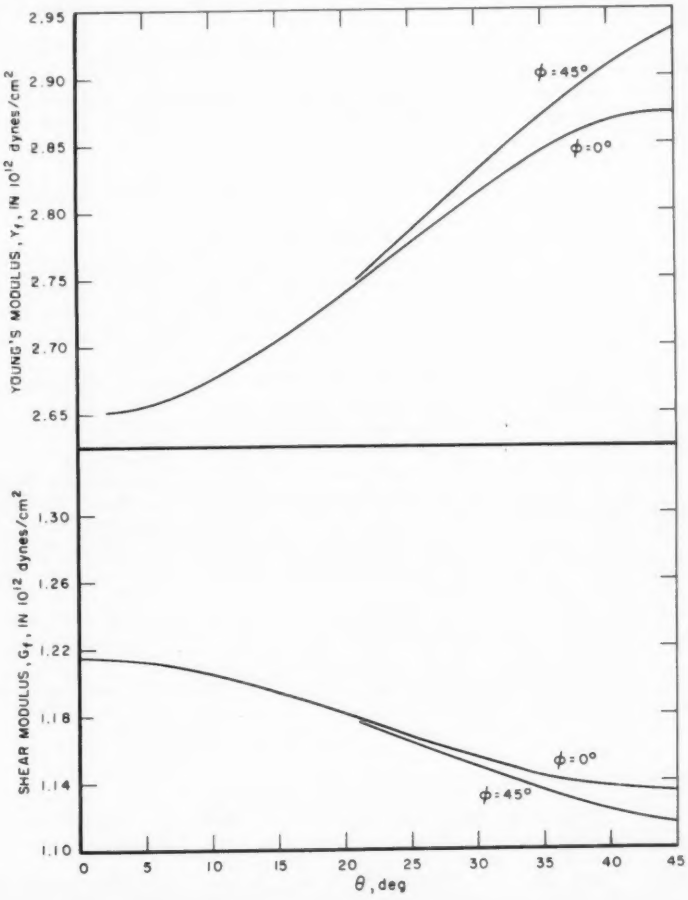

FIGURE 1. *Young's modulus, Y_f, and the shear modulus, G_f, as a function of orientation.*

The colatitude, θ, is the angle between the [001] direction and the direction of measurement. The azimuth, ϕ, is the angle between the [100] direction and the projection of the direction of measurement on the (001) plane. The subscript f indicates that the elastic moduli are for a free specimen which is under no constraint.

7. Summary

(1) Velocity measurements in a single direction in a cubic crystal provide enough information to determine the three elastic constants, c_{ij}, except for the [100] and [111] directions which are therefore excluded from consideration in this paper.

(2) For the [110] direction the computation of the elastic constants and their standard deviations is simple and is given in eqs (104) through (108).

(3) For all other directions the calculations are much more complex. The general procedure for the elastic constants (applicable also to the [110] direction) is given in eqs (2) through (54). The general procedure for the standard deviations (not applicable to the [110] direction) is given in eqs (59) through (102).

(4) The procedure for calculating the elastic compliances, s_{ij}, and their standard deviations is given in eqs (109) through (123). Throughout the statistical treatment the covariance terms are included and their importance is emphasized.

(5) The method is applied to $SrTiO_3$ and results in good agreement with previous workers are obtained.

The writers thank W. E. Tefft of the National Bureau of Standards for bringing eqs (55) and (58) to their attention, and M. D. Beals of the National Lead Company for supplying the $SrTiO_3$ specimen.

8. References

[1] R. F. S. Hearmon, The elastic constants of anisotropic materials, Rev. Mod. Phys. **18** 409–440 (1946); The elastic constants of anisotropic materials II, Adv. in Phys. **5,** 323–382 (1956).

[2] M. F. Markham, Measurements of elastic constants by the ultrasonic pulse method, British J. Appl. Phys. Suppl. **6,** pp. 556–563 (1957).

[3] H. B. Huntington, The elastic constants of crystals, Solid State Phys. **7,** 213–351 (Academic Press, New York, N.Y., 1958).

[4] K. S. Aleksandrov and T. V. Ryzhova, The elastic properties of crystals, Soviet Physics-Crystallography **6,** 228–252 (1961). Translated from Kristallografiya **6,** 289–314 (1961).

[5] J. R. Neighbours and Charles S. Smith, An approximation method for the determination of the elastic constants of cubic single crystals, J. Appl. Phys. **21,** 1338–1339 (1950).

[6] J. R. Neighbours, F. W. Bratten, and Charles S. Smith, The elastic constants of nickel, J. Appl. Phys. **23,** 389 (1952).

[7] J. R. Neighbours, An approximation method for the determination of the elastic constants of single crystals, J. Acoustical Soc. Am. **26,** 865–869 (1954).

[8] D. L. Arenberg, Determination of elastic constants in single crystals with especial reference to silver chloride, J. Appl. Phys. **21,** 941–942 (1950).

[9] H. Kolsky, Stress Waves in Solids (Oxford Univ. Press., London, England, 1953).

[10] G. W. Farnell, Elastic waves in trigonal crystals, Canadian J. Phys. **39,** 65–80 (1961).

[11] G. A. Alers and J. R. Neighbours, Crystal stability and elastic constants, J. Appl. Phys. **28,** 1514 (1957).

[12] O. L. Davies, Statistical Methods in Research and Production, (Oliver and Boyd, London, 1957).

[13] H. E. Swanson, R. F. Fuyat, and G. M. Ugrinic, Standard X-ray diffraction powder patterns, NBS Circ. 539, Vol III, 44 (1954).

[14] R. O. Bell and G. Rupprecht, Preliminary values were given in Elastic constants of single crystal strontium titanate, Bull. Am. Phys. Soc. **7,** 7 (1962). Refined values given in private communication with the authors and submitted to Phys. Rev.

[15] E. Poindexter and A. A. Giardini, Elastic constants of strontium titanate ($SrTiO_3$), Phys. Rev. 110, 1069 (1958).

(Paper 67A2–205)

JOURNAL OF RESEARCH of the National Bureau of Standards—A. Physics and Chemistry
Vol. 67A, No. 2, March–April 1963

Publications of the National Bureau of Standards*

Selected Abstracts

A new type of computable inductor, C. H. Page, *J. Research NBS* **67B** (*Math. and Math. Phys.*), *No. 1* (*Jan.-Mar. 1963*), *75 cents.*
The mutual inductance analog of the generalized Thompson-Lamparo theorem (for cross-capacitances) is developed. An infinitely long cage of five parallel wires can yield an absolute inductance of

$$10^{-7} \ln \frac{3+\sqrt{5}}{2}$$

henries per meter. End-effects of order $1/l^2$ occur in a finite cage, but can be reduced to order $1/l^4$ by using eight wires.
The eight wire cage has the advantage of overdetermined relations among the inductances to be measured, allowing an estimate of experimental error in the calibration of a standard. Errors due to faulty cage geometry are shown to be of the order of 1 in 10^7.

Numerical computation of the temporal development of currents in a gas discharge tube, W. Börsch-Supan and H. Oser, *J. Research NBS* **67B** (*Math. and Math. Phys.*), *No. 1* (*Jan.-Mar. 1963*), *75 cents*
The behavior of electrical currents in a gas discharge tube including space charge effects is investigated by numerical integration of the governing nonlinear partial differential equations. Both stationary solutions and the temporal development, under the influence of space charge effects, are considered. The numerical integration is done by a difference method. It is found that the truncation error can be greatly reduced by comparison with formal solutions for constant fields. The discussion is essentially restricted to the more mathematical questions.

Equipment for single crystal growth from aqueous solution, J. L. Torgesen, A. T. Horton, and C. P. Saylor, *J. Research NBS* **67C** (*Eng. and Instr.*), *No. 1* (*Jan.-Mar. 1963*), *75 cents.*
The growing of large single crystals of high quality from solution requires the precise control of supersaturation and the avoidance of thermal amd mechanical shock. Uniform growth conditions and cleanliness need to be maintained. Good seed crystals are necessary and the accidental introduction or generation of new nuclei should be prevented insofar as possible. In the apparatus and equipment assemblies here described, the crystal-growth bath is designed for uniform growth conditions and the exclusion of contamination. The support for the crystals provides for convenient mounting of the seeds, holds the crystals firmly, and allows their easy removal with minimum damage. A new reversing rotation mechanism promotes equal washing of the crystal surfaces and achieves uniform temperature and composition of the solution without, at the same time, producing significant mechanical stresses in the crystals. The temperature controller gives regulation of the temperature an order of magnitude more sensitive than those hitherto used and provides for stepless change of temperature. The crystals are thus free from liquid inclusions found to result from sudden acceleration of growth. The electrolytic conductance of ionic solutions may be used as a precise and sensitive measure of solution concentration and supersaturation. The crystal-growth procedures which are reported have resulted in the production of very good single crystals of a considerable variety of chemical phases.

An automatic multichannel correlator, R. F. Brown, Jr., *J. Research NBS* **67C** (*Eng. and Instr.*), *No. 1* (*Jan.-Mar 1963*), *75 cents.*
Very early in our Infrasonic Research Program it become apparent that the only way to differentitate between local meteorological pressure variations and the infrasonic signals from distant sources was through the relative time of arrival of the pressure disturbance at pickups spaced several miles apart. The "Multichannel Correlator" is an analog computer that was designed to detect these infrasonic signals.
At each pickup the pressure variations are converted to FM audio signals which are transmitted over leased telephone lines to the correlator. At the correlator these FM signals are demodulated and recorded on a ¼ inch per minute multichannel magnetic tape. The recorded data frequency range is 0.02 to 1.0 c/s and the pressure range is 0.1 to 50 dynes per square centimeter. 10 minute blocks of data are read from the tape and amplitude equalized to a constant rms value. A programmed time delay device produces the equivalent delays appropriate to a continuous horizontal azimuth search for velocities in the range of 280 to 400 meters per second. The correlator output is a continuous record of the average of the rectified sum of the delayed channel signals.

Elastic constant—porosity relations for polycrystalline thoria, S. Spinner, F. P. Knudsen, and L. Stone, *J. Research NBS* **67C** (*Eng. and Instr.*), *No. 1* (*Jan.-Mar. 1963*), *75 cents.*
The relations between the elastic constants and porosity for about 300 thoria specimens have been determined. Both Young's and the shear modulus for each specimen were obtained by a dynamic resonance method. From these two moduli, Poisson's ratio was computed. The tendency for all these elastic constants to decrease with increasing porosity is in qualitative agreement with theory. However, the decrease in the experimental values was greater than would be expected from the theory. This greater decrease for the experimental values is attributed to the fact that the specimens do not conform to the idealized assumptions of the theory.

New fast-opening, large-aperture shutter for high-speed photography, E. C. Cassidy and D. H. Tsai, *J. Research NBS* **67C** (*Eng. and Instr.*), *No. 1* (*Jan.–Mar. 1963*), *75 cents.*
This shutter consists essentially of a metallic foil in a capacitor discharge circuit. The opening action is obtained when the foil is compressed by the electromagnetic forces which accompany the heavy surge current through the circuit, during a transient discharge. A shutter made up of two foils in a loop arrangement may be opened to an area 1 in. x 3 in. in less than 45 μsec. The factors affecting the design and operation of this shutter are analyzed. These factors include the circuit parameters, the energy input to the foil, and the materials and the size of the foil. Some experimental results are also given.

Perturbation method in a problem of waveguide theory, D. Fox and W. Magnus, *J. Research NBS* **67D** (*Radio Prop.*), *No. 2* (*Mar.–Apr. 1963*), *70 cents.*
The reflection coefficient for the basic mode in a widening, straight, two-dimensional waveguide is computed for small wave numbers by using the perturbation method with the electrostatic case as the unperturbed case. The problem is treated as a perturbed infinite system of inhomogeneous linear equations, and it is shown that the matrix of the unperturbed system (which corresponds to the electrostatic case) can be inverted explicitly by using conformal mappings and physically unrealistic modes. Questions of convergence are discussed, and other examples for application of the method are indicated.

Some wave functions and potential functions pertaining to spherically stratified media, C. T. Tai, *J. Research NBS* **67D** (*Radio Prop.*), *No. 2* (*Mar.–Apr. 1963*), *70 cents.*
The wave functions pertaining to a bilinearly stratified medium are presented in this paper. Solutions to the equation $\nabla \cdot [\kappa(r)\nabla\psi]=0$ have been investigated for several profiles of $\kappa(r)$. An analysis is given to the equation

$\nabla \cdot [\overleftrightarrow{\epsilon} \cdot \nabla\psi] = -\rho/\epsilon_0$ which arises from the formulation of the quasi-static electric field in a homogeneous anisotropic medium.

Radiation from a plasma-clad axially-slotted cylinder, W. V. T. Rusch, *J. Research NBS* **67D** (*Radio Prop.*), *No. 2 (Mar.–Apr. 1963), 70 cents.*
Expressions have been developed for the complete radiation pattern from a finite axial slot on an infinite circular cylinder covered with a homogeneous, uniform plasma sheath. The resulting field expressions are functions of both the longitude angle, ϕ, and the polar angle, θ. Numerical results have been obtained for a thin lossless plasma to determine the variation of the field pattern with plasma frequency, plasma thickness, slot width, and cylinder radius. These results are presented graphically to illustrate various properties of the radiating system.

Report of the 47th National Conference on Weights and Measures, 1962, *NBS Misc. Publ. 244 (November 23, 1962), 75 cents.*
A report of the proceedings of the forty-seventh National Conference on Weights and Measures, held in Washington, D.C., June 4, 5, 6, 7, and 8, 1962, and attended by State, county, and city weights and measures officials. 167 p.

Radiation quantities and units, International Commission on Radiological Units and Measurements (ICRU) Report 10a, 1962, *NBS Handb. 84 (Nov. 14, 1962), 20 cents.*
This Handbook presents definitions of twenty-three fundamental radiation quantities and units. It resulted from a three-year study by the *Ad Hoc* Committee on Quantities and Units of the ICRU. It includes new names for certain quantities and clarified definitions for others. It presents a system of concepts and a set of definitions which is internally consistent and yet of sufficient generality to cover present requirements and such future requirements as can be foreseen.

Controlled temperature oil baths for saturated standard cells, P. H. Lowrie, Jr., *NBS Tech. Note 141 (August 1962), 25 cents.*
Two oil baths for the temperature control of saturated standard cells have been designed and fabricated at the Boulder Laboratories of the National Bureau of Standards for operation at 28° C and 35° C respectively. Short term control to better than ± 0.001° C with day-to-day variations no greater than 0.002° C has been achieved with the use of a mercury-toluene thermoregulator incorporating a temperature anticipating device. The circulating system limits temperature gradients in the oil to less than 0.001° C across any 10 inch section. The baths incorporate pre-heat and drain tanks as well as the main temperature regulated tank to facilitate the insertion and removal of cells and to minimize oil spillage.

Applications of resistance thermometers to calorimetry, G. T. Furukawa, *Book, Temperature, Its Measurement and Control in Science and Industry III, pt. 2, 317–328 (1962).*
The importance of the resistance thermometer in the accurate measurement of both temperature and the heat leak of the calorimeter is discussed. The final accuracy of the determination of heat capacity is shown to be dependent upon the accurate and consistent measurement of heat input to the sample and the corresponding rise in temperature. The various heat-capacity calorimeters used in the range from 10 to 400 °K are briefly described with emphasis upon the applications of resistance thermometers, the methods for calibrating them, and the problems associated with the design of calorimeter vessels. Comparison is made of the thermometric properties of platinum, copper, indium, lead and gold-silver alloy. The need for high relative accuracy in the measurement of $\triangle$R is emphasized. The various temperature scales used in calorimetry are compared and their applications are described.

Absorption spectrum of carbon vapor in solid argon at 4° and 20°K, R. L. Barger and H. P. Broida, *J. Chem. Phys.* **37,** *No. 5, 1152–1153 (Sept. 1, 1962).*
Absorption spectra have been observed photoelectrically for C_3 and C_2 in solid argon at temperatures of 4° K and 20° K. A molecular beam of carbon from a Knudsen cell at 2550° K was deposited simultaneously with argon onto a quartz surface, cooled either with liquid helium or with liquid hydrogen. The spectra consist of 21 lines and a continuum between 3797A and 4221A attributed to C_3, and two lines at 5208A and 5269A attributed to C_2. Measured wavelengths, half-widths, peak absorption intensities and f-values are given. An f-value of 2×10^{-4} was found for the 5269A line of the C_2 and the 4102A line of C_3.

Vibrational-rotational spectroscopy, H. C. Allen, Jr. and W. B. Olson, *Ann. Rev. Phys. Chem.* **13,** *221–240 (1962).*
The literature on molecular spectroscopy has increased significantly each year with the increased availability of high-quality commercial infrared spectrometers. This year is no exception. It is quite impossible to give a complete review of all the work in the space available, hence the authors will take advantage of their prerogative of discussing a limited number of topics. We shall, thus, stress work of a general nature on theoretical advances, fine structure of simple molecules, vibrational spectra, intensities of gases, and computer applications. For the spectra of specific molecules the reader is referred to *Chemical Abstracts.*

Realistic diatomic potential function, H. W. Woolley, *J. Chem. Phys.* **37,** *No. 6, 1307–1316 (Sept. 1962).*
An examination of recently published data for diatomic molecules as obtained by the Rydberg-Klein-Rees method has suggested a useful form for the potential energy function. This term provides an inverse power dependence at large distance and an extrapolation to infinity at the extreme of close approach. A three parameter potential obtained by fitting in lowest approximation is compared with empirical data on $\omega_e X_e$ and α_e. Relations are also given to permit an arbitrarily close fit of observed spectroscopic constants. Theoretical formulas covering seven new Y_{ij}'s of the Dunham-Sandeman series for the rotating-vibrator are included. Potential curves for H_2 and HF are shown as examples, including effects of previously determined higher order spectroscopic constants. Other applications of the new potential are also discussed.

Optical constants of aluminum in vacuum ultraviolet, R. LaVilla and H. Mendlowitz, *Phys. Rev. Letters* **9,** *No. 4, 149–150 (Aug. 15, 1962).*
Values of the frequency dependent complex dielectric constant $\epsilon(\omega)$ of aluminum in the photon energy region of 12–16 ev were derived from the characteristic electron energy loss spectra. A two-parameter Drude model with N, the number of "free" electrons per atom, as 2.6 and τ, the relaxation time as 1.1×10^{-15} sec. was found to give a good approximation to the optical properties of aluminum.

Microwave spectrum of methyldifluoroarsine, L. J. Nugent and C. D. Cornwell, *J. Chem. Phys.* **37,** *No. 3, 523–534 (Aug. 1962).*
The spectrum of CH_3AsF_2 was investigated over the range 10–33 KMc/sec. Three Q-branches ($K=5-4$, $6-5$, $7-6$) and two R transitions ($J=2-3$, $K=2-3$; $J=3-4$, $K=3-4$) were fitted by a Hamiltonian which included terms for overall rotation, internal rotation, nuclear quadrupole coupling, and centrifugal distortion. The reciprocal moments of inertia are $A=5414.49\pm0.04$ Mc/sec, $B=5381.28\pm0.03$ Mc/sec, and $C=3871.88\pm0.03$ Mc/sec. The b-axis is perpendicular to the plane of symmetry. The height of the internal rotation barrier (assumed to be sinusoidal) is 466 ± 10 cm^{-1}. With the bond length $r_{CH}=1.095$ A assumed, the spectral data yield $r_{As-C}=1.930\pm0.010$ A, $r_{As-F}=1.734\mp0.005$ A $\angle HCH=109°9'\pm1°$, $\angle CAsF=95°40'\pm14'$, $\angle FAsF=96°18'\pm16'$. The quadrupole coupling constants for As^{75} are $eQq_{cc}=-220\pm4$ Mc/sec and $\eta_0=(q_{bb}-q_{aa})/q_{cc}=-1.20\pm0.05$. The indicated uncertainties of all parameters are limits of error obtained directly from the estimated maximum imprecision in the measured frequencies.

New wavemeter for millimeter wavelengths, R. W. Zimmerer, *Rev. Sci. Instr.* **33,** *No. 8, 858–859 (Aug. 1962).*
A new wavemeter of simple design is described. The principle of operation makes use of a new development in physical optics. The actual performance of the devise was measured and compared with the theory.

Electron energy losses in solids and their influence on the electron diffraction diagram, L. Marton, *J. Phys. Soc. Japan* **17,** *Suppl. B–II, 68–73 (1961).*
The electron diffraction diagram is considered from the point of view of the influence of characteristic energy losses of the electrons in the solid. Some of the present theories of these losses are reviewed, together with the experimental evidence, leading to a new viewpoint. While the influence of these characteristic losses on the average electron diffraction diagram is negligible, for precise measurements a knowledge of the losses and a corresponding correction (either theoretical or experimental) is needed.

Optical detection of microwave transitions in electronically excited CN produced by a chemical reaction, R. L. Barger, H. P. Broida, A. J. Estin, and H. E. Radford, *Phys. Rev. Letters* **9,** *No. 8, 345–346 (Oct. 15, 1962).*
Population inversions and non-equilibrium populations produced by chemical reactions should be useful for molecular structure studies by double resonance and possibly for maser or laser action. Atomic flames of nitrogen atoms mixed with hydrocarbons provide a particularly good example of a chemical reaction which produces population inversion. A TE_{011} microwave cavity of volume 40 cm³, from 8750 to 10,200 Mc and having a Q of approximately 2×10^4, was used with a power input of ½ to 1 watt. At each of the frequencies 9855, 9740, and 8810 Mc, a resonant increase in the optical emission was observed; the increases had ralative magnitudes of 5, 4, and 1, respectively.

Sum rules for vibrational-rotational energy levels including centrifugal distortion, H. C. Allen, Jr., and W. B. Olson *J. chem. Phys.* **37,** *No. 2, 212–214 (July 15, 1962).*
Sum rules are developed for the vibrational-rotational energy levels of an asymmetric rotor. These sum rules contain the corrections for centrifugal distortion correct for terms of the order P^8 in the Hamiltonian. If the P^6 terms of the Hamiltonian are neglected these sum rules reduce to those derived for a rigid asymmetric rotor by Mecke.

Rotational perturbations in CN I. Zero-field theory, optical Zeeman effect, and microwave transition probabilities, H. E. Radford and H. P. Broida, *Phys. Rev.* **128,** *No. 1, 231–242 (Oct. 1963).*
The theory of rotational perturbations in doublet states of diatomic molecules is developed and is applied to the long-standing problem of perturbations in the violet bands of the CN radical. Analysis of the available optical data yields experimental values of two reduced matrix elements:

$$(\Pi|AL_y|\Sigma) = -0.39 \pm 0.04 \text{ cm}^{-1}$$
$$(\Pi|BL_y|\Sigma) = 0.011 \pm 0.001 \text{ cm}^{-1},$$

where the uncertainties shown are estimated upper limits. These account satisfactorily for all the observed line shifts in the violet spectrum. These two parameters are then used to predict the Zeeman effect of the rotational perturbations, and these predictions are checked against new observations of the CN violet specturm at magnetic field strengths up to 28 kgauss. Finally, the zero-field analysis is used to examine the feasibility of a proposed microwave resonance investigation of the perturbed excited states of CN.

The system Bi_2O_3–B_2O_3, E. M. Levin and C. L. McDaniel. *J. Am. Ceram. Soc.* **45,** *No. 8, 355–360 (Aug. 1962).*
The phase diagram for the system Bi_2O_3–B_2O_3 has been determined experimentally. The melting point of Bi_2O_3 has been redetermined as 825° C with an estimated overall uncertainty of about ±3° C, and the molal heat of fusion of Bi_2O_3, calculated from the slope of the liquidus curve, is 2050 cal per mole. The system contains a body-centered cubic phase of approximate composition $12Bi_2O_3{\cdot}B_2O_3$, which melts incongruently at 632° C. Four congurently melting compounds exist in the system: $2Bi_2O_3{\cdot}B_2O_3$, $3Bi_2O_3{\cdot}5B_2O_3$, $Bi_2O_3{\cdot}3B_2O_3$, and $Bi_2O_3{\cdot}4B_2O_3$, with melting points, respectively, of 675°, 722°, 708°, and 715° C. The $Bi_2O_3{\cdot}4B_2O_3$ compound exhibits a sluggish transformation at 696° C. Compositions containing up to 97.5 wt% (85 mole %) Bi_2O_3 can be partly or totally quenched to glass. Indices of the quenched glasses are greater than 1.74. A region of liquid immiscibility extends at 709° C from almost pure B_2O_3 to 19.0 mole % Bi_2O_3. The extent of immiscibility theoretically calculated agrees with the experimentally determined value when 1.20 A is used for the ionic radius of Bi^{3+}.

Wavelengths, energy levels, and pressure shifts in mercury 198, V. Kaufman, *J. Opt. Soc. Am.* **52,** *No. 8, 866–870 (Aug. 1962).*
The vacuum wavelengths of 27 lines in the spectrum of Hg^{198} have been measured relative to the international standard of length, the Kr^{86} line at 6057.80211 Å by photographic Fabry-Perot interferometry. These measurements were made using Hg^{198} electrodeless lamps containing argon gas at pressures of ¼, 3 and 10 mm Hg. Energy level values have been derived for each of the Hg^{198} sources. On the basis of these values, the energy level shifts per unit pressure of argon have been calculated. The suitability of the Hg^{198} electrodeless lamp as a source of wavelength standards for interferometric measurement of length and wavelength is discussed.
The standard source used was a Kr^{86} hot cathode lamp operated according to the conditions proscribed by the International Conference on Weights and Measures in 1960.

A network transfer theorem, G. F. Montgomery, *IRE Trans. Audio.* **AU–10,** *No. 3, 88 (May–June 1962).*
For a linear, passive, reciprocal two-port network, the forward, open-circuit voltage transfer ratio is equal to the reverse, short-circuit current transfer ratio.

Acoustical interferometer employed as an instrument for measuring low absolute temperatures, *J. Acoust, Soc. Am.* **34,** *No. 8, 1145–1146 (Aug. 1962).*
Values of absolute temperatures at 2 and 20° K have been determined from experimental measurements of the speed of sound as a function of pressure in helium gas. The acoustical interferometer was the instrument employed in the measurements, and the accuracy achieved in the experiment indicates that sonic thermometry at low tempertures may be competitive with other conventional thermometry techniques.

Kinetics of Cs^+ desorption from tungsten, M. D. Scheer and J. Fine, *J. Chem. Phys.* **37,** *No. 1, 107–113 (July 1962).*
The mean absorption lifetime (τ_3) of Cs^+ on tungsten has been measured in the 1000–1200°K temperature range, using a pulsed beam technique. Under conditions of low surface coverage and with either Cs or CsI as beam materials,

$$\tau_3 = (1.0 \pm 0.5) \times 10^{-12} \exp\left[\frac{23{,}6000 \pm 500}{T}\right] \text{sec.}$$

was obtained. The heat of desorption can be calculated as the energy required to remove an isolated Cs^+ ion from the surface of an electrical conductor. The presence of an absorbed contaminating layer, arising from residual vacuum gases, decreased the $Cs^+ - W$ binding energy by 0.5 ev and increased the pre-exponential factor by about two orders of magnitude. Anomolous results were obtained when CsCl was used for a beam material, suggesting a reaction between the surface tungsten atoms and atomic chlorine.

Structure and structure imperfections of solid β-oxygen, E. M. Horl, *Acta, Cryst.* **15,** *No. 9, 845–850 (Sept. 1962).*
Electron diffraction studies were carried out on thin films of solid oxygen. The structure of β-oxygen was investigated and a rhombohedral structure of the space group $P\bar{3}_121$ found. Its corresponding hexagonal cell has the dimensions $a = 3.307 \pm .008$Å, $c = 11.256 \pm .015$Å and contains three molecules parallel to the hexagonal axis at the positions: $(\frac{1}{3}, \frac{1}{3}, 0)$, $(-\frac{1}{3}, 0, \frac{1}{3})$ and $(0, -\frac{1}{3}, \frac{2}{3})$. Faults in the stacking sequence of the (00.1)-layers were observed and the experimental results compared with the Paterson treatment of growth faults in fcc crystals.

Neutral meson photoproduction from complex nuclei, R. A. Schrack, J. E. Leiss, and S. Penner, *Phys. Rev.* **127,** *No. 5, 1772–1783 (Sept. 1, 1962).*

The angular distributions of neutral mesons produced by 170 Mev bremsstrahlung on carbon, aluminum, copper, cadmium, and lead have been obtained through the coincident detection of the decay photons by a scintillation counter system. The experimental data have been analyzed by means of a Monte Carlo prediction based on an impulse-approximation elastic coherent production model. The nuclear density distributions which were used in the synthesis of those predictions which were in best agreement with the experimental data from this experiment have been compared to the charge density distributions inferred from electron scattering experiments. The values of the rms radii of nuclear matter obtained in this experiment are, within the limits of error of the experiment (about $2.\times10^{-14}$cm), consistent with the values of charge distribution radii obtained in electron scattering.

The spin-independent part of the neutral meson photoproduction cross section used in the synthesized predictions is obtained using the dispersion theory of Chew, Low, Goldberger, and Nambu. The dependence of the cross section on the meson-nucleon phase shifts used is investigated and a set of phase shifts is presented that results in a correct prediction of the absolute cross sections observed in this experiment; however, this particular set of phase shifts is not unique.

Rotation-vibration spectrum of matrix-isolated hydrogen chloride, L. J. Schoen and D. E. Mann, *J. Chem. Phys.* **37,** *No. 5, 1146–1147 (Sept. 1, 1962).*

An infrared vibration-rotation spectrum of hydrogen chloride molecules isolated in solid argon matrices at 1:500 dilution has been observed at 4 and 20 °K in the region of the fundamental. From the contraction in spacing of the P(1) and R(0) it has been deduced that the HCl molecules undergo quantized but hindered rotation in cavities having cylindrical symmetry.

Other NBS Publications

Journal of Research 67B (Math. and Math. Phys.), No. 1 (Jan.–Mar. 1963) 75 cents.

Evaluation of a generalized elliptic-type integral. L. F. Epstein and J. H. Hubbell.

An algorithm for obtaining an orthogonal set of individual degrees of freedom for error. J. M. Cameron.

Recognition of completely mixed games. A. J. Goldman.

A new type of computable inductor. C. H. Page. (See above abstract.)

Numerical computation of the temporal development of currents in a gas discharge tube. W. Börsch-Supan and H. Oser. (See above abstract.)

Tables of genera of groups of linear fractional transformations. H. Fell, M. Newman, and E. Ordman.

Journal of Research 67C (Eng. and Instr.), No. 1 (Jan.–Mar. 1963), 75 cents.

Method for calibrating a standard volt box. B. L. Dunfee.

Stability of residual thiosulfate in processed microfilm. C. I. Pope.

Equipment for single crystal growth from aqueous solution. J. L. Torgesen, A. T. Horton, and C. P. Saylor. (See above abstract.)

An automatic multichannel correlator. R. F. Brown, Jr. (See above abstract.)

Elastic constant—porosity relations for polycrystalline thoria. S. Spinner, F. P. Knudsen, and L. Stone. (See above abstract.)

An oxygen partial pressure warning instrument. L. Greenspan.

New fast-opening, large-aperture shutter for high-speed photography. E. C. Cassidy and D. H. Tsai. (See above abstract.)

Equations for the radiofrequency magnetic permeameter. C. A. Hoer and A. L. Rasmussen

Journal of Research 67D (Radio Prop.), No. 2 (Mar.–Apr. 1963), 70 cents.

The protection of frequencies for radio astronomy. R. L. Smith-Rose.

Radar reflections from the moon at 425 Mc/s. G. H. Millman and F. L. Rose.

Sunset and sunrise in the ionosphere: effects on the propagation of longwaves. J. Rieker.

Correction of atmospheric refraction errors in radio height finding. W. B. Sweezy and B. R. Bean.

Empirical determination of total atmospheric refraction at centimeter wavelengths by radiometric means. A. C. Anway.

Propagation of radiofrequency electromagnetic fields in geological conductors. V. Fritsch, translated from German by A. P. Barsis.

WWV reception in the arctic during ionospheric disturbances. G. E. Hill and J. R. Herman.

Height-gain for VLF radio waves. J. R. Wait and K. P. Spies.

Perturbation method in a problem of waveguide theory. D. Fox and W. Magnus. (See above abstract.)

Some wave functions and potential functions pertaining to spherically stratified media. C. T. Tai. (See above abstract.)

Radiation from a plasma-clad axially-slotted cylinder. W. V. T. Rusch. (See above abstract.)

Two- and three-loop superdirective receiving antennas. E. W. Seeley.

Hallen's method in the problem of a cavity-backed rectangular slot antenna. J. Galejs.

Relative convergence of the solution of a doubly infinite set of equations. R. Mittra.

Periodicals received in the Library of the National Bureau of Standards, July 1962, N. J. Hopper, NBS Mono. 57 (Nov. 23, 1962), 25 cents (Supersedes NBS Circ. 563 and the 1st supplement to NBS Circ. 563).

Corrosion of steel pilings in soils, M. Romanoff, NBS Mono. 58 (Oct. 24, 1962), 20 cents.

Hydraulic research in the United States 1962, H. K. Middleton, NBS Misc. Publ. 245 (Oct. 26, 1962), $1.00.

Quarterly radio noise data, March, April, May 1962 and corrigendum for Technical Notes 18–1 through 18–11, W. Q. Crichlow, R. T. Disney, and M. A. Jenkins, NBS Tech. Note 18–14 (Aug. 9, 1962), 50 cents.

Mean electron density variations of the quiet ionosphere, No. 8—October 1959, J. W. Wright, L. R. Wescott, and D. J. Brown, NBS Tech. Note 40–8, (Sept. 1962) 35 cents.

Synoptic radio metrology, B. R. Bean, J. D. Horn, and L. P. Riggs, NBS Tech. Note 98, (Oct. 1962) 50 cents.

Bibliography on direction finding and related ionospheric propagation topics 1955–1961, O. D. Remmler, NBS Tech. Note 127, (Oct. 1962) 60 cents.

Equatorial spread F, W. Calvert, NBS Tech. Note 145 (Aug. 1, 1962) 60 cents.

The thermodynamic properties of helium from 6 to 540° R between 10 and 1500 psia, D. B. Mann, NBS Tech. Note 154A (Jan. 1962), 50 cents.

The energy parameter B for strong blast waves, D. L. Jones, NBS Tech. Note 155, (July 1962) 25 cents.

Emission stabilization of thermionic diode noise sources, M. W. Randall and M. G. Arthur, NBS Tech. Note 160 (Sept. 1962), 15 cents.

Evaluation of unexpectedly large radiation exposures by means of photographic film, W. L. McLaughlin, NBS Tech. Note 161, (Aug. 1962) 15 cents.

Spectrophotometric determination of hydroperoxide in diethyle ether, W. C. Wolfe, Anal. Chem. **34,** No. 10, 1328–1330 (Sept. 1962).

Exchange behavior of kaolins of varying degrees of crystallinity, W. C. Ormsby, J. M. Shartsis, and K. H. Woodside, J. Am. Ceram. Soc. **45,** No. 8, 361–366 (Aug. 1962).

Analysis of the hydroxyl radical vibration rotation spectrum between 3900 Å and 15000 A, A. M. Bass and D. Garvin, J. Mol. Spectry. **9,** No. 2, 114–123 (Aug. 1962).

Microwave measurements in the NBS electronic calibration center, R. E. Larson, Inst. Elec. Engrs. **109,** pt. B, suppl. No. 23, 644–650 (1962).

Effect of additives on silver iodide particles exposed to light, G. Burley and D. W. Herrin, J. Appl. Meteorol. **1,** No. 3, 355–356 (Oct. 1962).

A modulated sub-carrier technique of measuring microwave attenuation, G. E. Schafer and R. R. Bowman, Inst. Elec. Engrs. **109,** pt. B, suppl. 23, 783–786 (1962).

A survey of microwave power-measurement techniques employed at the National Bureau of Standards, G. F. Engen, Inst. Elec. Engrs. **109,** pt. B, suppl. No. 23, 734–739 (1962).

Symposium on teaching of materials: Aspects of material behavior significant to engineers, J. M. Frankland, J. Eng. Mech. Div.–Proc. Am. Soc. Civil Engr. Paper No. 3246. **75**–81 (Aug. 1962).

Excitation of modes at very low frequency in the earth-ionosphere wave guide, J. R. Wait, J. Geophys. Res. **67,** No. 10, 3823–3828 (Sept. 1962).

The growth and roots of electronic computers, J. L. Little, Student Quart. and EE Digest, Joint Publ. of Am. Inst. Elec. Engr. and IRE **1,** No. 1, 64–70 (Sept. 1962).

Acoustical interferometer employed as an instrument for measuring low absolute temperatures, G. Cataland and H. H. Plumb, J. Acoust., Soc. Am. **34,** No. 8, 1145–1146 (Aug. 1962).

The Hall effect, D. O. Webster, Student Quart. & EE Dig. p. 82–86 (Sept. 1962).

Dimensional changes in complete dentures on drying, wetting, and heating in water, G. C. Paffenbarger and W. T. Sweeney, J. Am. Dental Assoc. **65,** No. 4, 495–505 (Oct. 1962).

A variable-parameter direct-current switching filter, G. F. Montgomery, Proc. IRE **50,** No. 9, 1986 (Sept. 1962).

The vapor phase radiolysis of propane-d^8 in the presence of other hydrocarbons, S. G. Lias and P. Ausloos, J. Chem. Phys. **37,** No. 4, 877–883 (Aug. 15, 1962).

Synthesis of an immittance function with two negative impedance converters, S. B. Geller, IRE Trans. Circuit Theory **CT–9,** No. 3, 291 (Sept. 1962).

A note on the propagation of electromagnetic pulses over the earth's surface, J. R. Wait, Can. J. Phys. **40,** 1264–1269 (1962).

Surface behavior of silver single crystals in fused sodium chloride, J. Kruger and K. H. Stern, J. Electrochem. Soc. **109,** No. 10, 889–894 (Oct. 1962).

The spontaneous martensitic transformations in 18% Cr, 8% Ni steels, R. P. Reed, Acta Met. **10,** 865–877 (Sept. 1962).

A high speed pyrometer, G. A. Hornbeck, Book, Temperature, Its Measurement and Control in Science and Industry, III, pt. 2, 425–428 (Reinhold Publ. Corp., New York, N.Y., 1962).

The viscous heating correction for fiscometer flows, E. A. Kearsley, Trans. Soc. Rheology **VI,** 253–261 (1962).

Strengthening of hot work die steels, C. R. Irish and S. J. Rosenberg, Trans. Quart. **55,** No. 3, 613–623 (Sept. 1962).

Correlation of factors influencing the pressures generated in multi-anvil devices, J. C. Houck and U. O. Hutton, Am. Soc. Mech. Engrs. Paper 62–WA-254 (1962).

The temperature dependence of flow and fracture characteristics of an age-hardenable alloy, W. D. Jenkins and W. A. Willard, Trans. ASM **55,** No. 3, 580–598 (Sept. 1962).

The effect of experimental variable including the martensitic transformation on the low-temperature mechanical properties of austenitic stainless steels, C. J. Guntner and R. P. Reed, Trans. ASM **55,** No. 3, 399–419 (Sept. 1962).

A new ionospheric multipath reduction factor (MRF), R. K. Salaman, IRE Trans. Commun. Systems **CS–10,** 220–222 (June 1962).

The effect of electrolytes on the sodium chromotropism of bix-(meso-2,3–diaminobutane)-nickel (II) ions, D. L. Leussing, J. Harris, and P. Wood, J. Phys. Chem. **66,** 1544–1546 (Aug. 1962).

Characteristics of resistance strain gages, R. L. Bloss, Book' Semiconductor and Conventional Strain Gages, ed. Mills Dean, III and R. D. Douglas, ch. VII, 123–142 (Academic Press, Inc., New York, N.Y., Oct. 1962).

The photodisintegration of bismuth and the lead isotopes, E. G. Fuller and E. Hayward, Nuclear Phys. **33,** 431–448 (1962).

Comparison of the relative acidic strengths of the isomeric dinitrophenols in benzene and water, M. M. Davis, J. Am. Ceram. Soc. **84,** 3623–3627 (1962).

The basis of the measurement system, A. V. Astin, Proc. IRE **50,** No. 5, 614–616 (May 1962).

Predicting the performance of long distance tropospheric communication circuits, A. P. Barsis, K. A. Norton, and P. L. Rice, IRE Trans. Commun. Systems **CS–10,** 2–22 (Mar. 1962).

A neuron model which performs analog functions, D. R. Boyle, (Proc. San Diego Symp. Biomedical Engr., San Diego, Calif., R. 256–263 June 19–21, 1962).

Scattered radiation from large Cs^{137} sources, L. Costrell, Health Phys. **8,** No. 5, 491–498 (Oct. 1962).

Standard tests for electrical properties, A. H. Scott, SPE J. **18,** 1375–1378 (Nov. 1962).

The industrial significance of National Bureau of Standards research, G. M. Kline, Mod. Plastics **40,** No. 2, 149 (Oct. 1962).

Comments on "A new precision low level bolometer bridge," G. F. Engen, Proc. IRE **50,** No. 9, 1997 (Sept. 1962).

Solar particles in interplanetary space, C. S. Warwick, Sky and Telescope **XXIX,** No. 3, 133–136 (Sept. 1962).

The kinetics of the heat precipitation of collagen, J. M. Cassel, L. Mandelkern, and D. E. Roberts, J. Am. Leather Chem. Assoc, **LVII,** No. 11, 556–575 (Nov. 1962).

Chromium plating by thermal decomposition of dicumene chromium, W. H. Metzger, Jr., Plating **49,** No. 11, 1176 (Nov. 1962).

Oxidation of high polymers, M. Tryon and L. A. Wall, Book, Autoxication and Antioxidants II, ch. 19, p. 919 (Interscience Publ. Inc., New York, N.Y., 1962).

The use of a Venturi tube as a quality meter, R. V. Smith, P. C. Wergin, J. F. Ferguson, and R. B. Jacobs, J. Basic Eng. **84,** 411–412 (Sept. 1962).

Dislocation loops in deformed copper, A. W. Ruff, Jr., Fifth Intern. Congress for Electron Microscopy, p. J–10 (Academic Press, Inc., New York, N.Y., 1962).

**Publications for which a price is indicated are available from the Superintendent of Documents, U.S. Government Printing Office, Washington 25, D.C. (foreign postage one-fourth additional). Reprints from outside journals and the NBS Journal of Research may often be obtained directly from the authors.*

U.S. GOVERNMENT PRINTING OFFICE:1963

UNIVERSITY MICROFILMS
313 NORTH FIRST STREET
ANN ARBOR, MICHIGAN
SJR-A-OCT

UNITED STATES
GOVERNMENT PRINTING OFFICE
DIVISION OF PUBLIC DOCUMENTS
WASHINGTON 25, D.C.
OFFICIAL BUSINESS

PENALTY FOR PRIVATE USE TO AVOID PAYMENT OF POSTAGE, $300 (GPO)

JOURNAL OF RESEARCH of the National Bureau of Standards — Vol. 67A, No. 2 — March–April 1963
A. Physics and Chemistry

Contents

Page

Third spectrum of palladium (Pd III). A. G. Shenstone. 87

Broadening of the rotational lines of carbon monoxide by HCl and by argon. R. J. Thibault, J. H. Jaffe, and Earle K. Plyler. 113

Theory of frustrated total reflection involving metallic surfaces. T. R. Young and B. D. Rothrock. 115

Quantitative metallography with a digital computer: application to a Nb-Sn superconducting wire. G. A. Moore and L. L. Wyman. 127

Moiré fringes produced by a point projection X-ray microscope. Sanford B. Newman. 149

Cyclic polyhydroxy ketones. I. Oxidation products of hexahydroxybenzene (benzenehexol). Alexander J. Fatiadi, Horace S. Isbell, and William F. Sager. 153

Effect of pressure and temperature on the refractive indices of benzene, carbon tetrachloride, and water. R. M. Waxler and C. E. Weir. 163

Pressure-density-temperature relations of fluid para hydrogen from 15 to 100 °K at pressures to 350 atmospheres. Robert D. Goodwin, Dwain E. Diller, Hans M. Roder, and Lloyd A. Weber. 173

A method for determining the elastic constants of a cubic crystal from velocity measurements in a single arbitrary direction; application to $SrTiO_3$. J. B. Wachtman, Jr., M. L. Wheat, and S. Marzullo. 193

Publications of the National Bureau of Standards. 205

For sale by the Superintendent of Documents, U.S. Government Printing Office, Washington 25, D.C. Price 70 cents (single copy)
Subscription price: $4.00 a year; 75 cents additional for foreign mailing.
UNITED STATES GOVERNMENT PRINTING OFFICE, WASHINGTON : 1963

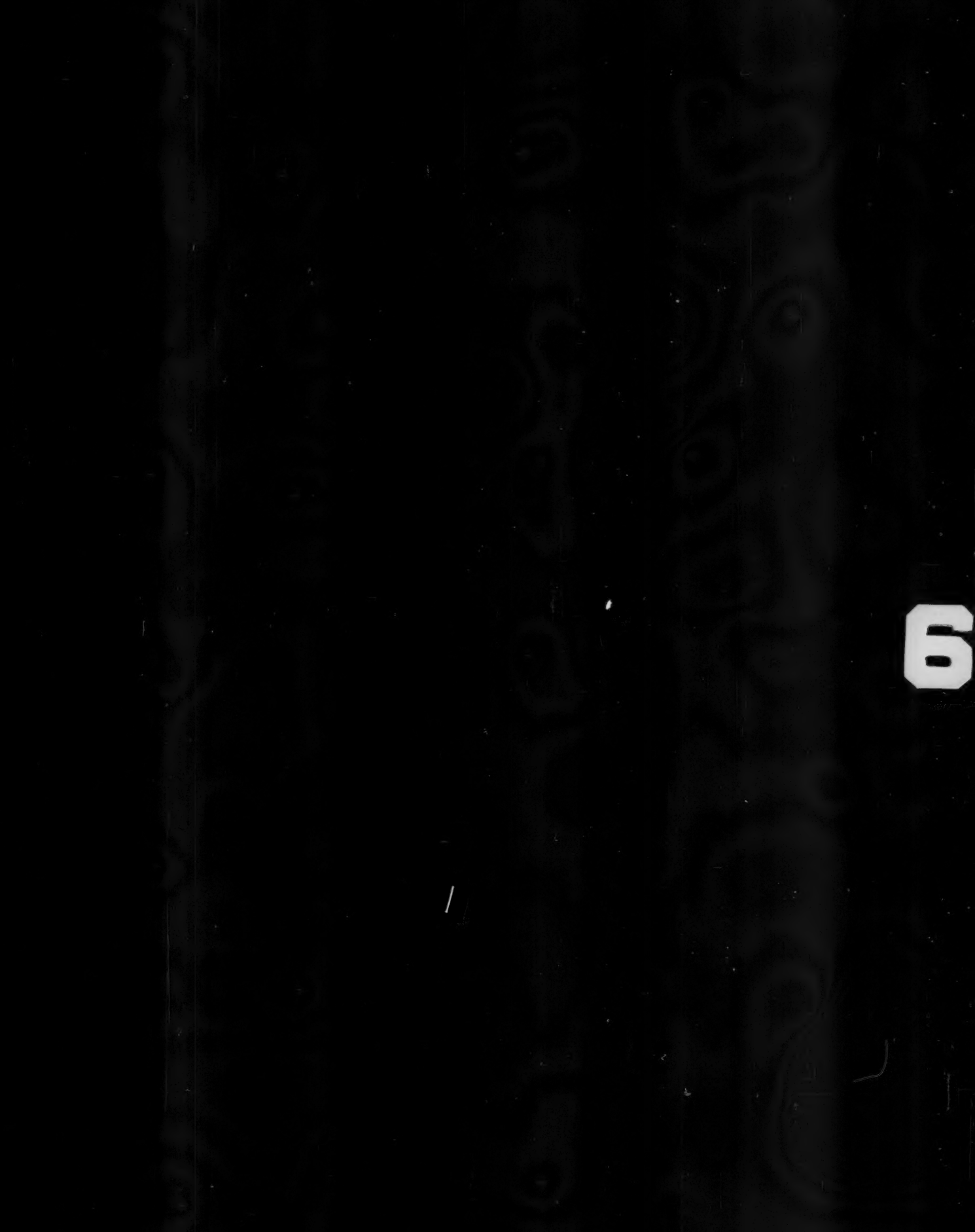
6